Volume 52 Number 11/12 November/December 1982

The Radio and Electronic Engineer

Journal of the Institution of Electronic and Radio Engineers

GUEST EDITORIAL

NEWS AND COMMENTARY

PAPERS ON MILLIMETRE WAVE SYSTEMS

Waveguides and Components

Editor:
F. W. Sharp, FIERE

Production Editor:
J. I. Secluna

Subscription Rates (1983)

	Annual	Single Copies
United Kingdom and Ireland	£44.00	£3.66
Overseas	£50.00	£4.16
North and South America	$(US)106	$(US)8.83

Subscribers outside the British Isles receive copies by Accelerated Surface Post.

Sworn statement of average monthly circulation:
January–December 1981, 13,393

Member of the Association of Learned and Professional Society Publishers

Papers published in *The Radio and Electronic Engineer* are listed or abstracted as follows:

Title listings: 'British Technology Index'; 'Current Papers'; 'Topics'; Current Contents'; 'Science Citation Index'; ASCA.

Abstracted fully: 'Science Abstracts'; 'Referativni Zhurnal'.

Abstracted selectively: 'Chemical Abstracts'; 'Computing Reviews'; 'Acoustic Abstracts'; 'Solid State Abstracts Journal'; 'Nuclear Science Abstracts'.

The Institution is not, as a body, responsible for expressions of opinion appearing in its publications, unless otherwise stated.

ISSN 0033-7722

All Advertisement Enquiries to
Electronic Engineering Publications Ltd.
PO Box 29 STEVENAGE, Herts SG1 1HJ

Telephone: 0438 727371

Published monthly by the Institution at
99 GOWER STREET
LONDON WC1E 6AZ

Telephone: 01-388 3071
Telegrams: INSTRAD LONDON WC1

Founded 1925
Incorporated
by Royal Charter 1961
To promote the advancement of radio, electronics and kindred subjects by the exchange of information in these branches of engineering

Volume 52, Number 11/12 November/December 1982

The Radio and Electronic Engineer

The Journal of the Institution of Electronic and Radio Engineers

Progress in Millimetre Wave Systems

A SPECIAL edition of this Journal in July/August 1979 focused attention on the exploitation of the 100–1000 GHz frequency range. Since that time considerable advances have been made, particularly at the low frequency end of the range. The presence of atmospheric windows of reduced attenuation at 96 and 140 GHz, and a military demand for small antenna dimensions and narrow beam-width systems, have resulted in a considerable increase in activity in the short-millimetric wavelength region. Subsequent developments will undoubtedly extend applications for other purposes but right now the basic need of sources, detectors, waveguide and components must be met before any solution is possible for a particular practical requirement. A timely one-day Colloquium on Waveguides and Components for the 80–300 GHz Frequency Range was organized by this Institution in April 1981 and, as reported in the November/December 1981 Journal, ten presentations outlined progress by UK research groups. The objective of the present Special Edition is to survey advances to date in both components and systems in some important areas in this part of the spectrum.

It is fair to state that there have been no startling developments during the past three years but rather expectancy has given way to a sense of maturity. There have been solid engineering achievements mainly up to 100 GHz and a more critical view has been formed of what technological and conceptual concepts should be addressed. The availability of solid-state devices and transmission components has remained at much the same level with little reduction in cost and conventional metal waveguides have yet to be replaced by other waveguiding structures. Military projects have been the main inspiration for development and both components and measurement equipment continue to be viewed as a high cost, highly specialized, constrained market. Active device reliability is not helped by small production runs and together with all the other factors has made R and D work in this field somewhat arduous at times. A breakthrough into the civil applications with costs spiralling downwards now seems less likely than a gradual build-up of activity in diverse applications through progress in printed circuit techniques, packaging of modules and simplifying manufacturing test procedures. Beyond 100 GHz new concepts will almost certainly be required.

Progress can be considered under the general headings of sources, detectors, waveguides, systems and applications. Solid-state sources at 100 GHz are now readily available, although expensive. Impatt oscillators will give several watts under pulsed conditions and approach 1 W c.w., whilst Gunn oscillators will deliver many milliwatts with a low noise content. Magnetrons and b.w.o. tubes have been available for many years at around 100 GHz. Gyratrons giving a pulse power of 100 kW at 140 GHz have been recently reported, and have given 1 kW cw even at 300 GHz. (Solid-state sources have been made to oscillate up to 300 GHz, but at very low power levels.) Detector development has more than kept pace. Beam lead diodes are especially convenient for microstrip and fin-line configurations, but conversion losses become high for balanced mixers much above 150 GHz. A significant development that has yet to reach this frequency range is the raising of f.e.t. operating frequencies: it looks as if 60 GHz operation will be feasible, and 100 GHz could well be achieved in the relatively near future. A number of different guide types are available, particularly at around 100 GHz when rectangular waveguide, microstrip, fin-line (E plane circuits across rectangular guide), and dielectric image lines are all applicable. Rectangular guide and associated components are the only form readily available commercially, but microstrip is convenient to make using photolithography, and fin-line components are finding increasing favour. Above 150 GHz the choice becomes much more limited. Rectangular guide and components are available but at great expense. Lower loss microstrip configurations, e.g. suspended stripline using Z-cut quartz, can be used, or new approaches such as groove-guide or optical techniques must be taken. Many components are available around 100 GHz, but a conspicuous absence of non-reciprocal devices using, for example, ferrites above 150 GHz is apparent. The systems situation is unclear, being shrouded by security considerations in many cases. Radar systems have been operational at 96 GHz however, whilst receiver technology extends above 200 GHz.

This special edition includes papers on waveguides and circuits, active devices, antennas, systems, propagation and measurements.

Booton and his colleagues have developed manufacturing techniques to produce a range of components in rectangular waveguide up to 325 GHz, with emphasis on electro-forming and selective chemical etching, and have also

constructed components using planar photolithography in Duroid-based fin-line. Fin-line is also the guide-base in the work of Nightingale *et al*, who have realized a range of components and circuits up to 140 GHz, while Bornemann *et al.* have developed low-insertion loss filters using fin-line and metal inserts. Two types of dielectric guide, insular and image guide, are described by Gelsthorpe and colleagues, and the design and performance of a number of components is given. The feasibility of construction by thick film printing for low-cost mass production is demonstrated.

Two papers relate to active devices. Eddison and Davies compare indium phosphide with gallium arsenide for oscillator construction and the theoretical prediction of superiority of InP for transferred electron oscillators at short-millimetric wave-lengths has been verified. Mixer diode developments are described by Sisson, who gives the design and performance of GaAs beam-lead diodes, together with information on microstrip mixer characteristics at 90 and 140 GHz.

The need for new types of antennas for millimetre equipment has opened up new frontiers but many problems exist as critically reviewed by Henderson and James. Dewey describes the considerations leading up to development of a novel imaging lens antenna.

The state-of-the-art in millimetre subsystems is crystallized in papers by Booton *et al* and Nightingale *et al.* and it is both fascinating and reassuring to see designers get to grips with this new technology. Beyond 100 GHz new concepts must be introduced and the paper by Clancy gives perhaps a preview of what is in store.

A paper by Johnston gives a critical comparison of millimetre wave propagation measurement techniques, and indicates additional measurements that need to be made. Finally a comprehensive review is given by Birch and Clarke of methods for measuring dielectric properties from 30 to 100 GHz. Knowledge of dielectric and other material properties is basic to the exploitation of this part of the spectrum. Reference is made to measurement on low-loss solids, reflecting surfaces, liquids, gases and biological materials.

Millimetre wave technology up to 100 GHz has been available for a considerable period, but with a severe cost penalty. This may not be prohibitive for many military applications, but is a bar for commercial or high-number requirements. Advances in lower-cost circuits and active devices, including integrated circuits for millimetre wavelengths, are now rapidly changing the situation however. Low-cost substrates can be used, even at 100 GHz. We can look forward to relatively low-cost systems for such frequencies in the near future with a resultant expansion in areas of application. The development of really high-power practical sources looks encouraging, but is still some way in the future. Widespread utilization of even higher frequencies is probably a decade or so away. Attenuation in the 140 and 220 GHz windows is considerably higher than at 96 GHz, devices are much less developed, and the waveguiding systems that are adequate below 100 GHz look unpromising above that frequency. New approaches will thus need to be explored. However it can be predicted that within five years low size, weight and cost systems with the enhanced performance possible at wavelengths down to 3 mm will be relatively commonplace, and find extensive application. It is our hope that this Special Edition will contribute to that end.

J. R. JAMES
D. J. HARRIS

The Guest Editors

Jim James (Fellow 1975, Member 1960, Graduate 1956) holds a research professorship at the Royal Military College of Science. He has published widely in the fields of microwaves, antennas, speech processing, radar absorbent materials and, more recently, electromagnetic heating of living tissues. He was appointed a Senior Principal Scientific Officer in 1976 and a Deputy Chief Scientific Officer in 1982, both by special merit promotion. He was Chairman of the IERE Papers Committee from 1972–1975 and is a Vice President of the Institution. He is currently Chairman of the IEE professional group on antennas and propagation and also Chairman of the IEE International Conference on Antennas and Propagation to be held in Norwich in 1983. He is editor of a series of research monographs.

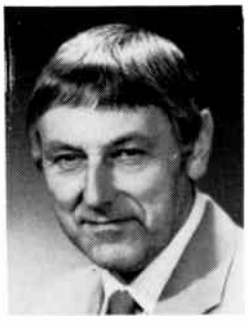

J. R. JAMES

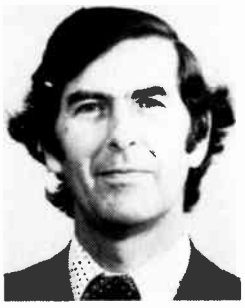

D. J. HARRIS

Douglas Harris (Fellow 1975) graduated in electrical engineering and obtained his Ph.D. from Queen Mary College, University of London. Subsequent research and lecturing appointments were held at the Admiralty Laboratory, Baldock, Stanford University, California, Sheffield University and Portsmouth Polytechnic. He was Professor and Head of Electrical Engineering at Ahmadu Bello University, Nigeria, for seven years, and a visiting Professor at University College London. Since 1975 he has been Professor and Head of the Department of Physics, Electronics and Electrical Engineering at the University of Wales Institute of Science and Technology, Cardiff. Research interests have included high voltage and microwave discharges, microwave electron tubes, m.h.d. generation and atmospheric electricity, but present research centres around millimetre and submillimetre waves. He was Guest Editor for the special issue of the Journal in 1979 on Exploitation of the 100–1000 GHz Frequency Range and was Chairman of the April 1981 Colloquium.

New Training Requirements

Applicants for admission to the IERE in the classes of Corporate Member, or of Associate Member, should be employed at the appropriate level or responsibility, and in addition need to satisfy the Institution's requirements relating to academic qualifications and initial training.

The assessment of academic qualifications is generally straightforward. Most applicants qualify by means of success in well-established examinations, and there are clearly defined procedures for dealing with 'special cases'. However, the Institution takes the view that no rigid formula can be applied to the assessment of initial training, firstly because needs vary for different kinds of employment and secondly because fast developing technologies such as electronics necessitate a more flexible approach than is perhaps required in the more traditional disciplines. It is therefore all the more essential for prospective Corporate Members or Associate Members to seek approval in advance of any training scheme which they propose to follow and to ensure that training received is properly recorded and authenticated.

The Council of Engineering Institutions (CEI) in its endeavour to establish comparable and adequate standards for all branches of the engineering profession, has tightened its procedures for implementing CEI Statement No. 11, which deals with general requirements for the training of engineers and is an interpretation of CEI Bye-laws 52(d) and (e). To publicize this revision of procedures the IERE issued in July 1982 a new edition of its Membership Regulations, which explains in some detail the steps which must be taken to satisfy the new requirements. Basically, these pertain to new methods for the proper certification of training rather than to any changes in course structure or content.

In future candidates will be required to submit a properly authenticated Training Record if following approved schemes, or a fuller Training Report if following a non-standard route. Exceptionally, candidates unable to produce documentary evidence of their initial training will be required to attend a professional interview conducted by a Corporate Member, and if necessary either to complete a further period of training and/or responsible experience or to satisfy a test of competence acceptable both to CEI and the Institution.

The Institution recognizes that some members may be handicapped by the limited availability of comprehensive training schemes, or the reluctance or inability of employers to develop and establish such schemes; it therefore recommends those members in employment who are in this situation to consult the Institution.

Members' Appointments

CORPORATE MEMBERS

J. A. Myers, M.Sc. (Fellow 1971, Member 1968), formerly Deputy Head of the Department of Electrical Engineering at Birmingham Polytechnic, has been appointed Reader in Electrical Engineering at the University of Malawi.

F. H. Wise, B.Sc. (Fellow 1977) has recently taken up an appointment as Head of Telecommunications (SM) with the Hong Kong Post Office. Mr Wise has been with the Independent Broadcasting Authority since 1958, latterly as Head of Network and Planning Department.

J. A. Akinwumi, M.Sc. (Member 1979, Graduate 1971), a Principal Engineer in the Nigerian Ministry of Communications, Transmission and Planning Group since 1980, has been promoted to the post of Assistant Chief Engineer; he recently successfully completed an M.Sc. course at the University of Wales Institute of Science and Technology.

B. W. Barnes (Member 1973, Graduate 1966) has been appointed Senior Engineer (Security System Design) at the Head Office of the Electricity Supply Commission of the Republic of South Africa, based in Johannesburg. His previous appointment was as Head of Telephony for the Rand and Orange Free State Region of ESCOM.

N. Brayford (Member 1973, Graduate 1975) who has been with the British Steel Corporation since 1969, has joined N. G. Bailey (Instrumentation), Bradford, as Engineering Manager.

D. Chadwick (Member 1973, Graduate 1970) has taken up an appointment as Works Manager with Malayan Cables at Petaling Jaya, Selangor. Since 1975 he has been Technical Manager of BICC Telecommunication Cables, Blackley, Manchester.

D. K. Craig (Member 1971) who has been with British Airways since 1953, has recently been appointed Chief Engineer, Technical and Industrial Services. He previously held the post of Overhaul Manager.

R. M. Everitt (Member 1973, Graduate 1970) who joined the Westinghouse Brake and Signal Company in 1972, has been appointed Engineering Manager, Mass Transit Group.

D. Fielden, B.Sc.(Eng.) (Member 1981) who has been with the Copperbelt Power Company, Kitwe, Zambia since 1980, has been appointed Head of the Electrotechnical Department. Mr Fielden is the Council's representative in Zambia.

F. Goodall, B.Sc., M.Sc., Ph.D. (Member 1970) who was Head of Engineering at Salford College of Technology, has taken up the post of Vice-Principal at Granville College, Sheffield. Dr Goodall has been a member of the Institution's Education and Training Committee since 1977 and is currently a member of the Accreditation Working Group and Training Working Party.

Sqdn Ldr M. Joseph, RAF (Member 1973, Graduate 1961), Officer-in-Charge, Training Headquarters Squadron at RAF, Cosford since 1979, has taken up an appointment as Lecturer, Electrical Training Squadron at No 1 School of Technical Training, RAF Halton.

E. C. Mupeso (Member 1980, Associate 1979) who has been with the Zambia Broadcasting Corporation since 1965, has been promoted to Senior Development Engineer with responsibilities as Deputy Chief Engineer of the Corporation.

T. L. Pearce (Member 1966, Graduate 1962) is now Head of the Telecommunications and Support Division with REME Telecommunications and Radar Branch at Leigh Sinton Road, Malvern. For the past six years he has held an appointment as Principal Professional and Technology Officer at the Weapons and Fighting Vehicles Headquarters of MOD (PE), based at ROF Leeds.

S. J. Piper (Member 1980, Graduate 1973) has recently taken up an appointment as Senior Software Engineer with Altos Computer Systems in San Jose, California.

N. J. Price (Member 1973) who has been a Project Manager with GEC (Telecommunications) in Nigeria since 1976, has returned to the United Kingdom and is now a Systems Planning Engineer with the Company's Transmission Division in Coventry.

R. A. Rao (Member 1968) is now Manager, Technical Development, TRW LSI Products Division, in La Jolla, California.

J. Richardson, M.Sc., B.Sc. (Member 1969) has taken up an appointment as Senior Engineer of the Electrification and Shipping Planning Office of New Zealand Railways, Wellington. Since 1971 Mr Richardson had been on the staff of Newcastle upon Tyne Polytechnic as a Senior Lecturer in the Department of Electrical and Electronic Engineering; from 1977 to 1980 he was seconded to the Department of Electrical and Electronic Engineering of Mombasa Polytechnic, Kenya.

R. A. Stewart (Member 1973) is now Head of the Cable and Broadcasting Satellite Branch at the Home Office, Directorate of Radio Technology. Mr Stewart was formerly in the Research and Development Section of the Home Office Directorate of Telecommunications.

NON-CORPORATE MEMBERS

M. M. Fok (Graduate 1979) is now a Technical Instructor at the Training Centre, Cable and Wireless (Hong Kong) in Wanchai.

J. B. Goodall (Graduate 1969) is now a Senior Lecturer in Electronics at Charles Keene College of Further Education, Leicester. He was previously a Lecturer Grade II at Tresham College, Corby.

S. D. Lawrence (Associate Member 1977) has formed his own company, Prototype Development Systems, based on Walton-on-Thames, Surrey; he was previously for six years Principal Engineer with Analog Devices.

K. A. Logan, B.Sc. (Graduate 1982) is now an Electronic Engineer with International Aeradio, based in Abu Dhabi. From 1975 he was an Air Traffic Engineer with the Civil Aviation Authority.

S. O. Ogunkomaiya (Associate Member 1979) who is with the Nigerian Federal Ministry of Aviation, has been posted to Benin Airport as Officer in Charge of Signals Section. He previously held the post of Senior Technical Officer, Signals Section, at Kano Airport.

Poon Hing Wai, Ph.D. (Graduate 1981) has taken up an appointment as an engineer in the First Research Institute, Ministry of Posts and Telecommunications, Shanghai, in the People's Republic of China. For the past five years he was a Research Assistant at the University of Bradford from whom he received his Doctorate.

R. H. Stoner (Graduate 1969) is now an Executive Engineer with Telecom Enterprises in Felixstowe, Suffolk.

P. J. Watts, B.A., M.Ed. (Associate Member 1973, Associate 1969) has been appointed Head of Department of Engineering at Stamford College for Further Education; he was previously Lecturer responsible for Electronics at Oswestry College.

R. A. Walters (Associate Member 1975) has taken up an appointment as Design and Development Engineer with Abacoud of Ealing in London. Mr Walters previously held the post of Director, RLW Developments.

A. G. Wilson, B.A. (Associate 1979) is now a ATE Design and Reliability Consultant with Hill Moss Ltd, Chippenham. He was formerly a Reliability Engineer with Sperry Gyroscope.

W. S. Wong (Associate Member 1979) is now a Senior Technician in the Department of Psychology at the Queen Mary Hospital, University of Hong Kong, following a course of Psychopharmacology at the Institute of Psychiatry, London.

Obituary

The Institution has learned with regret of the deaths of the following members.

Edward Albert Henry Bowsher (Fellow 1949) of Romford died on 11th August 1982, aged 82.

'Eddie' Bowsher received his technical education at Leyton Technical Institute whilst training as a telegraph plant engineer with Western Union Cable Company. He served as a pilot in the RFC and RAF during the 1914–18 war, and in 1921 joined the Standard Telephones and Cables (then known as Western Electric), supervising the installation of numerous telephone exchanges, etc. For four years prior to the 1939–45 war he was in charge of the Circuit Laboratory of the Telephone Division and was responsible for a number of patents, which included a method of signalling by d.c. over power supply networks. Between 1939 and 1945 Mr Bowsher was for some time in charge of production and planning for radar equipment and later became Chief Inspector for the Company. From 1945 to 1951 he was in charge of the Development Department of Central Rediffusion Services. He became Chief Engineer of the Company's subsidiary, Television Research, in Jersey in 1951 and presented a paper on 'Television wire broadcasting' at the Institution's 1951 convention at Cambridge. In 1952 he joined Argosy Radiovision as Technical Director. From 1956 until his retirement he was with the Plessey Company, initially as Head of Laboratory, Special Equipments Division, and subsequently with the Patents Department.

Mr Bowsher served on the Technical Committee from 1949 to 1956 and was for two years its Chairman. He was a member of the Council from 1950 to 1954 and became the founder Chairman in 1966 of the East Anglian Section.

William Walter Smith (Member 1971) of East Grinstead died on 26th January 1982, aged 56 years.

The earlier part of Walter Smith's career was spent in general engineering with the London County Council following an apprenticeship in light construction engineering. In 1940 he entered the radar industry, working first with Decca Radar as a trainee test engineer and subsequently with Mullard Equipment where he became, in 1956, head of the Electronics Test Department. From 1961 to 1966 he was head of the company's Technical Training Department. In 1966 Mr Smith joined the newly-formed Engineering Industry Training Board as a Senior Training Officer. He was later Senior Training Adviser at the London South Eastern Regional Office.

Mr Smith was responsible for drawing up various EITB training schemes in the electronics field and he also wrote a text-book on 'Electronics for Technician Engineers'.

Sydney Ernest Allchurch, O.B.E. (Companion 1964) of Tadworth, Surrey, died on 24th April 1982, aged 74 years. Sydney Allchurch will have been known to many members of the Institution, particularly those in the consumer electronics side of the industry because from 1946 to his retirement in 1973 he was with the British Radio Equipment Manufacturers Association. He joined BREMA immediately after the war as Secretary, becoming Director in 1960 and in 1962 Chairman of its Executive Council. He was also Director and Secretary of the Radio Industry Council from 1967 until his retirement, and he was for a number of years Honorary Treasurer of the Radio, Television and Electronics Examination Board.

Trained as a draughtsman and designer for Pullman rail cars in the 20s and 30s, he put to practical use his talents as an amateur musician by starting a retail music shop which subsequently expanded to include musical instruments and later radio and television. During the war years he served in the Ministry of Aircraft Production, dealing with the supply and installation of special radio and radar equipment for the Royal Air Force.

For his work during this period he was awarded the OBE.

Edgar Henry Kenneth Dibden (Fellow 1966, Member 1946) of Paddington, London, died on 2nd May 1982, aged 65 years. After war time service in the Royal Navy as a Radar Officer—his final appointment being Fleet Radar Officer, Home Fleet—Kenneth Dibden was for some twelve years Secretary of the Cavendish Laboratory, Cambridge. During this period he was elected to a Fellowship at Sidney Sussex College and was for a time Senior Bursar of the College. From 1960–62 he was Registrar of the Middle East Technical College, Ankara, Turkey, and on returning to the United Kingdom he became Secretary to the Appointments Board of the University of London. He subsequently became Director of the University's Careers Advisory Service and in this capacity he was Chairman of the Association of Graduate Careers Advisory Services. On his retirement in 1980, he was appointed a Director on the Board of the New Opportunity Press. In 1971 Mr Dibden was elected a Fellow of King's College from where he had graduated in physics 31 years earlier.

UDC 621.396.96.029.64+621.372.622.029.64

Indexing Terms: Radar systems, Microwave mixers

Millimetric wavelength components and coherent radar systems

M. W. BOOTON, Ph.D., B.Sc.,*

M. C. CARTER, MInstP*

and

E. G. STEVENS, C.Eng., MIERE*

SUMMARY

The construction of radar systems operating at millimetric and sub-millimetric wavelengths has necessitated the design and manufacture of a wide range of new microwave components. Manufacturing techniques have been developed for the production of components to operate in the frequency range from 30 GHz to 325 GHz using the fundamental mode in rectangular waveguide. Descriptions of some of these components and techniques are given, together with details of other higher frequency open structure and non-fundamental mode components. Planar millimetric circuitry, produced by photolithography, has been developed for use in harsh environments and the characteristics of a sub-system constructed in this manner are described. Finally, both the design and operation of two millimetric coherent radar systems are discussed and some details of their performance are given.

* *Thorn EMI Electronics Limited, Communications Division, Wookey Hole Road, Wells, Somerset, BA5 1AA*

1 Introduction

For more than two decades, millimetric and submillimetric radar systems have been made and operated by Thorn EMI Electronics at Wells in Somerset.[1,2] Many of these systems are still in regular use, observing accurately scaled models of aircraft, ships and land-based vehicles, to obtain detailed data on the scattering characteristics of all types of radar target. The scaling factors employed normally lie within the range from 0·01 to 0·3 so that, since the measurement radar wavelength must also be scaled by the same factor, it has been necessary to construct equipments to cover the frequency range from 1 GHz, throughout the millimetric waveband and beyond, to a frequency of 2500 GHz. Many of the components required to produce these millimetric and submillimetric radars are not commercially available and it has been necessary to design and manufacture them at Wells. Although produced primarily for modelling purposes, these components have also been used in full-scale systems.

Two of the more recently developed millimetric systems are described here together with some of the necessary components and fabrication techniques.

2 Components

A number of transmission media are employed in the production of r.f. components and various fabrication techniques are necessary to meet the wide range of frequencies and different environmental conditions to which the systems are subjected. For use at millimetric wavelengths, components are produced to operate in the fundamental waveguide mode or, if constraints of weight, size or vibration exist, they can be produced in planar form. For operation in the submillimetre band, devices are constructed using either the higher order, non-fundamental, modes in waveguide or quasi-optical, open structures.

2.1 Open Structure Components

Laser radar systems have been constructed, for the frequency region between 250 GHz and 2500 GHz, which use an optically pumped c.w. laser as a source of transmitter power. Pumped by a carbon dioxide laser, a suitable active organic gas is excited inside a resonant cavity and is stimulated to emit any one of hundreds of spot frequencies throughout the submillimetric spectral region. By stimulating specific transitions within the organic molecule, output powers up to 100 mW are obtained at some of these frequencies. The radar systems are produced in a homodyne configuration and employ receivers which, depending on frequency, use either liquid helium cooled photoconductive mixers, or Schottky barrier diodes mounted in corner-cube reflectors.

Prototype corner-cube mixers have been fabricated using 'in-house' manufactured diodes and Fig. 1 shows such a mixer designed to operate over a band centred at a wavelength of 900 μm. Details of the antenna region are shown in the inset. Initial measurements have shown that this device is also a sensitive detector, with a voltage responsivity of 200 V/W for r.f. power at 379 GHz. Voltage responsivities of 50 V/W and 18 V/W at

0033–7722/82/1100499+07 $1.50/0

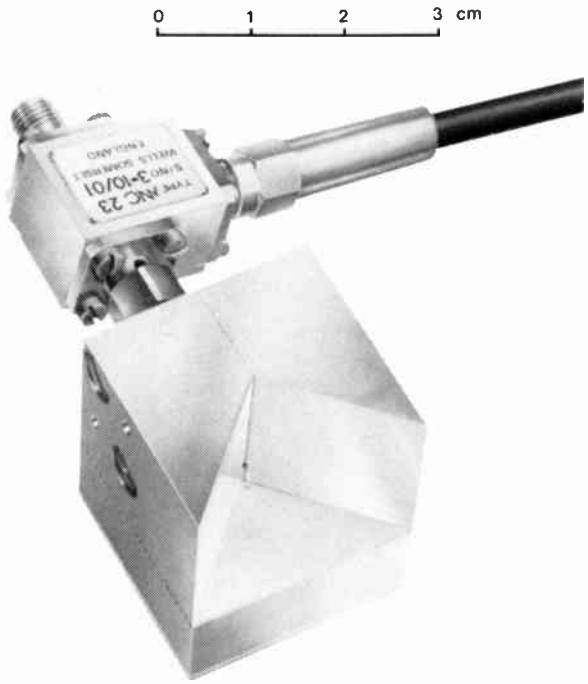

Fig. 1. Corner-cube mixer for operation at a centre band wave-length of 900 μm. Detail shows construction of antenna region.

761 GHz and 891 GHz respectively have been obtained for a similar device designed for a centre frequency of 750 GHz. Measurements of the conversion losses of these components, when they are used as mixers, are now being carried out.

The open construction of the corner-cube mixer minimizes electrical loss and also gives efficient coupling of the signal into the diode; it does, however, render the device somewhat sensitive to electrical interference.

2.2 Non-fundamental Mode Waveguide Components

For environments which preclude the use of a corner-cube mixer, an alternative, earlier design of mixer/detector is used. This consists of a Schottky barrier diode mounted in a circular waveguide. The signal is introduced via a horn fitted with a phase-correcting lens and tuning is effected by an adjustable short circuit. This unit has a very wide tuning range, from 70 GHz to more than 1000 GHz, and signals have been detected at 2500 GHz. However, the penalty of this type of construction is a reduction in sensitivity: at 891 GHz the voltage responsivity is an order of magnitude worse than that of the corner-cube detector and conversion losses are in the range from 40 to 45 dB at this frequency.

2.3 Fundamental Mode Waveguide Components

The fundamental waveguide mode is used for components at frequencies up to 325 GHz. The range of waveguide sizes in which components have been produced is typified by the series of Schottky barrier mixers whose performance is shown in Fig. 2. This MC10 series of mixers covers the frequency range from 18 GHz to 325 GHz. Single mixers, with tunable full waveguide band coverage, have been fabricated in all waveguide sizes from WG20 (WR-42) to WG32 (WR-3) inclusive, and an example of such a component is shown in Fig. 3. Balanced mixers have been constructed in waveguide sizes up to WG29 (WR-7) but the upper frequency and the bandwidth are limited, by the matched hybrid-tee section, to 170 GHz and the lower 90% of each relevant waveguide band respectively.

All these devices use 'in-house' manufactured GaAs Schottky barrier diodes mounted in a modified Sharpless[3] style of replaceable waveguide wafer. These diodes are produced with junction diameters varying from 2 μm to 6 μm depending upon the required operating frequency and have cut-off frequencies of 4500 to 2500 GHz respectively. The insert to Fig. 3 shows an SEM photograph of a 'honeycomb' array of diodes produced on a chip of epitaxial GaAs. The current I

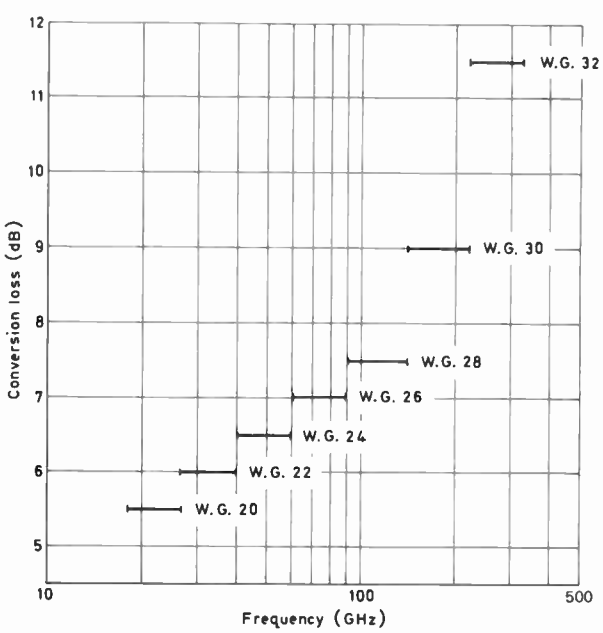

Fig. 2. Typical conversion losses of MC10 series of mixers.

resulting from a voltage V across a metal–semiconductor Schottky barrier is given by the expression:

$$I = I_0\left[\left(\exp\frac{eV}{nkT}\right)-1\right]$$

where I_0, e, k and T are the saturation current, the charge on the electron, Boltzmann's constant and the absolute temperature of the junction respectively. n is the 'ideality factor' which is equal to unity for a theoretically perfect I-V characteristic. Values of n better than 1.10 are obtained with the fabricated diodes.

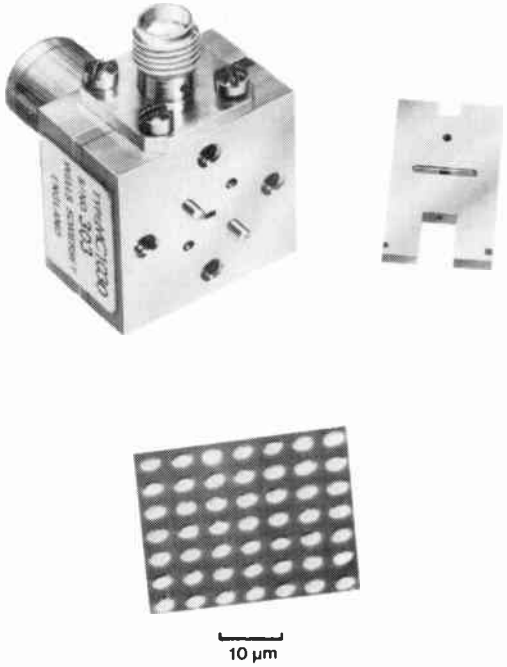

Fig. 3. A 140 to 220 GHz (WG30) single-ended mixer and replaceable Schottky barrier diode wafer. Insert shows SEM photograph of array of Schottky barrier diodes.

A typical conversion loss, obtained using 1 mW of local oscillator power, is 5·5 dB at 22 GHz rising to 11·5 dB at 280 GHz in the manner illustrated in Fig. 2. For clarity, the performance of mixers produced in even numbered waveguide sizes only are shown in the Figure. All devices are capable of operating with intermediate frequencies of several gigahertz. In general, the higher the designed r.f. operating band the higher is the i.f. capability. However, due to the limits of machining tolerances, above 170 GHz it is necessary to use an r.f. band-stop rejection filter in the i.f. output in place of the π-network low-pass filter used in the lower frequency units. Consequently the WG30 and WG32 mixers have a maximum i.f. of 6 GHz, while a maximum i.f. capability of 14 GHz is realized with the WG28 mixer.

In order to construct a radar system to be used for modelling at 280 GHz, it has been necessary to produce a complete range of passive components, including couplers, aerials, filters, attenuators, rotary and guillotine phase shifters and frequency meters.

As mentioned above, the highest frequency at which fundamental mode waveguide components have been employed is 325 GHz using WG32; this waveguide size

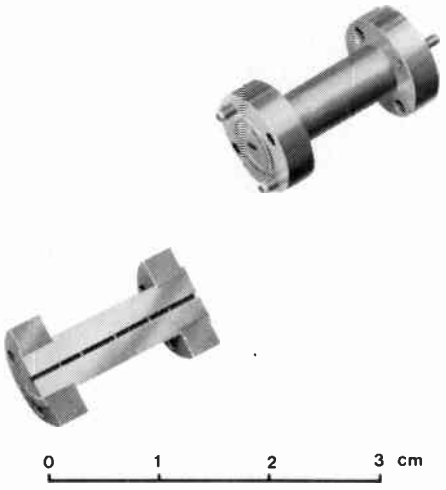

Fig. 4. 280 GHz waveguide bandpass filter. A section through the filter shows the electroformed pins within the WG32 structure.

has internal dimensions of 0·864 × 0·432 mm for which tolerances of 1% must be maintained. To achieve these tolerances, the components can not be made using conventional machining techniques. The method of manufacture chosen is copper electroforming on aluminium mandrels which have been machined and polished into the required male shape.

The mandrel is chemically treated and then the electroforming is carried out in an acid copper bath to a thickness of 1·5 mm. After the outside of the electroform has been machined and flanges have been attached, the aluminium mandrel is selectively etched away from the copper in a caustic solution, leaving the waveguide component. Using this technique, broadband, 3, 10 and 20 dB couplers have been made, with a directivity in each case greater than 30 dB, and rotary vane attenuators have been made and calibrated to 50 dB with an accuracy of ±1 dB at maximum attenuation.

One example of the electroforming technique is the 280 GHz band-pass Chebychev filter which has been produced in WG32 and is shown in Fig. 4. A similar device, also shown in Fig. 4, has been sectioned to reveal the electroformed pins spaced along the length of the waveguide. The filters have five pins which range in diameter between 0·1 mm and 0·2 mm. The frequency

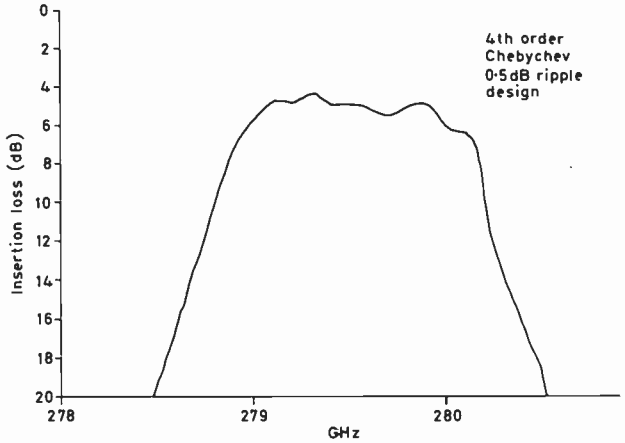

Fig. 5. Response of a 280 GHz waveguide bandpass filter. (WG 32)

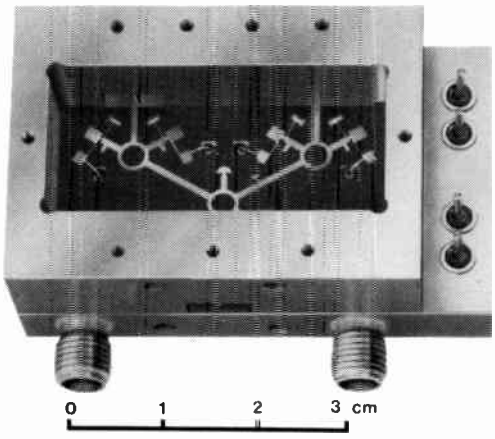

Fig. 6. A 35 GHz receiver module employing microstrip fabrication techniques.

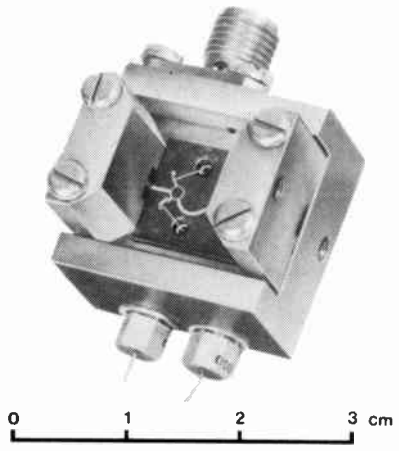

Fig. 7. O-band (E-band) microstrip balanced mixer in test jig.

response of such a waveguide filter is shown in Fig. 5, and the filter is seen to possess a 279·5 GHz $\pm$ 0·5 GHz pass-band. The insertion loss is approximately 5 dB with a ripple of 1 dB and the rejection, 3·5 GHz away from the band centre, is greater than 50 dB.

2.4 Planar Components

The construction of components for radio modelling purposes facilitates the production of other millimetric systems. However, for an assembly that is required to be lightweight and rugged, alternative fabrication methods are necessary and planar circuitry suitable for millimetric wavelengths has therefore been developed. Both microstripline and fin-line circuits are employed; they have the attributes of ease of component integration and are produced using photolithographic techniques. The use of planar components leads to miniaturization of the overall system and to low-cost mass production. Integrated millimetric circuits are produced on substrates of low permittivity, PTFE being favoured for most applications. The pliable nature of such a material allows systems and sub-systems to be designed to withstand harsh vibration environments and also enables good yields to be obtained during component assembly.

An example of such a construction is a Q-band (Ka-band) receiver module, as shown in Fig. 6. Two balanced mixers and a 3 dB power splitter with centre frequencies of 35 GHz have been produced in microstrip and they are excited via ridged waveguide-to-microstrip transformers contained within the walls of the receiver case. Using GaAs mixer diodes in a beam lead

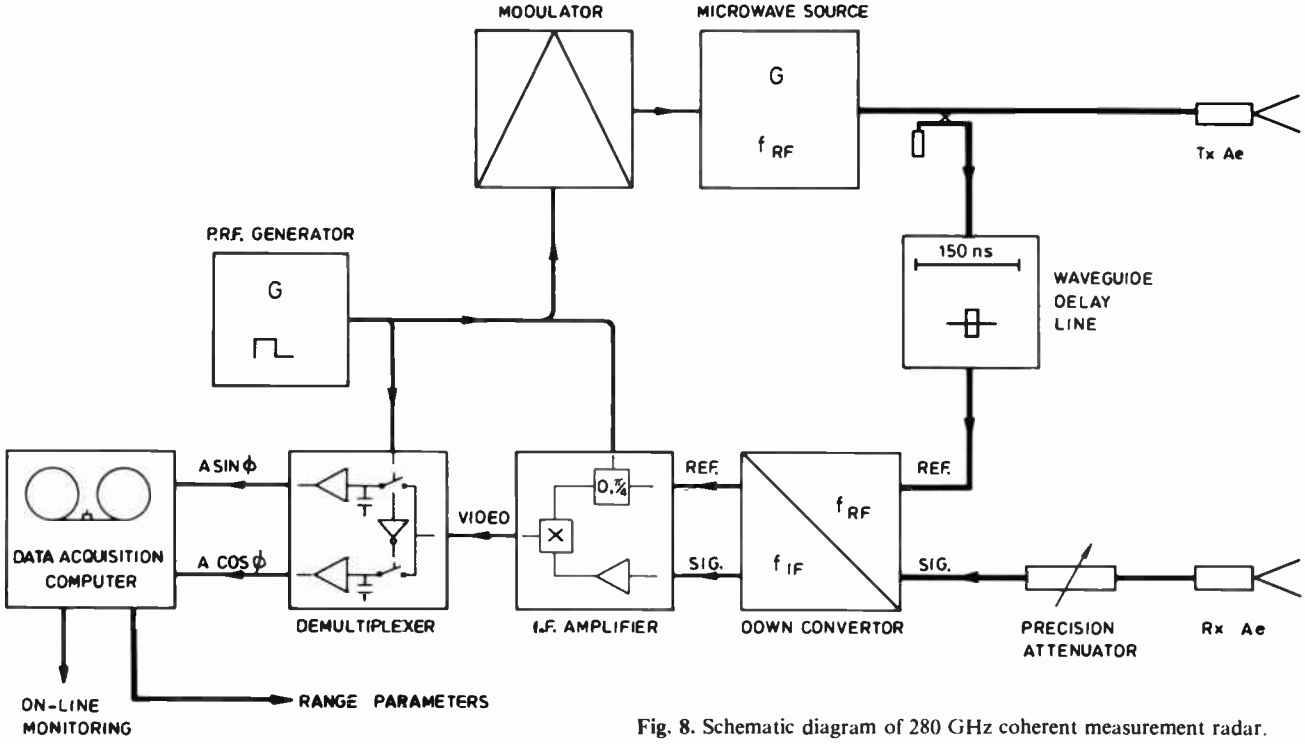

Fig. 8. Schematic diagram of 280 GHz coherent measurement radar.

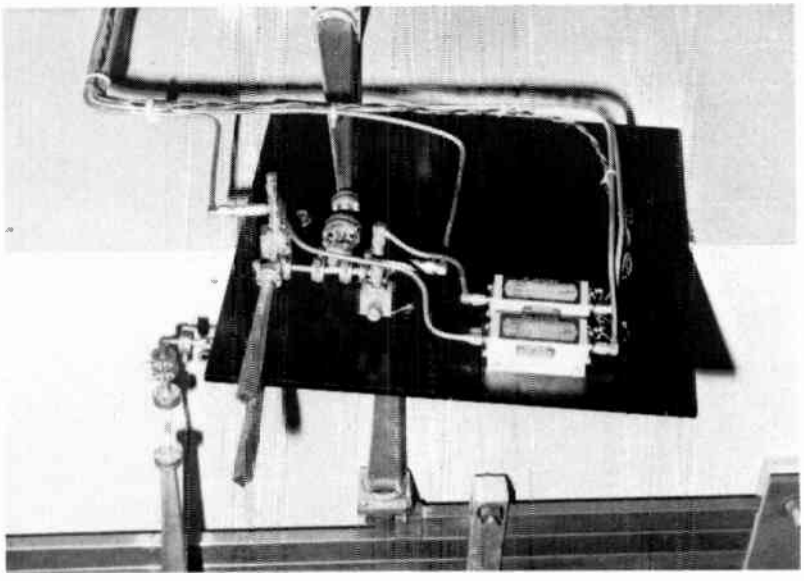

Fig. 9. Microwave circuit of 280 GHz coherent measurement radar.

configuration, typical conversion losses of 7 dB are obtained at room temperature and these increase by approximately 0·5 dB at 100°C.

Microstripline circuits produced on a substrate material with a permittivity as low as that of PTFE can be expected to be susceptible to r.f. coupling between the various integrated components. A suitable arrangement of the circuit elements, however, ensures a good performance as is borne out by the measured r.f. port-to-port isolation of the module shown in Fig. 6. This isolation is typically better than 25 dB. A further indication of the isolation between circuit elements is given by the r.f. to i.f. breakthrough between the two mixer channels. Measured as the ratio of the two i.f. outputs resulting from a single r.f. input, cross-talk figures of −20 dB are obtained.

Development of this form of circuit fabrication for operation at frequencies up to 100 GHz is demonstrated by the microstripline balanced mixer shown in Fig. 7, which has a conversion loss in O-band (E-band) of typically 9 dB. The penalty incurred with planar circuitry is seen to be an increase in mixer conversion loss which, at Q-band and O-band respectively, is approximately 1 and 2 dB worse than that shown in Fig. 2. However, the rugged nature and low cost of this type of assembly makes possible a greater range of system applications.

3 Millimetric Wavelength Systems

Using both fundamental and non-fundamental mode waveguide components, a microwave system has been built for a 280 GHz radar.[2] Illustrated in Fig. 8 and 9, this is a pulsed coherent system using a heterodyne receiver.

The transmitter and the local oscillator in the downconverter are both carcinotrons and the transmitter produces a 50 ns pulse with a peak power of about 1 W. A 10 dB coupler is used to direct a sample of the transmitter signal through an oversize-waveguide delay line to form a reference signal. The remainder of the power is fed to the aerial.

The signal returned from the target and the delayed reference signal are mixed with the local oscillator in the

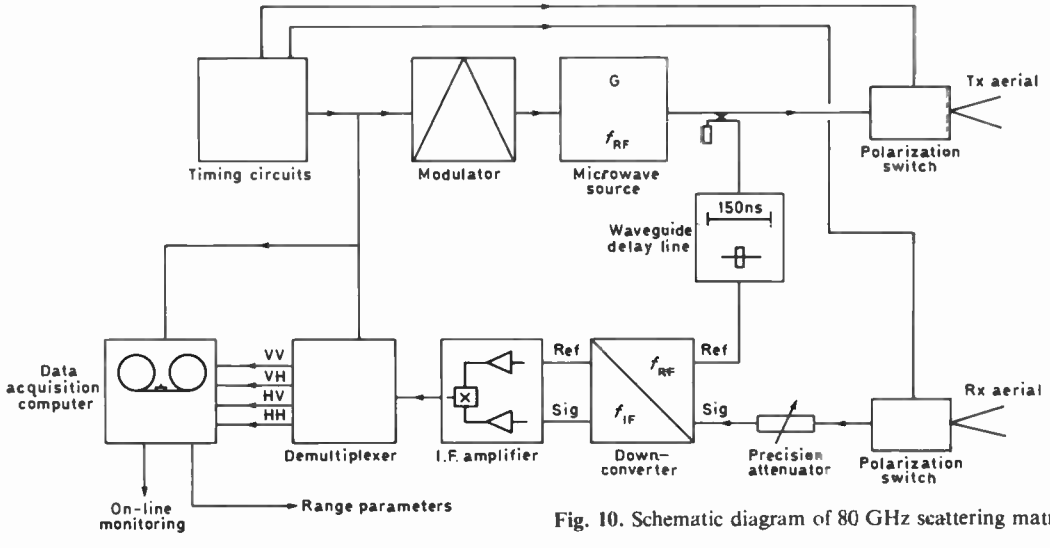

Fig. 10. Schematic diagram of 80 GHz scattering matrix radar.

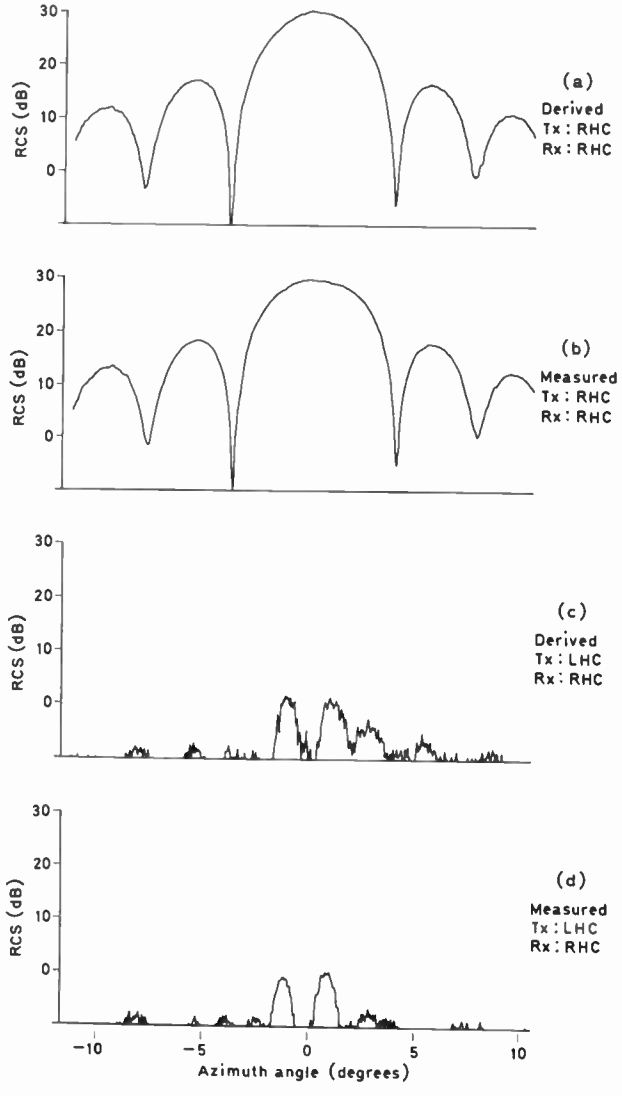

Fig. 11. Comparison of derived and measured radar cross-section of a dihedral reflector for circularly polarized radiation. (a) Derived from scattering matrix radar data: Tx, right hand circular (RHC); Rx, RHC. (b) Measured with circularly polarized radar: Tx, RHC; Rx, RHC. (c) Derived: Tx, left hand circular (LHC); Rx, RHC. (d) Measured: Tx, LHC; Rx, RHC.

downconverter. The two i.f. signals are amplified by means of the parametric amplifier, filtered and mixed together in order to obtain signals, dependent on the amplitude A and phase ϕ of the received signal, in the form $A \sin \phi$ and $A \cos \phi$. The two signals are fed to an on-line computer from which plots are obtained of target amplitude and target phase.

The latest millimetric systems to be built for radar scale modelling are the scattering matrix radars.[4,5] A 4 mm wavelength (80 GHz) scattering matrix radar has been in operation for about a year, and a 2 mm wavelength (140 GHz) version will be in operation shortly. A schematic diagram of the 80 GHz system is given in Fig. 10 and, as with the 280 GHz radar described above, this has been built as a pulsed coherent radar to produce target amplitude and phase information. However, the system is also fitted with polarization switches so that after each transmitter pulse, the polarization of the receiver aerial is rotated through 90 deg, while the transmitter aerial polarization is similarly rotated after every second pulse. Thus, four combinations of the linearly polarized transmitted and received electric vectors, E, are obtained as follows:

Tx Aerial	Rx Aerial
E Vertical	E Vertical
E Vertical	E Horizontal
E Horizontal	E Vertical
E Horizontal	E Horizontal

The radar provides sufficient phase and amplitude information to enable the full target scattering matrix to be calculated by the on-line computer, which gives the eight different polarization reflection coefficients from the target including those of right-hand circular polarization (RHC) and left-hand circular polarization (LHC):

Tx Aerial	Rx Aerial
E Vertical	E Vertical
E Vertical	E Horizontal
E Horizontal	E Vertical
E Horizontal	E Horizontal
RHC	RHC
RHC	LHC
LHC	LHC
LHC	RHC

In Fig. 11 recordings are reproduced of information obtained using a dihedral reflector as a target which has two reflecting surfaces and hence produces two reversals in the sense of rotation of circularly polarized incident and reflected radiation. Figure 11(a) shows the calculated radar cross-section based on data obtained from the linearly polarized scattering matrix radar and Fig. 11(b) gives the corresponding information obtained when measurements were made directly, using circularly polarized radiation from a conventional radar. Comparison of the recordings of Figs. 11(a) and 11(b) shows a close similarity for those conditions where the receiving antenna is polarized to accept the circularly polarized radiation (i.e. recordings for Tx: RHC, Rx: RHC). The results correspond to within a fraction of a decibel with respect to azimuth angle. Figures 11(c) and 11(d) relate to the condition in which the circularly polarized radiation is rejected by the receiving antenna; both signals are 30 dB lower than those obtained with the accepted polarization. It may be seen, therefore, that the scattering matrix radar system can adequately synthesize the circular polarization information after analysis of the linearly polarized radar returns in both amplitude and phase.

4 Conclusions

The mechanical tolerances necessary to construct components for use at millimetric wavelengths have required specialized construction techniques to be

developed. Copper electroforming onto an aluminium mandrel, followed by selective etching away of the mandrel, has proved to be a successful fabrication process for waveguide components. Components can be manufactured in this manner for use in the fundamental waveguide mode at frequencies up to 325 GHz.

An 80 GHz scattering matrix radar using linear polarization has been demonstrated to have a performance which permits the reproduction, to within a fraction of a decibel, of results that would otherwise require a more complicated circularly polarized radar system.

A wider application of millimetric components is made possible by producing lightweight, rugged devices and development has been undertaken to produce planar components and integrated sub-systems using photolithographic processes. Using PTFE-based substrate materials, good yields are obtained during production so that low-cost millimetric systems are now feasible. The technology has been demonstrated to be applicable to frequencies up to 100 GHz and has been found to have a performance that, although inferior to that of technology employing rectangular waveguide, is adequate for many applications.

Open structure and oversized waveguide components also are required in order to extend the operational frequency range beyond 325 GHz. They are required for radar systems which are being operated in the sub-millimetric wavelength band for radio modelling purposes. A single mixer can be produced in non-fundamental mode waveguide to cover the complete range from 70 GHz to 1000 GHz. Although radiation has been detected at 2500 GHz using this device, work has continued to achieve an improvement in the performance of mixers at these higher frequencies by developing the open structure corner-cube mixer. Evaluation of these mixers is continuing.

5 Acknowledgments

This work has been carried out with the support of MOD(PE), DCVD and Thorn EMI Electronics Ltd. The authors wish to thank their Directors for permission to publish this work. Gratitude is also expressed to their colleagues, Mr B. Milner and Mr R. J. Henderson, for the fabrication of the mixers and mixer diodes.

6 References

1 Cram, L. A. and Woolcock, S. C., 'Review of two decades of experience between 30 GHz and 900 GHz in the development of model radar systems', AGARD Conference Proceedings No. 245, September 1978.

2 Brown, E. G., Plaster, M. W. and Woolcock, S. C., 'Millimetre wave measurement radars for 140 GHz and 280 GHz', Conference Proceedings Military Microwaves '80, London, October 1980, p. 60.

3 Sharpless, W. M., 'Wafer type millimetre wave rectifier', *Bell Syst. Tech. J.*, **35**, pp. 1385–1402, November 1956.

4 Bird, D., Plaster, M. W. and Wilson, C. G. C., 'Measurement of the depolarization of radar scattering using scale modelling techniques', Conference Proceedings Military Microwaves '82, London, October 1982, p. 429.

5 Huynen, J. R., 'Measurement of the target scattering matrix', *Proc. IEEE*, **53**, August, p. 936, 1965.

Manuscript received by the Institution on 26th August 1982.
(Paper No. 2052/AMMS 112)

UDC 621.372/3/6.029.65

Indexing Terms: Millimetre wave techniques, Waveguides, Waveguide components, Couplers, Isolators, Oscillators, Gunn, Radiometers, Radar systems.

Millimetre-wave E-plane components and subsystems

R. N. BATES, B.Sc., Ph.D., C.Eng., MIEE*

S. J. NIGHTINGALE, Dip. E.E., Ph.D., MIEEE, C.Eng., MIEEt

and

P. M. BALLARD, B.Sc.*

Based on a paper presented at the IERE Colloquium on Waveguides and Components for the 80–300 GHz Frequency Range in London in April 1981

SUMMARY

This paper describes a variety of E-plane transmission lines which have been shown to be suitable for realizing microwave circuits for frequencies up to at least 140 GHz. A wide range of components has been developed using E-plane circuit techniques and some of these have been integrated together to form complete r.f. subsystems. Several examples of both components and subsystems are described.

* *Philips Research Laboratories, Redhill, Surrey, RH1 5HA.*
† *Formerly with Philips Research Laboratories; now with General Electric Company, Electronics Park, EP3-207, Syracuse, New York 13221.*

1 Introduction

In recent years the increased interest in the frequency spectrum above 30 GHz has led to a requirement for high performance millimetre-wave components and subsystems. E-plane circuit techniques have been found to be suitable for realizing millimetric components for frequencies up to at least 140 GHz.[1,2] The circuit patterns are defined on the substrate using standard photolithographic techniques and potentially the mass-production cost is low. The waveguide housing may be machined from solid aluminium or made from metallized moulded plastic. This paper describes a variety of components made using E-plane circuits together with examples of how they have been integrated into subsystems.

2 The E-plane Circuit

The E-plane circuit consists of a thin, low permittivity substrate which is mounted between the broad walls of a rectangular waveguide in the plane of the E-field. The conductor pattern, which forms the various transmission lines and circuit elements, is defined on one or both sides of the substrate and processed using standard photolithographic techniques. The substrate used is a PTFE material reinforced with randomly orientated glass microfibres and metallized with copper. This material has a dielectric constant of 2·22. A variety of different types of transmission line can be realized and some of these are shown in Fig. 1. These transmission lines fall broadly into two classes: (a) the quasi-TEM lines such as microstrip, coplanar line and suspended stripline, (b) the non-TEM lines which support a hybrid mode such as the various forms of finline. Finline can be considered as a modified form of double-ridged waveguide where the ridges are very thin and are supported by the dielectric substrate. Four different types of finline (unilateral, bilateral, isolated and antipodal) are shown in Fig. 1.

Unilateral and isolated finline are metallized on one side of the dielectric and are identical except for the presence of an insulating gasket. This allows a d.c. voltage to be developed across the fins and enables bias to be applied to active components such as Schottky and

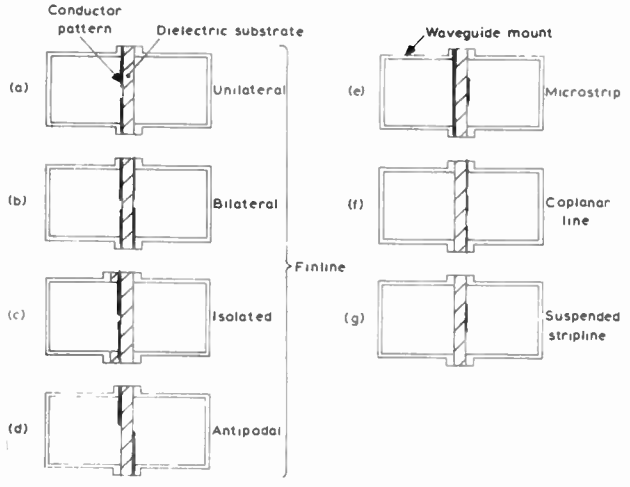

Fig. 1. E-plane transmission lines

0033–7722/82/11506+07 $1.50/0

Table 1 Typical characteristics of unilateral finline

Frequency (GHz)	Waveguide Number	Waveguide Size (mm)	Slot Width (mm)	Characteristic Impedance (Z_o)	Normalized Wavelength (λ_g/λ_o)	Loss (dB/λ)
33·5	22	7·11 × 3·56	0·1–3·0	100–480	0·91–1·22	0·08–0·019
75·0	26	3·10 × 1·55	0·1–1·5	130–490	0·89–1·20	0·12–0·024
115·0	28	2·03 × 1·02	0·1–0·8	170–470	0·90–1·13	0·15–0·06

p-i-n diodes. Bilateral finline is similar to the unilateral form, but has metallization on both sides of the dielectric and can, in general, support two propagating modes. Antipodal finline is also metallized on both sides of the dielectric; however, unlike unilateral finline, it is possible to overlap the fins which enables very low impedances to be realized. In isolated finline r.f. continuity between the conductors and the waveguide wall is obtained by making the thickness of the broadwalls of the rectangular waveguide about a quarter wavelength long at the waveguide centre frequency when loaded with the dielectric material. This form of choke section has been found to prevent propagation out of the guide over at least the waveguide bandwidth. Typical parameters for unilateral finline are given in Table 1 for the centre frequencies of the operating bands for WG22 (27–40 GHz), WG26 (60–90 GHz) and WG28 (90–140 GHz).

The parameters given in Table 1 were calculated using the general analysis of Davies and Mirshekar-Syahkal[3,4] and the values for normalized wavelength and line losses have been confirmed by measurements made in our laboratory. Microstrip loss on the same material has been found to be 2·5 to 3 times that of unilateral finline giving 0·25 dB/wavelength at 33·5 GHz and 0·30 dB/wavelength at 75 GHz. In view of the lower loss, finline is used for parts of circuits where low loss is important, such as the signal input of mixers, etc.

A wide variety of components have been developed at our laboratories using E-plane circuit techniques. These components include balanced mixers, Doppler mixers, p-i-n switches, directional couplers and detectors. A number of these components have been described in recent publications[1,2,5–9].

3 E-plane Components

3.1 Mixers

Balanced mixers have been made for the frequency ranges 27–40 GHz, 60–90 GHz and 75–110 GHz, using E-plane circuits. Each circuit uses a combination of four different types of transmission line shown in Fig. 1. The 180° hybrid junction is realized using finline and coplanar line.[5] The signal is coupled to the mixer diodes via a waveguide to finline transition and the local oscillator via a waveguide to microstrip transition in conjunction with a microstrip-to-coplanar line transition. A microstrip low-pass filter is used on the local oscillator side to extract the i.f. When it is desired to optimize the mixer noise figure at a given frequency, a finline matching transformer is used to match the signal impedance of the mixer diodes to the input port of the mixer. The mixer diodes used are planar GaAs Mott diodes made using molecular beam epitaxial material. These diodes have been specially developed within our laboratories[6,7] to be compatible with finline circuits and the device parameters are optimized for the different frequency ranges. Single sideband noise figures of 6 dB at 35 GHz and 7·5 dB at 85 GHz (including a 1 dB i.f. contribution) have been achieved.

The external appearance of an E-band (60–90 GHz) mixer is shown in Fig. 2. Three similar units are shown in Fig. 3, one of which has had the cover removed to reveal the constant current bias circuit while another has been opened to reveal the E-plane circuit mounted in the waveguide cavity.

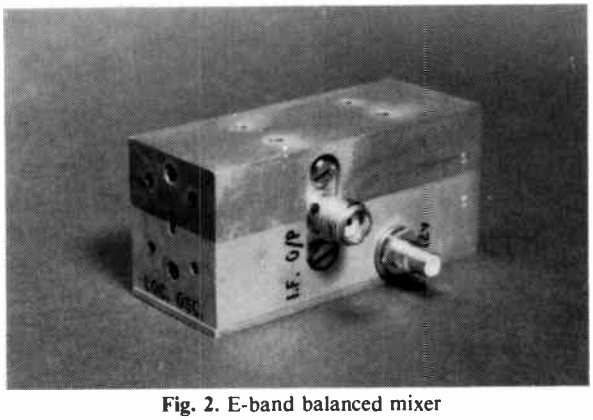

Fig. 2. E-band balanced mixer

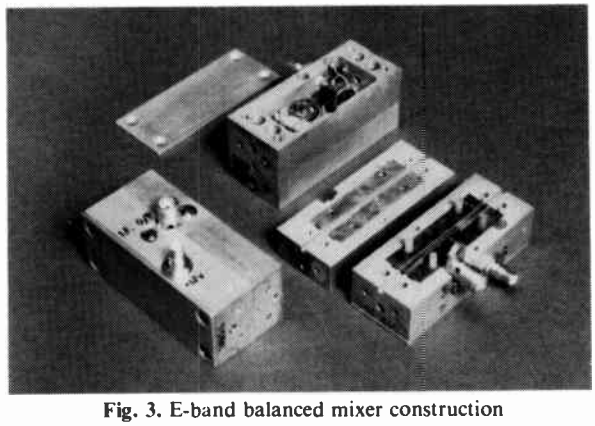

Fig. 3. E-band balanced mixer construction

Figure 4 shows the measured conversion loss and noise figure as a function of frequency from 80 to 90 GHz. It can be seen from this graph that over the frequency range 82 to 87 GHz the conversion loss is less than 6·5 dB. The performance degrades above 87 GHz due to the finite bandwidth of the matching transformer. However, the transformer centre frequency can be

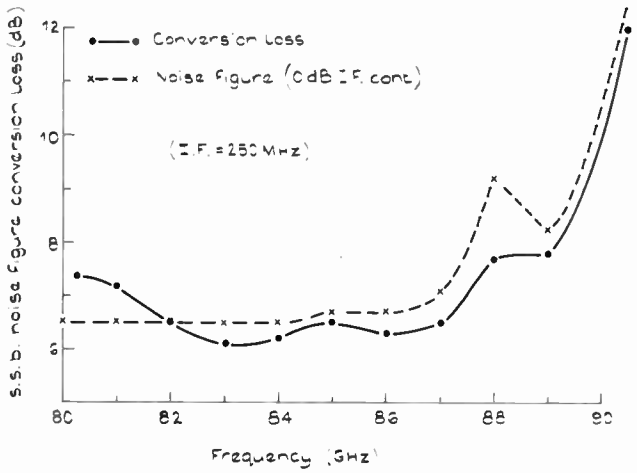

Fig. 4. E-band mixer conversion loss and noise figure versus frequency

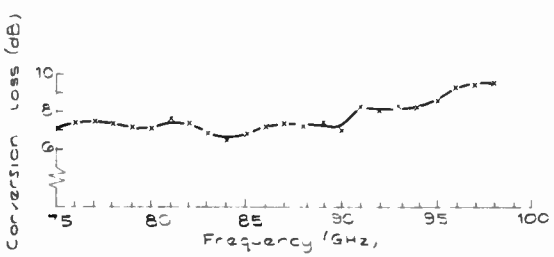

Fig. 5. W-band mixer conversion loss versus frequency

located anywhere in the band as required. The noise figure of the mixer was measured using a gas discharge tube.

If an input matching transformer is not employed then the mixer can be operated over a wider frequency range with slightly degraded conversion loss. Figure 5 shows the conversion loss performance of a W-band (75–110 GHz) mixer with an i.f. of 250 MHz.

3.2 Detectors

A range of detectors has been made for use up to 140 GHz. These detectors use silicon zero-bias Schottky-barrier detector diodes mounted on a finline circuit incorporating a broadband E-plane matched load. Figure 6 shows an E-band detector which has a typical sensitivity of 100 mV/mW at 90 GHz.

3.3 p-i-n Switches and Attenuators

Single-pole double-throw E-plane p-i-n switches have been designed for the frequency bands 30–40 GHz and 80–90 GHz. These components were developed for use in Dicke radiometers and the isolation in both bands is at least 20 dB. The insertion losses are typically 1·5 dB and 2·5 dB for the two bands respectively, but lower losses have also been achieved. A s.p.d.t. switch with an isolation of 50 dB has also been developed for the lower frequency band. Figure 7 shows an 89 GHz p-i-n switch with one half of the waveguide removed to reveal the substrate and insulating gaskets. This switch had an insertion loss of 2·0 dB. The p-i-n diodes used are beam lead devices and are mounted on the circuit using conducting epoxy cement.

Attenuators using p-i-n diodes have been designed for frequencies up to 100 GHz. These components, which may also be used as s.p.s.t. switches, have isolations of 20 dB with typical insertion losses of 0·6 dB at 35 GHz and less than 3 dB at 100 GHz.

3.4 Doppler Mixers

A Doppler mixer has been made for use at 35 GHz. The design is based on two single-ended mixers made on opposite sides of the same substrate using bilateral finline. The circuits are made so that there is $\lambda/8$ spacing between the two mixer diodes. By using this technique the Doppler i.f. outputs from the two diodes are in phase quadrature and can be used to obtain direction sense information.

3.5 Directional Couplers

A range of branch-guide couplers have been developed which are compatible with E-plane circuits. Figure 8 shows a Ka-band 3 dB coupler opened to reveal the construction. This unit operates from 27 to 36 GHz with a directivity of better than 30 dB and a return loss of better than 30 dB. Similar couplers with couplings from 3 to 10 dB have been made at E-band (60–90 GHz) and W-band (75–110 GHz). Each coupler operates over approximately 70% of the appropriate waveguide band with better than $\mp$ 1 dB coupling variation and a typical isolation of 25 dB.

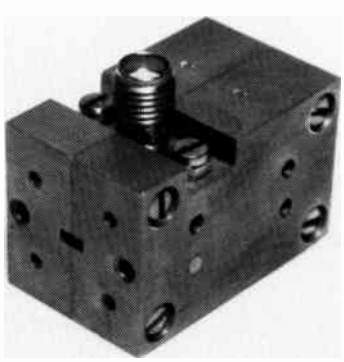

Fig. 6. E-band detector

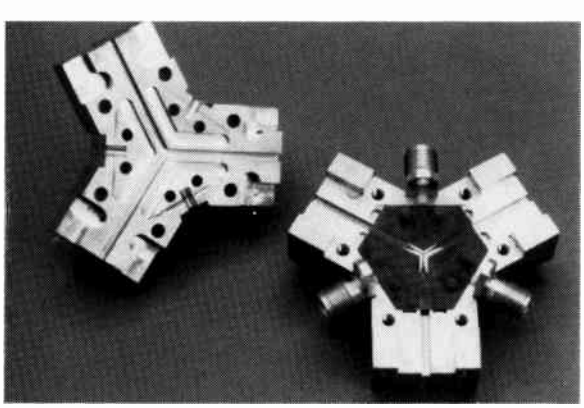

Fig. 7. 89 GHz p-i-n switch with one half of the waveguide removed

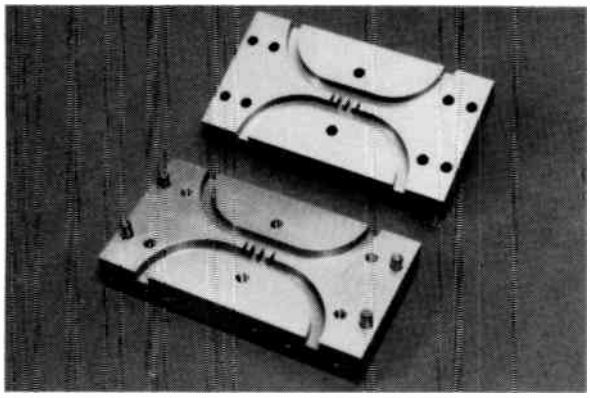

Fig. 8. Ka-band branch-guide 3 dB coupler

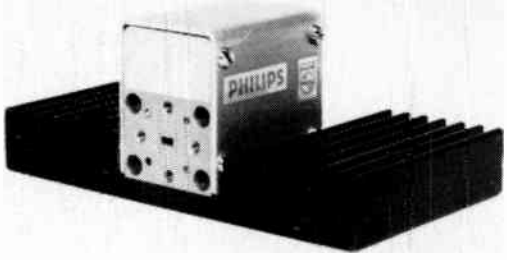

Fig. 9. 90 GHz Gunn oscillator

Table 2 Millimetre-wave oscillator data

Frequency range	70–95 GHz depending on diode and cap diameter used
Output power	5–15 mW depending on diode used
D.c. to r.f. efficiency	0·1–1% depending on diode used
External Q factor	1000–2000
F.m. noise	Typically −105 dBc/Hz at 1 MHz offset from carrier
Electronic tuning	200–300 MHz
df/dT	−3·4 MHz/deg C at 91 GHz

4 Transferred Electron Oscillators

The balanced mixers described above operate with minimum noise figure when operated at local oscillator levels of typically 5 to 10 mW. It has been shown that GaAs Gunn diodes can produce this order of power in the frequency range 60 to 100 GHz at the second harmonic. Therefore, for many applications, conventional Gunn diodes designed for use in the range 30 to 45 GHz are suitable. Oscillators are not generally made using E-plane circuitry since the Q is not high enough using this medium. However, conventional waveguide is compatible with E-plane components and therefore oscillators made in waveguide can be readily integrated with the components already described.

The circuit used for the millimetre wave oscillators is the resonant cap design[10-12] and the performance obtained is detailed in Table 2.

Figure 9 shows the appearance of a typical 90 GHz oscillator. This unit includes the heat sink and r.f.i. filter on the d.c. bias connection.

5 Subsystems

The components described in the previous Sections have been used to make a range of subsystems including radars and radiometers.[13-17] Examples of some of these are described below.

5.1 An E-plane Image Rejection Mixer

An image rejection mixer operating at 35 GHz has been assembled. The arrangement comprises two balanced mixers and two 3-dB branch-guide couplers together with an i.f. quadrature hybrid. The mixers are fed via the couplers so that the local oscillator and signal ports receive in-phase and quadrature signals respectively. The relative phase can be adjusted by adding waveguide shims on the coupler ports. The two mixers provide i.f. signals which are in phase quadrature and are combined in the i.f. hybrid to provide an i.f. signal at one of the output ports which is dependent on whether the input signal is above or below the local oscillator signal. Selection of one output enables the arrangement to be used as a single sideband or image rejection mixer.

A photograph of the complete image rejection mixer is shown in Fig. 10. At an i.f. of 30 MHz an image rejection of more than 20 dB at 35 GHz was obtained.

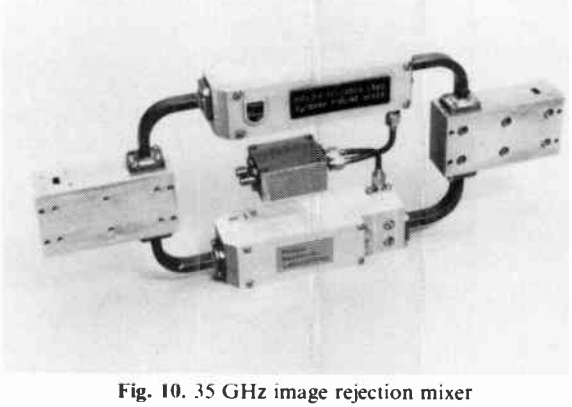

Fig. 10. 35 GHz image rejection mixer

5.2 Radiometers

Radiometers have been constructed for operation in Ka (27–40 GHz) and E (60–90 GHz) band.[13,14] Two radiometers, which were designed for operation centred at 35 GHz and 89 GHz, are shown in Fig. 11. Both units are similar in general construction, and Fig. 12 shows the two halves of the 35 GHz unit opened to reveal the E-plane circuits.

On the left-hand side of the mount is the p-i-n switch with an integrated reference load. This is followed by an isolator and then the balanced mixer. On the right-hand side of the figure the Gunn oscillator can be seen, which

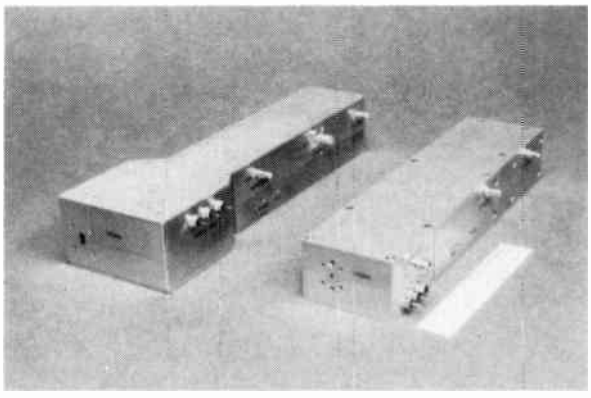

Fig. 11. 35 GHz and 89 GHz Dicke radiometers

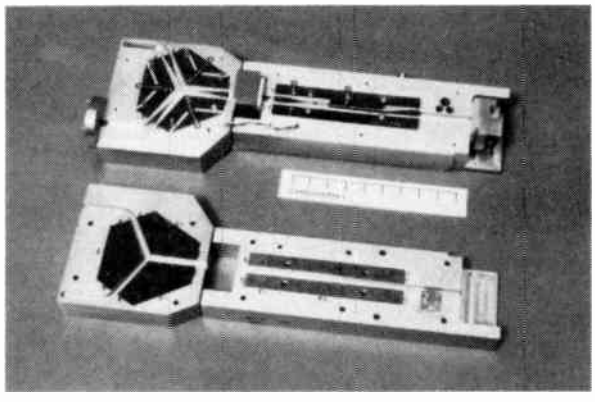

Fig. 12. 35 GHz integrated radiometer head (Opened to reveal the p-i-n switch, isolator, mixer and Gunn oscillator)

is followed by a variable card attenuator built into the waveguide mount in order to adjust the local oscillator power for minimum noise figure and to give some isolation between the mixer and the Gunn oscillator. Machined compartments in one half of the mount contain the low-noise, high-gain, wideband amplifiers, the mixer bias circuit and the BITE (built-in test equipment) circuit. The BITE circuit provides a visual indication, via two l.e.d.s, that the d.c. bias to the diodes is correct and the diodes are in order and that the Gunn oscillator is operating and producing the correct power level for the mixer. This radiometer has an overall noise figure of 7·5 dB which breaks down into 1·5, 0·5, 2 and 3·5 dB from the p-i-n switch, isolator, mixer and i.f. amplifier, respectively. The minimum resolvable temperature difference of the radiometer is 0·1 K when operated as a Dicke receiver with square wave switching (i.f. bandwidth = 1 GHz, post-detection integration time normalized to 1 second). The mixer uses coplanar GaAs Schottky barrier diodes which have been specially developed within our laboratories to be compatible with finline circuits.

Both radiometers have been incorporated into an imaging system as shown in Fig. 13. This system comprises a computer-controlled pan and tilt head in order to perform a raster scan of the field of view. The system is currently being used to gather target signature information from different scenes of interest.

A W-band 4-channel amplitude comparison radiometer for target tracking has also been constructed.[15–17] This receiver was developed within the constraints of small size and being low cost in mass production. The system comprises a 4-beam antenna with squinted beams and separate waveguide feeds for each beam. Associated with each feed is a mixer, of the type shown in Figs. 2 and 3, and with each pair of feeds a sampling switch, i.f. amplifier with detector and subsequent signal processing. The sampling is performed at i.f. where it is possible to realize lower insertion losses than with r.f. switching. A signal injection technique[18] is used to zero the system and compensate for any drift in the mixers as well as to allow testing of the complete system. The complete radiometer system, including signal processing, is shown in Fig. 14, together with the mounting tube. The system has been tested in the laboratory using scaled targets and has also undergone preliminary trials in a typical cluttered environment.

5.3 Doppler Radar

Some of the E-plane components described above have been incorporated into a 35 GHz Doppler radar module, shown in Figs. 15 and 16. The radar consists of two printed planar antennas with E-plane transitions. Each antenna has a 3 dB beamwidth of approximately 5° in each of the principal planes. The receive antenna is connected to a Doppler mixer with direction sense of the type previously described. The transmitter source is a Gunn oscillator using two diodes in a power combining

Fig. 13. Ka and W band radiometer imaging system

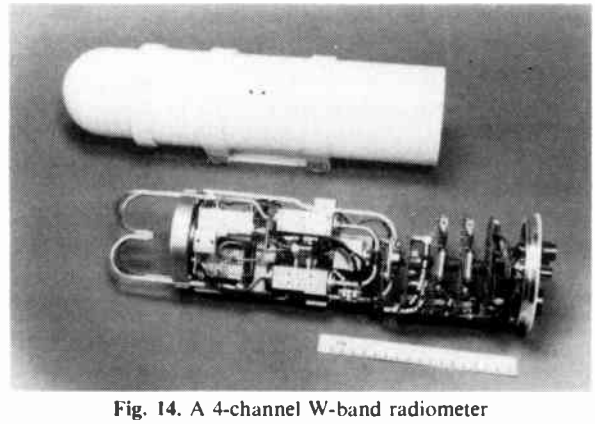

Fig. 14. A 4-channel W-band radiometer

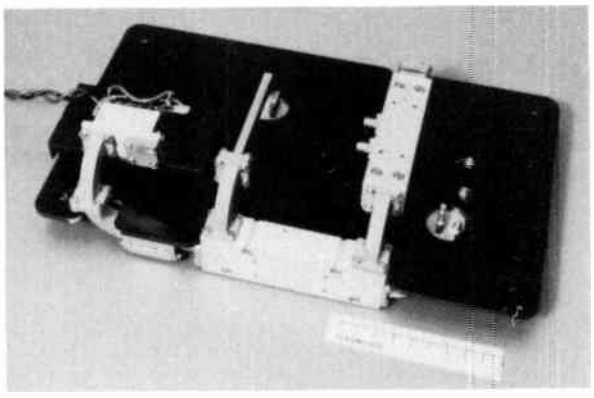

Fig. 15. 35 GHz Doppler radar (View of Gunn oscillator, Doppler mixer and coupler)

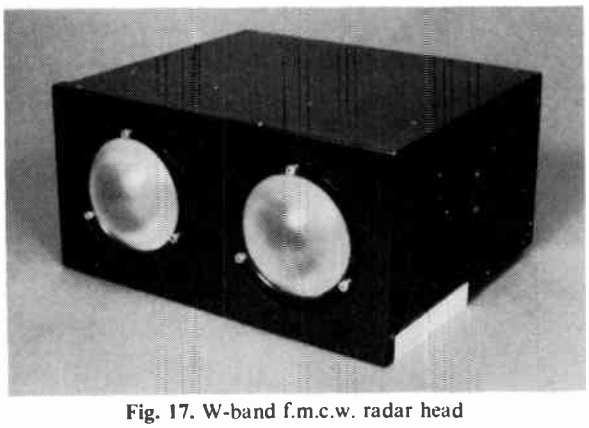

Fig. 17. W-band f.m.c.w. radar head

circuit which yields an output power of 230 mW with d.c. to r.f. efficiency of 2·7%. This oscillator is connected to the transmit antenna via an E-plane printed probe coupler.[8] The coupler has an insertion loss of 0·3 dB at 35 GHz with an associated coupling and directivity of 17 dB and 22 dB respectively. The coupled port is connected to the local oscillator port of the Doppler mixer and the isolated port is terminated in a matched load. The E-plane components in this unit could be readily integrated onto one substrate to form a compact low-cost system.

5.4 Solid State Radar

Short range f.m.c.w. radars have been investigated at Philips Research Laboratories[19] and an experimental W-band solid state radar head has also been developed using E-plane components and lens antennas.[20] The antennas have a 3 dB beamwidth of 2·7° and the complete r.f. head is shown in Fig. 17. This example further illustrates the potential compactness of a millimetric radar.

6 Conclusions

A wide range of components using E-plane circuit techniques has been described and it has been shown that the E-plane circuit approach enables high-performance, low-cost, lightweight components to be realized. A number of these components have been integrated or combined to form complete subsystems. It is believed that this technology will be widely employed in future millimetre-wave components and subsystems.

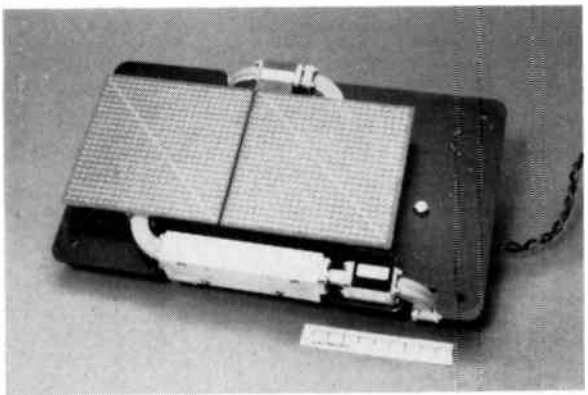

Fig. 16. 35 GHz Doppler radar (View of printed planar transmit and receive antennas and coupler)

7 Acknowledgments

Portions of the work described in this paper have been carried out with the support of the Procurement Executive, Ministry of Defence.

The authors also wish to acknowledge the following contributions from their colleagues at Philips Research Laboratories: Mr M. D. Coleman, for his technical assistance; Mr B. J. Hoad, for the manufacture of the E-plane circuits; Mr R. S. Watts, who mounted the devices and circuits; Mr G. Payne, who developed the signal processing for the radiometric tracker, and Mr R. Slater, our engineering designer.

The radiometric imager was built on a joint project between Philips Research Laboratories and Philips Elektronikindustrier AB, Järfälla, Sweden.

8 References

1 Nightingale, S. J., Bates, R. N. and Coleman, M. D., 'E-plane circuits and components for frequencies up to 140 GHz,' IERE Colloquium on Waveguides and Components for the 80–300 GHz Frequency Range, London, 23rd April 1981.

2 Bates, R. N. and Coleman, M. D., 'Millimetre wave E-plane mics for use up to 100 GHz', Proceedings of 2nd Military Microwaves Conference, MM '80, pp. 88–94, October 1980.

3 Davies, J. B. and Mirshekar-Syahkal, D., 'Spectral domain solution of arbitrary coplanar transmission line with multilayer substrate', *IEEE Trans. on Microwave Theory and Techniques* MTT-25, pp. 143–6, February 1977.

4 Mirshekar-Syahkal, D., Private Communication.

5 Bates, R. N. and Coleman, M. D., 'Millimetre wave finline balanced mixers', Proceedings of the 9th European Microwave Conference, September, 1979, pp. 721–5

6 Surridge, R. K., Summers, J. G. and Woodcock, J. M., 'Planar GaAs Mott low noise mm-wave (35 and 85 GHz) mixer diodes', Proceedings of 11th European Microwave Conference 1981, pp. 871–5.

7 Bates, R. N., Surridge, R. K., Summers, J. G. and Woodcock, J. M., 'Millimetre wave low noise E-plane balanced mixers incorporating planar MBE GaAs mixer diodes', IEEE MTT-S International Microwave Symposium Digest, 15th–17th June, 1982, pp. 13–15.

8 Bates, R. N. and Pearson, R. E., 'An extensive range of E-plane millimetric components', Philips Research Laboratories Annual Review 1981.
9 Bates, R. N. and Coleman, M. D., 'Finline for microwave integrated circuits (mics) at Ka-band (27–40 GHz)', Philips Research Laboratories Annual Review 1981.
10 Ruttan, T. G., 'Gunn diode oscillator at 95 GHz', *Electronics Letters*, **11**, no. 14, pp. 293–4, July 1975.
11 Bates, R. N., 'GaAs transferred electron oscillators operate above 60 GHz', Philips Research Laboratories Annual Review 1981.
12 Bates, R. N., 'Determination of resonant frequency for 2nd harmonic mode millimetre wave transferred-electron oscillators', *Electronics Letters*, **18**, pp. 198–9, 4th March 1982.
13 Nightingale, S. J. and Bates, R. N., 'A study of potentially low cost millimetre-wave radiometric sensors', Proceedings of the 2nd Military Microwave Conference MM 80, pp. 486–91.
14 Nightingale, S. J., 'An integrated 35 GHz radiometer', Philips Research Laboratories Annual Review 1980.
15 Nightingale, S. J., 'A 4-channel amplitude comparison millimetre-wave radiometer', Proceedings of 11th European Microwave Conference, Amsterdam, 7th–11th September 1981, pp. 365–70.
16 Nightingale, S. J. and Payne, G., 'An experimental millimetre-wave radiometric tracker', IEEE MTT-S, International Microwave Symposium Digest, 15th–17th June 1982, pp. 93–95.
17 Nightingale, S. J. and Payne, G., 'Performance trade-offs in radiometric tracker design', Proceedings of 3rd Military Microwave Conference MM '82, London, 20th–22nd October 1982, pp. 141–7.
18 Guildford, L. H. and Nightingale, S. J., 'Gain stabilisation in radiometers', British Patent Application No. 8115490, filed 20th May, 1981.
19 Vincent, R. P., 'Short range FMCW radar', Digest from the IEE Colloquium on Navigation Aids for Small Marine Craft, London, 1st June, 1982.
20 Dewey, R. J., 'Reflector and lens antennas for millimetre-wave radiometers', Proceedings of 11th European Microwave Conference, Amsterdam, 7th–11th September 1981, pp. 573–8.

Manuscript received by the Institution on 2nd June 1982. (Paper No. 2053/CC 359)

Letter to the Editor

From: **M. N. Sweeting**, B.Sc., Ph.D.

UOSAT Spacecraft Status Report*

The *UOSAT* spacecraft, built at the University of Surrey, ran into difficulties at the beginning of April this year after six months' successful operation.† Both of the v.h.f. and u.h.f. data transmitters were inadvertently switched on, causing a substantial degree of 'de-sense' to the two corresponding command receivers, thus preventing ground control. The problem was simulated on the engineering model of the spacecraft back at Surrey and an estimate of the worst-case de-sense made, including data from before and after launch. These measurements indicated that some 64 dBW e.i.r.p. at v.h.f. and 78 dBW e.i.r.p. at u.h.f. was necessary to override the de-sense and regain control of the spacecraft.

Attempts were initially made from Surrey with lower e.i.r.p.—just in case the measurements were unduly pessimistic—but it became clear that the de-sense was living up to the estimations! Further attempts were made by an American East Coast radio amateur on v.h.f. with a higher power 'Moon-bounce' station, but even this was still several decibels short. Finally, a group of radio amateurs at the Stanford Research Institute, California, obtained permission from the US Government to use the larger 150-foot antenna used previously on the *Pioneer* and *Mariner* missions and offered to help out. A small command generator was flown to S.R.I. and the antenna and high power (30 kW) klystron u.h.f. amplifier refurbished. After two months of preparation, and generating around 85 dBW e.i.r.p., Stanford succeeded in switching the v.h.f. data beacon on *UOSAT* off at just before midnight on 20th September 1982.

The Surrey Command Station then regained control of the spacecraft and switched the u.h.f. beacon off, the telemetry on and, finally, the v.h.f. beacon back on to receive housekeeping and experiment telemetry data. Analysis of the telemetry has shown that the spacecraft systems survived the five-month vigil without major problems. Two anomalies are evident, however, firstly the radiation experiment's e.h.t. voltage appears to have fallen to around 60% of nominal although the detectors still appeared to function, and secondly the secondary computer's c-m.o.s. memory current appears to have risen by 30%. At the time of writing, these two anomalies are being investigated. The attitude of *UOSAT* has also changed—the spacecraft is now spinning around its z-axis at a rate of 6 rev/min with about 15 degrees nutation and with the inertial axis roughly perpendicular to the orbit plane. This has altered the thermal condition of the spacecraft, causing slightly greater temperature gradients across the z-axis of the structure at this time of year. The battery temperature remains at around 5–8°C.

A rapid check-out of the spacecraft subsystems has been followed by the initiation of the attitude control programme. After the *UOSAT* has been re-oriented, the gravity gradient boom will be deployed and the spacecraft stabilized.

Department of Electronic and Electrical Engineering,
University of Surrey,
Guildford, Surrey GU2 5XH

MARTIN SWEETING
UOSAT Spacecraft Project Manager

8th October 1982

* Special issue on UOSAT, the University of Surrey's Satellite, *The Radio and Electronic Engineer*, **52**, no. 8/9, August/September 1982.
† Sweeting, M. N., *loc. cit.*, p. 377.

UDC 621.372.543.2.029.65: 621.372.852.1
Indexing Terms: Electric filters, bandpass, Waveguide components

Optimized low-insertion-loss millimetre-wave fin-line and metal insert filters

J. BORNEMANN, Dipl. Ing.,*
R. VAHLDIECK, Dipl.Ing.,*
Professor F. ARNDT, Dr.-Ing.*
and
D. GRAUERHOLZ, Dipl.Ing.*

SUMMARY

Low passband insertion-loss is achieved (1) by large-gap fin-lines, by which the high-Q potential increasing with gap-width is fully utilized, and (2) by pure metal inserts mounted in the E-plane of rectangular waveguides requiring no supporting dielectrics. This design combines the advantages of low-cost etching techniques and the low-loss performance of usual waveguide circuits. The theory described includes both higher-order mode interaction of the discontinuities and the finite thickness of dielectrics, metal fins as well as inserts. An optimizing computer program varies the filter parameters for a given number of resonators until the insertion loss yields a minimum in passband and an optimum in stopband. Data for optimized X-, Ka-, V-, E-, and W-band filters are given. Measurements verify the described theory. Measured minimum pass-band insertion losses are 0·3, 0·7, 1·5 dB for the fin-line filter for midband frequencies of about 12, 34, 75 GHz, and for the metal insert filter 0·1, 0·6, 0·5, and 0·7 dB at 12, 33, 63, and 76 GHz, respectively.

* *Microwave Department, University of Bremen, Kufsteiner Str. NW 1, D-2800 Bremen 33, West-Germany*

1 Introduction

In a fin-line structure,[1–14] metal inserts ('fins') are printed on a dielectric substrate (Fig. 1(a)), mounted in the E-plane of a rectangular waveguide. Besides the advantages of low-cost production through batch-processing techniques the fin-line configuration offers the potential for low-insertion loss filter designs if extremely high gap widths g (equal to the height b of the waveguide housing) are taken into account.[12,13] The reason is that the quality factor increases with increasing gap width, the optimum value being reached for the gap width $g = b$. (Ref. 2).

Low insertion-losses secondly result from a complete absence of supporting (lossy) dielectrics.[15–20] For the filter structure of Fig. 1(b) therefore the design is restricted to pure metal inserts, suitable for metal stamping or etching techniques, placed in the E-plane of rectangular waveguides.

For these two millimetre low-insertion-loss filter types design examples have been based on experimental data,[2,16,17] on equivalent-circuit theories,[18,19] and on an equivalent-waveguide approach.[5–7] These design methods neglect the higher-order-mode interaction which reduces the stopband insertion loss, or the finite thicknesses of substrates and inserts, which influence midband frequency, as well as ripple behaviour in the passband, and the stopband insertion-loss. Recently a design theory has been introduced by the

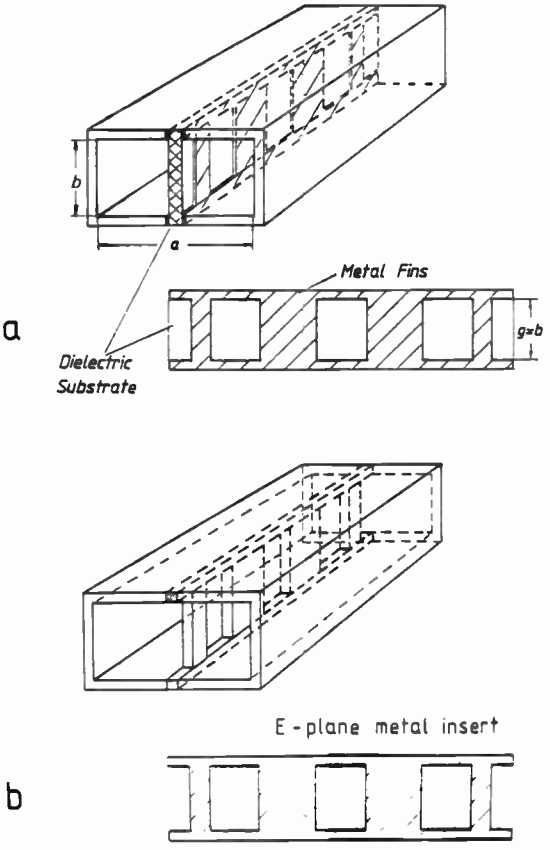

Fig. 1. Low-insertion-loss filter structures. (a) large gap fin-line filter; (b) E-plane metal insert filter.

The Radio and Electronic Engineer, Vol. 52, No. 11/12, pp. 513–521, November/December 1982
0033–7722/82/110513+09 $1.50/0

authors,[12,13,20] which includes both higher-order-mode interaction and finite thicknesses of substrates and metal inserts.

The purpose of this paper is to present new design examples, calculated with the method of Refs. 12, 13 and 20, and to compare the low-insertion-loss fin-line filter results with those of the pure metal insert filter. It will be shown that measured minimum insertion-losses in the passband are 0·3, 0·7, 1·5 dB for the fin-line filter at midband frequencies of about 12, 34, 75 GHz, and 0·1, 0·6, 0·5, 0·7 dB for the metal insert filter at 12, 33, 63, and 76 GHz, respectively.

Since millimetre-wave components require direct waveguide implementation, higher-order-mode excitation problems at the discontinuities are of great interest. For three typical waveguide discontinuities, waveguide with an E-plane metal insert of finite length, waveguide with a dielectric-slab structure mounted in the E-plane, and the abrupt transition waveguide to a shielded microstrip-line, the fundamental and higher-order-mode scattering parameters are calculated and compared with each other.

Further, the computer optimization method for the filter design is described. The optimization is based on an evolution strategy method,[21] where no differentiation steps are required. This reduces the involved computation time compared with commonly used methods, e.g. the Fletcher-Powell procedure.[22]

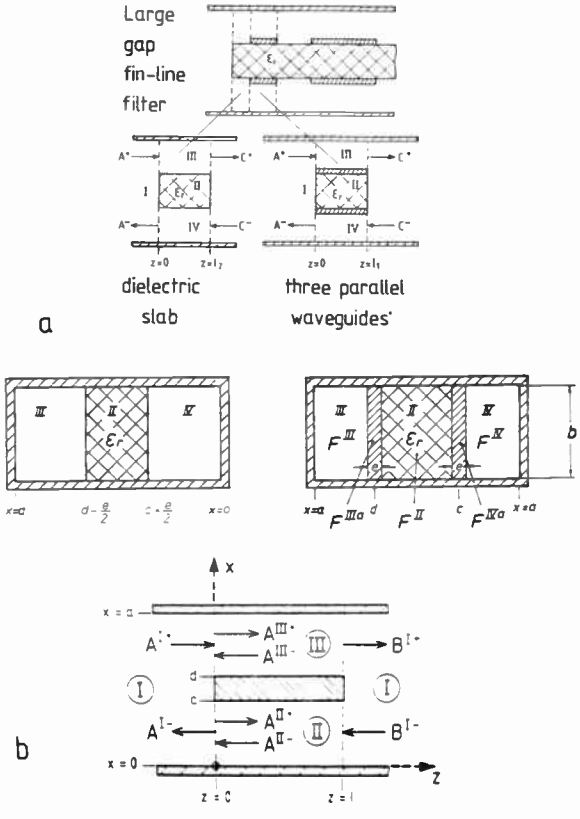

Fig. 2. Configuration for the field theory treatment. (a) fin-line structure (alternating three waveguides and dielectric-slab structure); (b) metal insert structure.

2 Theory

Since the theory is already explained in Ref. 12, its description can be abbreviated here and only the main aspects are elucidated. The fin-line filter (Fig. 1(a)) is regarded as consisting of alternating waveguide structure types: a waveguide with a dielectric slab and three parallel waveguides, the middle of which is filled with the same dielectric (Fig. 2(a)). The scattering matrices of each discontinuity are calculated including higher-order-mode excitation; the scattering matrix of the total fin-line structure is then obtained by suitably combining the transitions.

The metal insert filter (Fig. 1(b)) can be calculated by reducing the dielectric substrate thickness of the fin-line filter (Fig. 1(a)) to a negligible small value, or by directly calculating the simpler structure (Fig. 2(b)). The results are equivalent as has been proved in Ref. 20. In this paper only the first method is presented.

For the three waveguides structure of the fin-line filter in each subregion v = I, II, III, IV (Fig. 2(a)) the fields[23]

$$\mathbf{E}^{(v)} = -j\omega\mu\nabla X\boldsymbol{\Pi}_{hx}^{(v)},\quad \mathbf{H}^{(v)} = \nabla X\nabla X\boldsymbol{\Pi}_{hx}^{(v)} \tag{1}$$

are derived from the x-component of the magnetic Hertzian vector potential $\boldsymbol{\Pi}_{hx}$ which is assumed to be a sum of suitable eigenmodes satisfying the vector Helmholtz equation[23]

$$\nabla^2\boldsymbol{\Pi}_h + k^2\boldsymbol{\Pi}_h = 0,\qquad k^2 = \omega^2\mu\varepsilon \tag{2}$$

and the boundary conditions at the metallic surfaces:

$$\boldsymbol{\Pi}_{hx}^{(v)} = \sum_{m=1}^{\infty} A_m^{(v)\pm}\sin\left(\frac{m\pi}{p^v}\cdot f^v\right)\exp\left(\mp jk_{zm}^v z\right) \tag{3}$$

The propagation factor k_{zm}^v and the abbreviations p^v, f^v are explained in the Appendix. $A_m^{(v)\pm}$ are the still unknown eigenmode amplitudes of the forward and backward waves which are suitably normalized to the related power so that the power carried by a given wave is proportional to the square of the wave-amplitude coefficients. This leads directly to the desired scattering parameters.

By matching the transversal field components $\mathbf{E}_t$ and $\mathbf{H}_t$, which are given by (1) and (3), at the common interfaces F^{III}, F^{IIIa}, F^{II}, F^{IVa}, F^{IV} (Fig. 2a) across the step discontinuity at $z = 0$ the coefficients $A^{(v)\pm}$ in (3) can be related to each other after multiplication with the appropriate orthogonal function, which leads to the coupling integrals given in the Appendix. If the forward and backward waves at the two steps ($z = 0$ and $z = l_2$, Fig. 2(a)) of the structure of finite length l_2 are suitably related together, then (1)–(3) can be written as the desired scattering matrix

$$\begin{pmatrix}(A^-)\\(C^+)\end{pmatrix} = \begin{pmatrix}(S_{11})(S_{12})\\(S_{21})(S_{22})\end{pmatrix}\begin{pmatrix}(A^+)\\(C^-)\end{pmatrix}. \tag{4}$$

For details the reader is referred to Ref. 12.

The dielectric slab structure is treated in a similar manner. The common propagation factor k_{zm} in regions II, III, and IV is determined by the boundary conditions along the dielectric slab. A system of linear equations is obtained where the determinant is required to be zero. This leads to a transcendental equation which is solved numerically.[12]

The scattering matrix of the total fin-line structure is obtained by suitably combining the transitions, the length of waveguide I (Fig. 2(a)) being reduced to zero if the structures are joined together directly. A series of steps is commonly treated by transmission matrix parameters. But this is not appropriate if, like here, higher-order modes are included which are excited below their cut-off frequency. Since transmission matrix parameters for certain frequencies may then contain exponential functions with positive argument they exceed for many geometrical cases the available numerical range of the computer. The direct combination, however, of the resulting scattering matrices $(S)^{I}$, (S^{II}) is numerically stable as is shown for two steps I and II as an example, only containing exponential functions with negative arguments

$$\begin{bmatrix} b^{I} \\ b^{II} \end{bmatrix} = \left(\begin{bmatrix} S^{I}_{11} & 0 \\ 0 & S^{II}_{22} \end{bmatrix} + \begin{bmatrix} S^{I}_{12}D & 0 \\ 0 & S^{II}_{21}D \end{bmatrix} \times \right.$$
$$\left. \times \begin{bmatrix} ES^{II}_{11}D & E \\ F & FS^{I}_{22}D \end{bmatrix} \begin{bmatrix} S^{I}_{21} & 0 \\ 0 & S^{II}_{12} \end{bmatrix} \right) \begin{bmatrix} a^{I} \\ a^{II} \end{bmatrix}, \quad (5)$$

where I and II denote the steps I and II, respectively, and

$$E = (U - S^{II}_{11}DS^{I}_{22}D)^{-1}$$

$$F = (U - S^{I}_{22}DS^{II}_{11}D)^{-1},$$

a = incident waves, b = scattered waves, U = unit matrix, D = diagonal matrix with

$$D_{ii} = \exp(-\gamma_i l_i)$$

due to the section lengths l_i with the propagation constants γ_i between the step discontinuities. A series of more than two discontinuities can be treated in an analogous manner to (5).

3 Scattering Parameters of E-plane and H-plane Waveguide Discontinuities

Millimetre-wave components require direct waveguide implementation. As a first result of the given theory, therefore, the magnitude of the fundamental and higher-order mode transmission coefficients (scattering parameters $|S_{21}|$, eqn. (4)) is shown as a function of frequency of the complete discontinuity of a metal insert structure with finite length in the E-plane of a rectangular waveguide (Fig. 3). It can be stated that the power transmitted along the discontinuity is carried by H_{m0}-modes which are well compatible with the incident H_{10}-mode.

The good H_{10}-mode compatibility of E-plane structures is also demonstrated by the fundamental mode transmission coefficient $|S_{21}|$ of the transition waveguide to a waveguide with a dielectric slab mounted in the E-plane (Fig. 4), calculated according to Ref. 24. Below the H_{20}-mode cut-off frequency nearly all the energy is transmitted into the desired fundamental H_{10}-mode.

This is in contrast, for example to the common

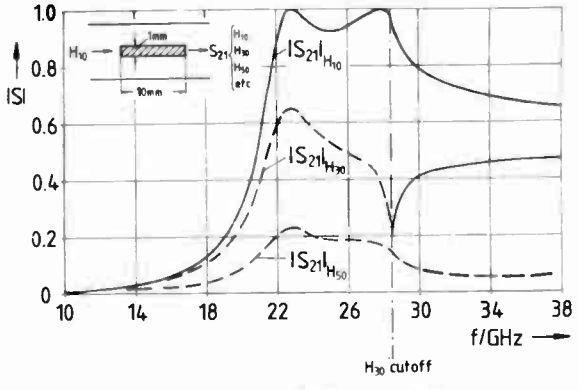

Fig. 3. Transition from a waveguide to a metal insert structure (Fig. 2(b)) and back to waveguide. Waveguide dimensions. $a = 15{\cdot}8$ mm, $b = 7{\cdot}899$ mm. Fundamental mode and first higher order mode scattering coefficients $|S_{21}|$ into the waveguide (right) if a H_{10}-mode is incident in the waveguide (left) as a function of frequency.

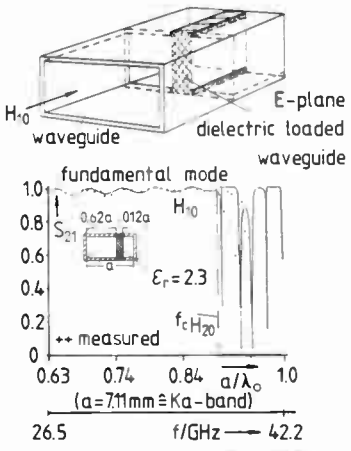

Fig. 4. Transition from a rectangular waveguide to a E-plane dielectric loaded waveguide. Scattering coefficient $|S_{21}|$ of the H_{10}-mode in the slab-line structure if a H_{10}-mode is incident in the waveguide as a function of frequency.

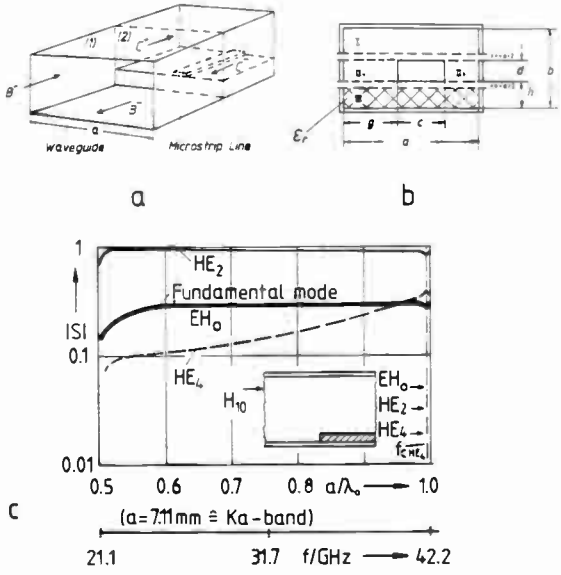

Fig. 5. Transition from a rectangular waveguide to a microstrip line. (a) View of the transition; (b) Cross-section of the shielded microstrip; (c) Transmission coefficient (scattering parameter $|S_{21}|$) of the step waveguide to microstrip as a function of frequency. Dimensions: $b/a = 8/16$, $c/a = 3/16$, $d/a = 1/160$, $g = (a-c)/2$, $h/a = 1/16$, $\varepsilon_r = 9{\cdot}7$ (— · — · — cut-off frequencies).

microstrip-line where the substrate sheet is mounted in the H-plane. Figure 5 shows the magnitude of the transmission coefficients of the transition from a rectangular waveguide to the shielded microstrip-line calculated according to Refs. 25, 26. The coefficients are a function of normalized frequency a/λ_0 (a = width of the waveguide housing, λ_0 = wavelength in air). It is shown that the principal part of the transmitted power is transported by the first higher-order HE_2-mode and not by the commonly desired fundamental microstrip mode EH_0. This is because of the incoherence of the incident waveguide H_{10}-mode with the EH_0-mode where an E-mode portion dominates. It indicates that a direct waveguide implementation of microstrip lines is inappropriate. Since suitable tapered transitions (e.g. ridged waveguide tapers) are relatively complicated, for millimetre-wave integrated circuits E-plane structures are more adequate.

4 Optimization Procedure

For the computer optimization of the filters an error function is defined (Fig. 6)

$$F(\bar{x}) = \sum_{i=1}^{N_{stop}} (a_{s(min)}/a_{21}(f_i))^2 + \sum_{i=1}^{N_{pass}} (a_{21}(f_i)/a_{p(max)})^2 \stackrel{!}{=} \text{Min.}, \quad (6)$$

where the filter resonator and coupling section dimensions $\bar{x}$

$$\bar{x} = (l_1, l_2, l_3, \ldots, l_n) \quad (7)$$

are optimized to yield a minimum. Here, f_i are the frequency sample points, N_{stop} and N_{pass} are the number of sample points in stopband and passband respectively. A number of 20 30 frequency sample points, both in passband and stopband, has turned out to be sufficient.

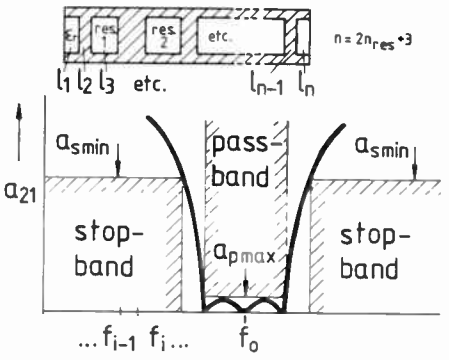

Fig. 6. Scheme for the computer optimization.

Values $a_{s(min)}$ and $a_{p(max)}$ are the given minimum stopband and maximum passband attenuation, respectively, and $a_{21} = 20 \log (1/|S_{21}|)$ is the insertion-loss at the frequency f_i, calculated according to Section 2. For first optimization results an expansion into five eigenmodes, see equation (3), is sufficient. The final results are proved by the expansion into twenty eigenmodes, and for the W-band filter in Fig. 11 into forty-five eigenmodes.

The initial values for l_2 to l_{n-1} (eqn. (7)) for the optimization procedure are chosen to be each $\lambda_0/2$, where λ_0 is the wavelength in air of the H_{10}-mode at the given midband frequency. Values l_1 and l_n, for the fin-line filter, are fixed by the given total substrate length L. For the metal insert filter l_1 and l_n are also initially chosen to be $\lambda_0/2$. In order to reduce the number of parameters the filters are assumed to be symmetrical with regards to the half of the total filter length.

A main optimization strategy parameter H and a secondary strategy parameter N influence[21] the alternation of the parameters $\bar{x}$ during the optimization process with a standard deviation $\sigma = H \cdot N$. Initial values for H and N are chosen to be $H = 0{\cdot}01$, $N = 1$.

Table 1

Computer-optimized design data for low-insertion-loss fin-line filters.

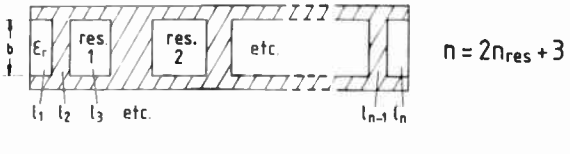

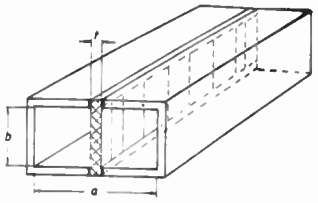

Frequency - band waveguide housing	Substrate material	Number of resonators n_{res}	Substrate thickness t	Copper cladding thickness	$l_1=l_n$ (mm)	$l_2=l_{n-1}$ (mm)	$l_3=l_{n-2}$ (mm)	$l_4=l_{n-3}$ (mm)	$l_5=l_{n-4}$ (mm)	$l_6=l_{n-5}$ (mm)	$l_7=l_{n-6}$ (mm)	Results see Fig.
X - band a = 22.86 mm b = 10.16 mm	RT/duroid 5880 ε_r = 2.22	4	1/32 "	17.5 µm	19.232	1.421	8.809	7.452	8.565	9.043		7 a
Ka - band a = 7.112 mm b = 3.556 mm	RT/duroid 5880 ε_r = 2.22	3	0.01 "	17.5 µm	19.77	0.705	3.75	3.9	3.75			8 a
E - band a = 3.10 mm b = 1.55 mm	Fused Silica (Quartz) ε_r = 3.8	3	0.220 mm	5 µm	11.016	0.336	1.457	1.462	1.459			10 a
E - band a = 3.10 mm b = 1.55 mm	Fused Silica (Quartz) ε_r = 3.8	5	0.220 mm	5 µm	5.595	0.305	1.477	1.333	1.493	1.554	1.488	10 b

During the optimization procedure the main strategy parameter H is altered as follows: For fewer than three trials, H is doubled, for more than three, H is halved; after a successful trial, H is left constant. If the deviation of the parameters $\bar{x}$ exceeds the limit $\lambda_0/2-0{\cdot}7\ \lambda_0/2 < x_i < \lambda_0/2+0{\cdot}7\ \lambda_0/2$, H is multiplied by 0·7. If the error function $F(\bar{x})$ is minimized three times by less than 1%, the result is interpreted as a local minimum. H is multiplied by 10^4. So the optimization process begins again for a different, perhaps better, parameter range, and the global minimum, if it differs from the already found local one, can be attained.

The secondary strategy parameter N is altered principally in the same manner. The altering factor for fewer than three trials is chosen to be 1·2, for more, 0·83. It is often convenient to adapt N to the individual parameters x_i: the resonator length variation should be less than the variation of the coupling sections, if, for

5 Results

Figure 7 shows the calculated and measured insertion-loss ($a = 20$ log $(1/S_{21})$) in decibels as a function of frequency for four-resonator X-band pseudo-highpass filters. Considered for prototypes for television communication satellite front-ends, the filters have been optimized according to specifications given by H. Kolbe & Co., Bad Salzdetfurth, W.-Germany. Figure 7(a) relates to the fin-line type, and Fig. 7(b) to the metal insert type. The filters yield a measured minimum insertion loss of about 0·3 dB for the fin-line filter and 0·1 dB for the metal insert filter, respectively.

Three-resonator Ka-band filter results are indicated in Fig. 8. The corresponding measured minimum insertion-losses are 0·7 dB (fin-line, a), and 0·6 dB (metal insert, b). The insertion-loss curve of a three-resonator V-band metal insert filter is given in Fig. 9 (0·5 dB measured minimum insertion-loss).

Table 2
Computer-optimized design data for low-insertion-loss metal insert filters.

Frequency - band waveguide housing	Number of resonators	Insert thickness t (mm)	$l_1=l_n$ (mm)	$l_2=l_{n-1}$ (mm)	$l_3=l_{n-2}$ (mm)	$l_4=l_{n-3}$ (mm)	$l_5=l_{n-4}$ (mm)	$l_6=l_{n-5}$ (mm)	Results see Fig.
X - band a = 22.86 mm b = 10.16 mm	4	0.9	1.96	9.439	8.686	9.251	10.065		7 b
Ka - band a = 7.112 mm b = 3.556 mm	3	0.51	1.009	4.778	3.87	4.796			8 b
V - band a = 3.76 mm b = 1.88 mm	3	0.1	0.708	2.243	2.26	2.252			9
E - band a = 3.045 mm † b = 1.55 mm	3	0.1	0.613	1.911	1.978	1.917			10 c
E - band a = 3.1 mm b = 1.55 mm	4	0.1	0.617	1.92	1.92	1.927	2.1		10 d
E - band a = 3.1 mm b = 1.55 mm	5	0.1	0.615	1.918	1.91	1.925	2.1	1.93	10 e
W - band a = 2.54 mm b = 1.27 mm	4	0.05	0.845	1.438	2.355	1.439	2.579		11

† The a-dimension of this filter housing differs from the nominal E-band value by about -55 µm (construction error!). This results in a mid-band frequency shift of about +1 GHz which has been included in the computation of this filter.

instance, the ripple behaviour has to be improved while the mid-band frequency behaviour of the filter is already satisfactory.

On the average, every sixth optimization step was successful. The results of the optimization procedure are given in Table 1 for the fin-line filters, and in Table 2 for the metal insert filters. The total computing time for the optimization process of one set of filter parameters was about 10–30 min. A Siemens-7880 computer was used for the computations.

Figure 10 shows the insertion-loss behaviour of several E-band filters. In Figs. 10(a) and (b) three- and five-resonator fin-line filters are chosen; fused silica (quartz) is chosen for substrate material, because of its lower loss compared with RT/duroid 5880, used for the lower frequencies. The measured minimum insertion-losses are 1·3 dB, and 3 dB, for the three- and five-resonator filters, respectively. The corresponding values of the three- to five-resonator metal insert filters are 0·7, 2·3, 2·4 dB, respectively. The calculated insertion-loss of a four-

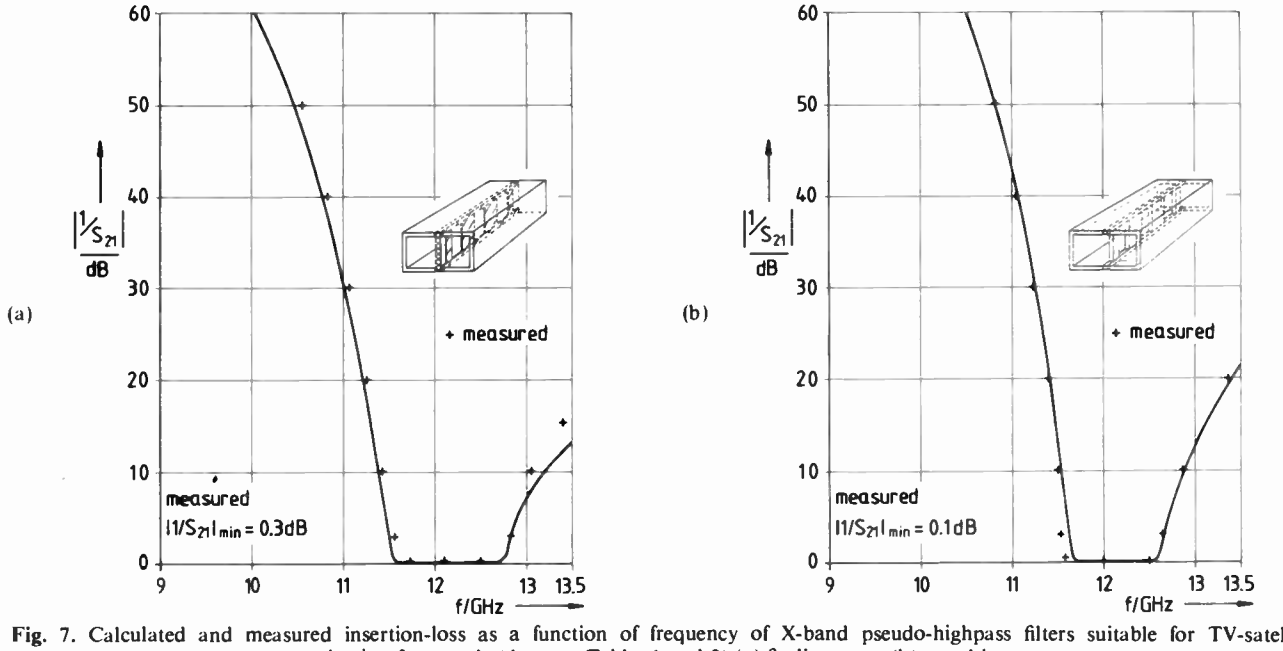

Fig. 7. Calculated and measured insertion-loss as a function of frequency of X-band pseudo-highpass filters suitable for TV-satellite-communication front-ends (data see Tables 1 and 2) (a) fin-line type; (b) metal insert type.

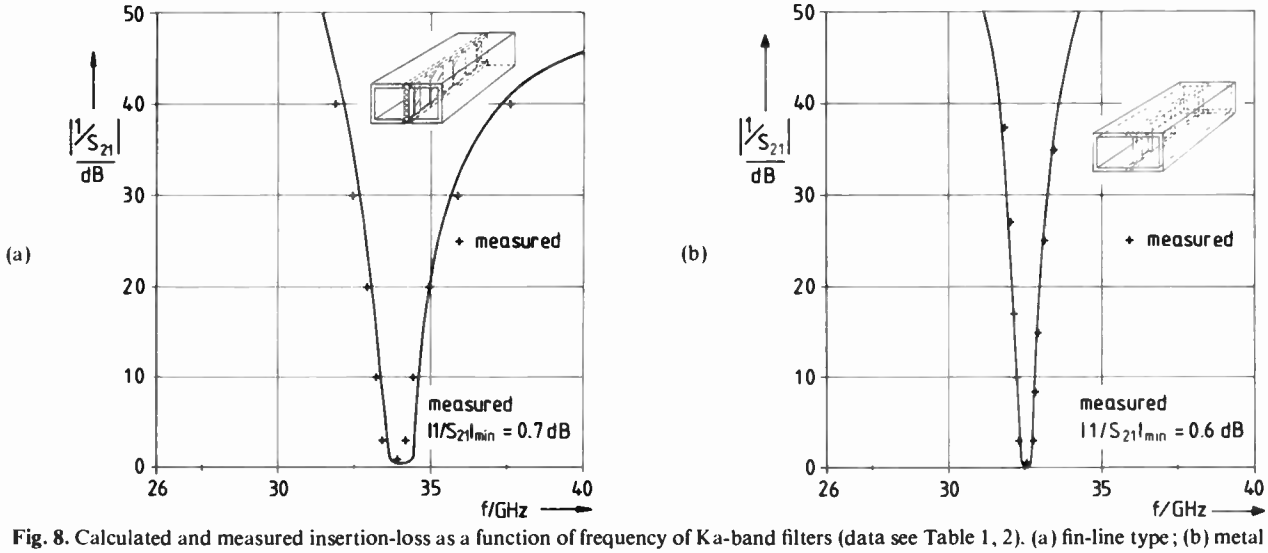

Fig. 8. Calculated and measured insertion-loss as a function of frequency of Ka-band filters (data see Table 1, 2). (a) fin-line type; (b) metal insert type.

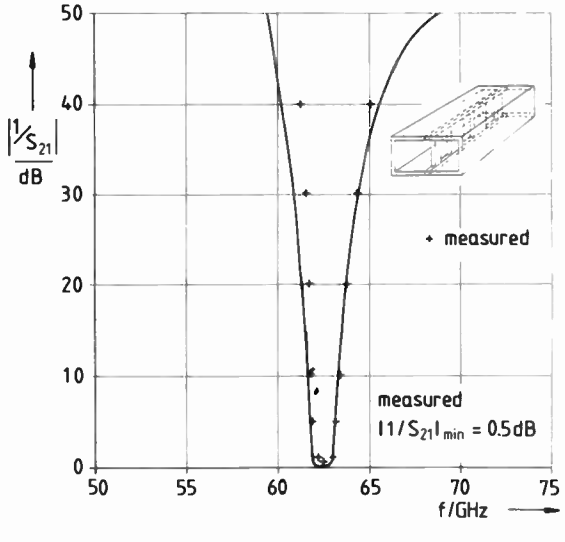

Fig. 9. Calculated and measured insertion-loss as a function of frequency of a V-band metal insert filter (data see Table 2)

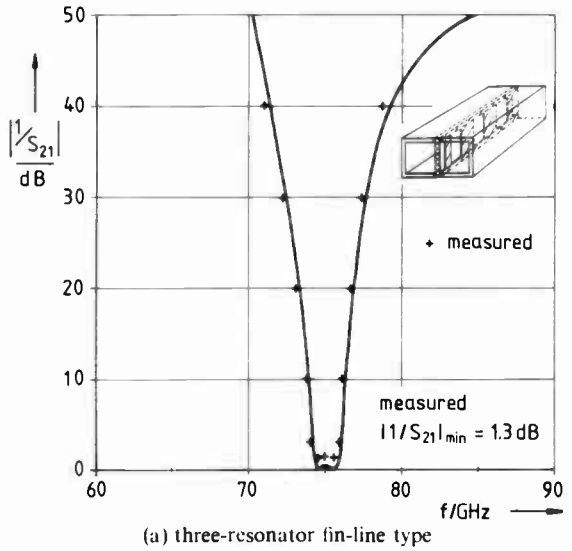

(a) three-resonator fin-line type

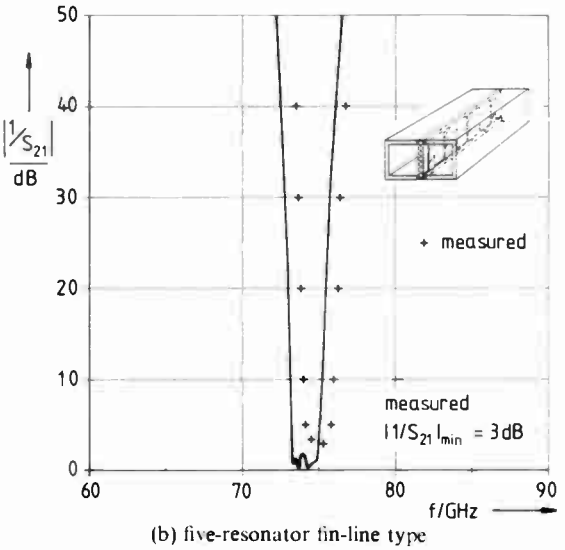

(b) five-resonator fin-line type

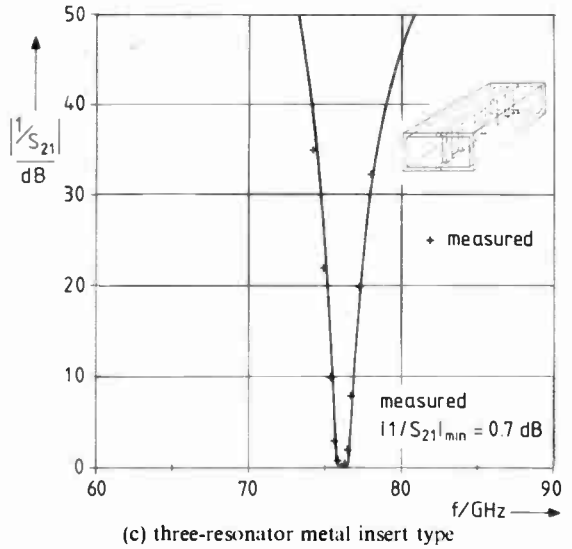

(c) three-resonator metal insert type

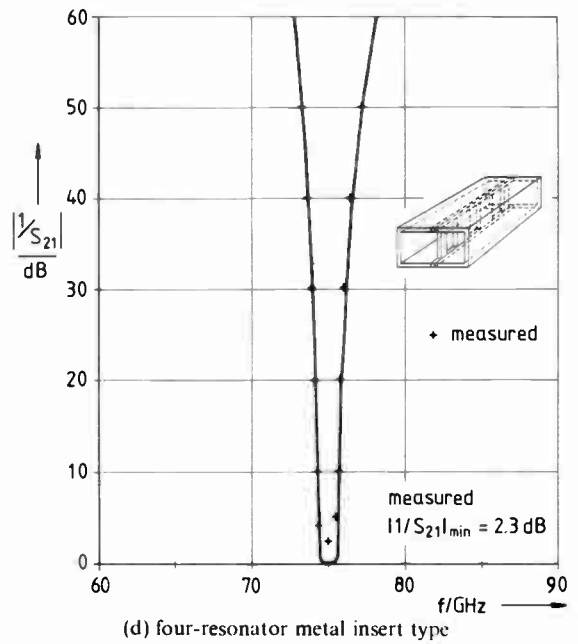

(d) four-resonator metal insert type

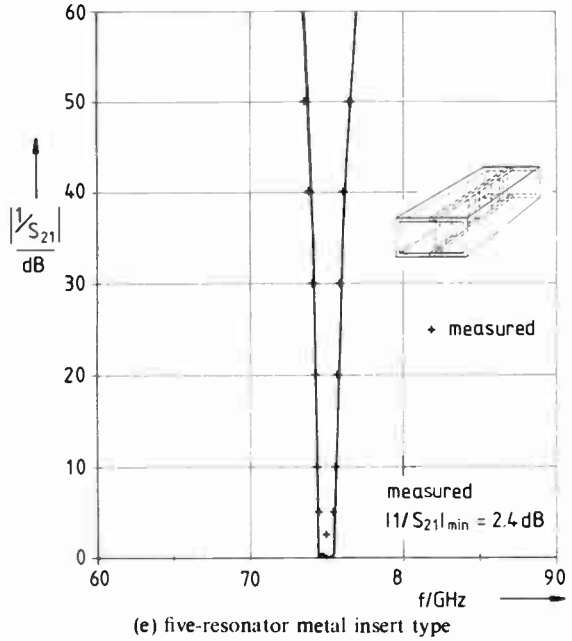

(e) five-resonator metal insert type

Fig. 10. Calculated and measured insertion-loss as a function of frequency of E-band filters (data see Tables 1 and 2).

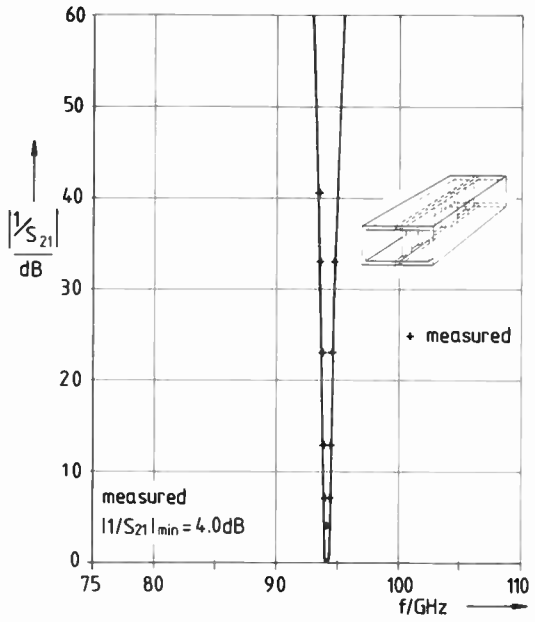

Fig. 11. Calculated insertion-loss as a function of frequency of a W-band metal insert filter.

resonator W-band metal insert filter is shown in Fig. 11. This filter is considered for application in millimetre-wave receiver systems and has been optimized according to specifications given by Dr Rembold, AEG-Telefunken, Ulm, W.-Germany. The measured minimum insertion-loss is 4·0 dB. Figure 12 shows the etched filter-structures of a fin-line and a metal insert E-band filter.

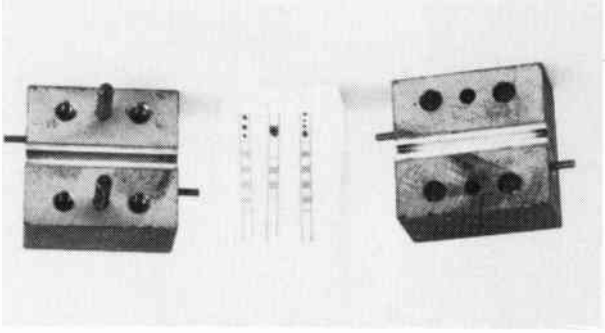

(a) fin-line type (two five-resonator and a three-resonator structure(s) on fused silica (quartz) substrate material).

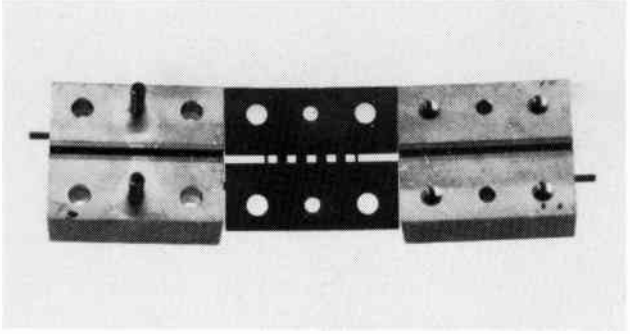

(b) metal insert type (five resonators).

Fig. 12. Etched E-band filter structures together with the corresponding waveguide housing.

The comparison of the measured and calculated filter responses shows a good coincidence between theory and practice. The slight frequency displacement between calculated and measured curves in some of the figures is caused by etching errors and production tolerances of the available material: copper cladding thickness about $\pm 2{\cdot}5$ μm (for the 17·5 μm thickness) and $\pm 0{\cdot}5$ μm (for the 5 μm thickness), substrate thickness about ± 20 μm, metal insert thickness about $\pm 5\%$. This has been checked by using the measured geometries of the filters in the theory.

6 Conclusions

A design theory has been described for low-insertion-loss fin-line and E-plane metal insert filters. The theory includes both higher-order mode interaction, and the finite thicknesses of dielectrics, metallic fins, and metal inserts.

The low-insertion-loss design is achieved by a large gap fin-line type, with a considerably higher unloaded Q compared with the common small gap design, and by a metal insert filter type requiring no supporting (lossy) dielectric substrate. The low-insertion-loss also results from the fact that no tapered transitions from waveguide to the E-plane printed circuit structures are required. For the fin-line, at lower frequencies, RT/duroid 5880 is used for substrate material. To reduce the losses fused silica (quartz) is chosen for higher frequencies because of its lower loss and surface roughness. The complete absence of supporting dielectrics, in the case of metal insert filters, achieves still lower insertion-losses.

A computer optimization leads to optimum design data for three-to five-resonator filters for X- to W-band application. Measurements verify the given theory. The low-insertion-loss E-plane integrated circuit filters combine the advantages of the low-loss design of common waveguide filters with the low-cost etching production technique of integrated circuit designs.

7 Acknowledgments

The E-band fin-line filters have been etched and measured and the V-, E- and W-band metal insert filters measured in the microwave laboratory of AEG-Telefunken, Ulm, W.-Germany. The authors are greatly indebted to Dr Rembold, the head of the laboratory, and the members of his staff, especially Dr Menzel, for this aid. Further, financial support for the W-band metal insert filter by AEG-Telefunken, via Dr Rembold, and for the X-band low-insertion-loss filters by Hans Kolbe & Co., Fuba, Bad Salzdetfurth, W.-Germany, via Dipl.-Ing. Begemann, is gratefully acknowledged as well as the permission for publication of results of the corresponding filter designs.

8 References

1 Meier, P. J., 'Equivalent relative permittivity and unloaded Q-factor of integrated fin-line', *Electronics Letters*, **9**, no. 7, pp. 162–3, April 1973.

2 Meier, P. J., 'Integrated fin-line millimeter components', *IEEE Trans. on Microwave Theory and Techniques*, **MTT-22**, pp. 1209–16, December 1974.

3 Meier, P. J., 'Millimeter integrated circuits suspended in the E-plane of rectangular waveguide', *IEEE Trans.* **MTT-26**, pp. 726–32, October 1978.
4 Mirshekar-Syahkal, D. and Davies, J. B., 'Accurate analysis of tapered planar transmission lines for microwave integrated circuits', *IEEE Trans.*, **MTT-29**, pp. 123–8, February 1981.
5 Saad, A. M. K. and Schünemann, K., 'A simple method for analyzing fin-line structures', *IEEE Trans.*, **MTT-26**, pp. 1002–7, December 1978.
6 Saad, A. M. K. and Schünemann, K., 'Design and performance of fin-line bandpass filters', Proc. 9th European Microwave Conf., Brighton, 1979, pp. 397–401.
7 Hennawy, H. E. and Schünemann, K., 'Analysis of fin-line discontinuities, Proc. 9th European Microwave Conf., Brighton, 1979, pp. 448–52.
8 Hoffmann, H., 'Dispersion of planar waveguides for millimeter-wave application', *Arch. Elek. Ubertragung*, **31**, pp. 40–4, 1977.
9 Beyer, A., 'Analysis of the characteristics of an earthed fin-line', *IEEE Trans.* **MTT-29**, pp. 676–80, July 1981.
10 Beyer, A. and Wolff, I., 'A solution of the earthed fin-line with finite metallization thickness', 1980 IEEE MTT-S Int. Microwave Symp. Digest Washington, DC, pp. 258–60.
11 Schmidt, L. P., Itoh, T. and Hofmann, H., 'Characteristics of unilateral fin-line structures with arbitrarily located slots', *IEEE Trans.*, **MTT-29**, pp. 352–55, April 1981.
12 Arndt, F., Bornemann, J., Grauerholz, D. and Vahldieck, R., 'Theory and design of low-insertion loss fin-line filters', *IEEE Trans.*, **MTT-30**, pp. 155–63, February 1982.
13 Arndt, F., Bornemann, J., Grauerholz, D. and Vahldieck, R., 'Low-insertion loss fin-line filters for millimetre-wave applications', Proc. 11th European Microwave Conf., Amsterdam, 1981, pp. 309–14.
14 Adelseck, B., Callsen, H., Hofmann, H., Meinel, H. and Rembold, B., 'Neue Millimeterwellenkomponenten in quasiplanarer Leitungstechnik', *Frequenz*, **35**, pp. 118–23, May 1981.
15 Konishi, Y. *et al.*, 'Simplified 12-GHz low-noise converter with mounted planar circuit in waveguide', *IEEE Trans.*, **MTT-22**, pp. 451–4, April 1974.
16 Reindel, J., 'Printed wg circuits trim component costs', *Microwaves*, pp. 60–63, October 1980.
17 Meier, P. J., 'Two new integrated-circuit media with special advantages at millimeter wavelength', Digest IEEE 1972 G-MTT Symp., May 1972, pp. 221–3.
18 Konishi, Y. and Uenakada, K., 'The design of a bandpass filter with inductive strip-planar circuit mounted in waveguide', *IEEE Trans.* **MTT-22**, pp. 869–73, October 1974.
19 Tajima, Y. and Sawayama, Y., 'Design and analysis of a waveguide-sandwich microwave filter', *IEEE Trans.*, **MTT-22**, pp. 839–41, September 1974.
20 Vahldieck, R., Bornemann, J., Arndt, F. and Grauerholz, D., 'Optimized waveguide E-plane metal insert filter for millimeter-wave applications', to be published.
21 Schmiedel, H., 'Anwendung der Evolutionsoptimierung auf Schaltungen der Nachrichtentechnik', *Frequenz*, **35**, pp. 306–10, November 1981.
22 Fletcher, R. and Powell, M. J. D., 'A rapidly convergent descent method for minimization', *Computer J.*, **6**, pp. 163–8, 1963.
23 Collin, R. E., 'Field Theory of Guided Waves', chap. 1.6., pp. 22–7, and chap. 6.2, pp. 232–44, (McGraw-Hill, New York, 1960).
24 Engel, W. and Kruse, J., 'Berechnung der Streumatrix verschiebbarer dielektrischer Stoffeinsätze in Rechteckhohlleitern', Diploma thesis, University of Bremen, 1978.
25 Arndt, F. and Paul, U., 'The reflection definition of the characteristic impedance of microstrips', *IEEE Trans.*, **MTT-28**, pp. 724–31, August 1979.
26 Paul, U., 'Berechnung des sprunghaften Übergangs vom Rechteckhohlleiter zur geschirmten Streifenleitung mit homogenem sowie mit inhomogenem Dielektrikum', Dr.-Ing. thesis, University of Bremen, 1976.

9 Appendix

Abbreviations in equation (3)

$$\begin{bmatrix} f^{\mathrm{I}} \\ f^{\mathrm{II}} \\ f^{\mathrm{III}} \\ f^{\mathrm{IV}} \end{bmatrix} = \begin{bmatrix} x \\ d-(e/2)-x \\ a-x \\ x \end{bmatrix}$$

$$\begin{bmatrix} p^{\mathrm{I}} \\ p^{\mathrm{II}} \\ p^{\mathrm{III}} \\ p^{\mathrm{IV}} \end{bmatrix} = \begin{bmatrix} a \\ d-c-e \\ a-(d+(e/2)) \\ c-e/2 \end{bmatrix}$$

$$\begin{bmatrix} k_{zm}^{\mathrm{I}2} \\ k_{zm}^{\mathrm{II}2} \\ k_{zm}^{\mathrm{III}2} \\ k_{zm}^{\mathrm{IV}2} \end{bmatrix} = k^{v2} - \begin{bmatrix} (m\pi/a)^2 \\ (m\pi/p^{\mathrm{II}})^2 \\ (m\pi/p^{\mathrm{III}})^2 \\ (m\pi/p^{\mathrm{IV}})^2 \end{bmatrix}, \quad k^{v2} = \omega^2 \mu_0 \varepsilon_v.$$

Coupling integrals

$$H_{mn} = \int_{x=c+e/2}^{d-e/2} \sin\left(\frac{m\pi}{a}x\right) \sin\frac{n\pi}{d-c-e}\left(d-\frac{e}{2}-x\right) \mathrm{d}x$$

$$H_{mk} = \int_{x=d+e/2}^{a} \sin\left(\frac{m\pi}{a}x\right) \sin\frac{k\pi}{a-d-\frac{e}{2}}(a-x)\,\mathrm{d}x$$

$$H_{ml} = \int_{x=0}^{c-e/2} \sin\left(\frac{m\pi}{a}x\right) \sin\frac{l\pi}{c-\frac{e}{2}}(x)\,\mathrm{d}x.$$

Manuscript received by the Institution on 7th June 1982
(Paper No. 2054/CC 360)

UDC 621.372.826.029.65 : 621.3.049.772.1
Indexing Terms: Waveguides, dielectric, Integrated circuits, thick-film.

Dielectric waveguide; a low-cost technology for millimetre wave integrated circuits

R. V. GELSTHORPE, B.Sc., Ph.D., C.Eng., MIEE*

N. WILLIAMS, B.Eng., Ph.D.*

and

N. M. DAVEY, B.Sc., C.Chem., MRSC*

SUMMARY

This paper describes the characteristics of two types of dielectric waveguide, the so-called insular and image guide configurations. The relevance of this technology to millimetre-wave integrated circuits is demonstrated and the design and performance of a number of dielectric waveguide components is described.

A thick-film printing method for the mass production of dielectric waveguide circuits is also described and the feasibility of using this technique for the production of complete millimetre-wave integrated circuits is demonstrated.

*ERA Technology Ltd, Cleeve Road, Leatherhead, Surrey KT22 7SA.

1 Introduction

Millimetre waves offer possibilities for the fabrication of high-resolution radar systems of small physical size.

Historically, millimetre wave systems have usually centred around rectangular metallic waveguide and as a result have been expensive and not suited to mass production. The application of millimetre waves to precision guidance has, however, stimulated demand for a low-cost mass-producible transmission medium of moderate performance.

In the lower portion of the millimetre wave spectrum, this demand may be satisfied by use of microstrip and its derivatives. As operating frequencies are raised however, such media, besides becoming extremely delicate physically, also become somewhat lossy electrically. Under such circumstances it is worthwhile to consider some of the broad features of the dielectric waveguide transmission medium, namely:

(i) the structure is mechanically robust;
(ii) its dimensions are relatively non-critical;
(iii) using suitable design procedures conductor losses can be reduced to a negligible level;
(iv) manufacturing techniques exist which render dielectric waveguide amenable to mass production.

It is these features which, when more conventional techniques are inapplicable, render dielectric waveguide an attractive medium for the fabrication of low-cost, moderate performance, millimetre wave integrated circuits.

2 The Dielectric Waveguide Concept

2.1 Dielectric Waveguide Structures

Although many dielectric structures may be envisaged for the guidance of electromagnetic energy, for practical reasons, two types of dielectric waveguides are of most significance. These are known as image guide and insular guide and are shown in cross-section in Figs. 1 (a) and (b) respectively. Image guide consists of a line of high permittivity low-loss dielectric material which is of rectangular cross section and mounted in intimate contact with a conducting ground plane. Insular guide, a related structure, is of a somewhat more complex construction and consists of a high permittivity line

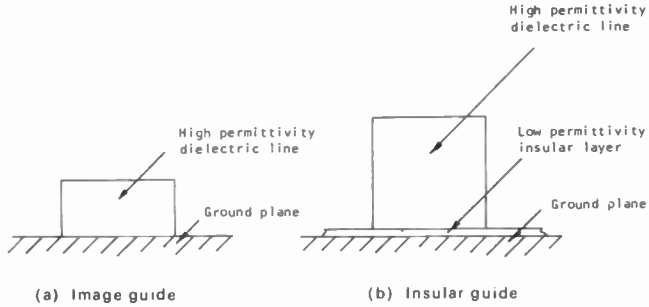

Fig. 1. Cross-sectional views of two important types of dielectric waveguide.

0033–7722/82110522+07 $1.50/0

(usually of square cross section) mounted on top of a thin low permittivity insular layer which, in turn, is situated above a conducting ground plane. Both types are attractive for the volume production of millimetre wave integrated circuits; image guide because of its simplicity and insular guide because of its potential in low-loss applications.

2.2 The Electrical Characteristics of Dielectric Waveguides

In seeking to implement a circuit design using dielectric waveguides an understanding of the electrical characteristics of the medium is essential. Three aspects of electrical performance are of importance: guide wavelength, attenuation coefficient and radiation losses occurring from curved sections of waveguide.

An exact analysis of the electrical characteristics of dielectric waveguide is not, in general, feasible since the medium supports only hybrid modes and the discontinuous nature of practically realizable cross-sections inhibits rigorous definition of the field structure. A range of numerical techniques does however exist which may be employed to ascertain the electrical characteristics of specific waveguide structures of known permittivity. Although approximations are made, the results predicted by these techniques are in general of sufficient accuracy to permit the formulation of engineering designs. Notable amongst the available analytical models is that formulated by Knox and Toulios[1] for the prediction of the phase-change coefficient of an image type waveguide; it is of significance because it may be readily extended to the analysis of insular guide and may also be employed as a starting point for the estimation of attenuation within dielectric waveguides.

The following discussion describes the salient electrical features of dielectric waveguide as predicted by the application of simple analysis techniques to particular waveguide structures.

2.2.1 *Guide wavelength characteristics*

Dielectric waveguide is capable of supporting two types of hybrid mode; in one instance the electric field is primarily parallel to the ground plane and in the other it is primarily perpendicular. These are designated the E_x and E_y modes respectively. The fundamental and higher order versions of both types of mode in both image and insular guide may be analysed using a method akin to that of Knox and Toulios.

In general terms, the analysis entails the assumption of sinusoidally varying fields within the dielectric waveguide itself and exponentially decaying fields in regions external to its walls. By sequentially considering the waveguide to be of infinite horizontal and vertical extent, field matching operations may be performed at the guide boundaries to yield a pair of transcendental equations which may be solved to derive firstly an effective permittivity for the dielectric medium, and ultimately to ascertain the propagation constant of the line itself. In general the method gives a good representation of the guide behaviour when energy containment within the line is high; in order to minimize radiation losses from bends it is necessary, in practice, to operate dielectric waveguides under this condition. For a given dielectric material, this is achieved by judicious adjustment of the line cross-sectional dimensions.

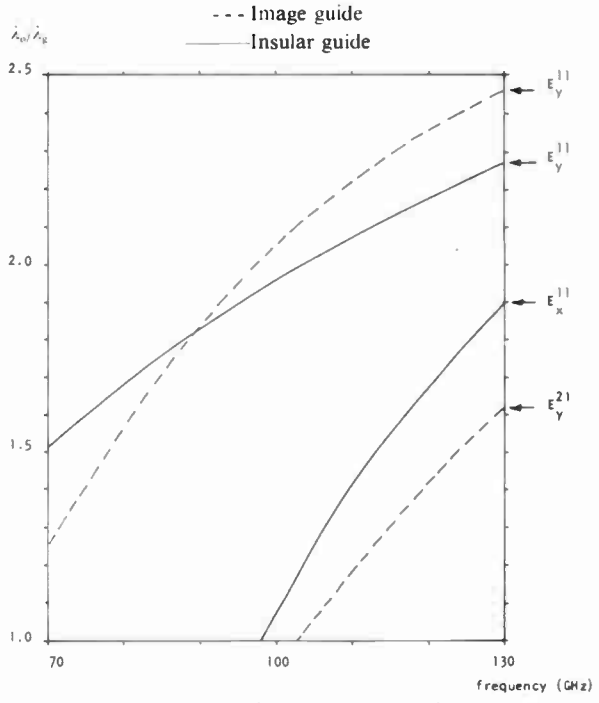

Fig. 2. Dispersion characteristics of specific image and insular waveguide structures.

The dispersion characteristics associated with image and insular guide structures designed for operation in the 90 GHz region are presented in Fig. 2 in the form of plots of λ_o/λ_g vs. operating frequency. In both instances lines of permittivity 9·8 are assumed and in the insular guide case an insular layer of 10% waveguide height and permittivity 2·25 is assumed. The cross-section of the insular guide (0·55 mm × 0·55 mm) has been selected to maintain as high phase velocity as is possible consistent with single mode operation. For comparison purposes an image guide of cross-section 0·7 mm × 0·35 mm is also analysed, this cross-section was selected since its phase velocity characteristic at 90 GHz is identical to that of the insular guide.

It is important to note from Fig. 2 that at relatively low frequencies for any given mode the ratio of λ_o/λ_g approaches unity; the dielectric medium exerts little influence on the propagation characteristic and energy containment within the guide is thus low. As the operating frequency is increased, the ratio λ_o/λ_g deviates monotonically from unity; this is consistent with increasing containment of energy within the dielectric guide.

An upper frequency limit is imposed on the operation

of dielectric waveguides by the onset of higher order modes. For insular guide this limit is, in theory (although not necessarily in practice since it need not be excited) established by the cut on of the E_x^{11} mode. In image guide, the early onset of this mode may be suppressed by the relatively small height of the guide and the presence of the ground plane. For very broad band performance image guide is a preferred choice.

2.2.2 *Loss in dielectric waveguides*

Two loss mechanisms exist in the aforementioned waveguide structures: dielectric loss due to the non-zero loss angle of the dielectric medium, and conductor loss due to the finite conductivity of the ground plane material. The two effects may be examined individually and summed to derive an estimate of the overall attenuation coefficient of the guide.

Using the transcendental relationships formulated by Knox and Toulios in conjunction with the complex permittivity of the dielectric media a perturbational analysis may be implemented to evaluate the component of attenuation arising due to the dielectric materials (see, e.g. Ref. 2).

Evaluation of conductor loss may also proceed from the field relations in the dispersion analysis. This loss term arises due to the fact that magnetic field components tangential to the ground plane surface give rise to a flow of current which, as a consequence of the finite conductivity of the ground plane, results in the dissipation of energy. Although tedious, estimation of the ground plane loss coefficient is essentially a simple process involving the computation of power loss in the ground plane via an analysis of its surface currents and the computation of power transmitted through the system by application of magnetic field and wave impedance considerations.[2]

Analyses of the dielectric and conductor losses of the two waveguide structures previously described have been performed for fundamental mode operation. Loss tangents of 0·001 and ground plane conductivities of $24{\cdot}7 \times 10^6$S/m (thick film gold) have been assumed in both cases. The results of these analyses are presented in Figs. 3 (a) and (b).

It is important to note that at the design frequency of 90 GHz, both the dielectric and conductor loss components are higher in the image than the insular configuration. The most significant change, a reduction of some 75%, is evident in the conductor loss term. This reduction is due to the rapid decay in tangential magnetic fields arising from the introduction of an insular layer; it is this feature of insular guide which renders it particularly attractive for low-loss applications.

2.2.3 *Radiation losses from bends*

Due to the open nature of dielectric waveguide its associated fields are not bounded and as a consequence,

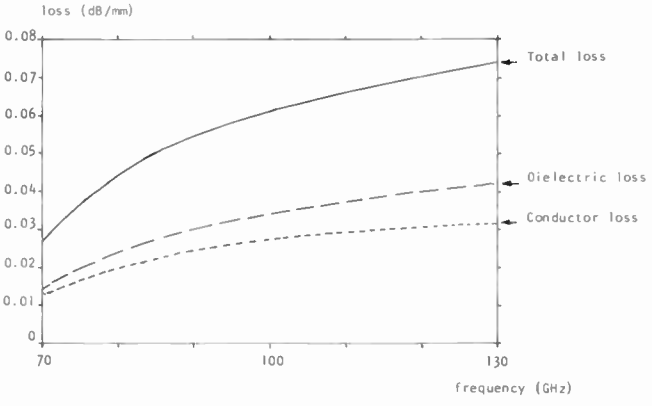

(a) Image guide

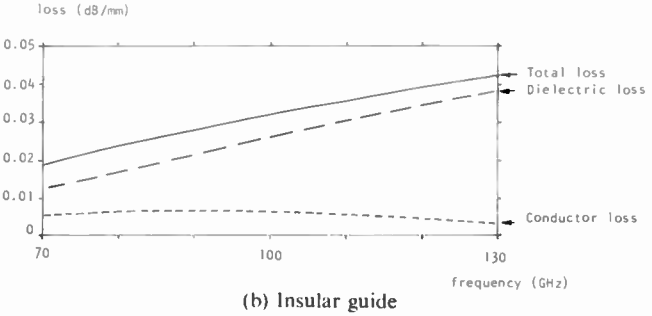

(b) Insular guide

Fig. 3. Loss components in specific image and insular waveguide structures.

on any curved section, some components of external field are required to propagate at a velocity in excess of that of light. This condition is clearly unrealizable and as a result radiation losses occur from the curved section.

Analysis of radiation losses from curved sections of optical guide has been performed by Marcatili and Miller[3] and this analysis has been extended by other workers to image line[4] and insular guide.[5] The analyses show the levels of bend radiation which take place to be a function of the waveguide parameters, the operating frequency and the bend radius. In general significant radiation levels occur at relatively low frequencies (when energy is only loosely bound to the guide) and in bends of small radius. By careful selection of guide cross-section and bend radius radiation losses may be reduced to insignificantly small amounts.

As a rule of thumb, a radius of four line widths generally results in insignificant losses for high permittivity lines operated well above cut-on.

3 Components

In attempting to apply dielectric waveguide technology to millimetre-wave integrated circuits the ability to manufacture a wide range of components is clearly an essential requirement. A typical integrated circuit requirement may be the design of a transceiver. Such a unit calls for basically two types of component: passive elements such as couplers and antennas, and active circuits such as mixers.

Hitherto, much emphasis has been placed on the manufacture of passive components and only recently

has attention been seriously directed towards the integration of active devices. The following Sections address the capabilities of active and passive components.

3.1 Passive Types

The feasibility of fabricating a large range of passive, dielectric-waveguide-based components has already been clearly demonstrated. It is inappropriate to present a lengthy discussion of the available component range here since all are well documented elsewhere (e.g. Ref. 2).

Two types of passive component are however worthy of note since they are essential for the design of almost any circuit; these are the directional coupler and the resonant filter.

A simple directional coupler can be manufactured in dielectric waveguide by bringing two axially parallel lines into close proximity. Coupling takes place in the forward direction and the level of power coupled is determined by the length of the coupling section and the separation of the lines. Using this technique both 3 and 10 dB type couplers have been produced and directivity figures in the region of 30 dB have been achieved.

Resonant filters may be produced by coupling dielectric ring or disk resonators into dielectric waveguide circuits. By appropriate measures these may be configured as band-pass or band-stop circuits; Q-values as high as 5000 have been achieved using alumina resonators at 30 GHz.

A difficulty arising in the design of ring and disk type filters is that in order to minimize radiation loss, their diameter must be fairly large; this results in the resonator exhibiting not a single resonant response but a multiple comb-like response. This problem, in practice, is easily overcome by cascading a pair of rings of differing characteristics so that the 'spurious' responses of each ring are mutually suppressed and only a single frequency response is ultimately evident.

3.2 Active Types

The integration of active devices may be achieved by the production of suitable dielectric waveguide to metallic waveguide transitions, the active elements being mounted in a standard metallic waveguide configuration. This arrangement is however not well suited to mass production and could conceivably lead to difficulties in high vibration environments. A simpler approach is clearly required.

Work on the direct integration of active devices with dielectric waveguide has been limited by a lack of theoretical models which can be used to analyse and optimize suitable mounting structures. For mixers, there are attractions in making a transition to microstrip which is directly compatible with rugged beam-lead diodes and for which designs are well established.

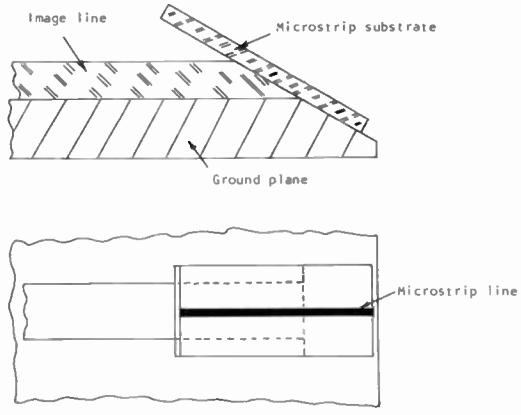

Fig. 4. Dielectric waveguide-to-microstrip transition.

(Obviously, at the higher frequencies, the length of the microstrip line must be kept short to minimize losses.)

One possible approach, first suggested by Brandt of the IIT Research Institute in a private communication to the authors, is shown in Fig. 4 and consists of a taper in the vertical plane of the dielectric line, on which is placed a low permittivity substrate with the microstrip line formed on its top surface. The metallization on the underside is terminated at the start of the taper. If a plastic substrate is employed, it can be pre-formed so that the output section is flush with the circuit groundplane; otherwise, the entire microstrip/mixer module is mounted at the required angle on the edge of the circuit (as shown).

An empirical investigation of the former configuration has been carried out in the 4–8 GHz band.[6] The microstrip line was formed on an RT-Duroid substrate and insular guide used for ease of fabrication. A range of taper angles, line widths, substrate thicknesses and lengths of the extension above the insular guide were considered. In general, the insertion loss increased with taper angle and line width; the height of the extension above the line primarily controlled the low-frequency performance.

The optimized design for 50 Ω microstrip was scaled to 30 GHz and the insertion loss of two back-to-back transitions measured using the set-up shown in Fig. 5. The response was relatively constant over the 26–40 GHz band and, on average, only 0·4 dB higher than an insular guide of the same length. A single spurious resonance was noted which is attributable to the discontinuities of the ends of the taper and may be suppressed by profiling the section.

The accuracy of return loss measurements was limited

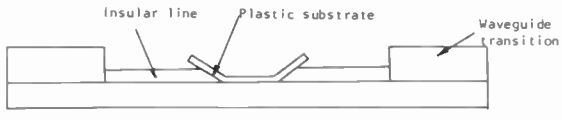

Fig. 5. Experimental test set-up for evaluation of dielectric-waveguide-to-microstrip transition.

by mismatches in the transitions to metallic waveguide; however, apart from a sharp peak occurring at the same frequency as the resonance on the insertion loss characteristics, the results were very similar to those obtained with the standard insular guide and it may be concluded that the return loss of the microstrip transitions themselves is relatively low.

An 80 GHz mixer incorporating the transition design is now under development.

4 A Low-cost Method of Fabricating Dielectric Waveguide Circuits

The development of dielectric waveguide components has relied on a piece-part fabrication technique which is relatively expensive to implement and is not, therefore, suited to mass production. A low-cost method of manufacture based on thick-film printing has been and still is under investigation. Results to date are encouraging.

4.1 Background

Over the last 20 years the use of thick-film techniques has grown from simply a method of mass manufacture of resistors to become a well-established technology capable of providing a wide range of products from simple resistor networks to complex multilayer hybrid circuits. While the complexity of circuitry produced using thick-film techniques has increased markedly the technology as a whole has remained essentially a low-cost method of mass manufacture.

During screen printing a highly viscous screen printing ink is forced through a fine stainless steel mesh, onto which a pattern has been delineated, by the forward movement of an angled squeegee blade. The ink is deposited onto a substrate (typically 96% alumina) in the form of a fine pattern of dots which, after the removal of the screen, collapse and coalesce to form a thick-film print. The solvents of the printing ink are then driven off at elevated temperatures (typically 125°C) after which the film is sintered at considerably higher temperatures (typically 850°C) in order to compact and adhere the thick-film permanently to the substrate.

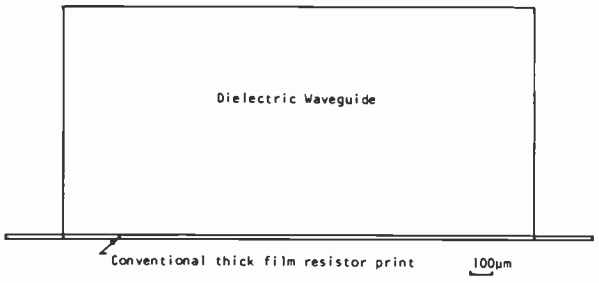

Fig. 6. Scale drawing showing the relative heights of conventional thick-film prints and printed dielectric waveguide.

4.2 The Application of Thick-Film Techniques to the Manufacture of Dielectric Waveguide

The fabrication of dielectric waveguide circuitry by a method analogous to that used to produce screened and fired thick-film circuits, requires a very significant upward extension of the range of thicknesses conventionally obtainable. Figure 6 shows the relative dimensions of a conventional thick-film resistor print and a dielectric image guide. It is clear that a massive increase in print height is required with little or no increase in print width. It is this factor above all others which dominates every aspect of deposition and processing of dielectric guide circuitry.

Since the emulsion of the screen not only delineates the print pattern but also meters the amount of paste being deposited, it is necessary to use screens with extremely thick emulsions—typically 750 μm thick compared to a conventional resistor screen which has an emulsion thickness of approximately 15 μm. The screen printing ink must also be extensively modified since it must maintain a uniform cross-section not only at the wet print stage but also during drying and firing. Its printing characteristics must also be heavily modified in order to release cleanly from the very thick emulsion screens being used.

Thick-film inks typically consist of a number of inorganic particles of controlled particle size distribution dispersed in a liquid vehicle. The liquid vehicle is usually an organic solvent (or solvents) in which a variety of organic thixotropes and binders are dissolved. It is the interaction between these thixotropes and the fine inorganic particles which gives the screen printing ink its desired rheological properties. For dielectric guide circuitry the screen printing ink must have an extremely high initial viscosity in order to maintain the very large height to width ratio required and prevent problems of edge slumping and ink spreading during the settling and drying stages of the deposition process. Under the moderate shear rates experienced in the early stages of print deposition the ink must exhibit a high degree of pseudoplasticity (rate-dependent shear thinning) in order to flow easily into the fine stainless steel mesh of the printing screen. At the higher shear rates experienced in the later stages of print deposition, however, the ink must maintain a significant viscosity. Then, through a process of micro-cavitation the ink will release cleanly from the mesh and emulsion of the very thick screens used for printing.

After printing the organic solvents of the vehicle system must be driven off at elevated temperatures in a manner analogous to more conventional thick film prints. Experience has shown that both the peak temperature and time at peak temperature are critical if significant voids are not to be created within the guide. A long drying cycle at a moderate peak temperature (100°C) has been shown to provide maximum densification.

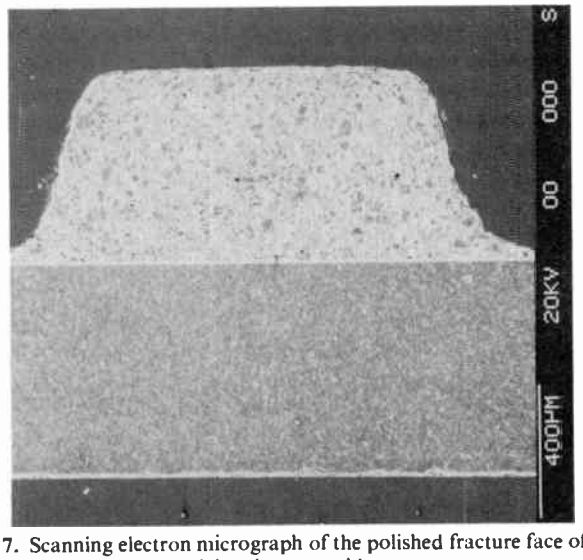

Fig. 7. Scanning electron micrograph of the polished fracture face of a dielectric waveguide.

At this stage of processing the inorganic particles of the waveguide are bound together by the organic binders and retained thixotropes of the vehicle system. Although these retained materials constitute less than 2% of the guide weight their low density relative to the inorganic components of the guide means that between 5 and 10% of the dried guide volume is retained organic material.

The purpose of the firing cycle is fourfold:

(i) Drive off retained organic materials
(ii) Sinter together the inorganic particles
(iii) Densify the guide structure
(iv) Firmly adhere the guide to a previously deposited metallic groundplane

It is essential that the retained organic materials are burnt off smoothly and cleanly at temperatures well below those used to sinter the inorganic guide constitutents. A compromise is required since, if the organic materials are driven off too quickly, the main body of the guide will be violently disrupted and if they are driven off too slowly they will be trapped within the guide. Trapped organic materials will decompose or react with the inorganic constituents causing the formation of voids and potentially lossy reaction products.

The inorganic constituents of the fired guide are most important since in order to produce high performance circuitry of small overall size it is necessary to have a relatively high permittivity material (with no voids) which exhibits a low dielectric loss at the frequencies of interest. In this work it was decided to use alumina as the main inorganic phase since it is well characterized at high frequencies and exhibits a relatively high permittivity (approximately 10) and low loss. Unfortunately alumina sinters at a temperature well above that obtainable using conventional tunnel furnaces and at temperatures considerably in excess of the melting points of suitable high conductivity ground planes. For this reason a small proportion of an inorganic binder in the form of a low melting point glass was included in the printing ink formulation.

While this had the benefit of enabling the guide to be sintered at relatively low temperatures the presence of even a small amount of glass was found to significantly degrade the electrical performance of the guide. Experiments have shown that this was due predominantly to the very much higher dielectric losses associated with the glass and also, to a lesser extent, to a variety of interactions between the glass and the other components of the guide during the firing process.

4.3 Assessment of Thick-Film Printed Image Guide

Although the thick-film printing technique is applicable to the manufacture of image and insular guide, initial emphasis has been placed on the image configuration. For convenience, studies have centred on the manufacture of waveguides for operation in the 60–70 GHz frequency range.

A scanning electron micrograph of a polished fracture face of such a waveguide, fabricated using the materials and processes described above, is shown in Fig. 7. It can be seen that the guide cross-section is very close to the ideal rectangular shape required. Measurements using a travelling microscope have confirmed that the guide dimensions are well within the tolerances required. Estimates of the level of retained porosity determined from micrographs such as these have shown that less than 2% of voids remain within the guide structure after firing. At the interface between the substrate and dielectric guide it is possible to observe the gold groundplane. This was deposited using conventional thick-film materials and techniques and serves to emphasize the massive upward extension in print height obtained in the course of the current study.

Two techniques have been employed to assess the electrical performance of the printed waveguides.

The first technique involves the examination of fields external to the waveguide by inspection of a standing wave pattern (generated using a metallic obstruction) with the aid of a travelling probe connected to a waveguide detector. This technique allows direct measurements of guide wavelength to be performed and has demonstrated the waveguide structure to be homogeneous. Transverse probing of the line has shown field containment within the line to be good.

In order to assess losses within the waveguide an insertion loss measurement has been employed which utilizes a pair of dielectric waveguides of differing lengths. This technique was selected in order to overcome difficulties in assessing the insertion loss of the transitions employed to launch and extract energy from the dielectric line. Currently, the attenuation coefficient of thick-film image guide is of the order 0·06 dB/mm at

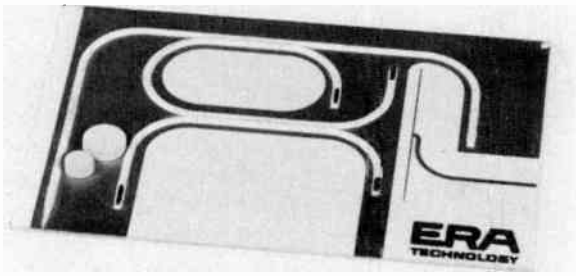

Fig. 8. 94 GHz transceiver model.

60 GHz. Whilst this figure may prove acceptable for a number of applications, work is currently in hand to identify lower loss inorganic binder phases and thus to improve guide performance still further.

As an exercise to demonstrate the feasibility of printing the circuit configurations necessary for dielectric waveguide integrated circuits a model of a 94 GHz transceiver was printed. This is shown in Fig. 8. With the exception of the high-Q disk filters at the input/output port (which are of piece-part alumina construction), the entire circuit consisting of a gold groundplane, two directional couplers, two matched loads, two metallized line sections and a microstrip i.f. output network was fabricated on a $7{\cdot}6 \times 5{\cdot}1$ cm ($3 \text{ in} \times 2 \text{ in}$) alumina substrate using thick-film technology. In this example fine gaps necessary for the directional couplers were produced using an air abrasive machine similar to the type used in the thick-film industry for the adjustment of resistors. Two alternative techniques using a laser and a wafer dicing saw have both been employed with a similar high degree of success.

5 Conclusions

The benefits to be gained from the use of dielectric waveguide in millimetre wave integrated circuit applications are those of non-critical dimensions, low-loss and, via thick-film printing, ease of mass production.

Adequate design data are already in existence and a large range of components for such systems already exists or is at an advanced stage of development.

Although for some applications, losses in thick-film printed lines are still unacceptably high, the feasibility of printing complete circuits has been clearly demonstrated and considerable scope is seen for further significant reduction of line loss.

6 Acknowledgments

The authors wish to acknowledge the significant contributions made by numerous colleagues, in particular Mr E. K. Browne and Mr I. Hutchinson. They would also like to acknowledge the support of Procurement Executive, Ministry of Defence and the sponsorship of DCVD.

7 References

1 Knox, R. M. and Toulios, P. P., 'Integrated circuits for the millimetre through optical frequency range', Symposium on Submillimetre Waves, Polytechnic Institute of Brooklyn, March 31—April 2, 1970, pp. 497–516.
2 Gelsthorpe, R. V. and Williams, N., 'The Dielectric Waveguide Handbook', ERA Report No 81-85, July 1981.
3 Marcatili, E. A. J. and Miller, S. E., 'Improved relations describing directional control in electromagnetic wave guidance', *Bell Syst. Tech. J.*, **48**, no 7, p. 2161, September 1969.
4 Knox, R. M., Toulios, P. P. and Howell, J. Q., 'Radiation losses in curved dielectric image waveguides of rectangular cross section', IEEE. MTT-S, International Microwave Symposium, Boulder, CO., June 1973.
5 Williams, N. and Rudge, A. W., 'Development of a Frequency Scanned Array: Technology Evaluation', Final report on MoD Contract, ERA-11TR1, RF Technology Centre, Leatherhead, June 1976.
6 Pretorius, J., Williams, N. and Brandt, K., 'A dielectric waveguide to microstrip transition' (*To be published*).

Manuscript first received by the Institution on 19th May 1982 and in final form on 16th August 1982
(Paper No. 2055/CC 361)

UDC 621.373.5.029.65: 621.382.232: 546.682.18

Indexing Terms: Oscillators, microwave, Semiconductor devices, transferred electron oscillators, Indium phosphide

Indium phosphide transferred electron oscillators for millimetre-wave frequencies

I. G. EDDISON, Ph.D.*

and

I. DAVIES, Ph.D.*

SUMMARY

This paper describes the development of indium phosphide TEOs for use in the millimetre wave frequency range. After presenting a brief theoretical basis for the superiority of indium phosphide over its chief rival gallium arsenide, details are given on the choice of epitaxial material used. Device fabrication is then considered with emphasis placed upon the special demands of mm-wave operation. Oscillator performances are presented which verify the theoretically predicted superiority of indium phosphide at these high frequencies. Finally, attention is drawn to the 2nd-order stability parameters exhibited by practical indium phosphide oscillator modules.

* *Plessey Research (Caswell) Ltd., Allen Clark Research Centre, Caswell, Towcester, Northants. NN12 8EQ.*

1 Introduction

There is a growing need throughout the mm-wave frequency range for solid-state, low-noise, local oscillator modules. To date this need has been partially satisfied by the gallium arsenide transferred electron oscillator (TEO) at frequencies below 100 GHz. However, the low output powers and low efficiencies of this device have limited its applications. Thus, there is a demand for higher efficiency and higher frequency TEOs, particularly in systems requiring multi-mixer drive levels and operating frequencies above 100 GHz. Indications that indium phosphide could provide the sought after improvements in TEO performance have come from theoretical studies of the transferred electron effect in III-V semiconductors.[1]

In order to obtain a general understanding of these theoretical studies it is necessary to consider the internal dynamics of electron transfer in the III-V semiconductor. The essential feature of the transferred electron effect is the transfer of electrons from the central Γ valley to the satellite L valley, a process which gives rise to the well-known electron velocity/field characteristics shown in Fig. 1. A comparison of these characteristics for indium phosphide and gallium arsenide highlights some important differences between the materials. In particular indium phosphide possesses a higher threshold field, a higher peak-to-valley electron velocity ratio and a less temperature dependent electron velocity/field behaviour.[2] This latter effect is due to the greater energy separation between the central and satellite valleys for electrons in indium phosphide. Thus the important electron peak-to-valley velocity ratio has a lower reduction with temperature in indium phosphide compared to the fairly rapid fall seen in gallium arsenide.

The dominant speed limitation of the transferred

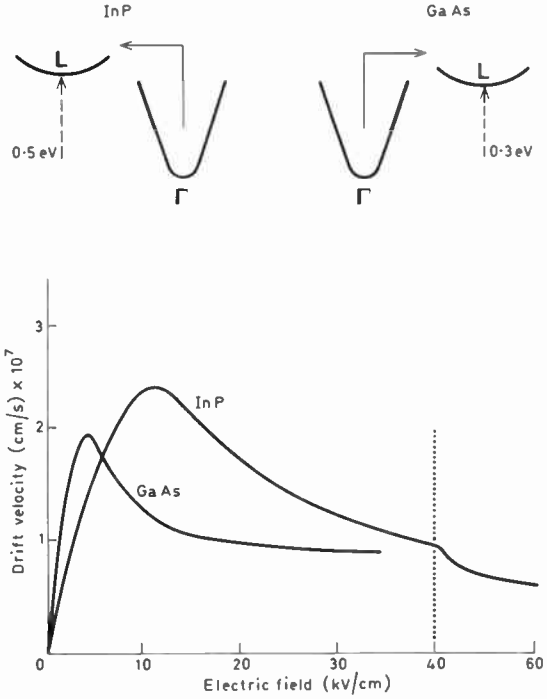

Fig. 1. Electron drift velocity vs. electric field in GaAs and InP.

The Radio and Electronic Engineer, Vol. 52, No. 11/12, pp. 529–533, November/December 1982

0033–7722/82/110529+05 $1.50/0

electron effect is the rate at which electrons gain or lose energy in the central valley during the rethermalization process in the low field part of the r.f. cycle. Now the associated energy relaxation time constant τ_0 is inversely proportional to the applied field. Thus it can be seen that the higher threshold field of indium phosphide permits faster electron transfer and hence higher operating frequencies than possible from gallium arsenide. Analysis shows that indium phosphide should operate to frequencies a factor of 2 higher than gallium arsenide. As well as this important advantage, the higher peak-to-valley ratio of indium phosphide promises better d.c. to r.f. conversion efficiency and hence improved output power levels. Further the less temperature dependent electron velocity behaviour in indium phosphide suggests a greater r.f. power stability with temperature from the final oscillator device.

Shown in Table 1 is a summary of the important differences between the properties exhibited by gallium arsenide and indium phosphide. The remainder of this paper describes the development of indium phosphide mm-wave devices and reports on oscillator performances which support the above theoretical predictions.

Table 1. Comparison of GaAs and InP

	GaAs	InP
Electron peak-to-valley velocity ratio	2·2	3·5
Threshold field (kV cm^{-1})	3·2	10·0
Temperature dependence of peak electron velocity (% deg C^{-1})	−0·15	−0·1
Inertial energy time-constant τ_0 (ps)	1·5	0·75
Diffusion coefficient/mobility ratio $D(E)/\mu(E)$ (cm^2 s^{-1}) ($E = 2E_{TH}$)	142	72

2 Material Growth

It has already been demonstrated that high d.c. to r.f. conversion efficiencies can be achieved at mm-wave frequencies using n-n$^+$ indium phosphide material on which an injecting cathode contact is utilized.[3] Indeed our recent work on this device structure has shown that excellent pulsed and c.w. mm-wave devices can be produced. Under pulsed operating conditions conversion efficiencies as high as 12% and power levels of 1 W peak have been achieved at 60 GHz (Ref. 4); at 80 GHz 9% efficiencies at 70 mW peak power levels have been seen. In the case of c.w. operation we have witnessed 53 mW with 7·2% efficiency at 88 GHz which probably represents the best efficiency from any W-band (75–110 GHz) TEO seen to date. Despite this good performance there are difficulties in producing a stable c.w. device. Unfortunately to date, the vitally important injecting cathode contact has shown strongly positive current with temperature (dI/dT) behaviour, a feature which makes manufacture of reliable n-n$^+$ c.w. devices for systems use problematical. Therefore, the likely system requirements of low-noise, good reliability and thermal stability have led us to initially investigate the inherently less efficient three-layer n$^+$-n-n$^+$ structure.

Our n$^+$-n-n$^+$ material is grown by vapour phase epitaxy on highly conducting n$^+$ substrates. The active

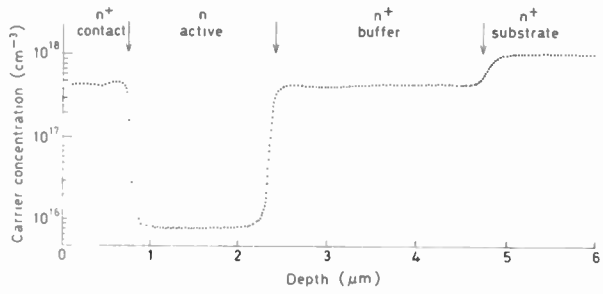

Fig. 2. Profile of typical InP mm wave epitaxial layer.

(n) region is grown at a carrier density of 5×10^{15} to $1{\cdot}5 \times 10^{16}$ atoms cm^{-3} at lengths (L) of 1·0 to 2·5 μm, these values being dependent upon the required operating frequency, efficiency and impedance level. In order to achieve adequate control of epitaxial growth and to identify those material parameters which critically affect device r.f. performance, it is essential to establish good material characterization facilities. Perhaps the most important facility is the material profiler which provides the information shown in Fig. 2. The equipment used in this case was an electrochemical impurity profiler manufactured by Polaron; the main advantage of this is that it allows accurate monitoring of doping level variations, layer thickness and interface sharpness for all three epitaxial regions as well as the substrate.

3 Device Fabrication

To achieve successful device operation at these very high frequencies great care has to be taken to design and fabricate device structures which possess low thermal and parasitic electrical resistances. Gold integral heatsink (i.h.s.) device structures with low resistance contacts have thus been developed to give the required features (see Fig. 3). Furthermore, in the mm-wave frequency range the skin depth of the substrate material is within the range 7–10 μm and this acts as a constraint upon the allowed device dimensions if skin effect losses and non-uniform current injection from the substrate into the active region are not to degrade the device performance. In addition to these considerations it has to be borne in mind that the high threshold field of indium phosphide does impose thermal constraints upon the device design. For these reasons the long established i.h.s. technology[5] has been modified to further improve its properties.

In particular other device geometries were considered as alternatives to the conventional solid disk device and the resultant annular and cross structures are shown in Fig. 4. These structures produce a 25–30% reduction in

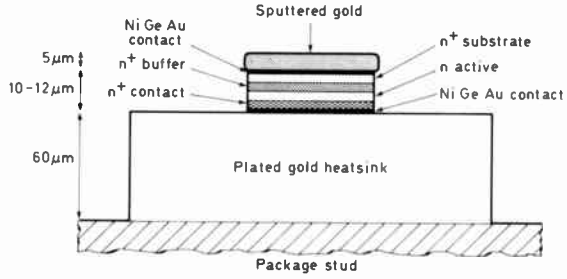

Fig. 3. Integral heatsink device structure.

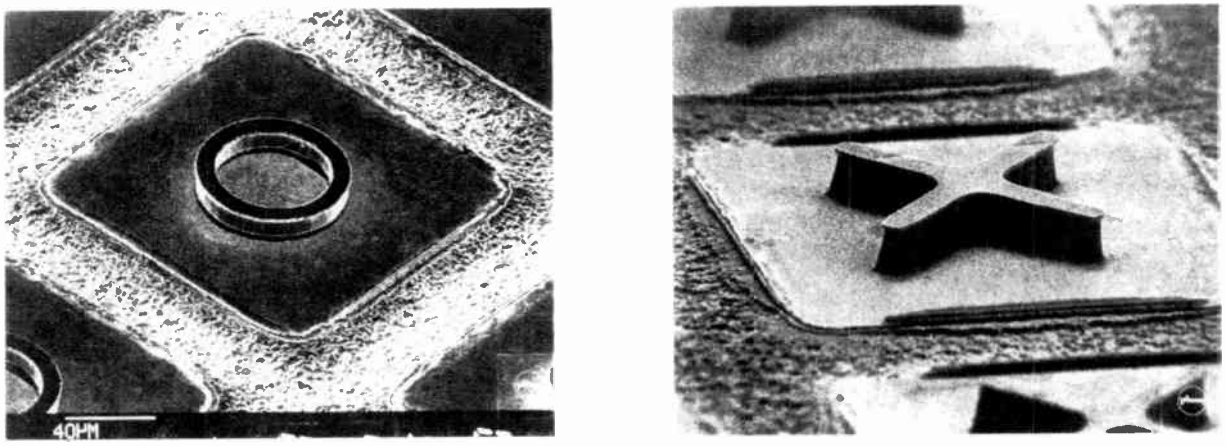

Fig. 4. Annular and cross structure InP devices.

the spreading resistance contribution to the device thermal impedance as well as allowing the semiconductor widths to be chosen to be less than twice the substrate region skin depth.

The development of this device fabrication technology has involved four distinct areas of consideration. Firstly, a low contact resistance metallization scheme was required to minimize the parasitic series resistance due to the contact. Alloyed NiGeAu contacts were developed giving typical values of contact resistance of 1 to 3×10^{-6} ohm cm^2. Secondly, the removal of substrate material had to be controlled in such a way that the total device height was approximately 10 μm in order to minimize the effects of any semiconductor parasitic resistances. A chemical polishing technique using bromine solutions together with a napless pad was found to be necessary in order to have sufficient control to be able to lap the slice down to 10 μm ± 2 μm. Thirdly, in order to realize the fine geometries demanded in the device design, conventional mask etching was found to be inadequate. In order to attain good control of the device area and enable the production of the annular and cross structures an etching system with a high degree of anisotropy was required. A photoetching system based on ferric chloride solution was found to meet these requirements.[6] Finally, it is necessary to embed the diodes in an environment for which the thermal and electrical parasitics have been minimized.

Owing to the thermal constraints imposed by indium phosphide's high threshold field the need for good device to package integrity demands that ultrasonic wafer bonding be used and that the bonding conditions in terms of ultrasonic power, weight and temperature be optimized and closely controlled. The choice of encapsulation used varies with the intended operating frequency. The ceramic pico-pill type package is favoured at the lower frequencies and a low parasitic quartz stand-off package is utilized at higher frequencies. In all cases the devices are wired with low inductance gold bonding tapes to minimize package parasitics.

4 R.F. Performance

4.1 Primary Characteristics

Using the above technology allied to a knowledge of the important material-related r.f. operating characteristics,[7] devices have been fabricated for TEO operation from 30 to 140 GHz. An investigation into the operating modes of TEOs throughout this frequency range has established that fundamental frequency operation is possible from indium phosphide up to at least 120 GHz but only up to 60–70 GHz from gallium arsenide.[8] At higher frequencies than these, both materials operate in a harmonic extraction/enhancement mode, with gallium arsenide ceasing to generate significant power above 110 GHz whilst indium phosphide is already capable of 10 mW power levels at 120 GHz and 1 mW at 140 GHz. Thus, the theoretically predicted higher operating frequency potential of indium phosphide has been practically verified.

Conventional resonant-cap and post-coupled waveguide circuits were used in the assessment of the indium phosphide device performances. Operating in a fundamental frequency mode, these devices have produced the high power and efficiency results presented in Table 2.

Table 2. R.f. performance of millimetre-wave InP transferred electron oscillators

Highest powers			Highest efficiencies		
Frequency GHz	Power mW	Efficiency %	Frequency GHz	Power mW	Efficiency %
50	210	4	57	140	4·75
70	160	3	75	70	3·25
			80	60	3·25
80	120	3	94	40	2·2
90	50	2	98	30	2·0
			106	19	1·3

A comparison of current device performances from both Plessey indium phosphide and gallium arsenide TEOs is also presented in Fig. 5. From these results it can be seen that the theoretically expected advantages of indium phosphide in terms of output power and efficiency are also borne out by the real device performance. Additionally, as material optimization is carried out for operation in the 90 to 140 GHz range we expect that the output power and efficiency capabilities predicted in Fig. 5 will be approached.

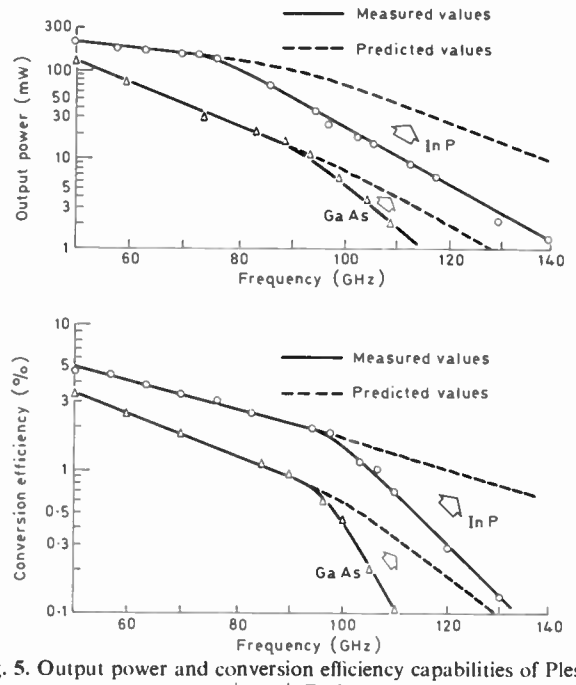

Fig. 5. Output power and conversion efficiency capabilities of Plessey n^+-n-n^+ TEOs.

4.2 Secondary Characteristics

The figures quoted above probably represent some of the highest powers and efficiencies generated from n^+-n-n^+ TEO structures. However, in themselves they are not sufficient to ensure the successful application of these devices, since often the oscillator 2nd-order parameters are the system designer's prime concern. For this reason we have started to study the noise performance, voltage stability and temperature stability of our devices.

Before discussing the noise performance of gallium arsenide and indium phosphide TEOs it is pertinent to consider the operating modes of these devices. In the mm-wave frequency range gallium arsenide devices operate in an harmonic extraction/enhancement mode which results in apparently high Q_e oscillator load pulling behaviour.[8] Thus it is difficult to determine the Q of the gallium arsenide device's local fundamental frequency environment. Conversely, the indium phosphide devices operate in the more efficient fundamental frequency mode in which the oscillator Q_e is relatively straightforward to determine.

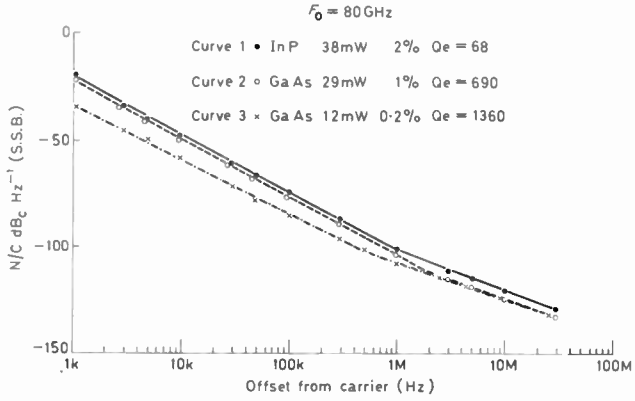

Fig. 6. Comparison of f.m. noise performance of Plessey TEOs.

Preliminary noise measurements made in W-band using an in-house f.m. noise facility[9] have shown that indium phosphide devices can exhibit a close-to-carrier f.m. noise performance very similar to that witnessed from gallium arsenide TEOs. This fact is seen in curves 1 and 2 of Fig. 6 which reveal almost identical noise-to-carrier ratios for the two materials despite the fact that the indium phosphide device generates more power at twice the efficiency of the apparently higher Q gallium arsenide device. Of course one can produce improved noise behaviour if sacrifices in power and efficiency are made as shown in the case of curve 3. However, for many systems the low output power and poor efficiency would be a severe drawback. Therefore it appears that, despite its relatively immature technology, indium phosphide already offers a competitive noise performance allied to an improved power and efficiency capability.

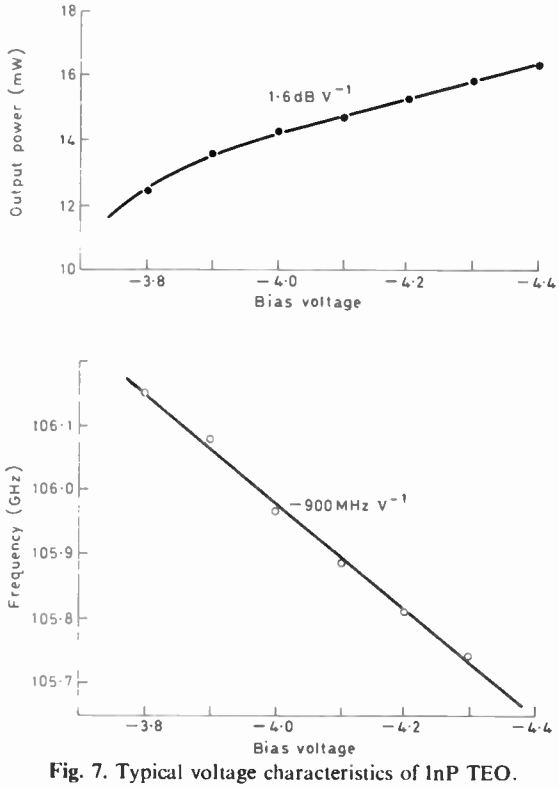

Fig. 7. Typical voltage characteristics of InP TEO.

With regard to the device voltage and temperature stability these characteristics are perhaps more clearly illustrated by considering the behaviour of a practical TEO. Figure 7 shows the output power and frequency variations with bias voltage (dP/dV and dF/dV) of a typical indium phosphide oscillator. It can be seen that, unlike gallium arsenide, this device exhibits an output power which monotonically increases with bias voltage. In fact this feature is a direct consequence of indium phosphide's more temperature stable velocity-field characteristics which results in the device output power and conversion efficiency being relatively insensitive to active layer temperature and hence input power. Further, this more stable velocity-field characteristic is evidenced in the device performance with temperature which shows a power and frequency variation (dP/dT

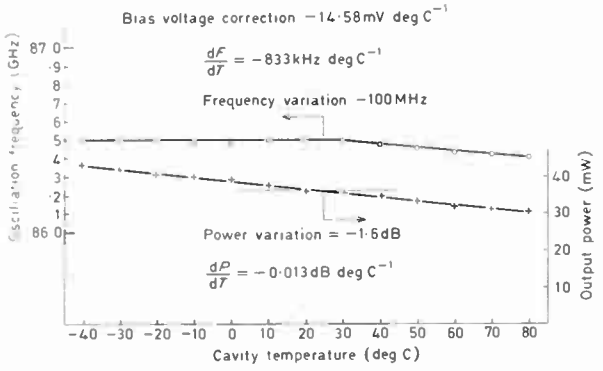

Fig. 8. Output characteristics of temperature compensated InP TEO.

and dF/dT) of −0·013 dB deg C^{-1} and −8 MHz deg C^{-1} respectively.

Although all these 2nd-order parameters are perfectly compatible with existing gallium arsenide TEO performances the linear voltage pushing behaviour of indium phosphide local oscillators could prove a real benefit to the system designer. Since there are no difficulties associated with frequency and power maxima, linear electronic bias voltage control can be simply implemented with indium phosphide TEOs. Thus for example frequency temperature compensation to track a known transmitter temperature drift becomes possible using basic electronic bias voltage control techniques.

Just such an approach has been used during the development of an indium phosphide mm-wave high stability oscillator. Shown in Fig. 8 is the compensated frequency and power performance of the oscillator over a −40 to +80 C temperature range. Here a bias voltage temperature correction of −14·58 mV deg C^{-1} has resulted in an overall output power variation of −0·013 dB deg C^{-1} and a frequency variation of −830 kHz deg C^{-1} for a 120 C temperature range. This type of characteristic is clearly superior to any currently available gallium arsenide W-band TEO performance.

Finally Table 3 presents comparison of the performance data for a harmonic mode gallium arsenide and a fundamental frequency indium phosphide device operating in the popular 94 GHz window. These data clearly demonstrate that indium phosphide can provide a higher power, more efficient alternative to the existing gallium arsenide TEO with similar stability parameters.

5 Conclusions

The results presented clearly support the theoretically expected advantages of indium phosphide over gallium arsenide as a TEO material. In addition to the greater output powers, better efficiencies and higher frequency capability, it has been shown that indium phosphide TEOs exhibit stability parameters compatible with system design needs. We therefore conclude that it should be possible to develop stable high power, efficient mm-wave oscillators with good bias tuning behaviour using indium phosphide n^+-n-n^+ devices.

6 Acknowledgments

The authors acknowledge with gratitude A. M. Howard and D. M. Brookbanks for their consistent support, advice and encouragement and P. L. Giles for provision of high quality epitaxial material. We are also indebted to T. J. Simmons and D. C. Smith for their help with the f.m. noise facility and to M. W. Geen for the provision of the results shown in Fig. 8.

This work has been carried out with the support of Procurement Executive, Ministry of Defence, sponsored by DCVD.

Table 3.

Parameter	Gallium arsenide (TEO273)	Indium phosphide
Frequency GHz	94	94
Output power mW	15	30
Input power W	5·2	1·8
dF/dV (±0·2 V) MHz V^{-1}	±300†	−640
dP/dV (±0·2 V) dB V^{-1}	±0·6†	+2·0
dF/dT (25–50 C) MHz deg C^{-1}	−6	−8·0
dP/dT (25–50 C) dB deg C^{-1}	−0·03	−0·012
Q_e	300‡	100

† Device operating at frequency and power maxima.
‡ Harmonic mode can give anomalously high Q_e values.

7 References

1 Kroemer, H., 'Hot electron relaxation effects in devices', *Solid State Electronics*, **21**, pp. 61–7, 1978.
2 Fawcett, W. and Hill, G., 'Temperature dependence of the velocity/field characteristic of electrons in InP', *Electronics Letters*, **11**, pp. 80–1, 1975.
3 Crowley, J. D. *et al.*, 'High efficiency 90 GHz InP Gunn oscillators', *Electronics Letters*, **16**, pp. 705–6, 1980.
4 Eddison, I. G. *et al.* '60 GHz high efficiency InP pulsed TEO', *Electronics Letters*, **17**, pp. 948–9, 1981.
5 Brookbanks, D. M., Griffith, I. and White, P. M., 'Integral heat sink contacts for cw indium phosphide transferred electron oscillators and amplifiers', I.O.P. Conf. Ser. No. 22, pp. 116–22, Institute of Physics, London, 1974.
6 Lubzens, D., 'Photoetching of InP mesas for production of mm wave transferred electron oscillators', *Electronics Letters*, **13**, pp. 171–3, 1977.
7 Eddison, I. G. *et al.*, 'Efficient fundamental frequency oscillation from millimetre wave indium phosphide n^+-n-n^+ transferred electron oscillators', *Electronics Letters*, **17**, pp. 758–60, 1981.
8 Eddison, I. G. and Brookbanks, D. M., 'Operating modes of millimetre wave transferred electron oscillators', *Electronics Letters*, **17**, pp. 112–3, 1981.
9 Simmons, T. J. and Smith, D. C., 'Direct measurement of fm noise in 80 GHz solid-state oscillators', *Electronics Letters*, **18**, pp. 308–9, 1982.

Manuscript received by the Institution on 26th May 1982.
(Paper No. 2056/CC 362)

UDC 621.372.622:621.382.23.029.65

Indexing Terms: Semiconductor diodes, Schottky, Electronic circuits, mixers

The development of millimetre wave mixer diodes

M. J. SISSON, B.Sc., M.Sc., Ph.D.*

SUMMARY

A new format gallium arsenide beam lead diode has been developed which allows the total capacitance to be reduced sufficiently for applications throughout the millimetre waveband. The design involves the use of low melting point glass and has high mechanical strength for ease of handling. Metal-organic chemical vapour deposition has been used to provide the thin epitaxial layer required to minimize series resistance in the device. Typical measurements from many batches are total capacitance at zero bias 0·03 pF, including 0·02 pF stray capacitance, series resistance 6 Ω and breaking force 4·5 g. The millimetre wave performance of the diodes has been demonstrated in microstrip mixer circuits operating at 90 GHz and 140 GHz. The microstrip single-ended mixer at 140 GHz extends the technology already established up to 100 GHz and includes a single crystal quartz substrate. The conversion loss of balanced mixers at 90 GHz is typically 6·5 dB and the single-ended mixer at 140 GHz displayed a loss of 7·0 dB.

* *The General Electric Company plc, Hirst Research Centre, Wembley, Middlesex HA9 7PP.*

1 Introduction

The exploitation of millimetre waves for radar systems has been the subject of research and development for many years. In the first investigations relatively large valve-based systems were constructed which employed waveguide components and the receiving elements were point-contact silicon diodes of the type developed by Ditchfield[1] and Sharpless.[2] These devices consisted essentially of a piece of silicon which was contacted by a tungsten whisker positioned across the waveguide and as mixers were able to produce a conversion loss of, for instance, 7 dB at 55 GHz.

There was a lull in the activity until a number of major developments caused a renewal of interest in the 1970s. Firstly, the arrival of microwave integrated circuit technology suggested the possibility of building compact systems. This, together with the availability of solid-state oscillators, would allow the construction of lightweight radars so enabling the potential advantages of the small millimetre wave antennas to be realized.

Secondly, detailed studies of the atmosphere had revealed a series of low attenuation transmission windows. This helped to establish the optimum frequencies for long range radiometry or alternatively for short range, covert radars. Thirdly, an increased understanding of the physics of metal semiconductor contacts led to the use of the Schottky barrier diode for microwave detection and mixing. Such devices showed a marked improvement in sensitivity compared with the point-contact diodes and could be tailored for use at any particular frequency. This latter feature was greatly facilitated by the arrival of the technology for growing epitaxial semiconductor material.

Many of the early microwave integrated circuits were based on either stripline or open microstrip for the transmission medium and their hybrid construction demanded the development of a new generation of receiving diodes since the whisker contacted diode was incompatible with such circuits. With the aim of developing a chip carrier which could be readily attached to open microstrip circuits the leadless inverted device (l.i.d.) was devised. The l.i.d. shown in Fig. 1 consisted of a ceramic carrier in which the semiconductor chip was soldered. The Schottky barrier which formed the rectifying junction was contacted by a thermocompression bonded fine gold wire of diameter ~7 μm. The device was applied successfully to a number of mixer circuits[3] at frequencies between about 1 and 12 GHz but was limited by the inductance associated with the package.

At about the same time people started to develop a new concept in device packaging in which there was no conventional encapsulation for the chip but contacts were made by planar gold plated leads. The beam leads were an integral part of the device construction and enabled the chips to be thermocompression-bonded directly into printed or integrated circuits. The idea stemmed from the work by Lepselter[4] who applied it to silicon integrated circuit chips and multi-beam leaded chips have since become standard components in the integrated circuit industry.

The application of beam leads to microwave devices

0033–7722/82/110534+09 $1.50/0

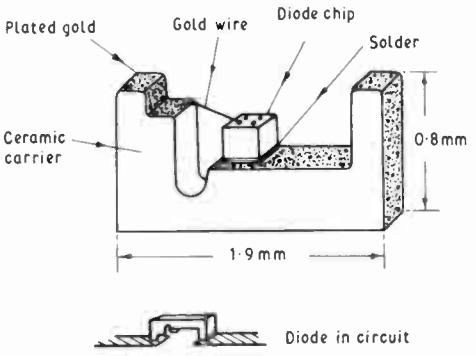

Fig. 1. Diagram of the l.i.d. diode.

required special consideration because of the inherent capacitance associated with the beams. Beam lead microwave diodes were reported for silicon mixers by Cerniglia *et al.*,[5] for germanium tunnel diodes by Davis and Gibbons[6] and by Oxley and Swallow[7] and Iizuka[8] for gallium arsenide mixer diodes.

Against this background the radio astronomers have steadily improved the performance of the whisker type of device in conjunction with waveguide circuitry. This has been achieved by changing to the semiconductor gallium arsenide and making closely packed arrays of Schottky barriers on one surface of the chip. The chip is positioned on one side of the waveguide wall and the finely pointed whisker is advanced from the opposite side until it contacts one of the Schottky barriers. Alternatively the chip and whisker are contained in a Sharpless wafer type of assembly. This technology has enabled whisker diodes to be applied throughout the millimetre waveband as has been shown by Schneider,[9] Held,[10] Vizard[11] and Keen.[12] Keen reports that for diodes with zero bias capacitance in the region of 0·01 pF the room temperature conversion loss is typically 6·0–6·5 dB at 115 GHz.

The present work stems from the beam lead diode developments originally reported by Oxley and Swallow[7] and indicates how the technology has improved sufficiently to allow the diodes to be designed for use at least to 300 GHz. After consideration of relevant theoretical aspects the practical implementation of the diodes is described. The performance of the devices in a number of millimetre wave integrated circuits is reported together with an indication of how the technology can be developed further.

2 Design Considerations

The basic requirements for a mixer diode are well understood and have been described previously for instance by Oxley.[13] The fundamental sensitivity parameter of the mixer is the overall noise figure given by:

$$F = L_c(F_{if} + t - 1) \qquad (1)$$

where the diode-related parameters are conversion loss L_c and noise temperature ratio t, and F_{if} is the noise figure of the following i.f. amplifier.

The conversion loss essentially is the loss incurred in the diode in converting the signal power from r.f. to i.f. It is related to the conductances present between the various signals present in the mixer and its value is set by the type of circuit used for mixing and how effectively the unwanted harmonics generated by the mixer are terminated. For the image matched case the basic loss of a resistive mixer is predicted to be about 3 dB. The conversion loss is however degraded by the parasitic elements of resistance, capacitance and inductance associated with the diode.

To understand where these elements arise consider Fig. 2 which shows the beam lead diode in its simple conceptual form and also the equivalent circuit of the device as mounted in a microstrip mixer. The series resistance R_s and the junction capacitance C_j are associated with the rectifying barrier and it has been shown (by considering the signal power absorbed by the barrier resistance R_b) that in its simplest formulation their contribution to minimum conversion loss is proportional to $(1+2\omega R_s C_j)$. This indicates that the $R_s C_j$ product must be made as small as possible and should furthermore be increasingly small as the operating frequency $(=\omega/2\pi)$ increases. An alternative view of the importance of the product is to consider the cut-off frequency f_{co} defined as $1/2\pi R_s C_{j0}$ where C_{j0} is the zero bias junction capacitance which again shows that for high-frequency operation the product should be minimized.

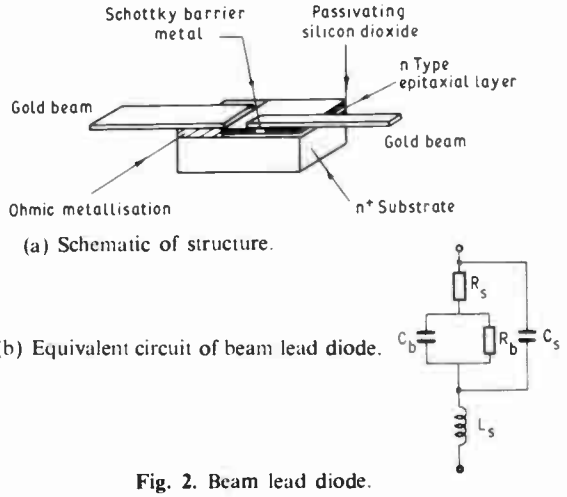

Fig. 2. Beam lead diode.

For the beam lead diode, however, the principal problem is that of ensuring that the power reaches the diode in circuit by preventing the reflection of power by the stray capacitance C_s and series inductance L_s. There are two possible sources of series inductance for a diode attached to a microstrip circuit. In general the width of the beams is different from the width of the microstrip feeder and there is therefore a discontinuity inductance at either end of the gap in which the diode is placed. Experiments carried out with a low-frequency circuit at 1.5 GHz have revealed that this inductance is much less than that caused by the change in width of the microstrip line at the diode. The resulting shift in characteristic impedance due to the short length of line equivalent to the length of the diode was equivalent to an inductive reactance. The tests were performed on relatively thick

alumina substrates and at 1·5 GHz it was found that the inductance due to the change in characteristic impedance was approximately ten times that of the discontinuity itself. In designing a beam lead diode circuit it is clearly important to make the diode gap as narrow as possible and to tailor the width of the beams to match the line width as closely as possible.

Referring to Fig. 2 it can be seen that the source of stray capacitance is the parallel plate configuration between the conducting substrate and the anode beam which lies on top of the surface passivation film of oxide. The capacitance appears in parallel with the junction. The options open for reducing the stray capacitance are an increase in the thickness of the passivating film, a change to a lower dielectric constant medium for the film or the reduction in contact area for the anode beam. All of these factors are considered in designing a diode for a particular frequency.

Although the equivalent circuit of Fig. 2 implies a complex impedance for the incoming r.f. signals the values of capacitance and inductance required for operation at a particular frequency can be estimated from the series resonant frequency ω_{res} of the circuit. ω_{res} is given approximately by:

$$\omega_{res} = 1/\{L_s(C_s+C_j\}^{\frac{1}{2}} \tag{2}$$

and it is desirable for the r.f. admittance of the diode to be in the region of series resonance in operation. If it is possible to evaluate L_s from the beam and circuit dimensions then the required junction capacitance can be calculated if the configuration of the anode beam is known.

The junction capacitance of a Schottky barrier diode of area A at zero bias is given by:

$$C_{j0} = A\left(\frac{\varepsilon q N_d}{2V_d}\right)^{\frac{1}{2}} \tag{3}$$

where ε is the relative permittivity of the semiconductor, N_d is the semiconductor doping level, V_d is the diffusion potential of the barrier and q is the electronic charge.

Using the series resonant frequency and calculated values for L_s and C_s, equation (3) for capacitance can therefore give an indication of the doping level and area required for the diode.

Other factors must, however, be considered in determining these design parameters more precisely. In particular, the series resistance tends to increase as area A decreases and therefore for a minimum value of R_sC_j an optimum value must be sought for N_d and A.

For a beam lead diode the series resistance is composed of contributions from the undepleted epitaxial layer, R_{epi}, from spreading resistance in the substrate, R_{sub}, from contact resistance between the ohmic contact and the substrate R_c, and if high frequency operation is envisaged from the influence of skin effect, R_{skin}, thus:

$$R_s = R_{epi}+R_{sub}+R_c+R_{skin}. \tag{4}$$

The effect of R_{skin} would not of course be observed at d.c. where series resistance is normally measured.

$$R_{epi} = \frac{1}{N_d q\mu}\cdot\frac{(t-x)}{A} \tag{5}$$

where t is the epitaxial layer thickness, x is the voltage dependent depletion layer width and μ is the semiconductor mobility.†

For a beam lead diode the spreading resistance must be calculated for the case of collection by an adjacent planar contact concentric with the junction. This has been expressed for $t < a$ as:

$$R_{sub} = \frac{\rho}{2\pi a}\tan^{-1}\left(\frac{b}{a}\right) \tag{6}$$

where ρ is the resistivity of the substrate, a and b are the radii of the barrier junction and collecting ohmic electrode respectively.

The fact that the collecting electrode for the beam lead diode is semicircular has been estimated to add no more than 25% to R_{sub} since most of the voltage drop occurs very close to the small circular junction.

The contact resistance R_c is determined by the specific contact resistance which can be achieved for the ohmic contact and is then inversely proportional to contact area.

For millimetre wave applications it is necessary to consider the influence of the skin effect which constrains the current to flow within a narrow channel close to the surface at high frequencies. The skin depth is frequency dependent and is given by:

$$\delta = \left(\frac{\rho}{\pi f m}\right)^{\frac{1}{2}} \tag{7}$$

where m is the permeability of the substrate material.† For a device well matched to the microwave circuit δ has been shown to add the contribution to R_s of:

$$R_{skin} = \frac{\rho}{2\pi\delta}\ln\left(\frac{b}{a}\right). \tag{8}$$

The total series resistance can thus be calculated from equations (5), (6) and (8), assuming that the specific contact resistance of the ohmic contact is known. Ideally for low series resistance the diode should display the characteristics of a Mott barrier diode, i.e. be fully depleted so that the contribution R_{epi} is zero. In practice, however, epitaxial technology cannot produce a perfectly sharp well-defined transition from active layer to substrate and there is a significant resistance from the interface layer. Also the diodes are generally forward biased when used in millimetre wave mixers to reduce the consumption of local oscillator power. Hence the term R_{epi} tends to dominate the series resistance.

From the equation for C_j and R_{epi} it is now possible to use the design criterion originally devised by Messenger and McCoy[14] which shows that the product R_sC_j is proportional to $t\varepsilon^{\frac{1}{2}}/N_d^{\frac{1}{2}}\mu$. For GaAs it can be shown[15] that the optimum doping level to produce a minimum value of R_sC_j is greater than 10^{19} carriers per cm^3. Since this would, however, produce an unacceptably low breakdown voltage the choice of N_d must ultimately be determined on the basis of ensuring that the diode can be driven without breaking down in the reverse direction.

† μ is used here for semiconductor mobility and m for permeability to avoid confusion although μ is the conventional symbol for the latter.

The dependence of breakdown voltage on carrier concentration is established in the literature[16] for ideal junctions. In practical terms, however, allowance must be made for the fact that the diode is unlikely to have the avalanche breakdown characteristics of an abrupt junction. To achieve a reverse breakdown voltage of greater than, say, 2 V in GaAs the doping level of the epitaxial layer should therefore be about 10^{17} carriers per cm^3. Having selected this value of doping level the junction area is now fixed in accordance with the r.f. considerations of equation (2), via equation (3), for junction capacitance.

Referring again to equation (1), the noise temperature ratio t is defined as the ratio of the noise generated by the diode to that generated by a resistor equal to the barrier resistance. Its value depends on the intermediate frequency at which the mixer is operating and is normally close to unity for i.f.s greater than about 1 MHz. It has been found experimentally that t is dependent on the factor n which appears in the relationship between current and voltage for a Schottky barrier diode and indicates the departure from ideal conduction:

$$I = I_0\left(\exp\frac{qV}{nkT} - 1\right) \qquad (9)$$

where I_0 is the saturation current of the diode,
k is Boltzmann's constant
and T is absolute temperature.

For an ideal Schottky barrier $n = 1$ but it has been found that there is no serious degradation in t for diodes with n in the range 1 to 1·2.

Below 1 MHz low frequency noise causes t to increase approximately inversely with frequency for GaAs.

3 Millimetre Wave Diode Design

It is now possible to illustrate how the foregoing design considerations have been used for the millimetre wave beam lead diode.[17] The aim was to produce a diode primarily for applications in different microstrip mixer circuits operating in the attenuation windows centred at 90 and 140 GHz. Early gallium arsenide beam lead diodes[7] were based on the conceptual diagram of Fig. 2 and reduction in stray capacitance was achieved by narrowing the anode as shown in Fig. 3 and making the passivating oxide as thick as possible. The consequence of this was that the beam strength relied on a narrow

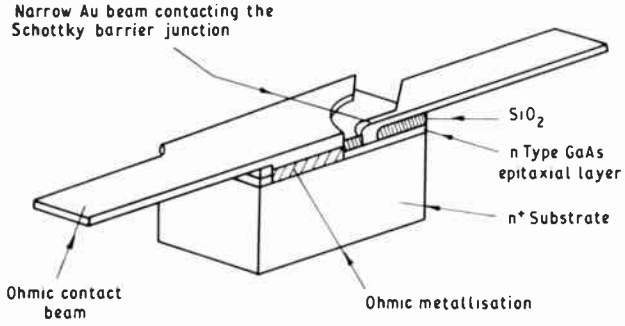

Fig. 3. 1970 beam diode for 12–18 GHz showing capacitance reduction by narrowing the anode beam.

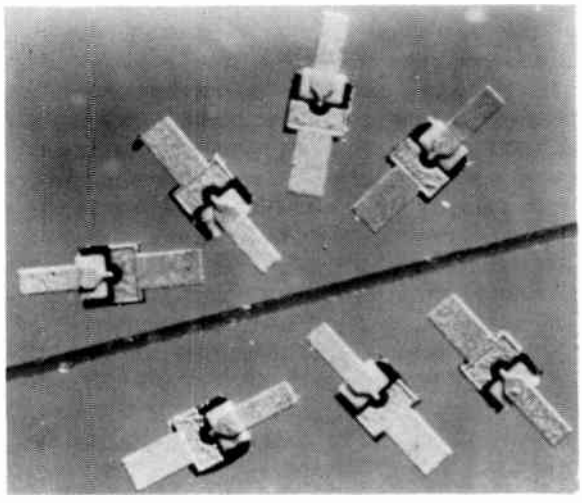

Fig. 4. Beam lead diodes with glass dielectric layer to reduce capacitance and maintain mechanical strength. Human hair shown for comparison.

finger of plated gold of about 100 μm^2 in cross section. Although this enabled the stray capacitance to be small (~0·05 pF) it did present problems in actual device handling.

Because of the mechanical problems a programme of work took place in 1977 to improve the strength of the diodes whilst maintaining the same electrical characteristics. A photograph of diodes produced at that time is shown in Fig. 4 and shows the technique which was adopted to allow the area of contact of the beam to the chip to be increased. A deep trough was etched into the gallium arsenide beneath the anode beam and this was subsequently filled with low melting point glass. The thick layer of low dielectric constant material allowed the stray capacitance to be the same as for the narrow beam diode but with a much improved mechanical strength. The force required to break the diode when bonded into a microstrip circuit increased from less than 0·5 g to greater than 2 g.

In designing the millimetre wave diode the question of mechanical strength was therefore regarded as being of fundamental importance. A sketch of the diode is shown in Fig. 5 and shows that the use of glass has been extended to surround completely the gallium arsenide chip. The strength of the device is thus in the glass and this has allowed the GaAs to be thinned much more than in previous diodes and to be removed totally from beneath the anode beam. A further consequence is that the rectifying junction can be placed immediately next to the glass edge thus minimizing the stray capacitance around the junction.

A 250-times scale model of the beam–glass–GaAs structure was built in order to estimate the stray capacitance and to optimize the shape of the beams. A diagram of the experimental arrangement and the results obtained are illustrated in Fig. 6. It was found that the stray capacitance was divided approximately equally between the narrow beam surrounding the junction and the broad part of the beam. The best compromise of beam shape, position and width predicted a total stray

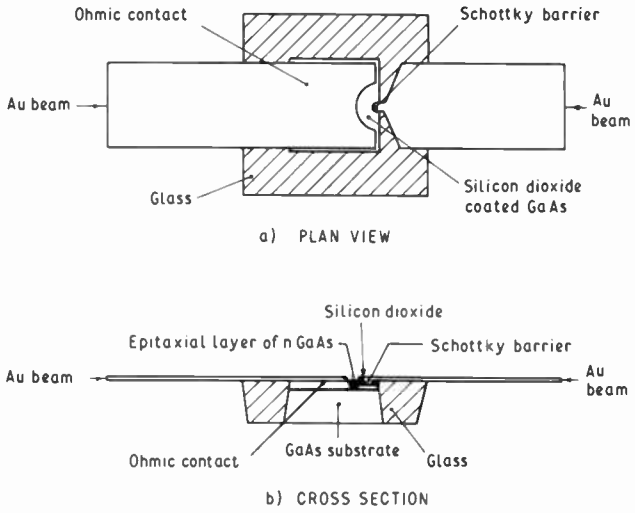

Fig. 5. Schematic diagram of the millimetre wave beam lead diode.

capacitance of about 10 fF for a beam width of 100 μm.†

With this information it was now possible to estimate the series inductance of the diode in a microstrip circuit in accordance with the 1·5 GHz modelling experiments. The microstrip circuit for 140 GHz was to be constructed from *Z*-cut single crystal quartz of thickness 100 μm. The width of a 50 Ω characteristic impedance feeder line was 205 μm. Selecting a gap of 200 μm to accommodate the diode chip it was calculated that the reactance equivalent to a length of line of width 100 μm would be 100 Ω at 140 GHz, giving a series inductance of 0·1 nH.

To ensure millimetre wave operation of the diode, it was now possible to use equation (2), in conjunction with the information on L_s and C_s to find the required junction capacitance. In series resonance the total capacitance, C_{t0} should be 31 fF at 90 GHz or 13 fF at 140 GHz. It was decided to aim for a C_{j0} of 10 fF which would give a $C_{t0}(=C_s+C_{j0})$ value of 20 fF. From equation (3), the required junction diameter should therefore be about 3 μm for a typical diffusion voltage of 0·75 V in the Schottky barrier.

It has been assumed that a circular contact is the optimum shape for the barrier. Other workers[18–21] have experimented with the alternative of a rectangular contact in the shape of a narrow finger. For millimetre wave applications the dimensions required would be 10×1 μm^2. This structure has the advantage that the barrier can be positioned close to the ohmic contact which is favourable from the point of view of spreading resistance and skin effect. However, there is additional complexity in defining such a narrow finger particularly if the gallium arsenide surface is to be passivated in the vicinity of the junction. It is known that passivation is advantageous for withstanding the environmental conditions likely to be experienced by real circuits and therefore a circular rectifying contact was preferred.

The diode design required that the epitaxial layer should be as thin as possible. The thickness of layer available is limited by the growth technology. At present high mobility layers of GaAs can be grown controllably to a thickness of about 0·1 μm which is also equal to the zero bias depletion width of 10^{17} cm^{-3} doped GaAs.

On the basis of a circular contact, the various contributions to series resistance for a 0·1 μm layer have been calculated for junction diameters 2, 2·5 and 3 μm using equations (5) and (6), and are given in Table 1. The calculation is for a typical d.c. measurement condition of 20 mA forward bias.

Table 1

Resistance	Diameter (μm) 2	2·5	3
Contact	0·25 Ω	0·25 Ω	0·25 Ω
Spreading	2·11	1·49	1·38
Undepleted epi at 20 mA forward bias	4·77	3·05	2·12
Total	7·13	4.79	3·75

The calculation assumes that the technology exists for making a low specific resistivity ohmic contact. The spreading resistance is for a typical substrate resistivity of 0·7 mΩ cm and for an ohmic contact radius of 20 μm. The mobility in the epitaxial layer has been taken to be 4000 cm^2 V^{-1} s^{-1} at 10^{17} cm^{-3} doping.

In addition to the figures quoted in the Table there is a contribution due to skin effect from equation (8) of 0·66 Ω at 94 GHz or 0·76 Ω at 140 GHz which would only become apparent in the millimetre wave circuit.

† 1 femtofarad (fF) = 10^{-15} F = 10^{-3} pF.

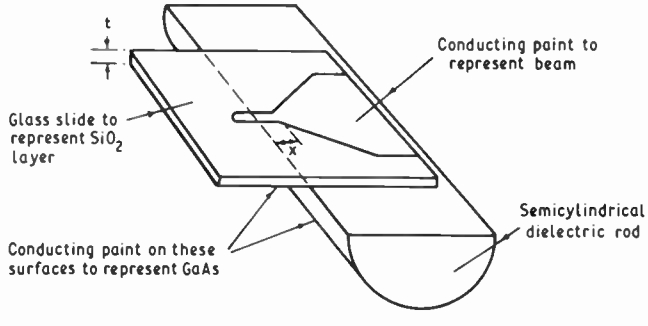

C_s fF			
X μm	t = 0·5 μm	t = 1 μm	t = 3 μm
0	19	12	8
5	15	10	7
10	11	8	6
15	7	6	4

Stray capacitance C_s as a function of length X and oxide thickness t.

Fig. 6. Scale model experiment for calculation of stray capacitance.

4 Practical Implementation

4.1 Technology

Epitaxial layers for the millimetre wave diode were grown on commercially obtained GaAs substrates by the method of metal organic chemical vapour deposition (m.o.c.v.d.).[22] Substrate resistivities were in the range 0·6 to 0·8 mΩ cm. The doping level in the epitaxial layer was in the range $1–2 \times 10^{17}$ cm^{-3} and the target thickness

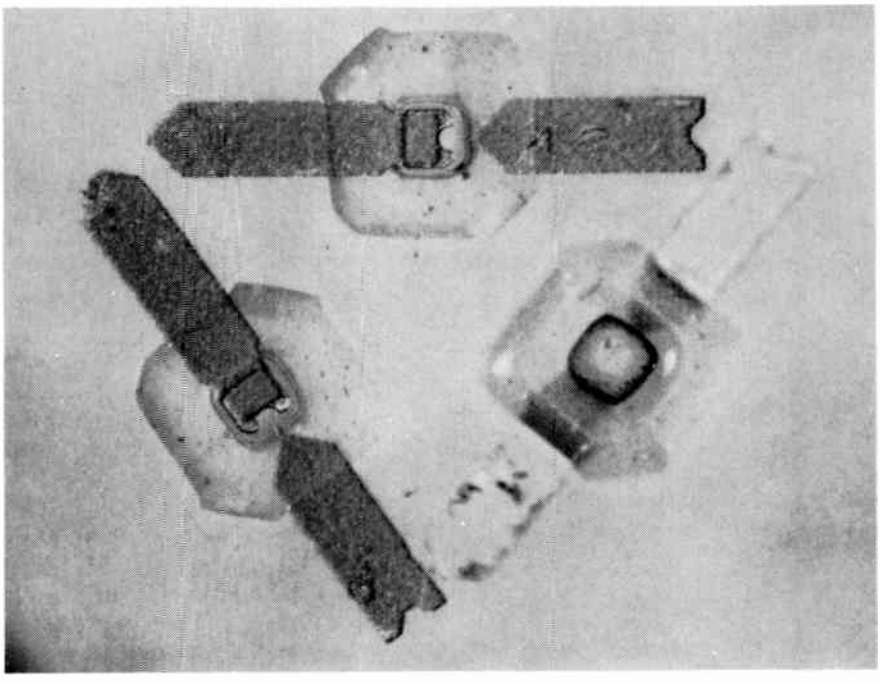

Fig. 7. Millimetre wave GaAs beam lead mixer diodes type DC1346.

was 0·1 μm. In some cases the layers were grown thicker than this and were then thinned to 0·1 μm by anodization. The use of m.o.c.v.d. allowed good control of deposition rate and sharp interfaces to the substrate were noted. For some slices a low resistivity buffer layer was included between substrate and active layer although this did not significantly affect device performance.

The main features of the process were then as follows:

(i) Etch deep moats into the GaAs.
(ii) Fill with low melting point glass and deposit a surface layer of SiO_2.
(iii) Apply the ohmic contact metallization of AuGeNi.
(iv) Define the active area window (diameter 2·5 μm) in the SiO_2.
(v) Deposit the barrier metal.
(vi) Define and electroplate the beam leads.
(vii) Thin from the back surface and separate the devices by etching.

The glass was selected to be a good expansion match to GaAs, to have a melting point which would prevent dissociation of the GaAs and to have a low dielectric constant and loss tangent. A suitable borosilicate glass was found and the dielectric properties were measured as a function of frequency using the waveguide method of Sucher and Fox.[23] At 90 GHz the dielectric constant was found to be 7·5 and the loss tangent was 0·014 indicating that there would not be significant dielectric loss at that frequency.

After a number of experimental runs AuGeNi was found to give the lowest specific contact resistance to the n^+ GaAs substrate, a typical result being $5 \times 10^{-6}\ \Omega\,cm^2$. The contribution to series resistance from contact resistance was measured to be about 0·25 Ω.

Figure 7 is a photograph showing some of the completed diodes. Overall length of the diodes is 800 μm and the width of the central glass region is 300 μm.

4.2 Results

D.c. and low-frequency evaluation of the devices was carried out with the aid of a test jig consisting of a microstrip line with a suitable gap for the diode. The diode was held in position across the gap with an insulating probe which applied pressure to the beam leads only. The forward conduction characteristics displayed good linearity over the range 10^{-9} to 10^{-3} A when plotted in the form log I_F against V_F.

The results of measuring C_{t0}, C_s, R_s, V_B and n value are summarized in Table 2 which also includes typical results for earlier GaAs beam lead diodes for comparison. Design values of the present diode, referred to as DC1346, are also included. The cut-off frequency f_{co} has been calculated from C_{j0} and R_s. The results are average values taken from many processing batches.

The mechanical strength of the diodes was assessed by thermocompression bonding a number of them into a test fixture, inserting a small hook under the body of the diode and raising the hook with a controlled force. The breaking strength was found to be in the range 4–5 g and the principal failure mode was the fracture of the gold plated beams at the edge of the glass body.

5 Microwave Evaluation

Circuits for the microwave evaluation of the diodes have been based on the microstrip type of mixer discussed by Oxley[24,25] and Scarman,[26] who have applied hybrid open microstrip techniques on quartz to circuits operating up to 100 GHz. Pairs of the new diode have been tested in conjunction with a number of balanced mixers operating in the vicinity of 90 GHz. Typical

Table 2

		Present diode, DC1346				
		Design	Measured (typical)	DC1309 DC1339	DC1308 DC1338	DC1306
Diameter	μm	3	2–3	3	6·5	7
C_{t0}	pF	0·02	0·03	0·055	0·08	0·1
		range: 0·02–0·04				
C_s	pF	0·01	0·02	0·04	0·04	0·05
C_{j0}	pF	0·01	0·01	0·015	0·04	0·05
R_s	Ω	3·75	6	10	6·5	5
		range:	4–10			
V_B	V	> 2	4			
n		1	1·15			
f_{co}	GHz		2650	~ 1000	~ 700	~ 600

Notes:
C_s was the typical capacitance of an open circuit diode.
C_{j0} by difference between C_{t0} and C_s.
R_s measured at 20 50 mA forward current.
V_B measured at 10 μA reverse current.

Diodes DC1309, DC1308 and DC1306 were designed primarily for use at 60–90 GHz, 26 40 GHz and 12–18 GHz respectively. DC1339, DC1338 and DC1306 are glass strengthened devices.

conversion losses are in the range 6·5 to 7·0 dB with local oscillator drive of 10 mW and bias per diode of 0·5 V.

The technology of open microstrip has now been applied to circuits operating at 140 GHz.[27] Because of its low loss and low dispersion characteristics, Z-cut single crystal quartz was again selected for the substrate material. This had the additional advantage that it was thermally compatible with metals such as copper, brass and nickel and hence allowed the substrates to be soldered to metal jigs for assembly. The substrates were thinned to 100 μm before deposition of the microstrip patterns by conventional photolithographic techniques.

Transition from waveguide to microstrip was by means of a five-step ridge built into the end of the guide (WG29). The same design principles were used for the transitions as for the earlier microstrip circuits. The inherent loss of the 50 Ω characteristic impedence microstrip lines was assessed by constructing different lengths of line and measuring the insertion loss including a pair of transitions. The loss was found to be equivalent to 0·1 dB per millimetre of line at 140 GHz.

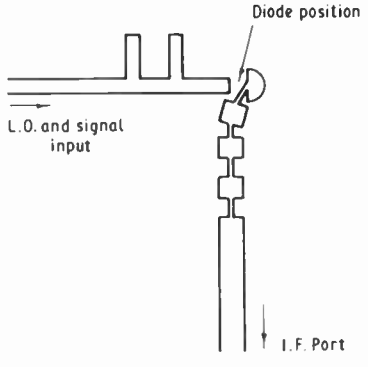

Fig. 8. Microstrip single-ended mixer pattern printed on 100 μm thick Z-cut quartz.

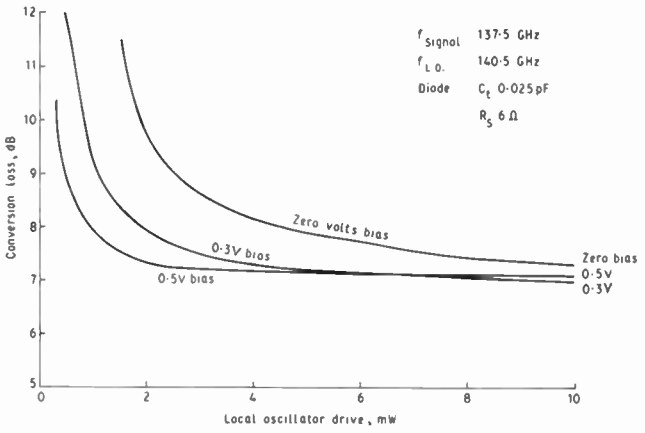

Fig. 9. Conversion loss v. l.o. power for single-ended mixer. Diode bias voltage as parameter.

A single-ended microstrip mixer circuit has been developed principally for the purpose of diode assessment. The main elements of the circuit are illustrated in Fig. 8 which shows that the r.f. input line is terminated behind the diode by a quarter wavelength r.f. short circuit pad. A twin-stub tuner was employed on the r.f. input line to bring the centre frequency of the mixer to 140 GHz. The high impedance elements of the high–low r.f. filter on the i.f. output line were optimized in length to give an r.f. insertion loss of 6 dB per section at 140 GHz. Extensive measurements have been made of conversion loss and r.f. input match and the results are illustrated in Figs. 9 and 10 for a diode of total capacitance 0·025 pF and series resistance 6 Ω. Figure 9 shows conversion loss as a function of local oscillator power for different diode bias voltages. The signal sources employed were a carcinotron local oscillator and a klystron for the r.f. signal. Figure 10 shows conversion loss and input match (return loss) as a function of signal frequency. The rectification efficiency at the optimum conversion loss of 7 dB was 1·2 mA per mW. It was found that there was no significant difference in conversion loss for intermediate frequencies in the range 1 to 4 GHz.

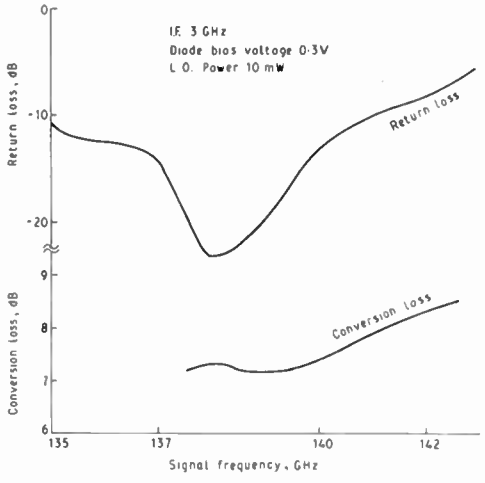

Fig. 10. Return loss and conversion loss v. frequency for single-ended mixer.

The measurements were repeated for a number of diodes with capacitances taken from the range 0·02 to 0·04 pF and typical conversion losses were between 7·5 and 8·5 dB at 140 GHz. The conversion loss was measured by direct measurement of the r.f. and i.f. powers available at the mixer input and output ports respectively.

6 Discussion

The application of the glass wall technology to beam lead diodes has enabled the parasitic elements of capacitance and resistance to be reduced significantly compared with earlier types (Table 2). Furthermore, this has been achieved with an improvement in the mechanical strength of the device. The stray capacitance is slightly higher than predicted and has been found to be critically dependent on the control of the oxide thicknesses and the beam lead plating at the junction.

Alternatives to the glass wall approach to producing low capacitance beam lead diodes have been explored by other workers. In particular, Immorlica,[19] Murphy[20] and Calviello[21] have produced diodes made on semi-insulating substrates which then become the low-loss dielectric supports for the beam leads. With this approach it was necessary to grow an n^+ buffer layer followed by the n-type active layer and ohmic contact was made to the n^+ layer. For this type of device it was essential to employ a finger-type barrier contact rather than a circular junction to minimize skin effect losses at the operating frequency. In general the n^+ layer thickness employed was about 5 μm and to isolate the diode areas within the layer proton bombardment was used. Thus the GaAs was completely semi-insulating apart from the localized areas where the diodes were defined. A slight modification was explored by Ballamy and Cho[18] who interposed a layer of silicon dioxide between the substrate and n^+ layer in the region outside the diode. The epitaxial layers were grown by molecular beam epitaxy and it was found that the gallium arsenide was polycrystalline and therefore semi-insulating on top of the silicon dioxide. Thus a structure similar to the proton-isolated device was produced. Although these techniques have produced low stray capacitance of about 0·02 pF it is suggested that capacitance reduction is likely to be limited ultimately by the relatively high dielectric constant of GaAs (12·5) compared to alternatives such as glass.

Other dielectrics have been considered as a means of reducing the parasitic stray capacitance. In particular Harada and Fukuda[28] have manufactured beam lead diodes for application at 12 GHz in which the top surface of the diode is coated with a 5 μm thick film of polyimide prior to electroplating the beam leads. The stray capacitance of the devices was typically 0·03 pF. This may be a candidate material for use at millimetre wave frequencies and preliminary work in this laboratory has shown that the dielectric properties are suitable. The dielectric constant of an addition type polyimide measured at 90 GHz was 3·0 with a loss tangent of 0·012. Parrish[29] has developed millimetre wave diodes in which the anode beam is supported on top of a 2–3 μm thick glass film. The junction characteristics are similar to the present diode but the mechanical strength of the diode reported here is incorporated in a 30 μm thick glass wall around the diode chip.

Millimetre wave operation of the diode as a mixer has been demonstrated in microstrip circuits at both 90 and 140 GHz. The high cut-off frequency of 2650 GHz represents a degradation in conversion loss in the region of 1 dB up to 140 GHz. This must be added to the fundamental loss of 3 dB for an image matched mixer. Compared with the measured losses of 6·5 dB at 90 GHz or 7·5 dB at 140 GHz the contribution from the junction is small showing that the design aims for the diode have largely been achieved. Thus other factors associated with the circuit, such as diode matching and the termination of unwanted harmonics, determine to a large extent the conversion loss achieved in practice.

Similar performance has been reported in a suspended strip line mixer operating at 140 GHz by Cardiasmenos[30] who claimed an overall noise figure of 8·9 dB with $F_{if} = 1·5$ dB (s.s.b.) implying a conversion loss of 7·4 dB assuming a noise temperature ratio of 1. For the present diode, the noise temperature ratio has not been degraded by a high n value. Thus it is expected that the noise temperature ratio of the mixer at normal intermediate frequencies will be close to unity and the overall noise figure of the diodes in millimetre wave circuits will be determined essentially by the conversion loss and the i.f. amplifier noise figure.

Although the diode was designed primarily for microstrip circuits it has been applied successfully to suspended stripline circuits for 90 GHz and 140 GHz in this laboratory, and has also been used as a groove guide detector at 100 GHz.[31] In all cases the important advantages associated with the beam lead diode of ruggedness, ease of handling and the ability to pre-select were maintained. The diode technology is adaptable for other circuit configurations and could readily be extended for the manufacture of integrated units of pairs or quads of diodes.

7 Conclusions

The interest in millimetre wave integrated circuits has led to the development of a new type of GaAs beam lead diode. The new diode has been designed with the aim of achieving low parasitic capacitance and yet maintaining the good mechanical strength required for rugged systems. The technology is based on a thick glass wall structure around the GaAs chip which supports the beam leads and produces a stray capacitance of only 0·02 pF. Series resistance has been reduced by employing m.o.c.v.d. epitaxial layers to give improved control of layer thickness such that the diodes are of the Mott–Schottky barrier type. Typical device parameters are total capacitance 0·03 pF, series resistance 6 Ω and breakdown voltage 4 V. The series inductance is determined by the relative geometries of diode and embedding circuit and was calculated to be 0·1 nH in the 140 GHz test mixer. The force required to break a diode which has been bonded into circuit is typically 4·5 g.

Further reductions in stray capacitance are predicted through the use of a lower dielectric constant material as a substitute for or in addition to the glass.

The millimetre wave performance of the diodes has been demonstrated in a number of microstrip mixers. At 90 GHz the conversion loss of a balanced mixer was 6·5 dB whilst at 140 GHz a single mixer based on a single crystal quartz substrate has been developed to give a conversion loss of 7·0 dB. In each case a forward bias of 0·5 V was applied to the diodes.

8 Acknowledgments

The author would like to thank Messrs P. N. Wood, D. G. Monk, A. M. Hansom and P. J. Magdani for assistance with the experimental work and Mr C. S. Brown and Dr J. E. Curran for discussions on some of the theoretical aspects of the work.

This work has been carried out with the support of Procurement Executive, Ministry of Defence, sponsored by DCVD.

9 References

1 Ditchfield, C. R., 'Crystal mixer design at frequencies from 20 000 to 60 000 Mc/s', *Proc. Instn Elect. Engrs*, **100**, pp. 365–71, 1953.
2 Sharpless, W. M., 'Wafer type millimetre wave rectifiers', *Bell Syst. Tech. J.*, **35**, pp. 1385–1402, 1956.
3 Oxley, T. H., Summers, J. G. and Hansom, A. M., 'The development of gallium arsenide Schottky barrier diodes', Proc. European Microwave Conference, London, September 1969.
4 Lepselter, M. P., 'Beam lead technology', *Bell Syst. Tech. J.*, **45**, pp. 233–53, February 1966.
5 Cerniglia, N. P., Tonner, K. C., Berkovits, G. and Solomon, A. H., 'Beam lead Schottky barrier diodes for low noise integrated microwave mixers', *IEEE Trans. on Electron Devices*, **ED-15**, no. 9, pp. 674–8, September 1968.
6 Davis, R. E. and Gibbons, G., 'Design principles and construction of planar Ge Esaki diodes', *Solid State Electronics*, **10**, pp. 461–72, 1967.
7 Oxley, T. H. and Swallow, G. H., 'Beam lead diodes and detector diodes for microwave integrated circuit applications', Proc. 8th International Conference on Microwave and Optical Generation and Amplification, pp. 10–31 to 10–36, September 1970.
8 Iizuka, H. and Kitaoka, S., 'Low noise GaAs Schottky barrier beam lead mixer diodes', *Proc. IEEE*, **58**, pp. 1372–3, September 1970.
9 Schneider, M. V., Linke, R. A. and Cho, A. Y., 'Low noise millimetre wave mixer diodes prepared by molecular beam epitaxy', *Appl. Phys. Letters*, **31**, pp. 219–21, 1977.
10 Held, D. N. and Kerr, A. R., 'Conversion loss and noise of microwave and millimetre wave mixers', *IEEE Trans. on Microwave Theory and Techniques*, **MTT-26**, pp. 49–61, 1978.
11 Vizard, D. L., Keen, N. J., Kelly, W. M. and Wrixon, G. T., 'Low noise millimetre wave Schottky barrier diodes with extremely low local oscillator power requirements', IEEE MTT-S, Symposium Digest, Orlando, 1979.
12 Keen, N. J., 'Low noise millimetre wave mixer diodes: results and evaluation of a test programme', *Proc. Instn Elect. Engrs*, **127**, pt. I, pp. 188–98, August 1980.
13 Oxley, T. H., 'Variable Impedance Devices', chap. 4 (Wiley, New York, 1977).
14 Messenger, G. C. and McCoy, C. T., 'Theory and operation of crystal diodes as mixers', *Proc. IRE*, **45**, no. 9, pp. 1769–83, September 1957.
15 Sisson, M. J., 'The development of microwave receiving diodes', Ph.D. Thesis, University of London, 1976.
16 Sze, S. M., 'Physics of Semiconductor Devices' (Wiley, New York, 1969).
17 Sisson, M. J., British Patent Application No. 7927031, 1979.
18 Ballamy, W. C. and Cho, A. Y., 'Planar isolated GaAs devices produced by molecular beam epitaxy', *IEEE Trans. on Electron Devices*, **ED-23**, no. 4, pp. 481–4, April 1976.
19 Immorlica, A. A. and Wood, E. J., 'A novel technology for fabrication of beam leaded GaAs Schottky barrier mixer diodes', *IEEE Trans. on Electron Devices*, **ED-25**, no. 6, pp. 710–3, June 1978.
20 Murphy, R. A. and Clifton, B. J., 'Surface oriented Schottky barrier diodes for millimetre and submillimetre wave applications', 1978 International Electron Devices Meeting Digest, pp. 124–7, December 1978.
21 Calviello, J. A., Wallace, J. L. and Bie, P. R., 'High performance GaAs beam lead mixer diodes for millimetre and submillimetre applications', *Electronics Letters*, **15**, no. 17, pp. 509–10, August 1979.
22 Glew, R. W., 'A comparison of H_2S and H_2Se n-type doping of GaAs by MOCVD', International Symposium on GaAs and Related Compounds, Japan, 1981.
23 Sucher, M. and Fox, J., 'Handbook of Microwave Measurements', vol. 2, chap. 9 (Polytechnic Press, Brooklyn, 1963).
24 Oxley, T. H., Ming, K. J., Swallow, G. H., Climer, B. J. and Sisson, M. J., 'Hybrid microwave integrated circuits for millimetre wavelengths', IEEE G-MTT International Microwave Symposium Digest, 1972.
25 Oxley, T. H., 'Millimetre mics rely on hybrid open microstrip', *Microwave Systems News*, **9**, no. 9, p. 75, September 1979.
26 Scarman, R. E., Lowbridge, P. L. and Brigginshaw, P. M., 'Millimetre-wave components of hybrid open microstrip form', Proceedings Military Microwaves MM-80, London, pp. 75–81, October 1980.
27 Sisson, M. J. and Brigginshaw, P. M., 'Microstrip developments at 140 GHz', Digest of 5th International Conference on Infrared and Millimetre Waves, Wurzburg, p. 115, October 1980.
28 Harada, Y. and Fukuda, H., 'A novel beam lead GaAs Schottky barrier diode fabricated by using thick polyimide films', *IEEE Trans. on Electron Devices*, **ED-26**, no. 11, pp. 1799–1804, November 1979.
29 Parrish, P. T., Cardiasmenos, A. G. and Galin, I., '94 GHz beam lead balanced mixer', *IEEE Trans. on Microwave Theory and Techniques*, **MTT-29**, no. 11, pp. 1150–9, November 1981.
30 Cardiasmenos, A. G., 'Practical mics ready for millimetre receivers', *Microwave Systems News*, **10**, no. 8, pp. 37–51, August 1980.
31 Harris, D. J. and Mak, S., 'Groove guide microwave detector for 100 GHz operation', *Electronics Letters*, **17**, no. 15, pp. 516–7, July 1981.

Manuscript received by the Institution on 1st June 1982
(Paper No. 2057/CC 363)

UDC 621.396.677.75.029.65: 621.396.96: 623.454.254

Indexing Terms: Antennas, planar, Waveguides, microstrip, Radar, military

A survey of millimetre-wavelength planar antenna arrays for military applications

A. HENDERSON, B.Sc., Ph.D.*

and

Professor J. R. JAMES, B.Sc., Ph.D., D.Sc., FIMA, CEng, FIERE, FIEE*

SUMMARY

The growing interest in the use of millimetre wavelengths for radar and communication systems stems principally from military requirements. Conventional component technology utilizing waveguides continues to feature but strenuous efforts are being made to devise new fabrication methods that lend themselves to further miniaturization, integration and cost saving. There is also a demand for a new generation of antenna types and this paper critically examines the progress made on planar antenna arrays using dielectric guides and substrate technology. Conclusions are reached on the feasibility of satisfying current system demands based throughout on published literature. It is conjectured that although the new planar devices have many performance shortcomings compared to conventional antennas, cost, weight and size advantages are significant and could in some cases bring new system concepts for submunition systems.

* *Department of Electrical and Electronic Engineering, Royal Military College of Science, Shrivenham, Swindon, Wilts. SN6 8LA.*

1 Introduction

A new generation of military systems including radars, radiometers, navigational and communications equipment is now being developed at millimetre wavelengths. No doubt many new millimetre wave system requirements will eventually arise in the civil sector but at present the demand is essentially of a military nature and this review is necessarily from the military standpoint. The advantages associated with the use of millimetre wavelengths arise both from the propagation aspects and the compactness of the antennas. The small size of the electronic equipment enables radiometry and radar acquisition to be employed on small missiles and submunitions in addition to the other more conventional installations on battlefield vehicles and guns. The term 'submunition'[1,2] refers to various types of small guided explosive projectiles. The use of millimetre wavelengths allows high spatial resolution to be obtained from an electronic package of smaller volume. Also penetration of fog and smoke is possible for operation in the propagation windows at 94, 140 and 220 GHz. For communications, use is also made of the high attenuation bands for security using line-of-sight transmission; 60 GHz is the commonly used frequency[6–8] for such purposes.

One might imagine that the antennas required by these new millimetre wave systems could be developed by scaling down in size such types as reflector and horn antennas which have been extensively engineered for the microwave bands. While this is indeed true for some millimetre wave systems, it is not generally the case particularly above 90 GHz, due to tolerance problems and costly manufacture. Where antennas are required to be conformal to a vehicle surface or concealed in a radome assembly for example, on a projectile or submunition[1,2] millimetre wave reflector and horn antennas are often too bulky and expensive particularly where some form of beam scanning is required. Figure 1 illustrates the relative shapes of the newer types of planar arrays and a conventional horn. Beam scanning can be achieved by either mechanical or electronic means, or a combination of both, and this requirement places severe constraints on the type of antenna which may be employed and on the method of connecting the feed circuits. For conformal applications, ideally the receiver/transmitter circuitry needs to be integrated as far as possible with the antenna structure and current trends in antenna design have been considerably influenced by the advances in semiconductor diode and source devices.

It is for the above reasons that increasing attention has been paid to developing new classes of low profile substrate-based planar antennas that can be flush-mounted on vehicles and missiles and can possibly allow some degree of circuit integration together with additional means of electronic scanning by semiconductor implants or frequency sweeping. Microstrip antennas[3] are obviously one type to consider but the main research effort has been directed towards dielectric guide antennas because these have intrinsically less loss at millimetre wavelengths than guides containing metal.

 0033–7722/82/110543+08 $1.50/0

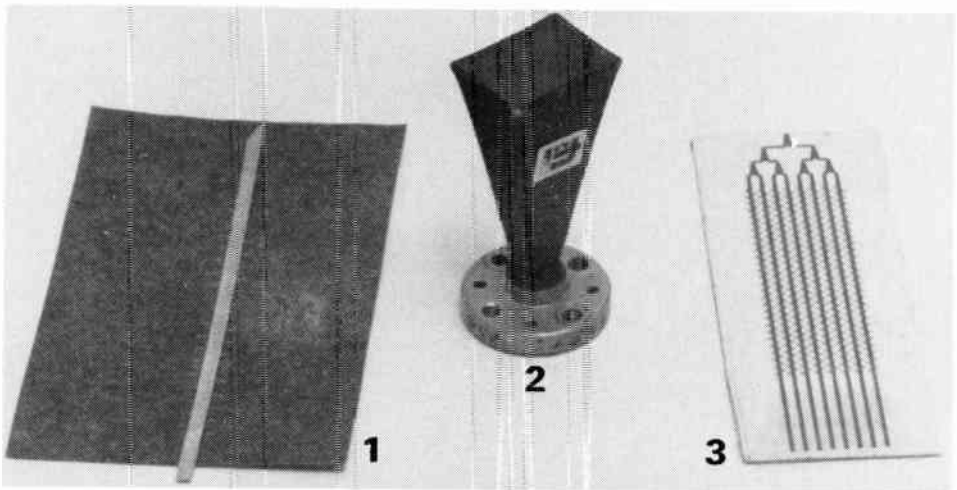

Fig. 1. Typical 70 GHz planar arrays, compared with metal horn. 1. Hybrid microstrip array as described in Fig. 9. 2. Conventional horn. 3. Alumina microstrip array with corporate feed as described in Fig. 6.

A large number of different forms of novel planar antenna structures have been devised but their fully developed capabilities are not yet realized and consequently their applicability to various systems requirements is not clear. For instance, it is becoming apparent that the new types of dielectric guide antennas are not physically compatible with conventional waveguide feeds which are still predominantly used at millimetre wavelengths. Radiometry demands wider bandwidth than radar systems and antenna efficiency will be important in some applications, while the integration of active or passive elements with the antenna would seem to favour a microstrip or waveguide type of antenna array to facilitate bias circuits etc. On the other hand, dielectric guides lend themselves to integrated optical techniques with semiconductor components grown into the structure[4, 5] which could be useful at the higher frequencies.

These are some of the many questions facing designers of new types of planar millimetre wave antennas. The purpose of the present paper is to critically review the new range of antennas currently available, giving due consideration to the demands of present day system requirements and to make recommendations for the future. Information about system requirements, antenna types and their properties are collated, in tabular form for clarity of presentation and an extensive bibliography is given.

2 System Requirements

The military applications at millimetre wavelengths fall broadly into six categories:

- radar
- radiometry
- seekers in large missiles
- electronic warfare
- submunitions, shells and small missiles
- communications

It is useful to extract as far as is possible the general antenna requirements for each of the categories mentioned and this is done in Table 1. The chosen frequency of operation will depend upon several parameters, such as the maximum antenna size allowable physically to achieve a specified resolution, the range of the target and whether an active or passive system is required.

Generally speaking the antenna specifications are constrained by both the rate of information being retrieved and the extent to which operation is being interfered with by enemy jammers. For instance a radar bandwidth of 100 MHz may be sufficient for many applications but if several channels are needed to escape from selective jamming, much larger bandwidths are demanded. Low sidelobe levels and good cross-polarization rejection may also be dictated by jamming requirements. Frequency scanning as a means of beam positioning would clearly be difficult to implement in such circumstances.

For radiometry, jamming cannot be tolerated and is unlikely to be a consideration but the need for very wide bandwidths make the antenna specification difficult. Antenna losses could also be an important issue as a source of unwanted noise whereas in many radar applications this would not matter if the incoming signal levels were high enough and the loss of efficiency was compensated for by additional semiconductor transmitting devices.

Seeker systems are housed in missile heads where limited space constrains antenna performance but for close-in acquisition the system demands may not be

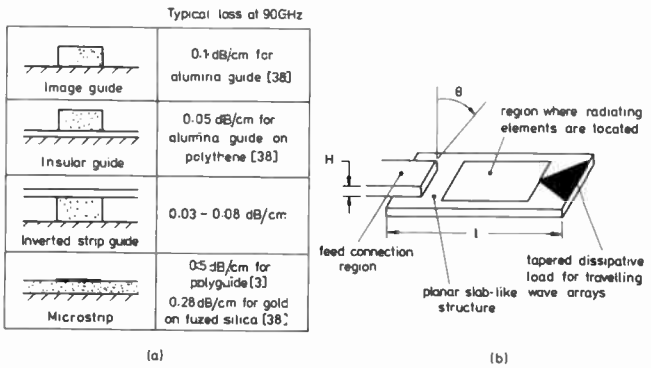

Fig. 2(a) Types of millimetre guide used in planar antenna arrays. (b) General outline shape of millimetre linear array. Dimension H depends on nature of launching device which is the transition region between the feeder line and antenna.

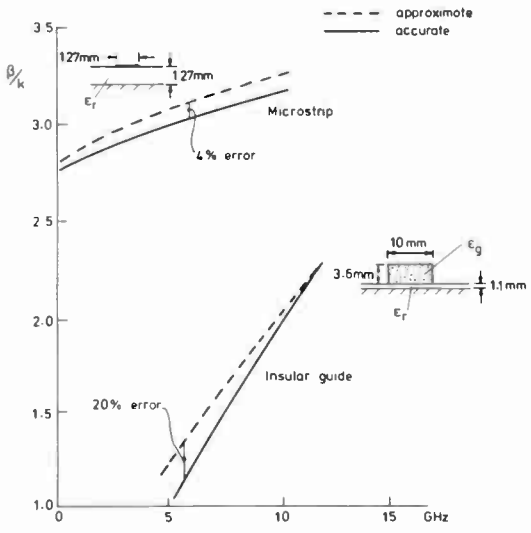

Fig. 3. Propagation coefficients for microstrip ($\varepsilon_r = 9{\cdot}7$) and insular guide ($\varepsilon_g = 10$, $\varepsilon_r = 2$) calculated by approximate and accurate techniques.

quite as critical as in high sensitivity radars. Communication systems have functions very different from those of radar yet the antenna specifications are equally demanding.

Submunitions[1, 2] are a challenging new area where attempts are being made to fit small projectiles with radar, radiometry and communication facilities. Much ingenuity is required and above all the antennas must be physically compatible with the submunition body.

In Section 3 the planar arrays available at the present time are discussed and their likely area of usage is considered in Section 4.

3 Survey of Antenna Concepts and Types

The planar antenna arrays for millimetre wavelengths published to date can be broadly characterized as—

- purely dielectric guides and radiating elements particularly suited for use at the upper millimetre band.
- metal radiating elements and/or metal-based elements, such as microstrip.

Most of the antennas mentioned in this paper are manufactured out of one of four types of open waveguide media—image guide, insular guide, inverted strip and microstrip, which are shown in Fig. 2(a). The outline shape of all the planar antennas is indicated in Fig. 2(b) and the launching transition matches the antenna to the

Table 1

System requirements for antenna arrays in military applications

System	Typical antenna requirement	Frequency band
Radar	1. Resolution determines gain > 30 dB 2. Sidelobes < −25 dB 3. Antenna efficiency > 80% 4. Frequency scanning possibly	35, 94, 140, 220 GHz
Radiometry	1. Gain > 30 dB 2. Sidelobes < −30 dB 3. Beam scanning, multi-beam operation 4. Wideband operation required for good image resolution 5. Low-loss antenna to reduce noise temperature	35, 94, 140, 220 GHz
Seekers	1. Gain ~ 30 dB 2. Sidelobes < −15 dB 3. Efficiency not critical 4. Frequency scanning possibly 5. Low cost	35, 94, 140, 220 GHz
Electronic warfare	1. Hemispherical coverage 2. Bandwidth ~5%	35, 60, 94, 140, 220 GHz
Submunitions	The requirements are similar to those above for radar, radiometry, electronic warfare and seekers, but the size and weight constraints are more severe.	
Communications	1. Beamwidth and system power budget set gain required 2. Low sidelobes < 25 dB for security and jamming protection 3. Large bandwidth for frequency hopping techniques (~ 5%) 4. Lightweight, compact 5. Cross-polarization could be a constraint, circularly polarization possibly desirable	60 GHz

Table 2

Planar array performances at millimetre wavelengths

Type	Reference	Efficiency and bandwidth	Number of elements	Pattern properties		
				Main beam	Sidelobes	Gross-polarization
Purely dielectric elements	(i) [12]		17	−26 at 15 GHz	−10 dB at 15 GHz −6 dB end-fire contribution	
	(ii) [11]†		12	20	−11·5 dB	
Microstrip planar arrays	(i) [20] comb-line	23% efficient including corporate feed at 70 GHz 3·5% bandwidth	8 × 60	Broadside	−13 dB	
	(ii) [22] patch		32 × 32	Broadside	−20 dB at 38 GHz	
Dielectric guides with metal elements	(i) [26]			−20	−8 dB	
	(ii) [32]		32	Broadside	−13 dB contributed by launcher at 70 GHz	Up to −10 dB of main beam level
	(iii) [34]		20	Broadside	−12 dB	
	(iv) [36]†	~ 50% efficient	5 × 20	−20	−25 dB at 33 GHz −20 dB contributed by launcher	
Conventional waveguide slot array	[37]	0·4% bandwidth for > −10 dB return loss. Surface roughness gives some attenuation	20	Broadside	~ −13 dB at 60 GHz	

† Indicates that absorbent material was used on launcher.

feeder with as little reflection or radiation loss as possible. These antennas are generally of a travelling-wave variety with a terminating load but resonant versions can be designed without the lossy load at the expense of a reduction in bandwidth.

The purely dielectric guides have less power loss at millimetre wavelengths than microstrip, as indicated in the Figure, and it is for mainly this reason that these guides are of interest. With microstrip, the main concentration of field is under the metal strip and ground-plane which together contribute the principal loss. Inverted strip and insular guide reduce the loss in the ground-plane by shifting the concentration of field into the dielectric regions by a suitable choice of permittivity and dimensions and therefore can have less loss than the simple image guide. There are however no closed form solutions for the propagation coefficients for both microstrip and dielectric guides and this complicates the design of antennas constructed from these open guides. Microstrip is much easier to quantify using approximate formulas.

Figure 3 shows the propagation coefficient $\beta(=2\pi/\lambda_g)$ values for microstrip and insular guide calculated by both approximate[3(p. 33),9] and more accurate formulations[10] for a high permittivity material; λ_g is the guide wavelength.

It is clear that formulation of the insular guide by approximate means can give very large errors in comparison with the microstrip case and this can make antenna array design calculations very inaccurate. For instance, an inaccuracy in β of 1% would result in an aperture phase error of $\pm 36°$ at the end of a $10\lambda_g$ travelling-wave microstrip array and is unacceptable for some specifications.[3]

Most of the arrays are designed from either a leaky-wave or a discrete element approach but in the final design no clear distinction exists. In the case of leaky-wave arrays it has been found necessary to use a tapered aperture distribution for high performance given that any array has to be finite in length.

A leaky-wave antenna ideally consists of an infinitely long series of perturbations made into a guiding structure and each individual element radiates a small proportion of the power travelling along the guide. Assuming that the perturbations are periodic, a beam is radiated at an angle θ to broadside determined by

$$\sin\theta = \lambda_0\left[\frac{1}{\lambda_g}+\frac{m}{d}\right]$$

λ_0 is the wavelength in free space, d is the distance between each perturbation and m is usually taken as -1.

If the frequency is changed then the angle of the beam

is shifted accordingly and it is, in principle, a simple operation to produce beam scanning; the extent to which this can be achieved is examined later on.

In contrast, the antenna can also be modelled as a linear array of discrete elements. The nature of the element is determined for the discontinuity in question, for example, a dielectric notch, metal strip or microstrip stub and patch, and mutual coupling can, in principle, be allowed for but is difficult to implement for more than 2 adjacent elements and is seldom addressed.

A summary of the performances of the main millimetre wave planar arrays is given in Table 2.

3.1 Purely Dielectric Arrays

These antennas have on the whole been derived from integrated optical techniques and have an intrinsic low loss. They are not at present easy to manufacture except possibly by thick film techniques[11] and cannot be made by simple etching processes as used for their metal counterparts which are described in Section 3.2. Thick film processing is discussed in a further paper by Gelsthorpe et al. in this issue.

Itoh[12] in 1977 reported measurements of one of the first dielectric grating structures for use at millimetres, whereby notches were cut out of an inverted strip dielectric guide as shown in Fig. 4. Measurements were made only at around 15 GHz on scaled-down versions of 60 GHz antennas and no indication of power loss could be given at the millimetric frequencies. The array had a beam off-broadside at 26° and sidelobes of −10 dB; a 15% frequency shift gave a 16° beam shift. Problems were encountered due to the termination of the antenna length and a large amount of energy was end-fired; additional unwanted radiation was contributed by the launcher. No further improvements in antenna performance have been reported using this construction which could be due to difficulties encountered in deriving useful design criteria, in view of the complicated radiation mechanisms involved.[13] Further analytical results have been given by the same author on simulated electronic scanning which gave a similar beam shift capability[14] to that of frequency scanning techniques.

One further type has been reported by Birand and Gelsthorpe[11] which consists of an insular guide with a uniform array of dielectric elements as shown in Fig. 5. Measurements at 35 GHz gave a main beam at 20° from broadside with −11·5 dB sidelobes. Again no indication of losses was given nor were any attempts at manufacturing a higher performance array published consequently. Birand and Gelsthorpe observed a 16° beam shift for only a 7% change in frequency. An alternative technique for electronic scanning using artificial dielectric materials has been analysed by Bahl and Bhartia[15] who predict that this method gives more beamwidth control than frequency scanning for large scan angles. No measurements were presented.

The optimum performance that could be obtained from these purely dielectric arrays has possibly yet to be realized; perhaps a more accurate analysis[11] of the radiating discontinuities would be beneficial and may also throw some light on the cross-polarization levels to be expected from these devices. Recent calculations by Peng and Oliner[16] have indicated that these could be highly significant.

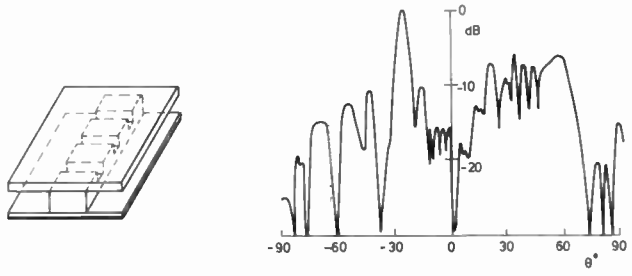

Fig. 4. Inverted strip leaky-wave array (Itoh[12])

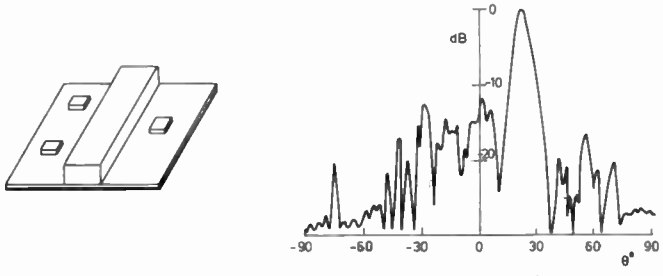

Fig. 5. 35 GHz insular guide array with dielectric radiating elements (Birand[11] and Gelsthorpe[11])

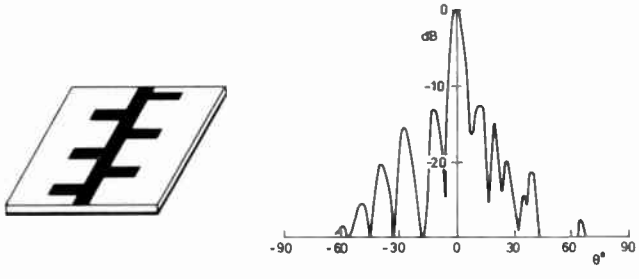

Fig. 6. 70 GHz microstrip travelling wave array (Hall *et al.*[20])

3.2 Arrays Incorporating Metal Radiating Elements or Slots

Microstrip antenna arrays are an obvious candidate for use at millimetre wavelengths and although it is generally reckoned that the power losses may well be excessive, particularly above 90 GHz, there is a well-established technology at microwave frequencies which is advantageous.[17–19] One of the earliest two-dimensional millimetric arrays was constructed by Hall *et al.* at 70 GHz where sidelobe levels of −13 dB were measured, as shown in Fig. 6, but very accurate antenna efficiency measurements were not possible. Estimations made indicated that losses were not greatly in excess of those experienced with similar microstrip antennas at microwave frequencies. Williams[21] using a 16 × 16 element cross-fed array claimed a radiation efficiency of 60% at 36 GHz with −20 dB sidelobes. More recently Weiss[22] has constructed a 32 × 32 element array at 60 GHz and showed that pattern control was difficult due to tolerance problems but that on a 4 × 4 array, the power losses incurred at 60 GHz were no worse than in a scale model at 38 GHz. The performance of the 32 × 32

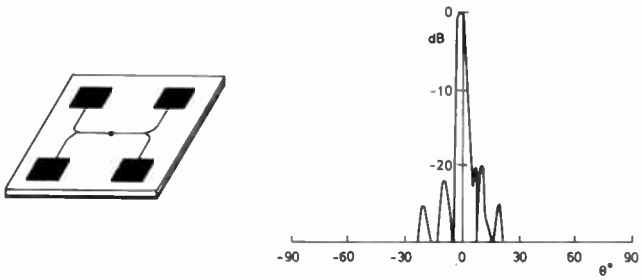

Fig. 7. 38 GHz 32 × 32 element microstrip patch array (Weiss[22])

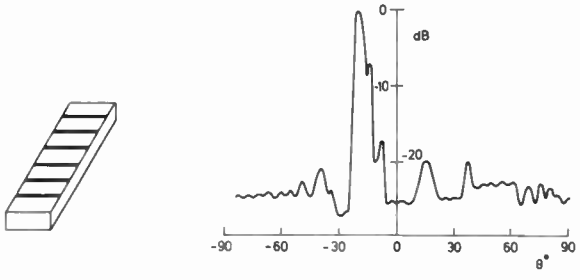

Fig. 8. Metal grating on dielectric guide (Kobayashi *et al.*[26])

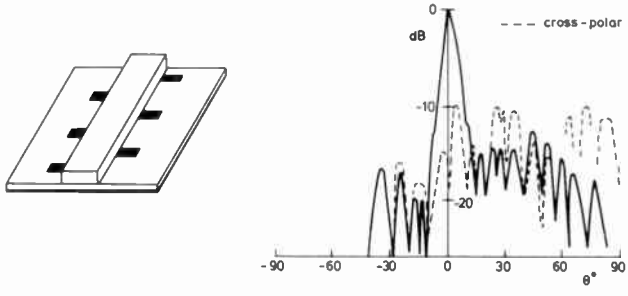

Fig. 9. 70 GHz hybrid microstrip/insular guide array (Henderson *et al.*[32])

element patch array at 38 GHz is shown in Fig. 7.

Microstrip antennas do however have a clear advantage over dielectric arrays in that there is a well-established technology in triplate feed systems. Because of the high metal line loss, alternative configurations to microstrip are being devised which still retain the metal radiating elements and can be easily etched off dielectric substrates using photolithographic techniques. Some of the earliest work on arrays of this type was done by Klohn *et al.*[23] using a silicon waveguide and based on leaky-wave gratings. Measurements at 58 GHz showed that very small dissipative losses were incurred but that as the beam was brought to broadside by frequency scanning, a severe mismatch resulted. The pattern had very poor sidelobes at −6 dB but good frequency scanning capabilities. Electronic scanning using implanted p-i-n diodes[24] proved to be difficult to control and further work has been done more recently on simulating these effects.[25] Analytical work by Kobayashi *et al.*[26] and Mittra and Kastner[27] has improved upon the performances of the metal grating antennas with −8 dB sidelobes previously reported but with large contributions to the radiation patterns from the launchers, as shown in Fig. 8. More recently improvements in horn launcher design[28,29] and the use of a long tapered aperture distribution[30] has resulted in −20 to −25 dB sidelobes. The beamwidth in the orthogonal plane may be reduced by incorporating a horn along the length of the grating but is not strictly planar in construction.[31]

Henderson *et al.*[32] describe a hybrid microstrip array where the lossy microstrip feeder line has been replaced by a dielectric insular guide yet retaining the metal radiators as shown in Fig. 9. A −13 dB sidelobe level was reported with a broadside beam at 70 GHz but no exact figures are yet available on antenna efficiency although it was observed that launcher radiation would be sufficient to seriously degrade the pattern of a high performance array. Cross polarization levels were high and this could be a prohibitive factor.

More recently, Itoh[40] has modified an image guide metal grating array by enclosing it on three walls by metal waveguide, which reduces the radiation at bends and would enable a corporate feed system to be made in the future. The antenna as yet is only 5% efficient and has high sidelobes when the main beam is brought to broadside but its performance could well be further improved by increasing the antenna length and this antenna could then be quite a useful structure at millimetre wavelengths.

Inggs *et al.*[34] have developed a similar array using dipoles printed onto an inverted strip waveguide but it involves a more complicated structure as indicated in Fig. 10. The radiation pattern at 30 GHz had −12 dB sidelobes with a similar level of contribution at 30° to broadside from the waveguide transition/launcher. Measurements indicated that about 60% of the available power was radiated and a good match was obtained at the input.

An alternative approach to using metal strip radiators is slots or indentations in ground-planes. Hori and Itanami[35] have used the orientation of the slots in a ground-plane as shown in Fig. 11 to give circularly polarized patterns. The power is fed to the slots by a dielectric image line and they claim that the new antenna is far superior to microstrip linear arrays at millimetre wavelengths due to a much reduced line loss. The image line loss is given as 0·4 dB and the launcher loss as 0·2 dB. Solbach and Wolff[36] have used transverse slot and circular holes drilled into a ground-plane to produce some good array patterns. At 60 GHz, a transverse slot array had −19 dB sidelobes with a 4·5° beamwidth and at 33 GHz a travelling wave array with circular holes, shown in Fig. 12, had sidelobes down at −25 dB. In both cases, the launcher radiation was −20 dB which severely limited the array performance. They estimated that about 1 dB of power was lost within the antenna and 2 dB of power was dumped into the absorbing load.

In comparison to the newer types of dielectric planar arrays, a conventional slotted waveguide linear array has been manufactured using electroforming techniques by Gelsthorpe and Aylward[37] who discuss the difficulties of pattern control associated with manufacturing tolerances. The array was linear and had a side-lobe level of −13 dB and some excess losses due to surface roughness were reported.

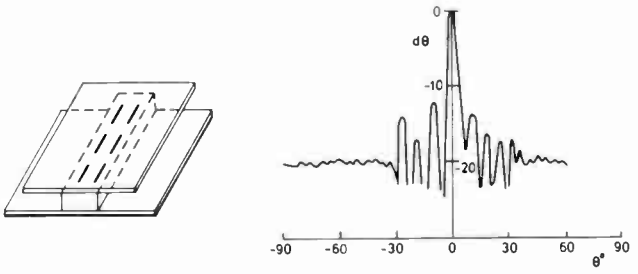

Fig. 10. 30 GHz inverted strip array with metal dipole elements (Inggs *et al.*[34])

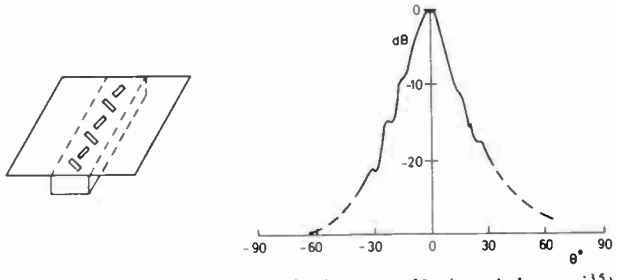

Fig. 11. 29 GHz circularly polarized array (Hori and Itanami[35]) consisting of slots cut into a ground-plane and fed by image guide

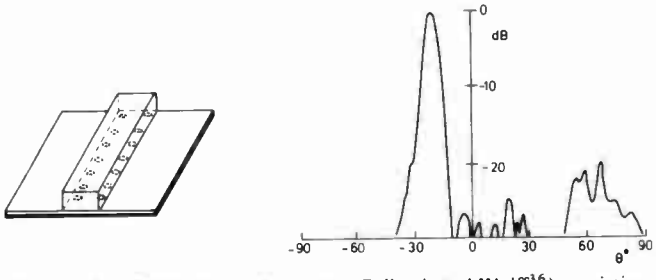

Fig. 12. 33 GHz travelling wave array (Solbach and Wolff[36]) consisting of indentations in ground-plane, fed by image guide

4 Application of New Antenna Arrays to Military Systems

The antenna types reviewed above are very new and the data available are not as complete as one would wish. Nevertheless, it is evident from a comparison of the system requirements given in Table 1 and the summary of the performances of the various antenna arrays in Table 2, that the new antenna arrays have in general a marginal performance. With the exception of microstrip antennas only linear arrays appear to have been devised, presumably due to the difficulty of designing a corporate feed in dielectric waveguide. Even if such an array were constructed, its efficiency and bandwidth would be lower than that of a reflector or horn antenna and, as in the linear array case, the sidelobe levels would be seldom better than −15 dB. Both microstrip and dielectric travelling-wave arrays can now be designed to radiate at broadside but only over a narrow bandwidth whereby the input matching condition is optimized. It is concluded therefore that the new types of arrays will only be used when space and weight economy or conformal requirements are demanded. Submunitions is an area of outstanding opportunity for these new devices particularly as the size of submunitions may well be smaller than the radiating aperture required for a specific resolution and synthetic aperture techniques can then well be an important factor in systems design.[2,39] It now remains to review the individual types more critically.

4.1 Purely Dielectric Arrays

From the evidence presented above it would appear that it is fundamentally difficult to control the radiation pattern characteristics by elements such as notches and slots in a dielectric guide, particularly over a short length. Very long antennas are needed if power is not to be wasted in the terminal load or endfired. Sidelobes are particularly poor, being very much a function of main beam squint, and cross-polarization levels are likely to be high although this aspect has not been reported fully as yet. The launching onto dielectric guides is seen to be a problem due to both the escape of unwanted radiation and the increase in the height profile of the antenna. Few precise data are available for the efficiencies of the launchers described in the literature particularly as radiation from launchers has been reduced by using absorbent material in some cases. An assessment by John *et al.*[33] cites the launcher as a major limitation for dielectric guides: this can possibly be reduced at the expense of a highly optimized horn which would be somewhat inconvenient for conformal applications. Alternatively feeding the guides from a system of similar dielectric materials would remove this launcher problem. An important conclusion here is that if transmitters and receivers were, in the future, to be constructed from dielectric transmission media, then the dielectric antennas would be compatible. These arrays, at present however, appear to offer no clear advantages, other than low transmission loss and have several drawbacks and it seems unlikely that they will find use in other than very special applications.

4.2 Dielectric Arrays with Metal Inserts

Like the purely dielectric array, these arrays have the same launching problems and have so far not been deployed as a planar array with a corporate feed. The use of metal radiating elements clearly improves the pattern control both in sidelobe level and frequency scanning performance. Little has been reported about cross-polarization properties but these are also likely to be improved. No data are available for the increase in antenna loss due to the metal inserts which clearly offsets the advantages of using dielectric guide structures.

4.3 Microstrip Antennas

These antennas have been successfully developed into a large variety of types at microwave frequencies and can be scaled down in size for millimetre applications. Unlike dielectric guide arrays, both linear and planar forms have been designed with corporate feeds[3] and a wide range of individual radiating elements capable of various polarizations and other properties have been developed.

5 Concluding Comments

1. The new types of planar millimetre wave arrays have performances which are generally inferior to conventional horn and reflector antennas and need much further design effort.

2. The new antennas will find applications where limited space is available and lower manufacturing costs are demanded such as in submunitions.
3. The use of purely dielectric antenna structures to obtain low loss does not give good radiation pattern control and the incorporation of metal radiating elements appears necessary to retain control but possibly increases the antenna loss. For low launcher loss, dielectric antennas need to be fed from a compatible feed system using similar dielectric waveguides.
4. Microstrip loss will not be an important factor in smaller arrays and feed circuits demanded by submunitions. Microstrip antennas offer the greatest design flexibility and possibly the best radiation pattern control. Two-dimensional arrays can be designed using corporate feeds.

6 References

1 Seashore, C. R. and Singh, D. R., 'Mm-wave component trade-offs for tactical systems', *Microwave J.*, **25**, pp. 41–62, June 1982.

2 Tipping, D. E. J., 'System requirements for the precision guided munition', IEE Colloquium on 'Millimetre-wave radar and radiometric sensors', 22nd April 1980, Paper 10a.

3 James, J. R., Hall, P. S. and Wood, C., 'Microstrip Antenna Theory and Design' (Peter Peregrinus, Stevenage, 1981).

4 Gulyaev, Y. V. and Lyubchenko, V. E., 'Semiconductor integrated-circuit technology in the millimeter band', *Sov. Phys. Dokl.*, **25**(2), pp. 119–120, February 1980.

5 Rosen, A. *et al.*, 'Millimetre-wave device technology', *IEEE Trans.*, **MTT-30**, no. 1, pp. 47–53, January 1982.

6 Whicker, L. R. and Webb, D. C., 'Potential military application of millimeter waves', 8th European Microwave Conference, Paris, 1978. Notes for Workshop on millimetre waves.

7 Gibbs, S. E., 'Potential for millimetre waves in radar and telecommunications', IEE Colloquium on 'Advances in millimetre-wave antennas and associated components', October 1977.

8 Hislop, A., 'A compact low cost 60 GHz communicator', IEEE MTT-S Digest, pp. 231–2. International Microwave Symposium, held in Dallas, Texas, 1982.

9 McLevice, W. V., Itoh, T. and Mittra, R., 'New waveguide structures for millimetre-wave and optical integrated circuits', *IEEE Trans.*, **MTT-23**, no. 10, pp. 788–94, October 1975.

10 Mittra, R., Hou, Y. L. and Jamned, V., 'Analysis of open dielectric waveguides using mode matching technique and variational methods', *IEEE Trans.*, **MTT-28**, no. 1, pp. 36–43, January 1980.

11 Birand, M. T. and Gelsthorpe, R. V., 'Experimental millimetric array using dielectric radiators fed by means of dielectric waveguide', *Electronics Letters*, **17**, no. 18, pp. 633–5, 3rd September 1981.

12 Itoh, T., 'Application of gratings in a dielectric waveguide for leaky-wave antennas and band-reject filters', *IEEE Trans.*, **MTT-25**, no. 12, pp. 1135–8, December 1977.

13 Itoh, T., 'Open guided wave structures for millimeter-wave circuits', invited paper of the 1981 IEEE MTT International Microwave Symposium, Los Angeles, CA, June 1981, pp. 3–4.

14 Itoh, T. and Hebert, A. S., 'Simulation study of electronic scannable antennas and tunable filters integrated in a quasi-planar dielectric waveguide', *IEEE Trans.*, **MTT-26**, no. 12, pp. 987–91, December 1978.

15 Bahl, I. J. and Bhartia, P., 'Leaky-wave antennas using artificial dielectrics at millimeter wave frequencies', *IEEE Trans.*, **MTT-28**, no. 11, pp. 1205–12, November 1980.

16 Peng, S. T. and Oliner, A. A., 'Radiation from grating antennas on dielectric waveguides of finite width', 11th European Microwave Conference, Amsterdam, 7th–10th September, 1981, pp. 757–61.

17 IEE Colloquium Digest No. 1982/19, 'Advances in printed antenna design and manufacture', 18th February 1982.

18 Mailloux, R. J., McIlvenna, J. F. and Kernweis, N. P., 'Microstrip array technology', *IEEE Trans.*, **AP-29**, pp. 25–37, January 1981.

19 James, J. R. *et al.*, 'Recent developments and trends in microstrip antennas', 2nd Military Microwaves Conference, London, 1980, pp. 309–314.

20 Hall, P. S., Garrett, C. and James, J. R., 'Feasibility of designing millimetre microstrip planar antenna arrays', Agard Conference Proceedings No. 245 on 'Millimeter and submillimeter wave propagation and circuits', held in Munich, 4–8 September 1978, pp. 31–1 to 31–7.

21 Williams, J. C., 'A 36 GHz printed planar array', *Electronics Letters*, **14**, no. 5, pp. 136–7, 2nd March 1978.

22 Weiss, M. A., 'Microstrip antennas for millimeter waves', *IEEE Trans.*, **AP-29**, no. 1, pp. 171–4, January 1981.

23 Klohn, K. *et al.*, 'Silicon waveguide frequency scanning linear array antenna', *IEEE Trans.*, **MTT-26**, no. 10, pp. 764–73, October 1978.

24 Horn, R. E. *et al.*, 'Electronic modulated beam-steerable silicon waveguide array antenna', *IEEE Trans.*, **MTT-28**, no. 6, pp. 647–53, June 1980.

25 Klohn, K. L., 'Metal walls in close proximity to a dielectric waveguide antenna', *IEEE Trans.*, **MTT-29**, no. 9, pp. 962–6, September 1982.

26 Kobayashi, S., Lampe, R. and Mittra, R., 'Dielectric rod leaky-wave antennas', Proc. Intl. Symposium on Antennas and Propagation, Quebec, June 2nd–6th, 1980, Vol. 1, pp. 31–4.

27 Mittra, R. and Kastner, R., 'A spectral domain approach for computing the radiation characteristics of a leaky-wave antenna for millimeter waves', *IEEE Trans.*, **AP-29**, pp. 652–4, July 1981.

28 Malherbe, J. A. G., Trinh, T. N. and Mittra, R., 'Transition from metal to dielectric waveguide', *Microwave J.*, **23**, no. 11, pp. 71–4, November 1980.

29 Trinh, T. N., Malherbe, J. A. G. and Mittra, R., 'A metal-to-dielectric wave-guide transition with application to millimetre-wave integrated circuits', Conf. Rec. 1980 Microwave Theory Tech. Soc. Int. Microwave Symp., pp. 205–207.

30 Kobayashi, S., Lampe, R., Mittra, R. and Ray, S., 'Dielectric rod leaky-wave antennas for millimeter-wave applications', *IEEE Trans.*, **AP-29**, no. 5, pp. 822–5, September 1981.

31 Trinh, T. N., Mittra, R. and Paleta, R. J., 'Horn image-guide leaky-wave antenna', *IEEE Trans.*, **MTT-29**, no. 12, pp. 1310–4, December 1981.

32 Henderson, A., England, E. and James, J. R., 'New low-loss millimetre wave microstrip antenna array', 11th European Microwave Conference, Amsterdam, September 1981, pp. 825–30.

33 John, G., Henderson, A. and James, J. R., 'Analysis of insular guide launcher radiation loss and comparison with microstrip counterparts', Proc. 12th European Microwave Conference, Helsinki, August 1982.

34 Inggs, M. R., Birand, M. T. and Williams, N., 'Experimental 30 GHz printed array with low loss insular guide feeder', *Electronics Letters*, 17, no. 3, pp. 146–7, 5th February.

35 Hori, T. and Itanami, T., 'Circularly polarized linear array antenna using a dielectric image line', *IEEE Trans.*, **MTT-29**, no. 9, pp. 967–70, September 1981.

36 Solbach, K. and Wolff, I., 'Dielectric image line groove antennas for millimeter waves', 2nd Intl. Conf. on Antennas and Propagation, York, IEE Conference Publication No. 195, 1981, pp. 59–62.

37 Gelsthorpe, R. V. and Aylward, M. J., 'A waveguide slot array for use at millimetric frequencies', *ibid.*, pp. 63–8.

38 Knox, R. M., 'Dielectric waveguide microwave integrated circuits—an overview', *IEEE Trans.*, **MTT-24**, no. 11, pp. 806–14, November 1976.

39 Schmieder, D. E., Loefer, C. R. and Weathersby, M. R., 'A segmented aperture approach to high resolution NMMW imaging', paper Th-4-3, 6th International Conference on IR and millimetre waves, December 7th–12th, 1981, Miami Beach, Florida, (IEEE Cat. No. 81 CH 1645-1 MTT).

40 Gelsthorpe, R. V., Williams, N. and Davey, N. M., 'Dielectric waveguide: a low-cost technology for millimetre-wave integrated circuits', *The Radio and Electronic Engineer*, **52**, no. 11/12, pp. 522–528, November/December 1982.

Manuscript first received by the Institution on 30th July 1982 and in final form on 3rd September 1982.
(Paper No. 2058/AMMS 113).

UDC 621.396.677.85.029.65
Indexing Terms: Antennas, microwave

Design considerations for millimetre wave lens antennas

R. J. DEWEY, B.Sc.(Eng.), Ph.D., C.Eng., MIEE*

SUMMARY

The operational background and some of the possible single and dual lens antenna options for use in a millimetric sensor with approximately 3° beamwidth have been examined. A particular single lens antenna design gave a scan of more than ±3 beamwidths and compatibility with conical scan, beam broadening and monopulse operation.

A dual lens antenna design was operated both with a single feed horn and with a rectangular matrix of plain waveguide radiators (with potential application in real time imaging). Good scan characteristics were obtained out to ±6 beamwidths with the single feed horn but the matrix feed assembly needed a group of elements to be fed in phase before equivalent performance could be obtained. The aim of the work was to simulate feeding the lens antenna with a monolithic array and whilst an array of waveguides can not accurately model all the properties of a monolithic array they are considered sufficiently representative to indicate some of the compromises that may have to be made.

* *Philips Research Laboratories, Systems Division, Cross Oak Lane, Redhill, RH1 5HA, Surrey.*

1 Introduction

With the increased availability of compact millimetre-wave components,[1] more work is now being carried out to implement systems operating above 30 GHz. The oft-quoted reduction in antenna size (or increase in resolution for the same antenna size) is at last being matched by proportionally smaller size mixers, solid-state amplifiers and integrated front-ends, so that the overall millimetre-wave systems are at last approaching a reasonably 'flyable' size.

An interesting aspect of the developing millimetric technology is the close interaction necessary with systems and potential applications. At millimetric wavelengths individual components are getting extremely small and it is no longer desirable to design high-performance components in isolation from each other. Furthermore the reduced size of the components also make them attractive for monolithic fabrication on a single semiconductor substrate.

The aim of this paper is to examine some of the possible antenna options for a millimetric sensor, starting with a single-channel tracking system and working towards a multi-beam arrangement with potential real-time imaging applications.

2 Background

To date most of the interest in millimetric systems has arisen in military circles[2] and follows successful development and operation of relatively short range infra-red (i.r.) surveillance, tracking and imaging systems. It has been realized however that such i.r. systems have severe limitations in fog, smoke, haze and inclement weather of the type often encountered in temperate climates. Millimetre-wave systems are less susceptible to the adverse effects of weather. Unfortunately millimetre-wave antennas are also smaller in terms of wavelengths than the i.r. antennas and consequently do not have such narrow beamwidths so the resolution is much poorer. Nevertheless they are considered to provide a useful addition or alternative to i.r. systems.

It is recognized that one of the main difficulties in short-range applications such as terminal guidance or homing heads, to which millimetre-wave systems are admirably suited, is in the initial acquisition of the target. Many conventional ground or shipborne weapon systems have separate surveillance and tracking radars. Thus the tracking radar may have to search only a small area before acquiring a target. Other terminal/homing guidance systems often rely on initial information from an operator immediately prior to launch or may even be television/optically guided to within a short distance of their target where the automatic guidance system is made operative. With advances in v.l.s.i.c. technology[3] and signal/information sorting techniques, the concept of a fully-autonomous system has become a feasible proposition. The problem of target acquisition is then one of the major limitations.

Several procedures can be adopted to search for the target within a given area:

(a) Variable beamwidth 'zoom' facility which allows a

0033-7722/82/110551+08 $1.50/0

wide beam for acquisition and a narrow beam for tracking.

(b) Narrow beam scanned over the required field of view (f.o.v.).

(c) Multi-beam arrangement with a wide instantaneous f.o.v.

In single-feed lens arrangements the first two procedures rely on mechanical movement to achieve their objective. The variable beamwidth property can be achieved by defocusing a lens antenna (Fig. 1(a)). The scanned beam configuration can be economically implemented by using a lens antenna system which incorporates a variable angle refracting plate between the feed and the lens as shown in Fig. 1(b). Whilst being conceptually simple, both these arrangements require fairly complex mechanical implementations, the latter particularly needing a complex mechanical linkage to allow changing the beam squint angle whilst maintaining conical scan. Both arrangements have been investigated at Philips Research Laboratories and the results will be summarized below.

A multi-beam antenna has the capability of either fast inertialess electronic scanning of a single beam or ideally, with sufficiently advanced signal/information processing, several simultaneous beams with the limiting case being a static 'staring array'.[4] The later device is very attractive for many applications as it allows real time imaging to be carried out or alternatively allows a compromise between update time and integration time. The term imaging means different things to different people—a simple sequentially scanned system can be used to build up an image as in a television-style raster scan whereas the synthetic aperture radar uses motion of the receiver to give a large apparent aperture with a corresponding narrow beam which is able to build up a very fine detailed image (usually of the ground). In the context of this paper, imaging will imply a staring array multi-beam application with the possibility of close to real-time processing.

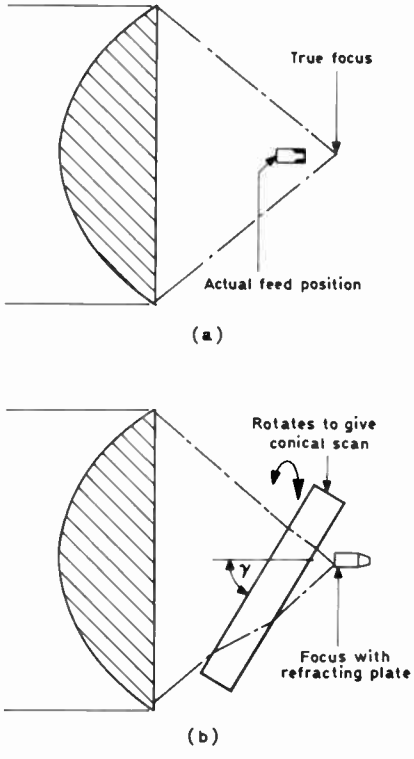

Fig. 1. Aplanatic lens arrangements
(a) Defocusing to produce variable beamwidth.
(b) With refracting plate to give conical scan capability.

The following Section will initially summarize results for a single-lens system which allows beam broadening by defocusing or beam squint by interposing a refracting plate between the lens and the feed, then examine the performance of a dual-lens multi-beam antenna using an open-ended circular waveguide matrix of feed elements and finally consider the implications of using instead an array of monolithic feed elements on a high dielectric substrate material.

A typical specification for antenna performance in the envisaged applications might be as follows:

Aperture size = approx 24λ
3 dB beamwidth = 2·9°
Sidelobe level $\leqslant -20$ dB
Beam cross-over level -2 dB to -3 dB
Field of view $\pm 20°$

3 Antenna Design

3.1 Single-lens Configurations

Lens antennas produce less beam squint than reflectors for a given feed displacement from the axis or conversely they allow larger (and more efficient) feeds to be used for the same beam squint (and cross-over levels). Thus they offer some advantage over front-fed paraboloids for antenna efficiency, have the feed package conveniently situated and do not suffer primary feed blockage of the aperture. For ease of manufacture plano-convex lenses have distinct advantages over those lenses which need both surfaces to be shaped. The more commonly encountered plano-convex lens is the hyperbolic profile lens.[5] This single-surface refraction lens adds substantial 'space taper' to the feed horn aperture taper which may be beneficial if the feed element produces a high edge illumination. However, like the classical paraboloid reflector, the hyperboloid lens is essentially a single-feed device with poor scanning properties.[6]

The two-refraction-surface aplanatic type of lens antenna[7] has better off-axis focusing properties and maintains the feed horn illumination across the subtended aperture. The plano-convex aplanatic lens profile is defined by the simplified equations:

$$z = t - \cos\beta\left\{\frac{(n-1)t - f\cos\delta(\sec\alpha - 1)}{n - \cos\beta}\right\}$$

$$x = f\sin\alpha\left\{1 + \frac{\left(1 - \frac{\cos\delta}{\cos\alpha}\right)(\cos\beta - 1)}{n(n-1)(n-\cos\beta)} + \right.$$

$$\left. + \cos\delta(\sec\alpha - \sec\delta)\left(\frac{n^2 - n - 1}{n-1}\right)\right\}$$

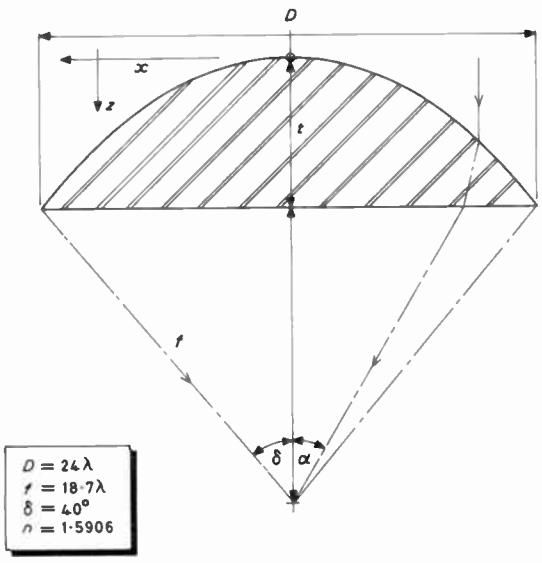

Fig. 2. Co-ordinate system and design dimensions for aplanatic lens antenna.

where

$$\beta = \sin^{-1}\left\{\frac{\sin\alpha}{n}\right\}$$

$$t = \frac{f(1-\cos\delta)}{(n-1)}$$

For the chosen value of dielectric constant and other dimensions as shown in Fig. 2, the Abbé sine condition was fulfilled at the axis and across the aperture the difference between x and $f\sin\alpha$ never exceeded $0{\cdot}01f$, which implies good scanning characteristics from a single-lens system. Typical E- and H-plane radiation patterns for this assembly as the feed horn is scanned away from boresight are shown in Fig. 3. It can be seen that the patterns are only useful out to about $\pm 10^\circ$ where the shoulder/sidelobe away from broadside has risen to about -12 dB and the gain has dropped by about 2 dB. Dissipation in the lens was estimated to be about 0·2 dB.

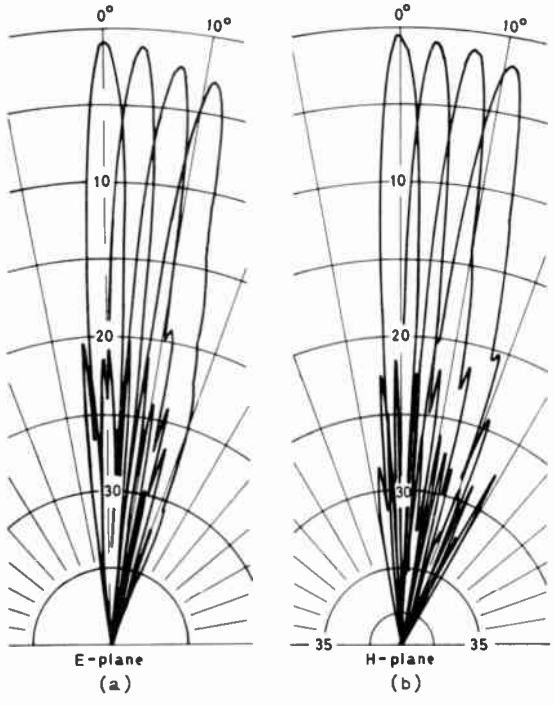

Fig. 3. Radiation patterns for aplanatic lens assembly

The aplanatic configuration lends itself particularly well to beam broadening by defocusing. As the focal distance is reduced the angle of incidence at the lens surface remains within reasonable bounds so that power is not unduly scattered or mismatched. Furthermore in the aplanatic lens neither profile presents an equiphase contour so that energy reflected at the boundaries does not add in phase at the feed to cause a large mismatch. A 30% reduction in horn/lens spacing was found to produce a 4·4 increase in beamwidth[8] and this beamshape was maintained over about a 9% frequency range.

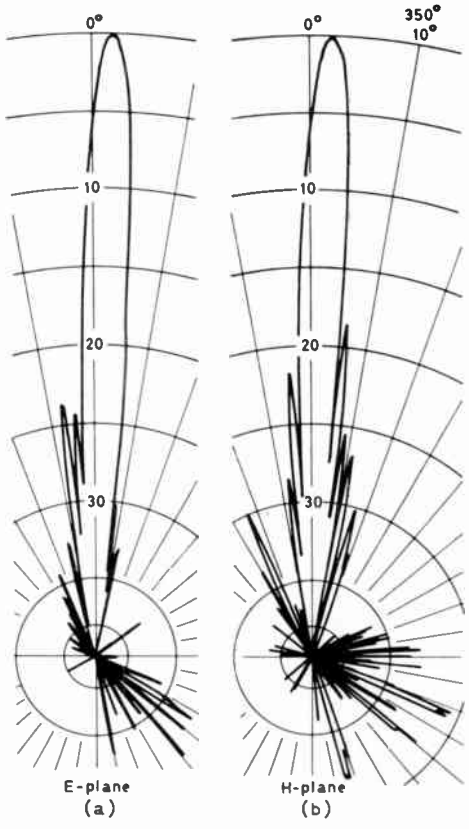

Fig. 4. Aplanatic lens radiation patterns with refracting plate

If a plane parallel sheet of dielectric is inserted in the focusing region between the feed horn and the lens then it acts as a refracting plate causing the beam to squint whilst maintaining the lens and feed horn stationary. Rotating the plate causes the beam to perform a conical scan. Parameters controlling the beam displacement and boresight cross-over level are plate thickness, angle and dielectric constant. Equal beamsquints for E- and H-plane polarizations were obtained and the beam shape and sidelobes showed little degradation with squint angle. Typical radiation patterns are shown in Fig. 4 and

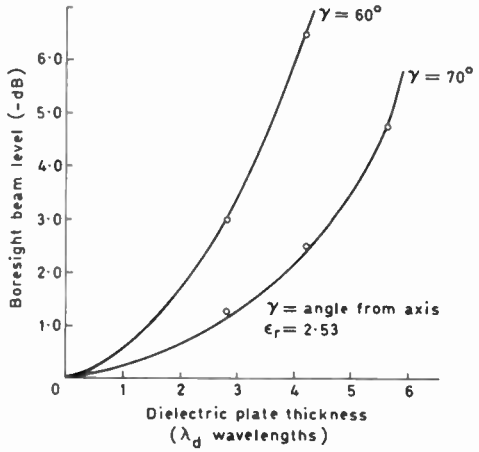

Fig. 5. Aplanatic lens beam cross-over characteristic with refracting plate.

the boresight cross-over characteristic in Fig. 5. The possibility of combining this conical scan arrangement with beam broadening by defocusing was examined. It was found however, that bifurcation of the beam occurred, precluding their simultaneous operation. Similarly in a four-horn feed arrangement, good focused patterns were obtained with the lens but bifurcation occurred when defocusing was included in an attempt to obtain beam broadening. A single-plane monopulse configuration was also examined and found to be compatible with either conical scan or beam broadening arrangements.

3.2 Imaging Antennas

A monolithic array fed lens system embraces many different antenna aspects which in the past have been treated largely independently of each other. A single array element involves novel concepts in the fabrication technology, in the mixer and r.f. front-end design and in the development of the radiating element itself. An array of elements is further susceptible to mutual coupling effects as has been widely studied for phased array applications. Whilst a lens system can be designed on geometrical optics principles and performs very adequately with an ideal feed, when such a lens arrangement is illuminated by a non-ideal element in a matrix array then unwanted effects can arise. The aim of this Section is not to study any of the constituent items in great detail but to investigate their inter-relation and identify any trade-offs that may have to be made.

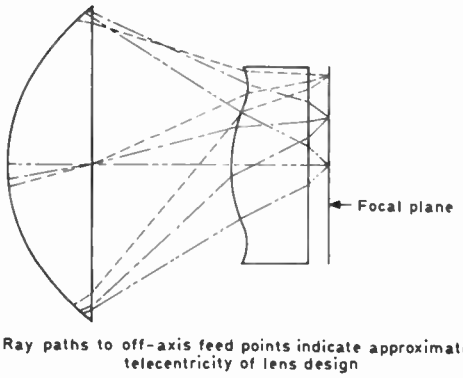

Fig. 6. Dual-lens antenna.

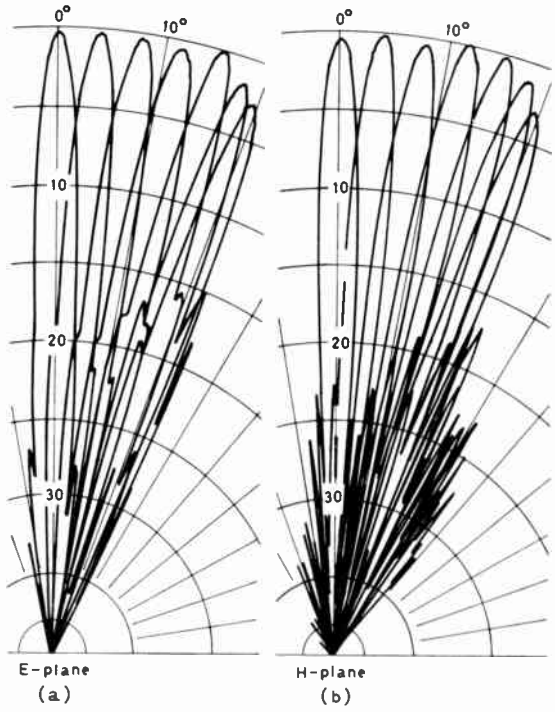

Fig. 7. Radiation patterns for dual-lens antenna

The basic lens system that has been examined is a two-lens arrangement as shown in Fig. 6. This is a logical progression from the single aplanatic lens arrangement described above and allows wider angle scanning whilst using plano-convex lenses and maintaining a planar focal plane with telecentric feeds (i.e. radiating normal to the focal plane and not angled inwards). As will be shown this configuration with both lenses having $\varepsilon_r = 2{\cdot}53$ is not altogether compatible with the favoured monolithic feed arrangements but many results have been obtained which are considered to be relevant to the overall antenna system operation.

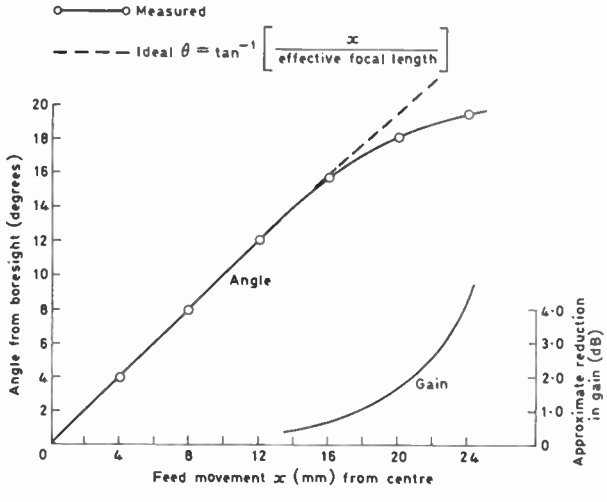

Fig. 8. Variation of scan angle and gain degradation with feed position in dual-lens antenna.

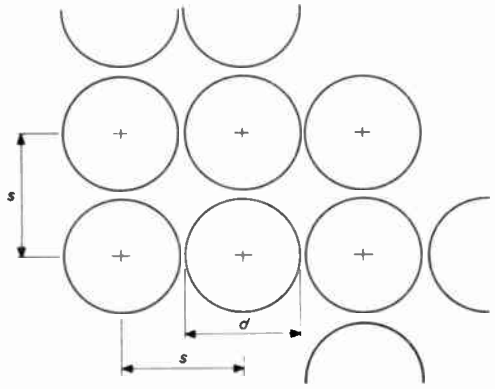

Fig. 9. Open-ended waveguide matrix feed.

the feed matrix. To obtain the required secondary beam spacings the feed elements must be quite small, yet if the primary feeds are small there is high edge illumination causing high sidelobes and high spill-over loss. Unfortunately there is no easy compromise between these two conflicting requirements yet in the foreseen applications gaps between the secondary beams could not be countenanced so initially the possibility of low efficiency and high sidelobes was accepted. In the event it will be shown that with the waveguide matrix, mutual coupling effects could largely determine the required compromise.

A matrix of open-ended waveguide elements was fabricated with the element spacings (see Fig. 9) chosen so as to give approximately $-2{\cdot}5$ dB secondary beam cross-over level. However when the element radiation patterns were measured in the coordinate axes they showed (Figs. 10(a) and 10(b)) characteristic effects of

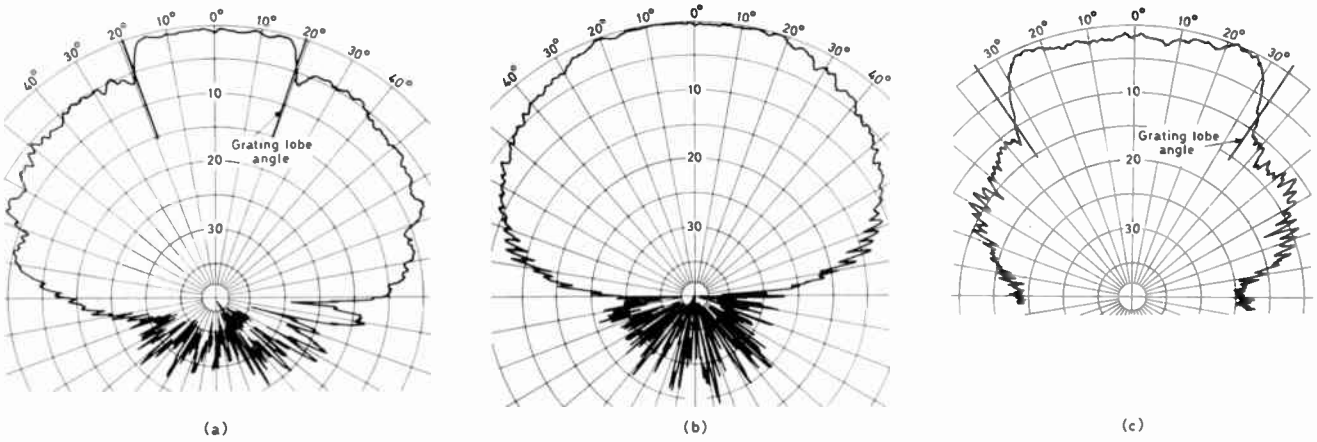

Fig. 10. Matrix feed element radiation patterns: $s/\lambda = 0{\cdot}75$
(a) E-plane and (b) H-plane: co-ordinate axes. (c) H-plane: 45° axis.

The lens design is based on a geometric optics procedure optimized to cancel spherical, astigmatic and coma aberrations. Two different types of feed arrangement were manufactured to be tested in conjunction with the lenses.

Firstly an idealized feed comprising a dual-mode Potter horn[9] was fabricated to test the lens arrangement under ideal illumination conditions. An edge illumination of -10 dB was chosen. The typical scanned radiation patterns are shown in Fig. 7 for E- and H-plane movement of the feed.

H-plane radiation patterns are very good, closely approximating the theoretical secondary patterns from a Bessel on a 10 dB pedestal primary illumination. Sidelobes are better than -20 dB except at the limit of scan (16°) where they rise to about $-18{\cdot}5$ dB. The E-plane patterns are not quite so good with sidelobes at -17 dB at the scan limit. The scan angle and gain degradation versus feed position characteristic is shown in Fig. 8. These curves indicate that the lens antenna has a useful field of view out to greater than $\pm 16°$. The lens combination was thus shown to be working very satisfactorily with an ideal feed so the next step was to simulate the multi-feed arrangement.

A number of problems were foreseen in connection with

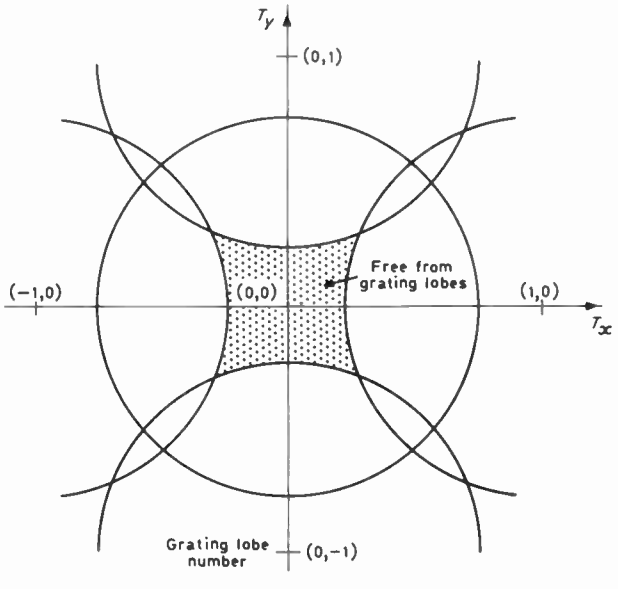

Fig. 11. Grating lobe diagram for matrix feed array $s/\lambda = 0{\cdot}75$.

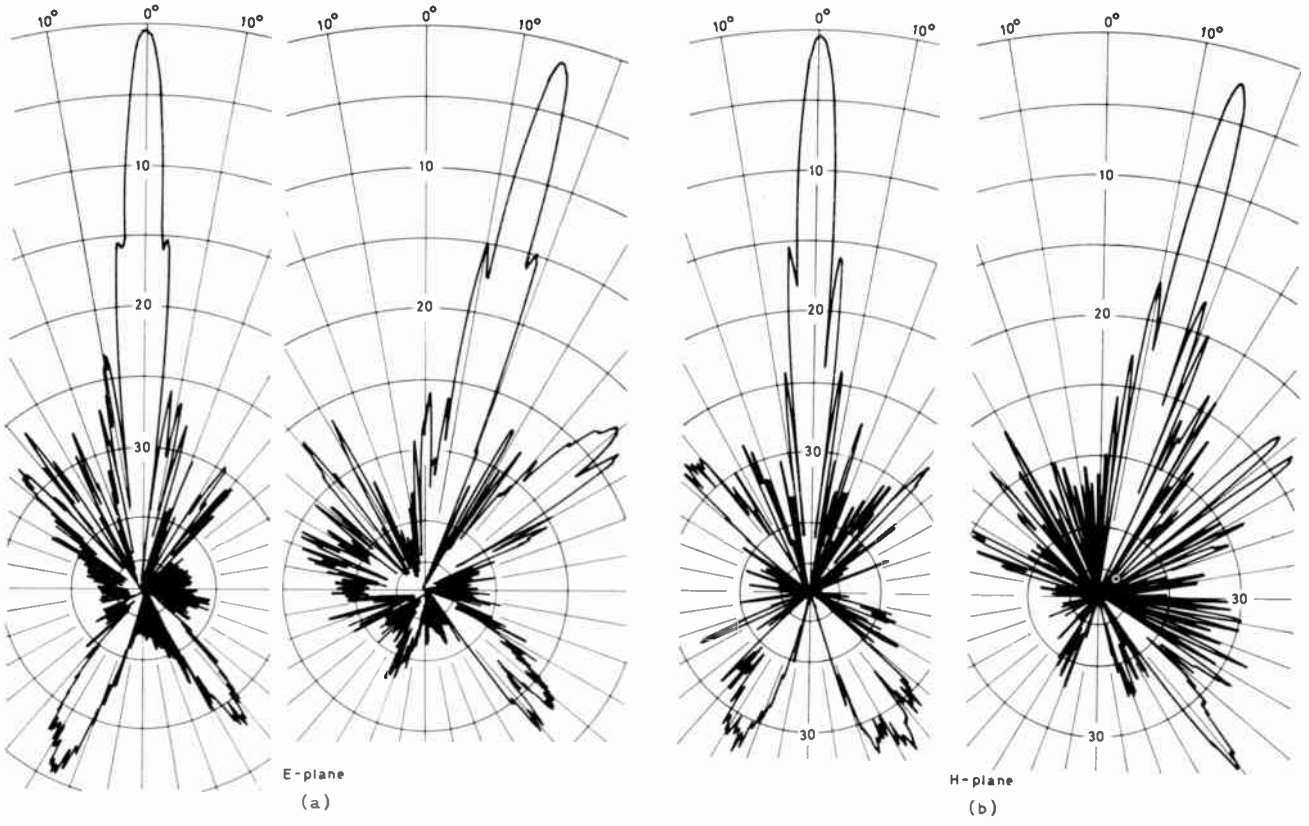

Fig. 12. Secondary radiation patterns for dual lens fed by single element in matrix feed array.

strong mutual coupling in the E-plane but only weak coupling in the H-plane. Notice that the included angle agrees closely with the grating lobe expression $\sin\theta_{max} < \lambda/d - 1$. Element radiation patterns were also measured in the 45° plane of the rectangular matrix for H-, E- and 45° polarizations. Surprisingly the strongest coupling here was in the H-plane (Fig. 10(c)), possibly due to the curvature of the field lines, but the grating lobe diagram shown in Fig. 11 was still useful in understanding the positions of the element pattern nulls.

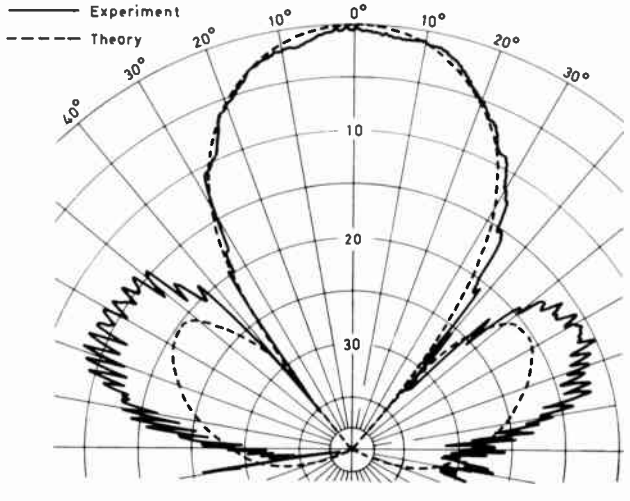

Fig. 13. Matrix feed element pattern with two elements excited in phase (H-plane). ($s/\lambda = 0{\cdot}75$).

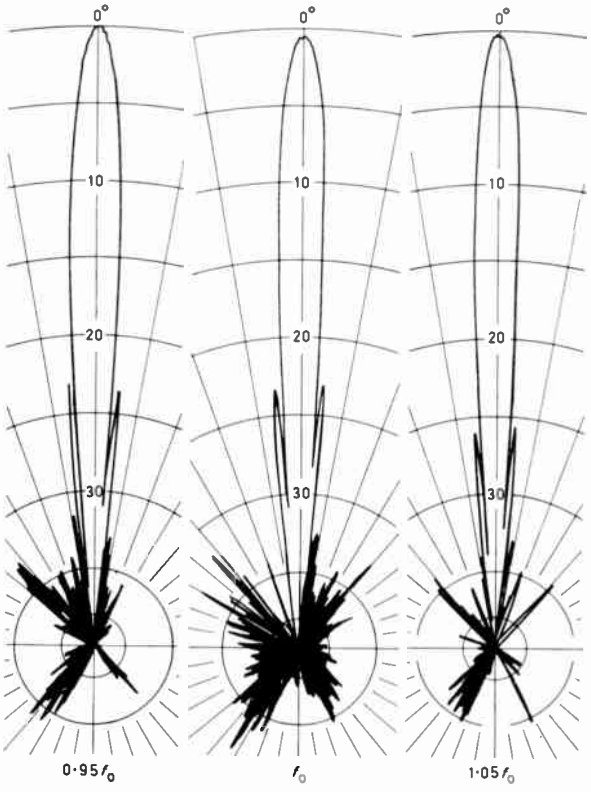

Fig. 14. Secondary radiation patterns for dual lens fed by dual elements in matrix feed array (H-plane).

Table 1

Measured values of mutual coupling in waveguide matrix array.

(a) $\frac{s}{\lambda} = 0.704$

E-plane ↓ / H-plane →				
	0	−27·0	−35·9	
	−24·7	−29·0		
	−29·7	−35·4		
	−33·2			
	−34·0			

(b) $\frac{s}{\lambda} = 0.75$

E-plane ↓ / H-plane →				
	0	−30·6	−32·7	< −39
	−21·3	−29·9	−39·0	
	−28·3	−31·5		
	−31·2	−36·3		
	−32·4			
	−36·4			
	< −38			

Approximate mutual coupling levels in the array were measured at two frequencies (Table 1) to ascertain the level of coupling required to affect the radiation patterns. These results indicate that E-plane mutual coupling is higher than H-plane and falls off more slowly.

As expected the secondary radiation patterns were poor (see Fig. 12) when the matrix feed was used in the lens system. E-plane sidelobes were about −15 dB on boresight rising to −13·5 dB at the scan limit whilst H-plane sidelobes were typically −16 dB.

Techniques to overcome high edge illumination in reflector and lens antennas are well known. Making the feed elements larger to increase their directivity has the desired effect on sidelobes but it also has the deleterious effect of increasing the secondary beam spacing. If adjacent feed elements are ganged together in phase the primary feed pattern is again narrowed as shown in Fig. 13 and, as can be seen, this takes the pattern well inside the limits imposed by grating lobe effects. It is gratifying to see that the well-known theory for plain conical horns[10] is reasonably accurate in modelling this situation. When dual-fed elements in the matrix array were used to feed the lens then excellent secondary radiation patterns were obtained as shown in Fig. 14. These give similar scan characteristics to the ideal Potter horn illumination.

The next problem to be resolved is whether the envisaged monolithic element radiation patterns resemble those for the open-ended waveguide matrix elements. If they do and low sidelobes are required then adjacent elements will need to be added in phase either by sequential switching or by first performing a static power split at each element as indicated in Fig. 15. This clearly has impact on the system configuration and subsequent signal processing.

There appear to be two different monolithic receiver approaches corresponding to using either a magnetic dipole[11] or electric dipole[12] as the primary feed element (Fig. 16). Both rely on coupling power through the back of the circuit into a high dielectric-constant substrate to obtain directivity and consequently need to couple power from the substrate out into free space. Problems arise with the restriction on emergence angle of radiation from the back of the substrate caused by total internal reflection at the dielectric boundary. This is governed by Snell's law $\{n_1 \sin\theta_1 = n_2 \sin\theta_2\}$ which for GaAs ($n = 3{\cdot}5$) requires the element 'capture angle' to be less than $\pm 16°$. This can be satisfied by covering the

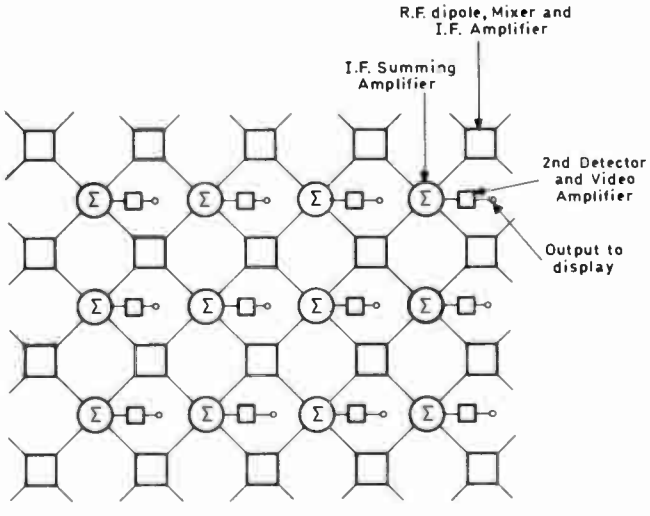

Fig. 15. Matrix arrangement for adding adjacent elements in phase.

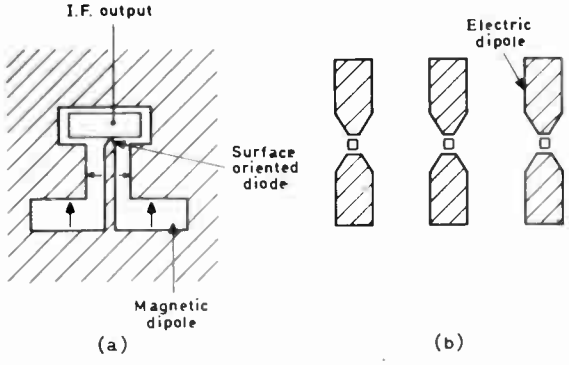

Fig. 16. Monolithic receivers
(a) Single-ended mixer (Clifton *et al.*[11] at M.I.T.)
(b) Detector diode array (Rutledge *et al.*[12] at Cal. Tech.)

monolithic elements with a high dielectric-constant hemisphere (incorporating quarter-wave matching layers if necessary) so that radiation is approximately normal to the boundary. The planar dielectric interface containing the circuit has a large effect on the shape of the far-field radiation patterns of the dipole elements and it remains to be seen which dipole will prove best in the lens assembly. It may be realized that the hemispherical primary-lens arrangement needed to match power out of the back of the high dielectric-constant substrate material is not altogether compatible with the dual-lens assembly investigated above. It is however directly compatible with the single-lens arrangement, but that has been shown to have limited off-axis imaging performance.

Initial calculations for the electric dipole element[13] suggest that the element radiation pattern will be much narrower than for the open-ended waveguide and may be multi-lobed in character. This will give rise to high spill-over losses and subsequent low efficiency. If the power in the sidelobes can be reduced then the narrower primary beamwidth for this type of monolithic feed is an advantage obviating the need for adding adjacent feeds in phase.

4 Conclusion

Whilst the ultimate aim of the work is to investigate monolithic feed elements and their interaction with lens antenna assemblies, a useful intermediate step, presented in this paper, has been to examine conventional horn feeds both individually feeding the lens assembly and also a matrix of feed elements. A matrix of plain waveguide radiators can not accurately simulate all the properties of a monolithic array but is considered sufficiently similar in many respects to indicate the compromises that will arise. In particular it was found that whilst mutual coupling to neighbouring elements was relatively low (< -20 dB), this was sufficient to significantly affect both primary and secondary radiation patterns. Furthermore it was found that to achieve both low secondary sidelobes and close beam spacing the primary elements had to be excited in pairs for single-plane scanning and groups of three or four for two-dimensional imaging.

Initially the performance of a single-lens antenna system (with $f/d = 0{\cdot}78$) for use in a millimetric sensor was presented. Satisfactory performance with better than ± 3 beamwidth scanning was obtained. The compatibility with conical scan, beam broadening and monopulse operation was examined.

Results for a geometric optics designed multi-beam dual-lens system was then presented and shown to give excellent scan characteristics out to ± 6 beamwidths. Some of the inter-related effects which must be taken into account when designing multi-beam imaging lens antennas have been investigated.

5 Acknowledgments

Mr J. A. Clarke of PRL Optics Group carried out the geometric optics design of the dual-lens profiles. Thanks are due to PRL Mechanical Techniques Department for careful design and manufacture of the experimental equipment.

6 References

1 Bates, R. N., Nightingale, S. J. and Ballard, P. M., 'Millimetre-wave components and subsystems', *The Radio and Electronic Engineer*, **52**, no. 11/12, pp. 506–12 November/December 1982.
2 Seashore, C. R., 'Missile guidance', Chap. 3 in 'Infrared and Millimetre Waves', Vol. 4, Ed. K. J. Button and J. C. Wiltse, (Academic Press, New York, 1981).
3 Special Issue on 'Very Fast Solid-State Technology' *Proc. IEEE*, **70**, no. 1, January 1982.
4 Lloyd, D. B., 'Staring IR Sensors' *Military Electronics/Countermeasures*, November 1979, pp. 58, December 1979, pp. 32–9.
5 Silver, S., 'Microwave Antenna Theory and Design', Sect. 11.3 (McGraw-Hill, New York, 1949).
6 Kreutel, R. W., 'The hyperboloidal lens with laterally displaced dipole feed', *IEEE Trans on Antennas and Propagation*, AP-**28**, no. 4, pp. 443–50, July 1980.
7 Friedlander, F. G., 'A dielectric-lens aerial for wide-angle beam scanning', *J. Instn Elect. Engrs*, **93**, Pt. IIIA, pp. 658–62, 1946.
8 Dewey, R. J., 'Reflector and lens antennas for millimetre-wave radiometers' 11th European Microwave Conference, Amsterdam 1981, pp. 573–8.
9 Potter, P. D. 'A new horn antenna with suppressed sidelobes and equal beamwidths', *Microwave J.*, **6**, pp. 71–8, June 1963.
10 Silver, S., *op. cit.*, Sect. 10.2.
11 Clifton, B. J., Murphy, R. A. and Alley, G. D., 'Integrated monolithic mixers on GaAs for millimetre and submillimetre wave applications', IEEE Fourth International Conference on Infra-red and Millimetre Waves, Miami Beach, Florida, December 1979, pp. 84–6.
12 Neikirk, D. P., Rutledge, D. B. and Muha, M. S., 'Far-infrared imaging antenna arrays', *Appl. Phys. Letters*, **40**, no. 3, 1, pp. 203–5, February 1982.
13 Brewitt-Taylor, C. R., Gunton, D. J. and Rees, H. D., 'Planar antennas on a dielectric surface', *Electronics Letters*, **17**, no. 20, pp. 729–31, 1st October 1981.

Manuscript received by the Institution in final form on 7th October 1982.
(Paper No. 2059/CC 364)

UDC: 621.372.622: 621.385.633: 621.396.62.029.65
Indexing Terms: Radio receivers, Microwave devices, Mixers, microwave, Oscillators, microwave, Spectrum analysers, Bragg cell

Broadband high-resolution receivers for the sub-millimetre region

P. F. CLANCY, Ph.D.*

SUMMARY

This paper describes the main features of high performance heterodyne receivers for the sub-millimetre frequency range. The great interest in the use of these receivers for scientific observations dictates that high performances in the areas of frequency resolution, sensitivity and tuneability are mandatory. The parallel interest in eventual space application of such receivers due to the high attenuation of the atmosphere to submillimetre waves also motivates technological efforts to minimize the mass and power consumption and maximize the reliability and automation of such systems. The implications of these constraints on hardware choices are examined especially in terms of input mixers, local oscillators and back-end spectrum analysers. Recent technological advances leading to improved performances of these components are described as well as work presently in progress on the realization of a fully automated, high-resolution, high-sensitivity receiver working in the 300–500 GHz band. Details of the applications potential of such systems are discussed with special emphasis on the importance of space-borne heterodyne receiver systems.

* *European Space Agency (ESA), ESTEC, Noordwijk, Netherlands.*

1 Introduction

The principle of heterodyne detection for the high-sensitivity, high-resolution, broadband reception of signals is well established at radio and microwave frequencies where the key technology areas can be regarded as mature with respect to their counterparts in the millimetre and submillimetre range. In these latter regions of the spectrum, performance improvements are at present occurring at a rapid rate as a result of technological advances in critical areas such as mixing, local oscillator power generation and broadband spectrum analysis. In many respects some of these technological advances are driven by the special requirements of low mass, low power-consumption and high reliability imposed by the employment of these technologies in space-borne systems. Some of the applications of these technologies in the 100–1000 GHz range have already been reviewed.[1]

At the present time and for the foreseeable future it appears that most of the interest in the use of submillimetre receivers of the type described here will come from the scientific side concerned with fundamental investigations of thermal and spectral line emissions from the Earth's surface and atmosphere and similar emissions from astronomical objects. As a consequence, user systems requirements tend to converge on state-of-the-art performances for each specification without the sophisticated trade-offs typical of more applications-oriented uses such as for example telecommunications or electronic counter measures. Broadly speaking, therefore, receiver systems likely to find wide applications in the scientific disciplines mentioned above will be those which offer a combination of high sensitivity (low noise temperature), high spectral resolution, and high bandwidth (tuneability). The only systems offering all these together are heterodyne receivers using tuneable local oscillators and multichannel spectrum analysers as back ends. In addition, when space applications are taken into account (this is particularly significant at these frequencies, due to the high attenuation of the atmosphere) then systems having high performances are mandatory in order to maximize the scientific return from costly space programmes. In consequence heterodyne systems of low mass and power consumption and high reliability are needed.

2 Heterodyne Systems

The principle of heterodyne detection at radio and microwave frequencies is well established and its application to higher frequencies employs similar concepts. The incoming signal is mixed in a non-linear mixer with a locally-generated coherent signal to produce an intermediate frequency signal at a lower frequency (usually in the radio or microwave region) which can then be processed or analysed for spectral content. The i.f. signal retains all the information contained in the original millimetre/submillimetre signal including phase. Figure 1 shows the schematic of a heterodyne receiver from front-end to back-end and a typical frequency plan of the system is given in Fig. 2.

The Radio and Electronic Engineer, Vol. 52, No. 11/12, pp. 559–564, November/December 1982 0033–7722/82/110559+06 $1.50/0

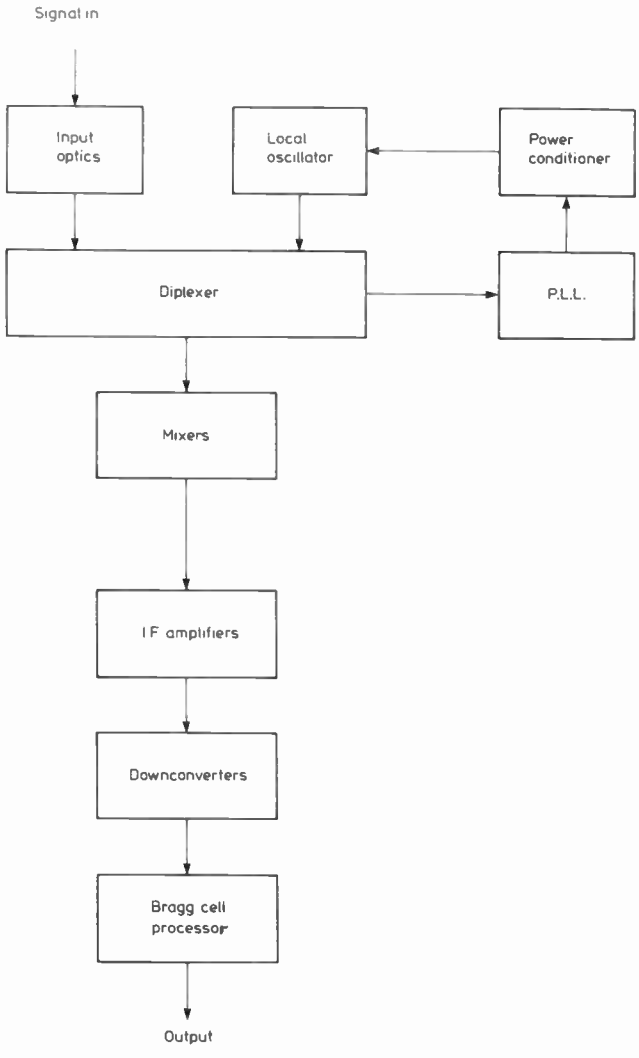

Fig. 1. Heterodyne receiver schematic.

The chief subsystems are (i) the input diplexer which is used to separate signal and local oscillator and suppress local oscillator noise at the signal frequency, (ii) the input mixer, (iii) the local oscillator, (iv) a phase-locked loop (PLL) for stabilization of the local oscillator frequency thus allowing high-resolution spectral analysis, (v) the i.f. amplification subsystem which may include a further frequency down-conversion, (vi) a back-end processor which is usually a spectrum analyser of some kind, and (vii) a control/data processing system which could be a microprocessor/microcomputer capable of carrying out functional control of the receiver such as tuning and housekeeping as well as performing data reduction and processing of the data emerging from the spectrum analyser. Such a system is currently under integration for ESA employing sub-systems already developed such as Schottky mixers, carcinotron local oscillators, and an acousto-optic spectrum analyser, all of which will be described later.[2]

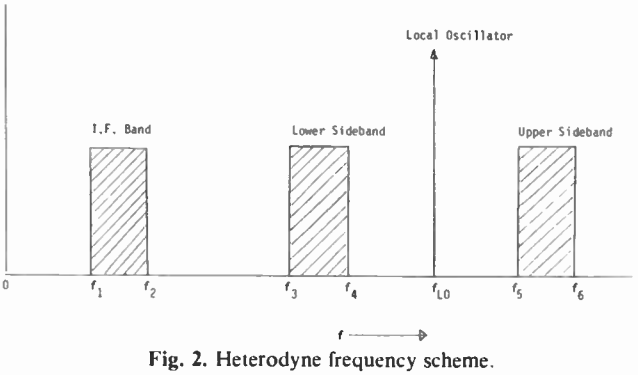

Fig. 2. Heterodyne frequency scheme.

To identify the key system parameters affecting the performance of a heterodyne system we may note first, that the total system noise temperature and hence overall sensitivity is given by

$$T_S = T_M + L_M T_{IF} + T_0 \quad (1)$$

where T_M is the mixer noise temperature and L_M is its conversion loss, T_{IF} is the i.f. amplifier noise temperature and T_0 is a temperature term arising from other contributions such as losses in the diplexer and mismatches between mixer and i.f. amplifier. These can be minimized by good system design so that the performances of the input mixer and the i.f. amplifier become the key factors in determining overall sensitivity.

Secondly, the resolution of the system is governed by the overall stability of the local oscillator subsystem and hence by the initial stability of the local oscillator in isolation, coupled with the performance of the phase-locked loop subsystem when the loop is closed. In addition the frequency resolution of the spectrum analyser determines the final frequency resolution of the system.

Thirdly, the broadband character of the heterodyne receiver derives ultimately from the tuneability of the local oscillator since, due to the additive nature of signal and local oscillator frequencies in determining the i.f. signal

$$f_{IF} = f_{SIG} - f_{LO} \quad (2)$$

the signal tuning bandwidth equals the local oscillator tuning bandwidth for a fixed f_{IF}. This is a crucial factor in determining the choice of local oscillator since at sub-millimetre frequencies only backward wave oscillator (carcinotron) tubes offer a high tuning bandwidth (up to 20%) and the necessary output powers (tens of milliwatts) to drive Schottky diode mixers. Laser local oscillators as well as being massive, bulky and inefficient

Table 1
Heterodyne systems key parameters and their hardware implication

Parameter	Implications
Sensitivity	Mixer noise temperature and conversion loss
	I.f. amplifier input noise temperature
	Diplexer losses, mismatches, l.o. noise contributions
Resolution	L.o. stability
	P.l.l. performance
	Spectrum analyser resolution
Bandwidth	L.o. tuneability
	Diplexer and mixer input
	E.m. configuration

offer only tuning bandwidths in the megahertz region. Solid-state oscillators such as impatts or tunettes offer only sub-milliwatt power levels in the sub-millimetre region. In addition to the basic tuneability dictated by the local oscillator the input system including the diplexer and the signal portions of the circuit in which the mixer is imbedded are also decisive. A resumé of these relations are shown in Table 1. At sub-millimetre frequencies this usually means that quasi-optical rather than conventional waveguide techniques are used.

3 Mixers

For the broadband, high-sensitivity mixing in the millimetre and sub-millimetre wave regions a broadband mixer diode imbedded in a suitable circuit of either the waveguide or quasi-optical variety is invariably used. There are essentially two candidates for the mixer diode —the Schottky barrier diode (or a variant such as the Mott diode) or a superconducting junction such as the Josephson, super-Schottky or the s.i.s. diode. The latter devices are all operated at superconducting temperature, i.e. a few kelvins, and consequently require the necessary cryogenic support hardware, a feature which makes their use unattractive for space applications. The Josephson junction device consists of two superconducting regions separated by a thin insulating barrier region. When suitably biased, both d.c. and oscillatory currents flow through the barrier. The interaction between these currents and those induced by incoming signal radiation gives rise to highly non-linear effects resulting in frequency mixing. In principle and often in practice conversion gain can be achieved.[3] The Super-Schottky diode is similar to a normal Schottky, but with superconducting metal electrodes[4,5] and non-linearities up to two orders of magnitude higher than those found for room temperature Schottkys have been quoted.[5] The s.i.s. diode is (like the Josephson junction) also a superconductor-insulator-superconductor. In this case, a dramatic increase in device current occurs when the applied bias exceeds the energy gap of the superconductors. This highly non-linear region gives rise to very efficient mixing and theoretical[6,7] studies indicate that conversion gains can be achieved at low oscillator power requirements (1 nW) up to 250 GHz. Measurements have shown conversion gain for these devices at the lower frequencies.[8,9]

As has been indicated all of these devices require a cryogenic environment with operating temperatures as low as 4K. No lightweight energy efficient coolers for these devices exist although work is presently going on at the Office of Naval Research and the Naval Research Laboratory in the US for the development of such coolers. These might typically be expected to weigh 5–10 kg and consume 100W d.c. power for every 100 mW of cooling power below 10K.[4]

By far the most widely used mixer diode presently employed for heterodyne detection in the sub-millimetre region is the uncooled Schottky diode mixer. A characteristic of such a device is that in the uncooled condition local oscillator powers of a few tens of milliwatts are required. The diode itself consists of a small metal contact deposited on an epitaxial semiconductor which is usually GaAs. Such a diode is sensitive, broadband and mechanically rugged. A good review of this device has been given by Kelly and Wrixon.[10] Diode diameters of about 1 μm are typical for high performances at submillimetre wavelengths. Although circular cross section anodes are the most common, studies[10] have shown that cross-shaped diodes have lower skin-effect components of series resistance. The important factors in this type of mixer are diode noise and diode conversion loss. As a guideline to the evolution of mixer performances with frequency we may note that, under the best circumstances and with diodes optimized for their particular frequency range of operation, a mixer conversion (s.s.b.) loss of 5 dB at 100 GHz would be expected to increase to 15 dB at 1000 GHz and a noise temperature (s.s.b.) of 100–200K at 100 GHz would be expected to increase to 10000–20000K at 1000 GHz.

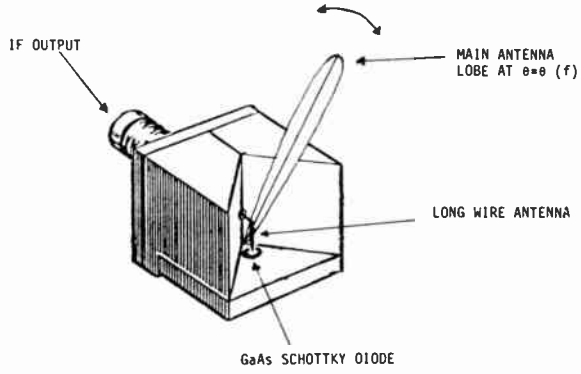

Fig. 3. Corner cube mixer.

Fundamental to the correct operation of such diodes is the optimum operation of the circuit in which it is imbedded. In the millimetre region conventional waveguide mounting with a tuning backshort has been successfully used. However, in the submillimetre region the difficulty of producing suitably small waveguide components with adequate tolerances has forced the adoption of quasi-optical techniques. This has resulted in the adoption of the corner-cube mount as the presently most favoured mixer mount for Schottky diodes.[11] Figure 3 shows the construction of such a mixer. It should be noted that the position of the main lobe of the antenna pattern of the corner cube is a function of frequency so that in a tuneable system the orientation of the mixer with respect to the incoming local oscillator beam has to be varied as tuning is carried out. Apart from the corner cube mount other mounts such as the double slot[11,12] and the biconical have been used in the millimetre and submillimetre regions.[11,13] Corner cube mixers operating in the 300–400 GHz and 400–500 GHz region have been developed for ESA,[14] and are now being integrated into a 300–500 GHz receiver to be described later.

4 Local Oscillators

Tuneable receivers for submillimetre wavelengths require local oscillator power levels of from tens of nanowatts for

some superconducting detectors to tens of milliwatts for Schottky mixers operating at room temperature. For the former, both impatt diodes and klystrons using multipliers can be used at frequencies extending up to many hundreds of GHz. However, for the tuneable operation (this eliminates the many sub-millimetre wave lasers) of room temperature Schottky mixers, the only device available is the backward wave oscillator (b.w.o.). A comprehensive review of the b.w.o. in the millimetre and submillimetre regions has been given by Kantorowicz and Palluel.[15] In essence, an electron beam generated in a suitable electron gun is caused to traverse a region of periodic electromagnetic field generated by a slow-wave structure. Interaction between the beam and the slow-wave structure is a maximum when the electron velocity equals the phase velocity of the e.m. wave and energy transfer occurs between the beam and the e.m. wave which is coupled out as useful local oscillator power. Tuning of the oscillator is effected by varying the electron velocity, i.e. by varying the accelerating voltage. Other features include a magnetic field for beam focusing along with water cooling of the collector electrode due to the inherently low d.c. to r.f. efficiency ($< 0{\cdot}1\%$) of such tubes at these frequencies.

Table 2

High-performance submillimetre-wave carcinotron performances

	Tube developed	Tube under development
Tuning range	405–500 GHz	850 1000 GHz
Output power	10 mW (405–500 GHz)	10 mW (920 1000 GHz) 1 mW (850 900 GHz)
Nominal lifetime	6000 hours	6000 hours
Mass	9 kg	10 kg
Power consumption	125 W	125 W
Maximum voltage	10 kV	10 kV

Leading the field in the development of such devices is the Electron Tube Division of Thomson-CSF which uses the trade-name 'carcinotron' for these tubes. Development contracts by ESA with this organization have been directed at (i) an increase in tuning bandwidth, (ii) a reduction in overall mass, (iii) an increase in efficiency, (iv) an increase in lifetime, and (v) extension of operation to higher frequencies. The electron-beam/delay-line region is exceedingly small with delay-line pitch of the order of tens of microns. This ensures low efficiency, narrow beam geometry and high cathode-emission densities. Output power and tuning bandwidth are trade-off related variables. However, mass can be reduced by the incorporation of advanced samarium-cobalt magnet technology and cathode/filament lifetime increased by the use of potted filaments and advanced low-temperature cathode materials. An earlier development which resulted in a tube operating in the range 330 to 400 GHz has now been supplemented by a tube operating between 405 and 500 GHz with enhanced lifetime, bandwidth and reduced mass. The specifications of this tube are given in Table 2. Also given in the Table are the specifications of a high frequency (1000 GHz) tube currently under development.

5 The I.F. Chain

After downconversion of the signal to the microwave region, conventional amplification techniques may be used to reach a level suitable for driving the back-end spectrum analyser/demodulator/data processor. A key factor, which is indicated by equation (1) is the noise temperature of the first stage. This will normally be of the GaAs f.e.t. variety so that noise temperatures of a few tens of kelvins at frequencies below 10 GHz can be expected with state-of-the-art components. The advantages gained by cooling this input stage to liquid nitrogen temperatures (77K) may be realized by incorporating the i.f. first stage on the cooling block if a cooled mixer is used. Another key factor related to i.f. design is its thermal stability. Gain instabilities arising from temperature drift of the i.f. gain block (typically 80–90dB) will be manifested as a signal. Experience with earlier receivers has shown that stabilization of the i.f. gain block to $\pm 0{\cdot}1°C$ is a good design goal. Typically this may be achieved by housing the i.f. system in a thermally stabilized enclosure using active thermal control.

The bandwidth of the i.f. stage and the back-end processor determine the instantaneous bandwidth of the receiver. Commercially available i.f. amplifiers operating in the communications band 3·7 to 4·2 GHz can be employed for systems having a 500 MHz bandwidth. For receivers with 1 GHz bandwidth (as determined for instance by the back-end processor) custom-designed 1 GHz amplifiers operating at a few gigahertz may be employed.

6 Back-end Processor

The spectroscopy applications towards which all of these receivers are directed means that some form of spectral analysis is to be performed on the 500–1000 MHz signal emerging from the i.f. chain. In the past with this kind of bandwidth, massive bulky and high-power-consumption filter banks have had to be employed for this purpose. In recent years, however, much attention has been given to the development of spectrum analysers based on the acousto-optic interaction in Bragg cells. This offers considerably reduced mass and power consumption and ultimately the promise of an 'analyser on a chip', i.e. an integrated optics unit.

The Bragg-cell device operates by diffracting a laser light beam in an acousto-optic cell by an acoustic wave which carries the spectral information, i.e. the i.f. signal. Since the angle of diffraction is proportional to the frequency, an angular dispersion of the frequencies present can be generated and read out by a photodiode array. The Bragg cell may either operate by using a bulk acoustic wave or a surface acoustic wave. Commercially-available bulk Bragg cells have been used to develop spectrum analysers for high bandwidth operation (up to 1 GHz).[16] In addition work has been sponsored in the

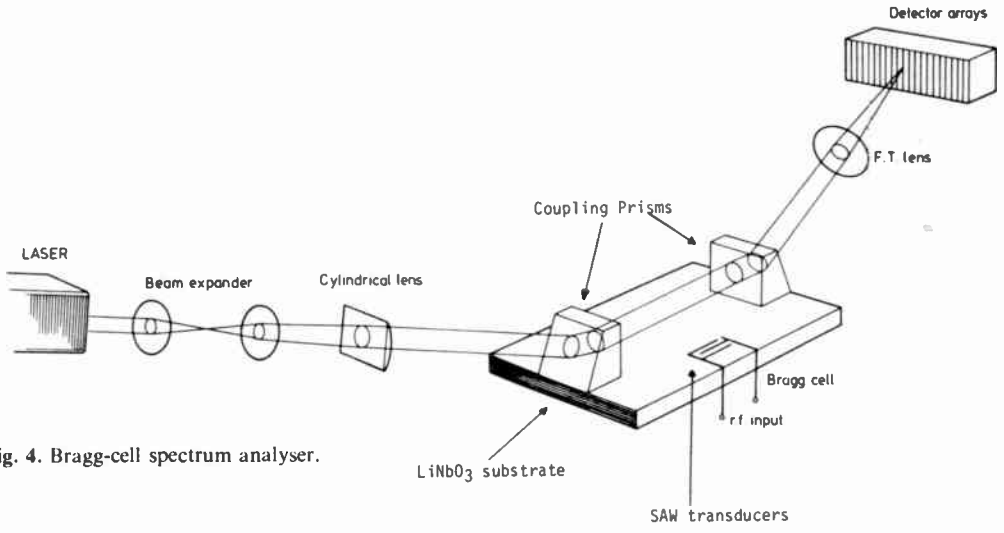

Fig. 4. Bragg-cell spectrum analyser.

US for the development of units based on the integrated optics approach.[17]

In general, analysers of this type will have bandwidths of some hundreds of megahertz and resolutions of some megahertz. Work sponsored by ESA with Plessey has been directed at the development of a system employing a surface acoustic wave (s.a.w.) device with the intention of eventually implementing an integrated optics approach. A schematic of the Bragg-cell arrangement and its working principle are shown in Fig. 4. The Bragg cell itself is a lithium niobate ($LiNbO_3$) crystal with a planar optical waveguide on the upper surface formed by the diffusion of titanium into the lithium niobate. The i.f. signal is converted into a surface acoustic wave at the transducer which is a key feature in defining bandwidth and ripple. A laser beam is coupled into the planar waveguide carrying the surface acoustic wave and the optical wave sees the acoustic wave as a diffraction grating so that Bragg diffraction of the laser beam occurs, the angle of diffraction being

$$\theta_B \approx \left(\frac{\lambda_g}{2V}\right) f, \quad \text{i.e. } \theta \propto f \tag{3}$$

where λ_g is the optical guide wavelength, V the acoustic phase velocity and f the acoustic frequency. The diffracted beam is then coupled out of the cell and focused onto a photodiode array which can be electronically read out to yield the spectral information present in the original i.f. signal. Within the context of the ESA sponsored work a 530 MHz bandwidth Bragg-cell at a centre frequency of 1·74 GHz employing a single tranducer has been developed.[18] A transducer geometry allowing frequency-controlled beam steering has been evolved for this cell. Present sub-systems specifications call for an operating bandwidth of 500 MHz, a design goal resolution of 1 MHz, a dynamic range of better than 40 dB, a mass of 20 kg and d.c. power consumption less than 20W. The output is a serial signal from the photodiode array carrying the spectral data of the i.f. signal.

7 A 300–500 GHz Receiver System

As has been indicated, ESA sponsored work on various critical sub-systems technologies for these heterodyne receivers has been in hand for some time. In order to prove these technologies a demonstration model receiver system is being integrated. This system will meet the specifications shown in Table 3. It incorporates two carcinotron local oscillators, one for 300–400 GHz and the other for 400–500 GHz using lightweight SmCo magnet technology. Quasi-optical diplexing using a polarizing Michelson interferometer along with a pair of quasi-optical corner cube mixers are also employed. A high stability phase-locked loop using both phase and frequency discriminators is used to lock the carcinotron local oscillators to a harmonic of an X-band (11–11·5 GHz) synthesizer which is used for tuning. The p.l.l. allows a frequency of 1 in 10^7 to be achieved, thus ensuring a frequency resolution of this order and hence resolutions of 30–50 kHz in the 300–500 GHz region.

Table 3

Specifications of 300–500 GHz Demonstration Heterodyne Receiver

Frequency range	300–500 GHz
Overall system noise temperature (double side band)	5000K (300–400 GHz) 10000K (400–500 GHz)
Spectral resolution	1 in 10^7 (with Bragg-cell processor, 1–2MHz)
Instantaneous bandwidth	500 MHz
Intermediate frequency	3·7–4·2 GHz
Maximum integration time	1 hour
Overall mass	70 kg
Overall d.c. consumption	120W typical 200W maximum

Spectrum analysers based on chirp/s.a.w. techniques and having bandwidths of tens of megahertz and resolutions of tens of kilohertz are presently commercially available, allowing the frequency resolution inherent in this type of

system to be realised. Conventional i.f. amplification (500 MHz bandwidth) and down-conversion to 1·7 GHz is followed by Bragg-cell spectral analysis.

A feature of this system is the incorporation of a high degree of automation resulting from the use of microprocessor control of all tuning functions such as diplexer tuning, local oscillator tuning and optimization, mixer tuning/orientation, receiver calibration, p.l.l. operation, spectral data processing and general housekeeping. Access to the receiver is by means of a terminal/microcomputer allowing the experimenter quickly and uncomplicatedly to select the type of observation (frequency, calibration type, integration time etc.) desired and carry it out with the minimum of time-consumption by the operational needs of the receiver itself.

8 Applications

Among the range of applications of such receivers such as laboratory molecular spectroscopy, plasma diagnostics, atmospheric physics and radio astronomy, the latter two represent the main drivers of technological improvements in the areas of sensitivity, tuneability and resolution. In the case of atmospheric physics the method of limb sounding of important trace gases in the atmosphere such as ozone, carbon dioxide, ClO and nitrogen oxides can be accomplished by heterodyne spectroscopy in the submillimetre wave region from high-flying aircraft platforms but potentially much more comprehensively from low-Earth-orbit spacecraft. Spaceborne radio-astronomy at submillimetre wavelengths is currently receiving increasing interest due to its potential return in the investigation of star formation in interstellar gas clouds, the evolution of galaxies, and the composition of comets and giant planets. In addition the increasingly perceived feasibility of sub-millimetre systems for space application is fuelling the thrust of system studies of large deployable telescopes for use in the submillimetre and far infra-red regions.[19]

9 Conclusions

High-resolution, sensitive spectroscopy in the sub-millimetre region of the spectrum is, and will in the future be, pushed forward by the development of highly tuneable heterodyne receivers of high sensitivity and spectral resolution. The key sub-systems for such receivers are the mixer front-ends, local oscillators and back-end spectrum analysers whose performances are presently being improved by technological advances often motivated by the potentially large scientific return from flying such receivers on spaceborne platforms free of the obscuring effects of the Earth's atmosphere. The high resolution spectroscopy which these receivers are suited to performing is likely to lead to increasing interest in their use for atmospheric physics and astronomical research. A broadband automated system currently being developed for ESA and employing advanced technological features such as quasi-optical Schottky mixers, lightweight highly tuneable local oscillators and a lightweight acousto-optic spectrum analyser is expected to serve as a demonstration model showing both the feasibility of such systems for future space applications and the scientific return achievable from high-resolution spectroscopy in the submillimetre region.

10 References

1 Clancy, P. F., 'Space applications and technology in the 100–1000 GHz frequency range', *The Radio and Electronic Engineer*, **49**, no. 7/8, pp. 395–402, July/August 1979.

2 Farran Research Associates (IRL), 'Sub-millimetre heterodyne spectrometer assembly' Phase I report on ESTEC Contract 4548/80/NL/HP, March 1982.†

3 National Physical Laboratory (UK), 'A theoretical and experimental study of Josephson frequency mixers for heterodyne reception in the submillimetre wavelength region'. Final report on ESTEC Contract 2334/74, 1978.†

4 Whickes, L. R., Nisenoff, M., Webb, D. C. and Spielman, B. E., 'Detection and mixer technology for millimetre waves', Sixth International Conference on Infrared and Millimetre Waves, December 1981, Miami Beach, Fla.

5 McColl, M., *et al.* 'The super-Schottky device at 30 GHz', *IEEE Trans. Magnetics*, **MAG-15**, p. 468, 1979.

6 Tucker, J. R., 'Predicted conversion gain in superconductor-insulator-superconductor quasi-particle mixers', *Appl. Phys. Letters*, **36**, p. 477, 1980.

7 Roesler, R. F. and de Zafra, R. L., 'Analysis of sis heterojunctions for use as mm-wave mixers exhibiting conversion gain', *Intl. J. Infrared Millim. Waves*, **3**, no. 2, p. 241, 1982.

8 Shen, T. M., Richards, P. L., Harris, R. E. and Lloyd, R. L., 'Conversion gain in mm-wave quasi-particle heterodyne mixers', *Appl. Phys. Letters*, **36**, p. 777, 1980.

9 Smith, A. D., *et al.*, 'Negative resistance and conversion gain in sis mixers', *Physica*, **108B**, p. 1367, 1981.

10 Kelly, W. M. and Wrixon, G. T., 'Optimization of Schottky barrier diodes for low-noise, low conversion loss operation at near millimetre wavelengths', 'Infrared and Millimetre Waves', Ed., K. J. Button, (Ed.) Vol. 3, p. 77, 1980.

11 Clifton, B. J., 'Schottky diode receivers for operation in the 100–1000 GHz region' *'The Radio and Electronic Engineer'*, **49**, pp. 333–46, July/August 1979.

12 Kerr, A. R., Siegel, P. H. and Mattauch, R. J., 'A simple quasi-optical mixer for 100–120 GHz' IEEE-MTT International Microwave Symposium Digest, 1977, p. 96.

13 Gustincic, J. J., 'Receiver design principles', *Proc. Soc. Phot. Opt. Instrum. Engrs*, **105**, p. 40, 1977.

14 Farran Research Associates (IRL), Final Report on ESTEC Contract 3767/78/NL/JS(SC) July 1980.

15 Kantorowicz, G. and Palluel, P., 'Backward wave oscillators' Infrared and Millimetre Waves, Vol. 1, pp. 185–212, 1979.

16 Chin, G., Buhl, D. and Florez, J. M., 'Acousto optic spectrometer for radio astronomy', Proc. Int. Conf. on Heterodyne Systems and Techniques Williamsbury, NASA Conf. Pub. 2138, p. 385, March 1980.

17 Barnoski, M. K., *et al.*, 'Integrated optic spectrum analyser', *Soc. Photo. Opt. Instrum. Engrs.*, **209**, p. 92, 1979.

18 Stewart, C., Stewart, W. J. and Scrivener, G., '500 MHz bandwidth guided wave L-band Bragg cell', *Electronics Letters*, **17**, no. 25/26, pp. 971–3, 10th December 1981.

19 Murphy, J. P., *et al.*, 'A large aperture space telescope for infrared and submillimetre astronomy', *Soc. Photo Opt. Instrum. Engrs.*, **228**, p. 117, April 1980.

† For availability of ESTEC contractor reports contact:— ESA Scientific and Technical Publication Branch, ESTEC, 2200 AG Noordwijk, Netherlands.

Manuscript received by the Institution on 9th June 1982
(Paper No. 2060/Comm 349)

UDC 621.317.335.3.029.65+621.317.39: 535.3
Indexing Terms: Electric measurements, Microwaves, Dielectric measurements, Optical measurements

Dielectric and optical measurements from 30 to 1000 GHz

J. R. BIRCH, B.Tech., Ph.D., MInstP*

and

R. N. CLARKE, B.Sc.*

SUMMARY

A review is presented of current measurement methods for the determination of dielectric and optical properties of materials at frequencies between 30 and 1000 GHz. The methods considered will fall into four main categories based on guided, resonant, free-space and stirred-mode geometries. The main applications of the measurements considered are in the study of materials that are relevant to telecommunication and radar developments. The significance of dielectric measurements for physico-chemical and biomedical studies is also briefly discussed. Among the methods covered are those based on waveguide bridges, closed cavities and open resonators, Fourier transform spectrometry and laser methods. The relatively new field of stirred mode (or untuned) cavity dielectric measurements is introduced and discussed. The application of these methods is illustrated by reference to measurements on low-loss solids, highly reflecting surfaces, liquids, composite materials and, briefly, on biological materials and gases.

* *Division of Electrical Science, National Physical Laboratory, Teddington, Middlesex TW11 0LW.*

1 Introduction

The optical or dielectric constants of a medium at a certain frequency are parameters which describe the way in which an electromagnetic wave propagates within the medium. They determine the spatial variation of both the wave amplitude and phase and the reflection and transmission effects occurring at interfaces between dissimilar media. This review will describe experimental methods currently used for the determination of these constants for liquids and solids in the frequency range approximately bounded by 30 and 1000 GHz, corresponding to wavelengths between about 10 and 0·3 mm. This spectral region therefore covers the near-millimetre wave and millimetre wave frequencies. A large number of measurement methods might be described as belonging to this metrological area, but our discussion will be restricted to those that determine both real and imaginary optical or dielectric constants of a medium. This requires a measurement of two quantities that are directly related to those constants. Thus the use of cavities in which the change in resonant frequency and Q-factor are determined will be considered in detail, as will guided wave and free-space methods which determine both the attenuation and the phase shift imposed on an electromagnetic wave by an interaction with a specimen. Methods which only determine the attenuation caused by a specimen will generally be omitted as it is not possible to calculate the optical constants exactly from a single measurement. Similarly, measurements where the phase information is inferred from an indirect parameter such as the period of a channel spectrum, or constructed from the use of Kramers–Kronig integral relationships will not be discussed. With one exception the techniques described will require specimens of well defined shape.

There are several important scientific and technological reasons why accurate knowledge of the optical or dielectric constants of materials are required in the spectral range between 30 and 1000 GHz. First, there is currently a great interest in telecommunications, radar, remote sensing and surveillance in this frequency range. This will necessarily create its own requirements for the knowledge of the optical or dielectric constants of materials that might be of interest to the designer and user of such systems.[1–4] A typical application would be in the design of radome materials[5] to meet the various electromagnetic, mechanical and thermal requirements that govern the use and protection of transmitter and receiver antennae for ships, civil and military aircraft, guided projectiles, missiles, and ground stations for satellite communications and astronomical observations. Other applications include microwave integrated circuit substrates, dielectric support materials and dielectric waveguides and resonators.[6] Secondly, the general increase in the use and application of the techniques of this frequency region in areas of potentially important scientific and technological development such as fusion plasma diagnostics[7,8] and biological studies,[9,10] in addition to those already mentioned, points to a requirement for standard reference materials. These would be specimens having known optical or dielectric

0033–7722/82/110565+20 $1.50/0

Table 1. Dielectric measurement techniques 30–1000 GHz. The figures in parentheses refer to the Sections of the paper in which individual techniques are discussed.

		Discrete Frequency		Broadband
		Guided	Free-space or quasi-optical (TEM propagation)	
Travelling wave	Single pass	Waveguide bridges (3.1) Microstrip measurements (3.1)	Free-space Bridges (3.2) Mach-Zehnder Interferometer (3.2)	
	Double pass	Waveguide reflectometers (3.3)	Free-space reflectometry Michelson interferometry (3.2,3.3,4)	Dispersive Fourier Transform Spectrometry (4)
Multi-pass	Resonant	Cavity resonators (5.1) Microstrip and dielectric resonators	Fabry–Perot resonators Open-resonators (5.2)	
	Non-resonant		Stirred-mode (untuned) cavities (6)	

properties for use in the calibration of spectroscopic instrumentation in order to assess levels of measurement uncertainty.[11] Similarly, calibrated attenuators will be required as will absorbing materials for the construction of thermal sources for the absolute calibration of radiometric response. All of these applications require accurate optical or dielectric constant data. Thirdly, the detailed origins of many loss mechanisms found in liquids and solids at these frequencies are poorly understood. Accurate knowledge of the spectral variation of the optical or dielectric properties associated with these mechanisms allows a discrimination between models of the dielectric response that is not possible with attenuation measurements alone.[12] This discrimination implies a better understanding of the microscopic dynamics of the system and should lead to advances in areas of technological and industrial interest.

The review is limited to a discussion of measurement methods for non-magnetic materials, though we recognize that there is considerable interest in the use of new magnetic materials in telecommunication related applications. Techniques for measurement on such materials are widely used at microwave frequencies, but few results have been reported in the frequency range covered here. However, these microwave techniques are closely related to some of those discussed in the review and, in principle, there is no reason why they should not be used at higher frequencies. This is evidenced by recent work of Josyulu *et al.*[191] at 34 GHz using reflectometric techniques and by resonant methods used for evaluating ferrites at millimetre wave frequencies.[192–4]

Table 1 is a guide to the techniques which will be discussed. Further introductory treatments of these techniques can be found in a number of recent publications.[13–16]

2 Notation

The division of the measurement methods of this frequency region into guided wave and cavity methods on the one hand and free-space methods on the other, and the long association of the former with microwave systems and the latter with far infra-red or sub-millimetre wavelength systems has led to a natural difference in the way the experimentally determined quantities are presented. In microwave usage the derived quantities are expressed as the real and imaginary parts, ε' and ε'' respectively, of the complex relative permittivity

$$\hat{\varepsilon} = \varepsilon' - j\varepsilon'' \tag{1}$$

where the symbol $\hat{}$ indicates a complex quantity, j is $\sqrt{-1}$, ε' is the relative permittivity and ε'', the imaginary part of $\hat{\varepsilon}$, is a measure of the loss of the material. The loss angle, δ, and its tangent

$$\tan \delta = \varepsilon''/\varepsilon' \tag{2}$$

are also widely used representations of loss. Loss angle is often conveniently expressed in units of microradians (1 μrad = 10^{-6} radian).

At frequencies above ~100 GHz, and in most non-resonant methods, the attenuation and phase of the wave are directly determined and this leads to expressing the derived quantities as the real and imaginary parts of the complex refractive index

$$\hat{n} = n - jk \tag{3}$$

where n is the refractive index and k the absorption index. Many free space measurements in this spectral region are made by the methods of Fourier transform spectroscopy for which the most common way of expressing the independent spectral variable is in terms

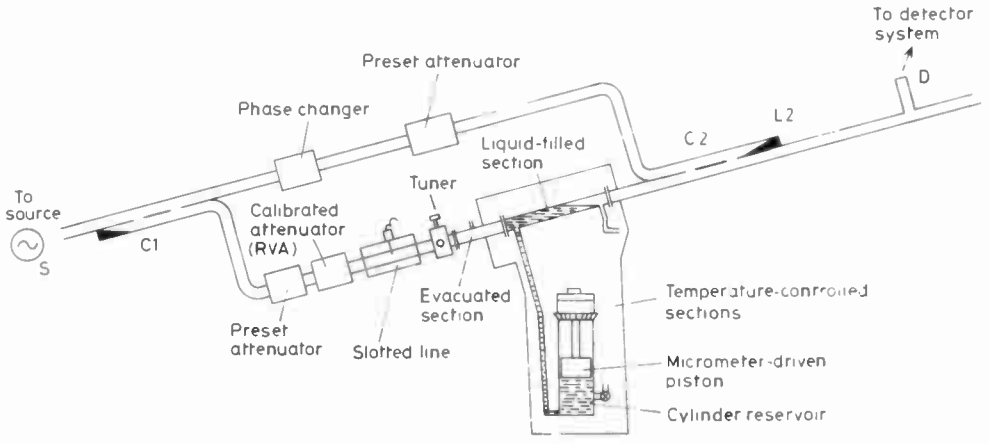

Fig. 1. Composite diagram of a waveguide bridge containing components used by Lynch and Ayers[17] and Hermiz *et al.*[20]

of wavenumber, $\tilde{\nu}$, the reciprocal of vacuum wavelength. This is related to frequency, f, and the speed of light, c, by

$$\tilde{\nu} = f/c \tag{4}$$

Wavenumber is usually quoted in terms of reciprocal centimetre, and so 1 cm^{-1} is approximately equivalent to 30 GHz. Although the absorption index k was introduced in equation (3), the equation for a plane wave propagating in a dissipative medium shows that the intensity decays with distance travelled, x, by the factor

$$\exp(-4\pi\tilde{\nu}kx) \tag{5}$$

It is, therefore, common practice to work with the power absorption coefficient, α, defined by

$$\alpha = 4\pi\tilde{\nu}k \tag{6}$$

For non-magnetic materials these two representations of the electromagnetic parameters are directly related through Maxwell's relation

$$\hat{\varepsilon} = \hat{n}^2 \tag{7}$$

leading to the simple transformations

$$\varepsilon' = n^2 - k^2, \qquad \varepsilon'' = 2nk \tag{8}$$

If a material is sufficiently transparent that $k^2 \ll n^2$ one also has the following approximate relationships

$$\varepsilon' = n^2 \tag{9}$$

$$\tan\delta = 2k/n = \alpha/2\pi n\tilde{\nu} \tag{10}$$

3 Discrete Frequency Single and Double Pass Measurements

It is generally convenient to distinguish between guided and free-space methods. The latter use transverse electromagnetic (TEM) propagation without continuous guiding constraints and are referred to as 'quasi-optical' if they mimic optical techniques or use focusing or collimating lenses or mirrors. Guided-wave methods are extensions of those used at microwave frequencies. Guiding structures: metallic or dielectric waveguide, fin-line or microstrip, are most commonly used at the lower millimetre frequencies, their upper frequency limit for metrological applications being governed by the difficulty of constructing the guide with sufficient accuracy.

3.1 Guided Single Pass Configurations

It is a well-establish metrological principle to compare a signal to be measured with a reference signal in a bridge technique. This principle is followed by the Lynch–Ayers waveguide bridge,[17,18] shown in Fig. 1, the operation of which is most easily appreciated for liquid measurements. One arm of the bridge contains a variable length column of the liquid under study. For a given setting of the phase shifter, a series of balance points can be achieved, between which the column length changes by $\lambda_g\lambda'_g/(\lambda_g - \lambda'_g)$, where λ_g and λ'_g are the guide wavelengths for air and liquid respectively. The calibrated attenuator must be adjusted for a complete balance, which occurs when the detector D is nulled and when all power which passes through the two arms of the bridge is dissipated in the load L2 of the 3dB directional coupler C2. The liquid's attenuation coefficient is derived from the set of attenuator readings on balance, taking into account multiple reflections.[19] Direct reflections from the fixed lower liquid boundary can be eliminated[20] but not those from the meniscus where reflections can only be minimized by tilting the bridge to produce a gradual transition. Bridges based on these principles have been implemented at 29 GHz,[17,19] 35 GHz[20] and 65 GHz.[17]

The detector geometry shown in the diagram is not obligatory but allows solid samples to be slipped into the waveguide at its open end to be measured by a liquid immersion techniques.[17] Innovations due to Hermiz *et al.*[20] included the stub tuner and slotted line, used to cancel reflections at the lower liquid boundary, and the calibrated reservoir to allow the volume of liquid transferred to the guide to be measured—this is necessary if one is to derive, rather than assume, ε' values. The bridge geometry is well suited for temperature control and Hermiz *et al.*[20] tabulate ε' and loss angle figures measured over a temperature range

−40°C to 25°C for pure liquid n-alkanes, C_5 to C_{14}. Uncertainties of the order 0·1% (standard deviation) in ε' and 1% in loss angle were achieved. These liquids exhibit relaxations in the 10−100 GHz region with loss angles peaking at 500 to 1000 μrad and the figures obtained, when taken with published results from other authors, allowed new estimates of molecular dipole moments and Frohlich relaxation time spread to be made.

Guided-wave techniques are not restricted to metal-waveguide implementations. Intrinsic dielectric properties, both permittivity[21] and loss[22], can also be obtained from calculable dielectric waveguides formed from the material under study. We cannot cover here the many techniques used for microwave integrated circuit substrate evaluation. The most common, economical and convenient methods do not involve evaluation of intrinsic properties but rather geometry-dependent equivalent parameters such as microstrip equivalent permittivity, a parameter of immediate value to the device designer. Intrinsic properties are, however, derivable from such measurements.[23–25]

3.2 Free-Space Transmission Measurements

Many accurate dielectric metrological techniques demand much of sample quality if they are to be used at all. Samples often have to be accurately machined to have uniform parallel faces, and may have to be rejected if they are warped. What is more, inhomogeneous materials scatter radiation—a mechanism which gives rise to spuriously high apparent loss if the scattered power is lost. Nevertheless, such materials are of great commercial importance and need to be assessed. One suitable technique that has recently become available, the stirred mode cavity, is discussed in Section 6. A second approach is to assess the material in a configuration which approximates to that in which it will be used. In these circumstances, systematic errors may parallel effects that will occur in practice and may possibly have less significant consequences. One has in mind, in particular, the assessment of radome composite materials[5] which are produced to fulfil mechanical specifications which often conflict with the optimization of electrical properties. Glass-fibre sheet composites of non-uniform texture and thickness used for this purpose may not meet the metrological requirements for some techniques. For such materials a free-space single-pass technique may be appropriate for medium and high-loss materials. The principle of the free-space bridge, shown in Fig. 2, is similar to that of the waveguide bridge in that signals pass through measurement and reference arms before being summed and nulled. In this case, the measurement arm has an unguided section situated between two horn antennae where relatively large cross-section samples are inserted. One such bridge operating at 35 GHz was used to measure a glass-fibre/epoxy-resin composite coated in graphite to give a resistance of 12 kΩ·m^{-1}.[26] The material was anisotropic and mean complex refractive indices were measured parallel to and perpendicular to the fibre orientation: $(n-jk) = (2{\cdot}53-j1{\cdot}58)$ and $(2{\cdot}10-j0{\cdot}165)$ respectively, there being a 1·5% standard deviation uncertainty associated with each component. Free-space bridges are also suitable for less-lossy and homogeneous materials and the same authors also measured nylon and intercompared the results with those from resonant methods. For normal-incidence multiple reflections must be taken into account[26,27] but this may be avoided if the sample is rotated to the Brewster angle.[27,28] Bridges operating at 70 GHz in which the sample is held in an oven have been used to measure properties up to approximately 2200°C.[28]

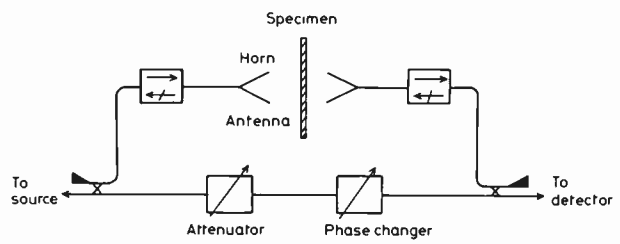

Fig. 2. A free-space bridge for dielectric measurements on large-sheet specimens. (After Cook and Rosenberg,[26] Crown Copyright).

A quasi-optical transmission measurement technique for liquid measurements at 285 GHz was described by Kilp.[29] The constant-length liquid cell was bounded by two collimating plano-convex lenses. Liquids could be contained on either side (or both sides) of an intermediate planar window which was translated to vary sample thickness. The cell was used in a number of configurations, but for low and medium loss dispersive measurements (i.e. those giving real and imaginary optical parameters), a Mach–Zehnder interferometer, or bridge-like, geometry was used. The cell was used in a recent large-scale intercomparison of liquid measurements which was carried out in seven European laboratories and sponsored by the EEC Community Reference Bureau (BCR).[11,30,31] Liquids measured included common non-polar solvents and solutions of chlorobenzene in cyclohexane. The exercise was of some importance since it involved a wide variety of measurement techniques covering the frequency range d.c. to 4 THz. Measurements in the constant-length cell exhibited typical uncertainties of 0·2% in ε' and 1·2−4% in ε'' and they provided a valuable check on the broad-band dispersive Fourier transform spectrometry results in the BCR exercise.[30,31]

3.3 Reflectometry in Waveguide Systems

For low-loss materials, reflectometry is a two-pass technique in which the sample (liquid or solid) must be backed by a high reflectivity mirror. For such materials the thickness of the specimen is an important parameter and multiple reflections must be taken into account. At the other extreme, very lossy materials such as water can be characterized by surface reflectometry if the sample is thick enough to absorb all transmitted power. There is a wide spectrum of measurements falling between these two conditions. Van Loon and Finsy[32–35] have developed reflectometric techniques for liquids in standard-waveguide cells for the range 5–140 GHz. The liquid is contained between a thin mica-foil window and

a shorting plunger. From the reflection coefficient of the cell measured as a function of liquid depth, the dielectric properties of the liquid can be computed by a curve-fitting procedure,[35] provided propagation mode-conversion is minimized. The design of a plunger which minimized conversion to higher-order modes was an important factor in the experimental development.[32] The method is most suitable for medium to very lossy liquids. For water measurements at 9–135 GHz, sample thickness was 0·5 mm or less for significant data. Complex permittivity of water at 135 GHz was measured as $(\varepsilon' - j\varepsilon'') = (5{\cdot}64 \pm 0{\cdot}2) - j(10{\cdot}42 \pm 0{\cdot}3)$. Uncertainties were typically similar at lower frequencies.[35] The authors also published results for solutions of trichloroethane in cyclohexane[34] and participated in the BCR intercomparison.[11,30,31] Medium and high-loss waveguide cells for liquid measurements at 70 GHz have also been described by Szwarnowski and Sheppard.[36] Their resolution for liquid thickness measurement was 0·01 mm and 0·001 mm respectively.

3.4 Free-Space Reflectometry and Ellipsometry

Free-space oblique-incidence reflectometry on variable-thickness liquid layers backed by a metallic reflector can also be based on a curve-fitting technique.[37,38] In general, oblique incidence is preferred in free-space reflectometry as it helps to alleviate the problems of multiple reflection, even if the angle of incidence is only a few degrees.[39] Measurements of this type on samples of relatively large surface area are convenient if the material under study is readily available and does not suffer from atmospheric contact. Examples of applications are millimetric measurements on ice and water[39] and on 'ground covers' such as concrete, asphalt, sand or snow.[40]

Ellipsometry uses a similar oblique-incidence geometry but has the advantage that it is a null technique based upon the properties of polarized light.[41,42] The sample is irradiated by elliptically-polarized light in such a way that at one angle of incidence the reflected wave will be plane-polarized and the detected power seen through a crossed-polarizer will be nulled. The sample dielectric properties are deduced from the instrument geometry and the polarization parameters of the incident radiation. Thorpe *et al.*[42] have proposed a millimetre-wave instrument based on this principle.

Normal incidence two-pass measurements can be carried out by Michelson interferometry, discussed in detail in Section 4, see Figs. 3 and 4. We introduce it here because it can, of course, be used with discrete-frequency sources. Like bridge techniques it follows the metrological principle of comparing the signal from the sample with a reference signal and accordingly is suitable for accurate measurements on low to high-loss materials.[43–46,28] The techniques used are not necessarily reflectometric, but involve two passes through the sample for all but surface reflectivity measurements. Measurements in Michelson interferometers at the University of Nancy[43–45] were an important contribution to the BCR intercomparisons.[11,30] Instrumentation already discussed in the context of transmission measurements has also been adapted for normal-incidence reflectometry. Thus, free-space bridges can be used for reflectance measurement,[26] as can the liquid cell of Kilp.[29]

Looking to the future, it appears that the 'six-port'-junction reflectometry principle[47,48] will be of value in dielectric metrology. The 'six-port' concept has proved very successful at microwave frequencies and excellent measurement repeatabilities are now possible for device impedance or scattering parameter determination. Dielectric measurements are also proving amenable to the technique. For near-millimetre wave reflectometry, Stumper[49] has described a possible quasi-optical, multi-Michelson six-port geometry which could be adopted for this purpose.

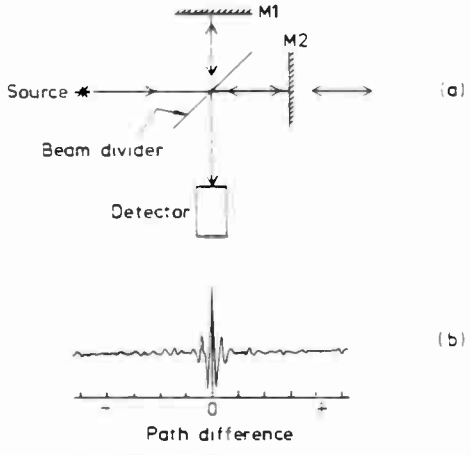

Fig. 3. (a) A schematic representation of a two-beam Michelson Interferometer used in Fourier transform spectroscopy. M1 and M2 are plane mirrors. M1 is fixed in position while M2 can be moved either way along the direction of propagation of the radiation incident upon it. (b) This shows a typical interference pattern recorded by such an instrument.

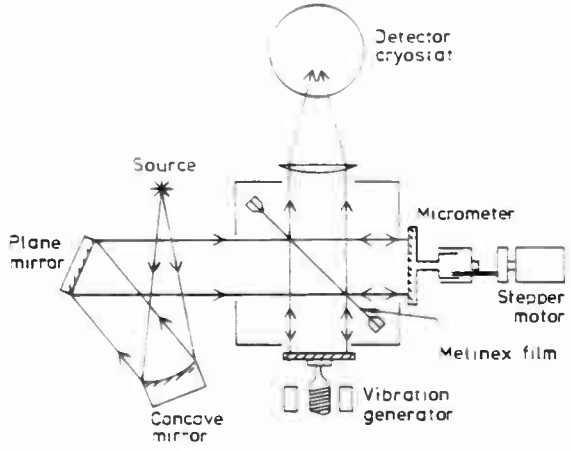

Fig. 4. A two-beam Michelson interferometer using a thin-film dielectric beam-divider and typical of those used for the determination of optical constants by DFTS at near-millimetre wavelength. (Crown Copyright).[68]

3.5 Near Millimetre Laser measurements

Little use has been made of lasers as sources in free space quasi-optical dielectric measurements below 1000 GHz, in spite of the large number of optically-pumped laser lines that are available for use as near-millimetre wavelength sources.[50,51] When such measurements are made the specimen is placed in one arm of a two-beam interferometer and an interference pattern observed as the optical thickness of the specimen is varied. The refractive index is derived from the oscillatory period of the pattern, while the absorption coefficient can be found from the decrement of the pattern. In measurements on solids the variation in specimen optical thickness is achieved by rotating the specimen in one arm of an interferometer. This should be a double-pass Michelson interferometer, as the double pass through the specimen automatically compensates for the lateral shear introduced by the specimen rotation. Polyethylene, PTFE and crystal quartz,[52] perspex, crystal quartz and polypropylene[53] and TPX[54] have been studied in this way at 891 GHz (0·337 mm wavelength) with uncertainties in the best measurements that varied between $\pm 0{\cdot}002$ and $\pm 0{\cdot}012$, depending on the level of absorption in the specimen. Measurements on liquids have been made with a Mach–Zehnder,[53] rather than a Michelson, interferometer to reduce the level of power returned to the laser by the interferometer. The specimen would be mounted in a variable thickness liquid cell, and the interference pattern recorded as the thickness is systematically varied. In this way measurements have been made on carbon tetrachloride, p-xylene, ethyl benzene, toluene, tetrabromoethane and chlorobenzene[53,55] with a random uncertainty in the refractive index that was typically $\pm 0{\cdot}0002$ in the better of the two sets of measurements.[53]

4 Broadband Quasi-optical Methods

Broad band spectroscopic measurements at the wavelengths with which this review is concerned are more difficult than in many other spectral regions due to the low power levels emitted by the thermal sources used. At the present time, there is only one broadband technique available for the determination of both optical constants of materials at frequencies from about 100 GHz to those in excess of 6000 GHz. It is known as dispersive Fourier transform spectroscopy (DFTS) and is a special form of the widely known technique of Fourier transform spectroscopy (FTS). In the following parts of this Section the general principles of DFTS are discussed, and its experimental application to the determination of the optical constants of weakly and heavily absorbing solids and liquids at frequencies up to 1000 GHz examined.

4.1 General Principles of FTS and DFTS

Fourier transform techniques are the best for broadband spectroscopic measurements in the near-millimetre and infrared portions of the electromagnetic spectrum. This is largely as a result of two advantages, the multiplex and the étendue advantages, that the method possesses over other spectroscopies. The first of these refers to the simultaneous observation of all spectral elements in an interferometric measurement. In a detector-noise-limited system this results in the observed spectrum having a signal-to-noise ratio that is $\sqrt{M}$ times greater than that found in a measurement of the same spectrum in the same time by a sequential observation method. (M is the number of spectral elements observed.) The second advantage refers to the large radiation throughput that interferometers possess as a consequence of their cylindrical symmetry. Non-interferometric techniques use narrow slits to achieve adequate resolving powers and these severely restrict the radiation throughput. These two advantages are also known as the Fellgett and Jacquinot advantages after their respective discoverers.[56–59] Detailed discussions of these advantages and of their practical consequences may be found in books on the subject.[60–62]

All Fourier transform interferometric spectrometers have two major components. First, a two-beam interferometer which produces an intensity delay pattern known as an interferogram. Second, a digital computer used to compute the Fourier components of the interferogram, leading to the observed spectrum. The most common form of interferometer used is the Michelson-type shown schematically in Fig. 3. Radiation from the source is divided into two orthogonal beams by the beam divider. These travel along separate paths to plane mirrors M1 and M2, one of which (M1) is fixed in position, while the other can be translated along the propagation direction of the radiation incident upon it. The two beams are reflected at the mirrors and recombine at the beam divider to give a pair of beams that return to the source and are lost to the experiment, and a pair that travel on to the detector.

In an FTS measurement the position of mirror M2 is varied in a systematic manner and a recording made of the voltage analogue of the intensity interference pattern between the two beams recorded by the detector. For a polychromatic source this is typically of the form shown in the second part of the Figure, having a unique grand maximum when the two arms are of equal length. As the path difference increases to either side of this position the signal goes through an oscillatory behaviour and tends to a constant value. The modulus of the complex Fourier transform of this interference pattern gives the detected intensity spectrum. In a conventional FTS experiment the ratio of such spectra obtained with and without the specimen placed between the interferometer and the detector gives either the power transmission or power reflection spectrum of the specimen, depending on the particular measurement made. There then exists a range of approximate methods of analysis which allow one, or sometimes both, of the optical constants to be deduced from the measured quantity.[63] Such a measurement is only of the power insertion loss of the specimen[64] as the power-law detector does not respond to the phase shift imposed symmetrically upon both output beams by the specimen.

In a DFTS experiment, however, the specimen is placed in one of the orthogonal beams within the interferometer and as only this beam interacts with the

specimen the interferogram now contains the desired phase information, which can be recovered by a complex Fourier transformation to give the complex transmission or reflection spectrum of the specimen. The optical constants are then calculated from this by the application of exact expressions derived from the Fresnel equations for the complex transmission and reflection coefficients of an interface between two dissimilar media.

4.2 Near-millimetre Wavelength DFTS Instrumentation

The previous Section has outlined the nature of the DFTS method and the general form of the instrumentation used. In this Section some details of the features of the two commonly used interferometers for near-millimetre wavelengths DFTS will be given.

The first is the Michelson interferometer using a thin film dielectric beamdivider illustrated in Fig. 4. The radiation from a 120 W mercury vapour arc in a quartz envelope is collimated before entering the main body of the interferometer. The beam divider would be a thin polymer film, usually of Melinex.† The best broad band performance at these frequencies can only be attained through the use of liquid-helium-cooled detectors, their low n.e.p.s ($\sim 10^{-12}$ WHz$^{-1/2}$) compensating for the low source power levels. Perhaps the most widely used detectors of this type are based on the hot electron bolometric effect in indium antimonide.[69] Such detectors are commercially available.[70]

A.c. modulation and detection of the radiation from such an instrument is always used. This may be accomplished in one of three ways. First, amplitude modulation of the source by a rotating mechanical chopper, which will give the type of interferogram shown in Fig. 3(b). Second, phase modulation of the radiation within the interferometer can be used.[71–73] This is the scheme illustrated in Figure 4. The fixed mirror of the interferometer is mounted on a mechanical transducer and given a small sinusoidal motion of peak-to-peak amplitude about equal to one-quarter of the mean wavelength of the spectral region being studied. The detected modulated signal then only contains interferometrically modulated information. In either amplitude or phase modulation the moving mirror of the interferometer is driven by a stepper motor. The third form of modulation used is that of rapid scan, in which the moving mirror is driven at a constant velocity over the range of path differences required in the measurement.[61] This automatically modulates the various radiation frequencies at audio frequencies which are then detected in sufficiently broad band post detector electronics. The last two of these forms of modulation can lead to systematic error when used for FTS due to the presence of interferometrically-modulated radiation from the detector port of the interferometer in the detected signal.[68] This can be particularly significant when phase modulation is used at long wavelengths with liquid-helium-cooled detectors. The error is not, however, present in DFTS, due to the greater symmetry

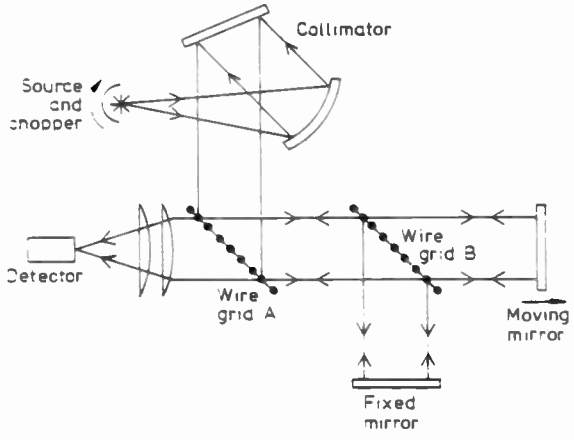

Fig. 5. A Martin-Puplett polarizing interferometer using wire grid beam dividers (From Ref. 75, reproduced by permission of Pergamon Press).

of the DFTS experimental configuration to all the radiation fluxes within the interferometer.

The second basic type of interferometer used for DFTS measurements at near-millimetre wavelengths is the Martin–Puplett, or polarizing, interferometer.[74] A version used for such measurements is illustrated in Fig. 5. This instrument avoids the limited spectral bandwidth of the thin film dielectric beam divider instrument by using the polarization properties of self-supporting two-dimensional wire grids. In the instrument shown in the Figure the wires of grid A are taken to be vertically arranged while those of grid B are oriented to give a projected angle of 45° to the radiation incident from A. Grid A acts as a polarizer to the input radiation and as an analyser to the output radiation. In the original configuration of the instrument of Martin and Puplett[74] only one grid beam divider was used, together with roof top reflectors instead of plane mirrors to terminate each arm of the interferometer. The advantage of this is that both sets of output beams travel to the detector, one is not lost to the source. As the interference patterns corresponding to the two sets are in antiphase a polarizing chopper can be used to chop between them and give an enhanced signal with a zero baseline. This configuration has not however been used for DFTS as the arrangement of the roof top reflectors changes the plane of polarization of the radiation incident on them by 90° on reflection. This means that a specimen placed in that arm for a double-pass transmission measurement would be probed by two orthogonal polarization states of the same beam. Thus, any information on the anisotropy of the optical constants would be lost by averaging. In Fig. 5 the source is shown as being modulated by an amplitude chopper. This is because the spatial separation of the two orthogonally polarized outputs by grid A means that polarization modulation cannot be used. Phase modulation can also be used in such instruments.[76,77] Polarizing interferometers used for DFTS have used free-standing wire grids wound from 5 to 10 μm diameter tungsten wire, and these have been demonstrated[78,80] to give interferometric response from about 2 to

† ICI trade name for polyethylene terephthalate.

700 cm^{-1}, although it is thought that the polarization behaviour of the grids fails in the region about $\sim 400\ cm^{-1}$ and that the higher wavenumber interferometric response observed was due to action of the grids as normal division of amplitude beamdividers.

4.3 DFTS of Transparent Solids

A specimen that transmits a reasonable fraction of the radiant energy incident upon it would be measured in instruments of the form of those shown in Figs. 4 and 5. It is difficult to be exact about what a resonable fraction would be as it depends on a number of factors, such as specimen size and resolution required, that vary from specimen to specimen. However, a power transmission factor of 0·05 (5%) would certainly be measurable in these instruments and should lead to good values of the optical constants. Under ideal conditions, relatively large aperture specimens and the use of a liquid helium cooled detector, good optical constant data at near-millimetre wavelengths can be obtained from specimens that transmit only 0·001 (0·1%) of the incident power. In these interferometers the specimen is placed in the fixed mirror arm and the probing radiation passes through it twice, once before and once after reflection at the mirror. The measurement is generally known as a double-pass measurement. The specimens are generally introduced into the interferometer by slide mechanisms that are manually operated from outside of the interferometer.[81,82] The main requirement on the specimen is that it be of a plane parallel form so that the measured attenuation and phase shift can be related to the optical constants through a simple application of Fresnel's equations. Thus, specimen preparation is important, and it is generally the case in current near-millimetre wavelength transmission DFTS measurements that either departures of the specimen form from this ideal shape, or inaccurate knowledge of the specimen thickness, provide the limiting (systematic) error in such measurements.

Most near-millimetre wavelength measurements of this type have been made in the last half decade or so, even though the technique has been established for nearly two decades. Early measurements on crystal quartz by Chamberlain *et al.*[83] came down to 600 GHz using a room temperature detector, while later measurements on ferrite materials for use in Faraday rotation modulators[84] reached down to 150 GHz using a liquid helium cooled detector. More recent double-pass measurements have included studies of the optical constants of silicon,[85] fused quartz,[81] soda-lime-silica glass,[86] some common low loss polymers[87,88] and alumina, beryllia, fused silica, titanium silicate and glass ceramics.[89] In the measurements on single crystal silicon[85] high levels of measurement reproducibility were attained through the use of the liquid-helium-cooled indium antimonide hot electron bolometer referred to previously.[69] This resulted in a measurement of the refraction spectrum that had a random uncertainty between 0·0001 and 0·0002 and a measurement of the absorption spectrum in which this was 0·05 $Np \cdot cm^{-1}$. The measurements on fused quartz[81] are of particular

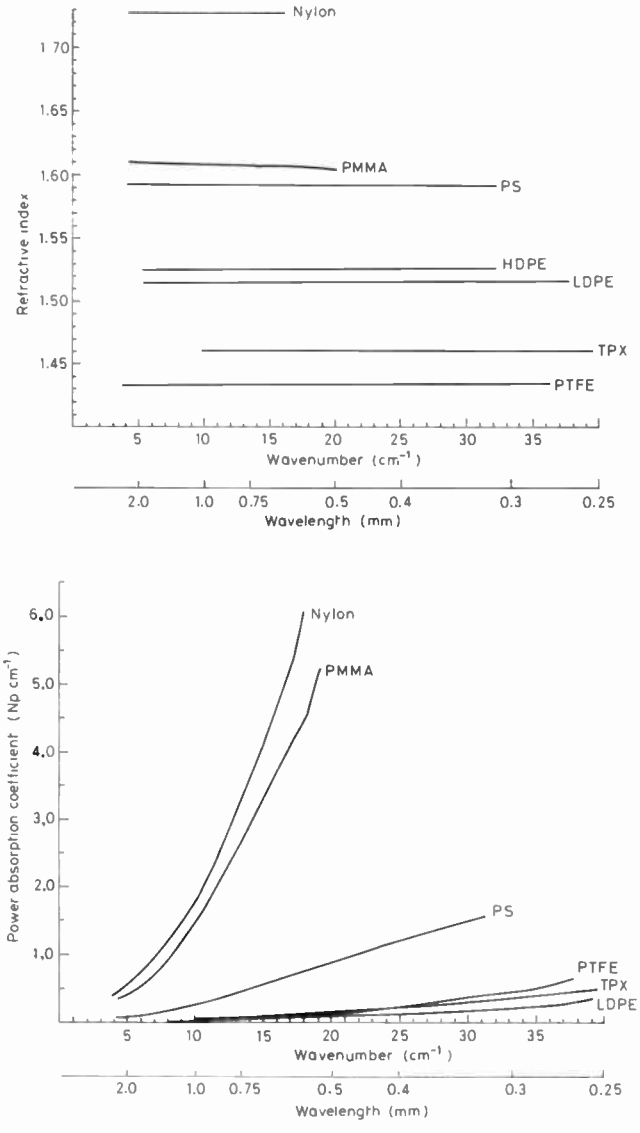

Fig. 6. The refraction and absorption spectra at 290 K of seven common low-loss polymers. HDPE—high density polyethylene. LDPE—low density polyethylene. TPX—poly-4-methyl pentene-1. PTFE—sintered polytetrafluoroethylene. PS—polystyrene. PMMA—polymethyl methacrylate (perspex, plexiglass). nylon—polyamide. (Crown Copyright).[87,88]

interest as they demonstrate a point referred to earlier. The level of random uncertainty in the measured refraction spectrum was sufficiently low that the overall measurement accuracy was limited by the systematic error in the determination of the specimen thickness. Thus one has the result that broadband optical constant measurements at near-millimetre wavelengths, a region of the spectrum that has traditionally been considered difficult to work with because of the low power levels emitted by the thermal sources, can now be limited by mechanical rather than electromagnetic uncertainties.

The measurements of the optical constants of the low-loss polymers[87,88] are reproduced in Fig. 6. Such polymers find widespread use as transmission components in millimetre and near-millimetre

wavelength equipment and absorption spectra. There was, however, little quantitative broadband information on their refraction spectra, particularly below 1000 GHz. Thus, DFTS measurements such as those of this figure provide a body of information of use to the designer and user of near-millimetre wavelength systems. These measurements also indicate current levels of measurement capability for transparent solids fairly well. For the lowest-loss specimens the random uncertainty in the refraction spectra typically occurred in the fifth decimal place, and in the fourth decimal place for the more absorbing specimens. The uncertainty in the measurement of thickness for these specimens was such that there could have been a possible systematic error of up to 10^{-4} in the calculated refraction spectra. Thus, the refraction spectra of the more absorbing specimens could have similar random and systematic errors, while in those of the more transparent specimens a systematic error could be the dominant uncertainty.

As the level of the absorption in a specimen increases and leads to smaller transmitted signals it becomes difficult to make double-pass measurements, and other DFTS techniques to be discussed in the following Section must be used. An indication of the transmission levels down to which the double pass method may be used is given in Fig. 6 which shows the optical constants and transmission spectra of a 0·44 mm thick specimen of a material known as Ferroflow. This is a castable microwave absorber for the 1 to 10 GHz region† consisting of chemically-formed carbonyl iron spheres uniformly dispersed in a plastic base. It is not apparent on the scale of the Figure, but the lowest fractional transmission levels measured are $\sim 0{\cdot}0006$, and reproducible values of the absorption and refraction spectra were obtained down to these levels.

4.4 DFTS of Heavily Absorbing and Reflecting Solids

When the absorption in a specimen has increased to such an extent that a double-pass transmission measurement cannot be made, it may be possible to make transmission measurements using the single-pass method in which the optics of the instrument are arranged so that the probing radiation only passes once through the specimen.[91,92] This is because of the amplitude advantage of single-pass measurements. In a double-pass measurement the power transmission of the specimen is determined while in a single-pass measurement it is the square root of the power transmission that is determined. In regions of very low transmission the latter can be an order of magnitude or more times greater than the former. The method has not been widely used below 1000 GHz and the only measurements in this region appear to be those of Russell and Bell who determined the optical constants of crystal quartz[93] and of sapphire[94] down to 20 cm^{-1} (600 GHz), although these materials are sufficiently low loss that they may be measured in a double pass configuration.

If the absorption of a specimen is so large that single pass transmission methods cannot be used, dispersive reflection measurements must be made. These differ from transmission DFTS in that the specimen becomes the mirror terminating one arm of the interferometer, and the amplitude and phase of its complex reflectivity are determined. Instruments for such measurements at ambient temperatures were developed by a number of workers, and these formed two types depending on how the reference measurement was made. In one group the specimen physically replaced the fixed mirror of the interferometer,[91,95–97] while in the other group the specimen was not moved. In this latter group part of the specimen surface was aluminized to provide the reference reflector, and the field of view of the interferometer divided by a set of screens so that either the aluminized or the non-aluminized areas could be illuminated.[98–100] Subsequently, several of these instruments have been developed to allow measurements at temperatures down to those of liquid helium and up to 500 K. These developments are covered in the two review papers on DFTS.[65,66]

Little use has been made of dispersive reflection spectroscopy for materials characterization below 1000 GHz. Most of the measurement interest has been above 50 cm^{-1} in studies on the lattice modes of materials such as the alkali halides and compound semiconductors, and the subsequent derivation of information about their microscopic dynamics from the measured optical constants. An application of DFTS reflection methods to the region below 1000 GHz has come from work on the absolute determination of complex reflectivity. The measurement of power reflectivity at millimetre and far-infrared wavelengths is generally a relative measurement in which the power reflected from a specimen is compared to that reflected from a reference which is assumed to have unity power reflection coefficient. The accuracy that can be achieved in such a measurement therefore ultimately rests upon the validity of this assumption. In the dispersive method the optical constants of a silicon specimen were determined by transmission DFTS. These were then used to calculate the complex reflectivity of the silicon specimen from Fresnel's equations. As the complex refractive index measurement only required knowledge of the defined refractive index of vacuum and of the length standard, the procedure can be taken as providing an absolute determination of complex reflectivity. The random uncertainty in the derived amplitude reflectivity was about 10^{-5} (10^{-3}%) with a possible systematic error of up to 10^{-4}. In the phase of the complex reflectivity the random uncertainty was about 7×10^{-5} rad. This specimen was then used as a reference reflector of known, rather than assumed, reflectivity in subsequent measurements.

4.5 DFTS of Liquids

In the study of liquids by DFTS the liquid specimen must be contained in a cell to produce a well-defined shape so that the results of such a measurement can be analysed. Recent developments in liquid-state DFTS have concentrated on the design and operation of a particular type of cell and have successfully combined in one piece

† Manufactured by the Microwave Filter Company Inc., East Syracuse, New York 13047, USA.

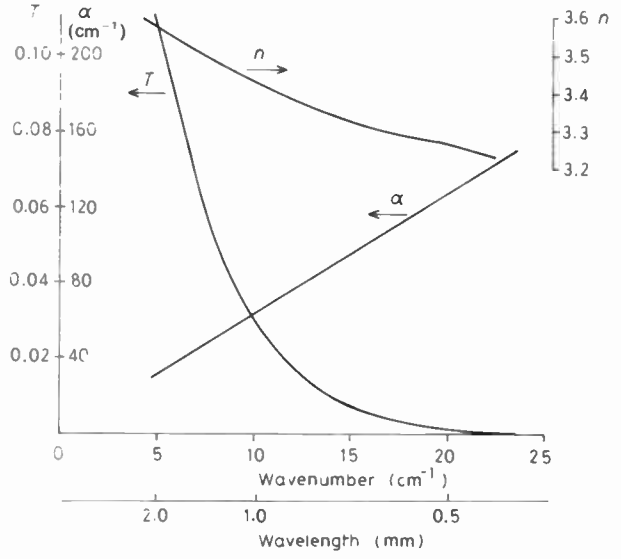

Fig. 7. The power transmission (T), absorption (α), and refraction (n) spectra of a 0·44 mm thick specimen of Ferroflow, a castable microwave absorber for the 1–10 GHz region (J. R. Birch, unpublished results).

of apparatus the several different techniques previously used for liquid studies. The early development of the various techniques used to study liquids can be found in the literature.[65,66,76,102–106]

Most of the measurements made with these early techniques used room temperature detectors and gave results that only just extended down into the present region of interest. An interesting point about this early work is that while the experimentalists believed the spectral variation of the measured refraction spectrum, they preferred to fix its overall level by reference to an independent measurement of the refractive index at a single frequency using a gas laser source such as an HCN laser at 891 GHz or an H_2O laser at ~ 2·5 THz. This arose in part from the difficulty of determining the thickness of the specimen in the particular experimental configuration used, and in part to possible errors introduced by the analytical procedure[102] followed in deriving the refraction spectrum from the measured spectra. This procedure has subsequently been shown to be unnecessary and susceptible to systematic error.[107,108] The improved experimental and analytic methods of current DFTS result in measurements of refraction spectra that have low levels of random and systematic error, and such level adjustment procedures are not now necessary. In spite of such systematic adjustments high radiometric precision was achieved in the early liquid DFTS studies and levels of random uncertainty in the derived optical constants were low. Davies and Chamberlain,[109] for example, in measurements on p-difluorobenzene in solution in both carbon tetrachloride and cyclohexane found it necessary to set the level of their refraction spectra by reference to measurements made with a HCN laser, but achieved levels of random uncertainty in their refraction spectra of $\pm 0{\cdot}0003$ at frequencies down to 600 GHz.

The low levels of measurement uncertainty that can presently be achieved in DFTS studies on liquids below 1000 GHz have been demonstrated in recent publications in which DFTS determinations of the optical constants of some pure liquids and solutions have been compared with microwave measurements.[110,111,11] The first two of these came to the conclusions that for measurements on reasonably transparent liquids the Fourier transform method is capable of giving the absorption spectrum with a precision of 2–3% over a wide frequency band, and the refraction spectrum with a random error of about 0·2% and a possible systematic error of up to 0·6%. When the DFTS data was combined with the comparison microwave data to produce an estimated smooth fit over the whole frequency range it was found that the overall uncertainty in absorption was $\pm 1\%$ and $\pm 0{\cdot}2\%$ in refraction. The third of these comparisons[11] was the result of a large international comparison on dielectric measurement methods aimed at producing standard reference liquids for dielectric spectrometers. It involved measurements by DFTS, open and closed cavity resonators, a waveguide reflectometer, oversized cavity resonators, an automated coaxial line, an oversize waveguide interferometer and a free space interferometric method based on the fourth harmonic of a 71 GHz klystron, all of which covered the range from

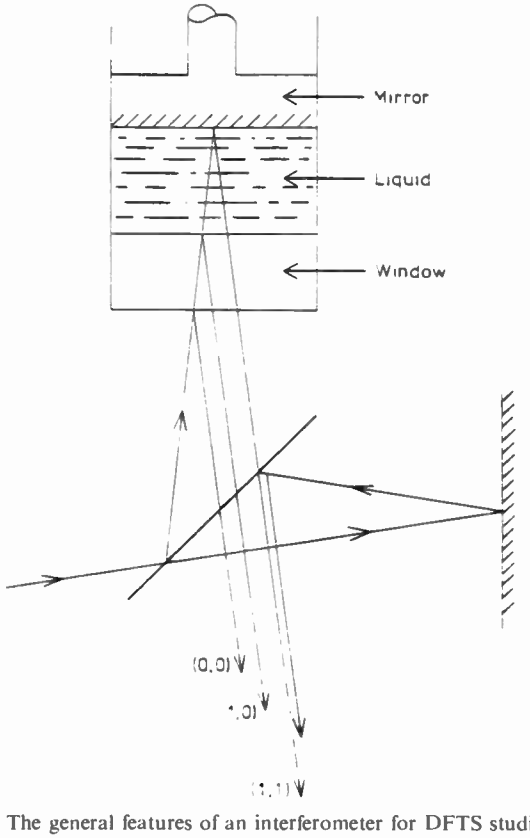

Fig. 8. The general features of an interferometer for DFTS studies of liquids using a closed, variable thickness liquid cell. The first rays reflected from the three interfaces of the cell: interferometer-window, window-liquid, liquid-mirror, are labelled according to the notation of Honijk *et al.*[111] (Crown Copyright).[66]

1 GHz to 4 THz. A large number of commercially available liquids, specially purified liquids and solutions were studied. The random error was assessed from the internal variability of each measurement method and was typically found to be $\pm 0{\cdot}2\%$ for ε' and $\pm 3\%$ for ε''. From the combined spectral data for a given liquid it was estimated that an overall uncertainty as small as $\pm 0{\cdot}1\%$ for ε' and $\pm 1\%$ for ε'' could be obtained over a wide frequency range.

It was mentioned earlier that the major recent developments in the techniques of liquid-state DFTS have been in the design and operation of a new type of liquid cell. The basic structure of such a cell is presented in Fig. 8 which shows such a cell in an interferometer. The cell is shown in the format of the early versions of these instruments[112,113] in which the liquid specimen was totally contained within a hollow cylinder between a transparent window sealing the lower part of the cell and a mirror which was free to slide within the cylinder. The position of the mirror was adjusted from outside of the cell to give the desired thickness of specimen for a particular measurement. Windows made of silicon, germanium, crystal quartz and TPX have been used with these early cells. In the Figure the rays shown reflected from the three interfaces of the cell have been labelled according to the notation of Honijk *et al.*[114]

Few accounts of systematic measurements made with these cells have been published, and of those that have been only one covers the range of frequencies of this review. It involved measurements on a dilute solution of acetonitrile in carbon tetrachloride in the spectral range from 2 to 200 cm^{-1} ($\sim$ 60 GHz to 6 THz).[115] Such studies on a dilute solution of a polar molecule in a non-polar solvent are of value because by dilution it is possible to distinguish between the single molecule contribution to the rotational correlation function and the contributions due to interaction-induced intermolecular correlations, the latter decreasing with increasing dilution.

Although the closed cells described above offered improved performances over the earlier methods that they replaced they suffered from the nature of their close fitting, piston-within-cylinder mechanisms. These made it difficult to align the mirror in the cell, and were susceptible to being jammed. A new variable-thickness cell has recently been developed[77] that avoids these problems by having a more open internal structure to avoid close fitting parts. It has been used in transmission measurements of the temperature variation of the optical constants of carbon tetrachloride,[77] and in dispersive reflection measurements on water and aqueous solutions of concentrated salt solutions[116] using a new experimental approach to such measurements.[117]

5 Resonant Techniques

In these methods the permittivity and loss of a dielectric specimen are derived from the resonance frequency, dimensions and Q-factor of a resonator into which the specimen is introduced. Most important at millimetre-wave frequencies are techniques involving open resonators but closed-cavity techniques can also be applied at the longer millimetre wavelengths. One advantage of the latter is that they may allow one to use smaller specimens. Cavities are also inherently more susceptible to temperature control. A number of common observations can be made for both types of resonator, however. Permittivity may be deduced from resonator dimensional changes required to preserve the same resonant frequency on insertion of the sample[118,119] or from measurement of wavelength in the sample.[120,121] For some years neither approach has presented major experimental difficulties since adequate displacement-measurement techniques and frequency counters have been available commercially. Experimental effort has therefore been aimed at accurate Q-factor measurement. For Q-factors of the order of 10^5 phase-locking and heterodyne techniques may be necessary to obtain uncertainties as low as 1%. One such method[119] follows tradition in relying upon observations of the resonance *amplitude* to determine the 3dB resonance width in terms of frequency. However, the recent significant progress in automation of Q-factor measurement has not only been based upon this method[122] but also upon detection of the *phase* changes associated with the resonance.[123,124] For lossy samples one restricts oneself to small sample volumes and to a perturbation technique[125] or else to placing the sample close to an electric field minimum[126] so as not to excessively load the resonator.

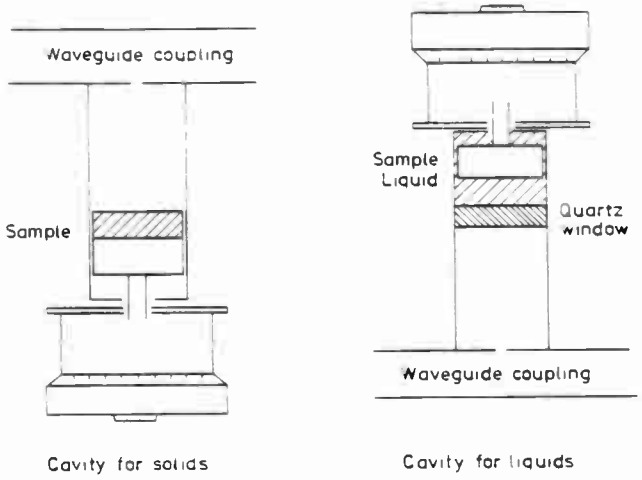

Fig. 9. Schematic diagram of TE_{01n} cylindrical cavities for measurements on solid and liquid specimens. The micrometer-driven piston is positioned to produce the same resonant frequency with and without the specimen. (After Cook[118] and Rosenberg *et al.*,[128] Crown Copyright).

5.1 Cavity Resonators

The use of purpose-built fundamental mode cavity resonators at frequencies above 30 GHz is uncommon since machining requirements for accurate measurements become very exacting. This can be overcome by the use of higher modes in significantly overmoded cavities. A common configuration having a cylindrical geometry is the TE_{01n} mode cavity in which the length is the frequency-determining dimension and where the diameter may amount to a few wavelengths. It

is possible to use a disk-shaped sample which fills the cavity,[127] but with a partially filled cavity having the sample at one end (Fig. 9) one has a calculable geometry which is well suited to the measurement of low-loss solids.[11] Such cavities require a mode filter to remove a degenerate TM_{11} mode. This has been implemented by forming all or part of the cavity from a helically-wound cylindrical section which does not allow longitudinal surface currents to propagate.[118,120] Stumper[120] used TE_{01n} cavities for measurements on non-polar liquids such as n- and cyclo-alkanes in the 26–70 GHz region and at 136 GHz. The liquid was allowed to fill only a portion of the cavity between a dielectric foil window and a moveable short-circuit. The waveguide coupling was located in the air-filled part of the cavity in order to retain constant coupling. Permittivity was determined from the guide-wavelengths in the air and liquid respectively. Q-factor measurement for these cavities was recently automated.[122] Rosenberg *et al.*[128] employed 50 mm diameter TE_{01n} helical waveguide cavities at 10 and 35 GHz for non-polar liquid measurements. Again, the cavity was partially-filled (see Fig. 9), with the liquid contained between a piston short-circuit and a window, in this case a quartz-crystal disk of significant thickness. The associated theory was derived without loss of generality for a three-layer TE_{01n} system, however, in practice, the intrusive effects of the quartz window were minimized by making it an integral number of half guide-wave lengths thick. The unloaded Q-factor of the 35 GHz resonator was approximately 10^5 and its insertion loss was kept as high as 70 dB to minimize coupling perturbations. Measurements[128] on n-alkanes were published in greater detail by Hermiz *et al.*[20] (see Sect. 3.1) and compared with reported results due to Stumper and other workers. Uncertainties of the order $\pm 0{\cdot}001$ (standard deviation) in permittivity and

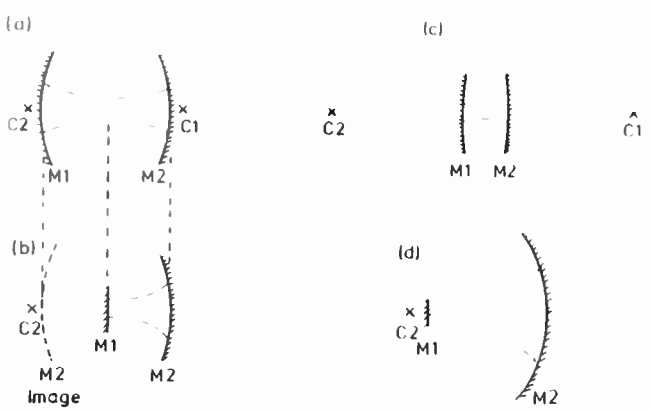

Fig. 10. Plano-concave and bi-concave open resonator geometries. Concave mirrors M1 and M2 have centres-of-curvature at C1 and C2 respectively. The beam geometry is shown (dashed lines). (a) Shows a *near-confocal* configuration; if the concave mirror M1 is replaced by the plane mirror M1 in (b) one contains a related *near-semi-confocal* geometry; (c) is a 'short' bi-concave resonator and (d) shows a *near-hemi-spherical* resonator. (The prefix '*near-*' is often dropped and the resulting terms should not be taken literally). The beam diameters are at a minimum at the waist. but waist diameters of (a) and (b) are greater than those of (c) and (d).

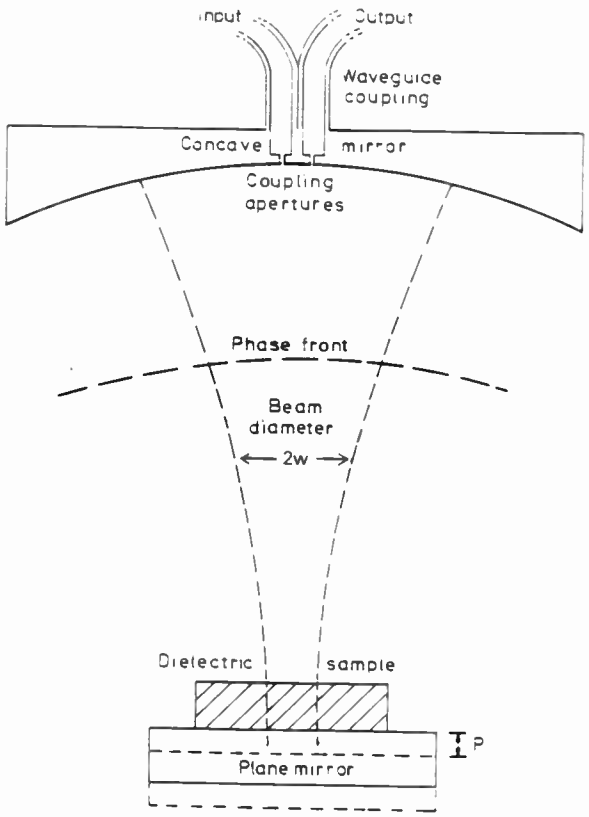

Fig. 11. A near-hemi-spherical open resonator with small-aperture coupling for transmission measurements. The plane mirror must be displaced a distance P to retain the same resonant frequency on insertion of the sample. The radius of curvature of the constant-phase fronts increases as the plane mirror is approached. (After Jones,[119] Crown Copyright).

($\pm 3 \pm 1\%$) in 200–700 μrad were achieved. The cavity was also used in the BCR exercise.[11,31]

Convenient measurement techniques can be based upon the (perhaps partial) evaluation of the scattering matrices (reflection and transmission coefficients) of cavity resonators with somewhat lower coupling losses. One technique has been described for thin film specimens.[129] An extension of such an approach for a critically coupled TE_{01n} mode cavity at 40–60 GHz employs frequency domain shuttle pulse measurements,[130,131] involving the use of a triangle-wave frequency-swept source and a spectrum analyser detector. Q-measurement from observation of reflectivity can also be used with open resonators[126] to which we now turn.

5.2 Quasi-optical Resonators

Millimetre-wave quasi-optical resonators are often referred to as *open resonators*, the most common configurations being conceptually derived from the optical Fabry–Perot resonator. Since a comprehensive review of this class of resonators has been published recently by Clarke and Rosenberg,[132] it will not be necessary here to dwell on their background or development. Suffice it to say that the open resonators which have proved to be most useful in dielectric

metrology are those that possess either (i) two concave mirrors whose poles and centres of curvature are all co-linear[133,134] or (ii) one concave mirror and one plane mirror[135,119,28] (see Fig. 10). The electromagnetic fields supported are conventionally derived in a scalar paraxial approximation which leads to the description of the resonant modes in terms of Gaussian beam resonances similar to those found in laser cavities. The basic theory was well summarized by Kogelnik and Li[136] and is also introduced elsewhere.[132,137–140] Dielectric samples usually take the form of planar laminae placed transversely in the resonator close to the waist of the beam as shown in Fig. 11. This positioning minimizes loss of power due to diffraction at sample edges since the beam width is minimized at the waist; smaller samples can therefore be employed there. The field constant-phase surfaces are also closest to planar at the waist. Since corrections for the mismatch between wavefront and sample surface geometry are the most significant that must be applied[133,141] (see below), it is as well to minimize them in this way.

From a practical viewpoint the preference for open resonators rather than closed cavities for millimetre-wave metrology arises from a number of properties of quasi-optical resonators:

(a) They are more accessible than closed cavities and do not require dismantling for sample insertion. This results in a higher intrinsic instrumental repeatability.
(b) Their mode spectrum is sparser,[142] this reduces the likelihood of error due to mode coincidences.
(c) Their Q-factors are higher than cavities of similar volume.
(d) Only the thickness of the dielectric specimen is critical, provided its radius is greater than that of the beam.
(e) TEM modes allow measurements of dielectric anisotropy to be carried out.[143,144]

One may set against these advantages some of the practical problems that arise in their use. These include stringent limitations on the nature of the samples to be measured—for instance warped or inhomogeneous samples can introduce large errors of measurement. Consideration of such points leads one to the conclusion that the open resonator is best suited to measurements on *low-loss, homogeneous* materials that can be readily machined to size, and that other materials should possibly be more efficiently measured by non-resonant techniques. Nevertheless, even these instrumental limitations allow for a wide range of materials, including low loss liquids, to be profitably measured by means of open resonators. Atmospheric propagation measurements are also possible.[145] In fact, open resonator techniques continue to produce some of the lowest values of uncertainty for low loss homogeneous samples.

The first application of the Gaussian beam-wave theory to solid dielectric measurements was reported in 1971.[133] Subsequent work demonstrated its applicability to confocal,[146] hemispherical[119,147] and short[134] resonators. Jones extended the approch to anisotropic materials[144] and to liquids.[148] The preferred technique for containing the liquid was again the use of an integral half-wavelength-thickness quartz window[31] similar to that used in cavity liquid[128] measurements. The requirement to minimize beam width to reduce sample size can be met by such a hemispherical geometry[119] but also by the adoption of a short bi-concave geometry as reported by Lynch.[134] In the latter, the repeatability of refractive index for polypropylene samples was better than 0·0004 in 1·50. Measurements on lossy materials can be designed to reduce resonator loading by placing the sample at electric field minima. One such technique for conducting samples involves the placing of a thin film of the material over the plane mirror.[126]

Confidence in assessed values of uncertainty is best obtained empirically through intercomparisons with other established techniques. Thus, compatibility between closed cavity techniques at 10 and 35 GHz and open resonators at 35, 72 and 144 GHz was tested at NPL[149] at the common frequency 35 GHz, the cavities and open resonators having been designed to allow the same samples to be measured in each system. For samples of unsintered PTFE, typical discrepancies were of the order 0·004 in a mean permittivity of 1·954 and 3 μrad in a mean loss angle of 48 μrad. More recently the BCR intercomparison of dielectric liquid measurements has been reported both in summary[11] and in greater detail.[30,31] Also incorporated in the latter are details of cavity/open resonator intercomparisons on high permittivity solids at 35 GHz. For alumina, agreement was of the order 0·01 in a permittivity of 9·75 and within 20 μrad in a loss of 570 μrad. For barium strontium zirconate ceramic corresponding figures were 0·3 in 34·0 (permittivity) and 150 in 1700 μrad.

The approximations[132] involved in the scalar paraxial beam-wave theory would be of doubtful validity in the absence of a more rigorous analysis. Theoretical advances have followed two approaches, (i) perturbation or variational theories[150–154] and (ii) attempts to find an exact solution of Maxwell's equations for an open resonator geometry. The significance of the perturbation theories has been discussed previously[132] but for fundamental modes they have now been superceded by the more comprehensive approach (ii). The attractive and powerful concept which has enabled this step to be taken is the 'complex source point' theory of Deschamps.[155,156] The theory provides an interesting insight into the nature of Gaussian beams since they are viewed as being generated by sources situated at complex, or purely imaginary, positions.[157] The value of the approach is not purely philosophical, however; in the absence of paraxial and other approximations, exact wavelike solutions can be derived for Gaussian beams which conform to Maxwell's equations. The derivation of the exact vector-field solution for an empty bi-concave microwave resonator was tackled by Cullen and Yu.[158] An important conclusion of their work, which confirmed the finding of the earlier perturbation approaches, was that for many practical purposes, the use of the scalar Gaussian beam

wave theory need not introduce significant errors for fundamental modes. This may not be the case for higher order modes.[153] More recently Yu and Cullen[159] have applied the approach to dielectric-loaded resonators. As already noted, the most significant correction for dielectric metrology is the interface correction which accounts for the phase-surface/specimen-surface mismatch.[133,141] The authors coupled the complex source point theory to a variational technique in order to tackle this problem in a more rigorous manner. Their derived correction proved to be compatible with the previous solutions for suitably thin samples, but the importance of their approach is that it provides criteria for deciding on the adequacy of the scalar beam wave theory for any geometry which may be empirically desirable. A companion paper by Lynch[160] described the application of the theory to measurement of samples of polypropylene, alumina and polymethylpentene (TPX) at 28–36 GHz. Lynch concluded that an accuracy of 1% in permittivity could be obtained even with specimens which depart considerably from the ideal thickness of an integral number of half wavelengths in the sample.

6 Stirred Mode Cavities (SMCs)

Stirred mode or 'untuned' cavities (SMCs) are finding increased application in electromagnetic metrology, but as their popularity for dielectric measurements is a recent phenomenon, we will commence with a brief introduction to the concept, illustrated in Fig. 12. The well-overmoded low-loss cavity contains at least one rotating mode stirrer which is used to disturb the internal fields to ensure that the radiation is time-averaged homogeneous. This term indicates that there is a substantial volume in the centre of the cavity where the time-averaged electromagnetic power density is the same (subject to acceptable limits) for all positions. There should therefore be no fixed nodes or antinodes in the central region of the cavity. The time-averaged power *flux* should also be isotropic, independent of position and of the polarization of the radiation. Specimens inside the cavity thus experience a time averaged uniform flux

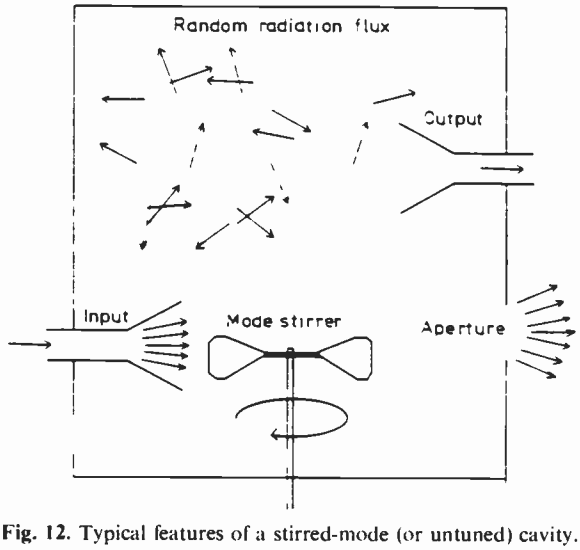

Fig. 12. Typical features of a stirred-mode (or untuned) cavity.

of incident radiation, although it is recognized that the specimen itself disturbs that uniformity. Electromagnetic SMCs have affinities with the reverberating chambers used in acoustic metrology[161,162] and the integrating spheres used at optical frequencies.[163]

The recent advances in SMC applications have been made on a number of fronts:

(a) Dielectric measurements, which are discussed in detail below.
(b) Isotropic power irradiation and dosimetry: industrial microwave heating,[164] microwave ovens[165] and studies on (possibly live) biological specimens.[165–168]
(c) Electromagnetic compatibility measurements (EMC). There is now a considerable literature on these measurements.[169–173]
(d) Power measurements: power-flux-density-meter calibration and *absolute* power measurements referenced to a black body radiator in the cavity.[169–171,174]

Reference to papers concerned with (b)–(d) will be made when they relate to dielectric measurements through common considerations such as the requirement for time-averaged isotropy, the design of mode stirrers, methods for checking the isotropy and the study of the statistics of the internal radiation.

SMCs usually operate in a transmission mode, having both input and output ports or apertures. On introduction of a lossy specimen, power is absorbed and the transmission coefficient falls. This process can be quantified in at least three ways:

(a) In terms of Q-factors,[171,175,176] using the same relationship as is used for resonant cavities, which relates the stored energy to the energy dissipated per cycle. A Q-factor can be associated with each loss-process: dissipation in cavity walls, flux through apertures or power dissipation in the dielectric specimen. These will combine in parallel in the normal way to give the overall Q-factor, which, however, unlike a that of resonant cavity, cannot be determined from cavity frequency response since the SMC is essentially broad-band. For an aperture with linear dimensions somewhat larger than a wavelength (i.e. ignoring diffraction effects) the aperture Q-factor is: $Q_a = 8\pi V/\lambda A_a$,[175] where V is the cavity volume, A_a is the aperture area, λ is the free-space wavelength.
(b) The loss cross-section description—each loss process is quantified in terms of an absorption cross-section for isotropic radiation σ_{iso}.[177] This is simply related to the Q-factor description through a modification of Lamb's formula:

$$Q = 8\pi V/\lambda\sigma_{iso} \qquad (11)$$

(c) The photon description: energy is carried by photons which are rebounding haphazardly inside the cavity. An absorption coefficient is associated with each loss process.[175,178,179] This approach is most appropriate for shorter wavelengths.

These approaches can be related to one another without too much difficulty and the most convenient can be chosen for any particular problem.

6.1 Stirred Mode Cavity Characteristics

Overmoding of SMCs helps to increase field homogeneity[171] but this is generally further improved on a time-averaged basis by stirring. Complexity and number of mode stirrers are to some extent interchangeable: one may use a single complex stirrer[177] or two or three orthogonally-mounted planar stirrers.[169,167] Kremer and Genzel[180] have achieved a high degree of homogeneity by forming their cavity from two circularly-symmetrical near-hemispherical shells with dimpled inner surfaces to scatter the radiation. One shell rotates at about 25 Hz and acts as a mode stirrer while the other remains stationary. As the dielectric properties of non-biological specimens vary slowly with frequency, it is also possible to sweep or frequency-modulate the source so as to launch a greater number of normal modes into the cavity. D'Ambrosio[167] has compared the efficiency of one to three stirrers with that of a swept source. Field homogeneity can be measured by moving a detector inside the cavity[169] or by monitoring transmission coefficient as a small absorber is moved between test positions.[167] Uniformity is not achieved near the cavity walls where all modes satisfy the same boundary conditions.[169] Stirring efficiency can also be tested by studying the coupling coefficient of co- and cross-polarized modes detected by rotation of the plane of polarization of a suitable detector with respect to a polarized source such as waveguide aperture.[181]

The transmissive properties of SMCs depend strongly upon the type of coupling used. Two methods are common: (a) single-mode coupling, (b) multi-mode coupling. The modes referred to here are those which propagate between the output port and the detector rather than those which characterize the fields in the cavity itself. An example of (a) would be an antenna coupling to a single-mode waveguide which carries the output signal to the detector;[169,178] (b) would correspond to an overmoded aperture through which a sample of internal radiation can escape to irradiate a Golay cell.[177] Some insight into coupling can be obtained from a thermodynamic analogue in which one associates a thermodynamic temperature T with the SMC isotropic radiation. Corona *et al.*[176] used such an analogue to relate the power detected via a matched, lossless antenna (case (a)) to the power flux density in the SMC. Thus within a bandwidth Δf, the Rayleigh power density is $2kT\Delta f/\lambda^2$, but the power transferred to the detector is, according to Nyquist, $kT\Delta f$, this being the power available per degree of freedom. A second approach to understanding coupling mechanisms looks at the statistical properties of the signals detected by a fast-response detector. The action of stirring causes the detected signal intensity to vary rapidly with time. Some features of this variation can be described in terms of a probability density function (PDF), $P(x)$, of detected intensity. This can be defined from the time-averaged probability, $P(x)\mathrm{d}x$, of instantaneously receiving a signal with intensity in the range x to $(x+\mathrm{d}x)$. Waterhouse[161] discussed this function in relation to a set of mean square pressure transducers dispersed throughout an *acoustic* reverberating chamber, but similar considerations apply to electromagnetic multi-mode detection or to the total power detected by a set of single-mode electromagnetic detectors. Fig. 13 demonstrates that PDFs for single and multiple-mode detection are quite different. One may conclude from such an analysis that improved signal-to-noise ratio will result from multi-mode detection which may therefore be preferable for dielectric measurements. Measured PDFs[169] for single mode waveguide coupling can show a response close to Fig. 13, curve A ($M = 1$). Lentz, however,[173] shows that the response of some practical SMCs varies widely from these theoretical predictions. In particular, a PDF similar to Fig. 13, curve F, results from a mixture of stirred and direct transmission, signifying inefficient stirring and a potential source of error.

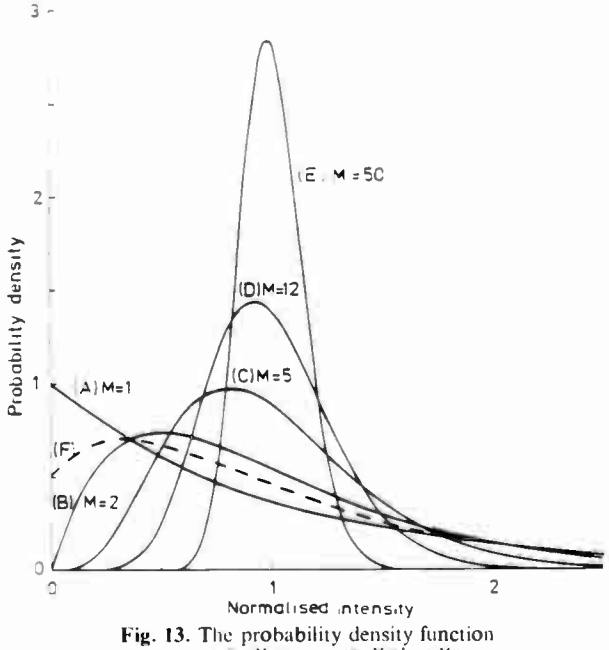

Fig. 13. The probability density function $P(x) = [M^M/(M-1)!]x^{M-1}\mathrm{e}^{-Mx}$ of total detected power for M single-mode detectors.[161] The response (F) may be obtained from a single mode detector if mode-stirring is not fully effective.[173] For large M, a constant level with added Gaussian noise is seen, corresponding to the power emitted from an overmoded aperture.

6.2 Dielectric Specimens

The earliest SMC dielectric measurements were reported by Becker and Autler (1946)[182] and Lamb[175] who measured loss in water vapour. Their work has only recently been superseded by that of Llewellyn-Jones, Gebbie and their co-workers[183,184] who have been largely responsible for the recent growth in interest in the SMC for dielectric measurements.[168] In such measurements the 'dielectric specimen'—water vapour—fills the cavity so that no consideration need be given to boundary conditions at interfaces between dielectric media. This is not the case for solid dielectric specimens or for liquids which are held in cells which introduce still

further complexity into the boundary conditions. Nevertheless, an attraction of the SMC for solid and liquid measurement lies in the possibility that absorption will depend substantially only on the specimen volume and not on its shape or permittivity. If this were so, the SMC would lend itself to a wide range of potential applications both in the laboratory and in quality control. That this can be accepted for certain samples has been shown experimentally by Llewellyn-Jones *et al.*[177] Conversely, Kremer and Izatt have shown that for *laminar* dielectric samples absorption can depend strongly on sample thickness and permittivity through multiple internal reflection and interference effects.[178,179] Indeed, they have made use of this very dependence on non-volumetric parameters for the determination of the *real* part of the relative permittivity. These approaches can be reconciled since the analysis is carried out at two levels of complexity, the former omitting the effects of interference and hence describing only the purely volumetric effects.

For the purposes of intercomparison we can define a numerical parameter F_i for suitable sample shapes which accounts for all effects which cause the specimen power absorption to depart from proportionality to the specimen volume. F_i takes a separate value for each face, i, through which radiation can enter the sample. It is a function of the frequency, f, the specimen dielectric properties and its dimensions. Approximating equation (5) for a low-loss material and for unidirectional power flow with normal incidence, the absorption cross-section, σ_n, of a slab of material of thickness d and cross-sectional area A is

$$\sigma_n = A\alpha d = \alpha v_s \tag{12}$$

where v_s is the volume of the sample. This can be generalized to three dimensions and to the cross-section for isotropic radiation:

$$\sigma_{iso} = \sum_{i=1}^{N} F_i(f, n, k, d_i)\alpha v_s \tag{13}$$

where σ_{iso} is related to the Q-factor associated with each face of the sample by equation (11). We assume there are N faces of the sample through which radiation can enter. For a cuboid, $N = 6$; for a lamina with perpendicular screened edges,[178] $N = 2$, $d_1 = d_2$ and $F_1 = F_2$. One can justify the neglect of laminar edge effects by noting[177] that, if $\varepsilon' > 2$, all radiation entering through a face will be totally-internally-reflected at perpendicular edges. (If $\lambda \approx d$, diffraction can occur and this statement will not apply). A similar argument applies to a cuboid specimen which may accordingly be treated as three laminae. For an approximate estimate of loss for a cuboid (assuming $n > 2$, and $k \ll 1$) one can apply equation (12) for each face giving

$$\sum_i F_i = 6.$$

This gives $\sigma_{iso} = 6\alpha v_s$, very close to the value found by Llewellyn-Jones *et al.*,[177] namely $\sigma_{iso} = 4\Theta v_s\alpha$, where Θ is a parameter which accounts for multiple internal reflections. The authors find both empirically and analytically that for $n > 1{\cdot}5$, $\Theta \approx 1{\cdot}6$. They also find that Θ is substantially independent of the shape of the sample for $n > 1{\cdot}5$ but its value must be modified for higher loss samples. If $\Theta = 1{\cdot}6$, the factor F_i will equal 1·07 for each face of a cuboid.

Kremer and Izatt[178] made use of the complete equations for the reflection coefficient and transmission coefficient of a lamina as derived by Hadley and Dennison.[185] The formulae explicitly involve real and imaginary parts of the complex refractive index (n, k) so that no limitation of their validity for high loss materials is necessary. One derives transmission coefficients and reflection coefficients for both parallel and perpendicular polarizations; the assumed isotropy allows one to use average coefficients T_{iso}, R_{iso} respectively. The absorption coefficient is just: $A_{iso} = (1 - T_{iso} - R_{iso})$ and $F_i = A_{iso}/\alpha d_i$ is now shown to be a function of complex refractive index and lamina thickness. By using samples of various thicknesses Kremer and Izatt were thereby able to derive both real and imaginary parts of the refractive index. The analysis was extended[179] to the

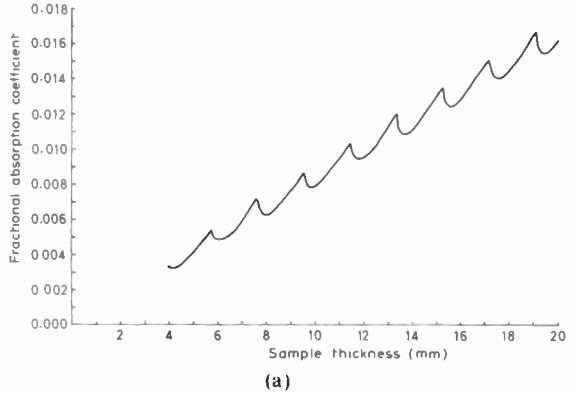

(a)

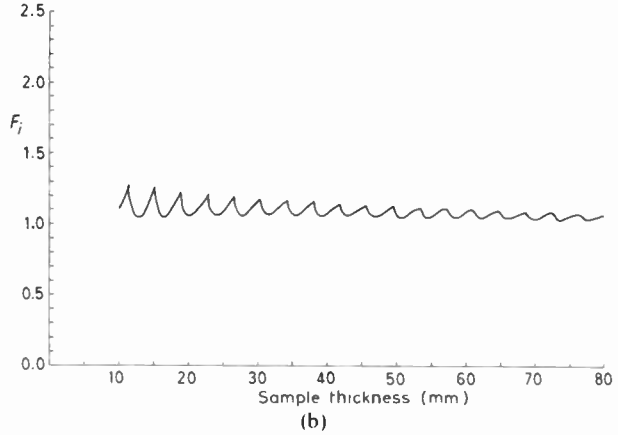

(b)

Fig. 14. (a) Calculated fractional absorption coefficient for a laminar sample subject to isotropic radiation. $n = 1{\cdot}5$, $k = 0{\cdot}0005$, $f = 70$ GHz. (After Kremer and Izatt)[178] (b) The parameter $F_i = A_{iso}/d_i\alpha$ at 35 GHz for similar material. The approximation F_i = constant = 1·07, which implies that the absorption is a purely volumetric effect, is better for thicker samples.

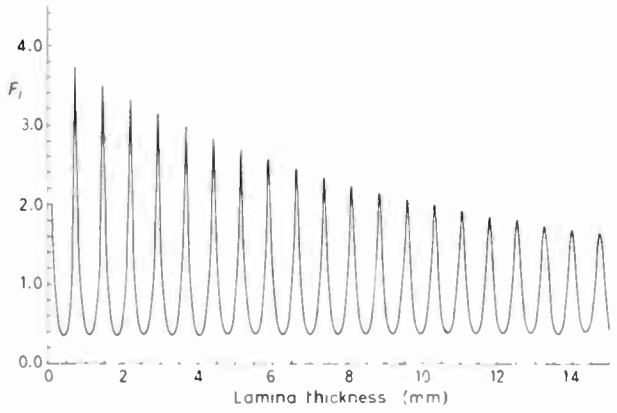

Fig. 15. As for Fig. 14(b) but for a high permittivity sample at 35 GHz: $n = 5{\cdot}848$, $k = 0{\cdot}005$, which correspond to the properties of barium strontium zirconate ceramic. The approximation: F_i = constant, is not valid if one assumes that standing-waves in the sample are not limited by diffraction.

multi-layer case of a liquid dielectric sandwiched between windows in a suitable cell.

The laminar treatment is valid only if radiation is prevented from entering through the sides of the lamina. This can be achieved by lining the edge of the sample with metal foil.[178] If such precautions are not taken, the total absorption could be (in the short wavelength limit) typically three times higher. It happens that for $n \approx 1{\cdot}5$, a typical value for a low-loss polymer, interference effects are quite small, see Fig. 14(b), but materials having higher refractive indices should have F_i values which vary dramatically with sample thickness, Fig. 15. The approximation F_i = constant (1·07) improves with sample thickness in both cases. It is, however, questionable whether the predicted behaviour for high permittivity materials would actually apply to a sample with dimensions of the order of a wavelength. Energy would be lost by diffraction at the edge of the sample and one would not expect standing waves to be as pronounced as the theory predicts.

6.3 Summary of Reported Measurements and Uncertainties

Willis *et al.*[186] reported loss measurements on sintered and unsintered PTFE at 156 GHz and also spectroscopic measurements 90–450 GHz using a broad-band source and interferometer. The measurements when extrapolated agree well with previously published figures[187] and show clearly the increase in loss after sintering; loss angles reported for 156 GHz were 103 ± 7 and 395 ± 29 microradians before and after sintering respectively (quoted uncertainties are standard deviations). The corresponding uncertainties in the interferometric measurements were in the region 10–30%.

Both Llewellyn-Jones *et al.*[177] and Kremer and Izatt[178] reported measurements on solid PTFE and polyethylene samples, at 156 GHz and 70 GHz respectively. The latter obtained values for n and k by using three techniques to ensure that the properties of the sample and cavity were being properly interpreted. These involved either cavity transmission measurements on (a) a sample having known dielectric properties or (b) a measurement on a calculable cavity aperture, or else (c) measuring the material under test using a number of different sample dimensions. The latter has the advantage that it allows one to estimate edge effects. For plexiglass, quoted uncertainties for loss were of the order of 10%.

Determination of the complex refractive indices of water and of glycerine[179] was based on an extension of the theory for solids. Three cells having differing thicknesses were used to point to a unique value for n and k. Values quoted for 70 GHz were $n = 3{\cdot}91 \pm 0{\cdot}16$, $k = 2{\cdot}33 \pm 0{\cdot}09$ for water and $n = 4{\cdot}6 \pm 0{\cdot}2$, $k = 1{\cdot}00 \pm 0{\cdot}05$ for glycerine. The uncertainty analysis indicated that for 0·5% accuracy in n and k for water, the cell thickness would have to be uniform to ± 1 μm and the detected power ratios would have to be reproduced to 0·1%.

Earlier work[175,182,188] on gas and vapour absorption has led to the latest determinations[184] of the absorption coefficient of water vapour as a function of temperature and pressure. The measurements were carried out at 213 GHz in a cavity 60 cm in diameter and 1 m long. The functional variation of attenuation with pressure and temperature was found to contain linear and quadratic terms attributed to monomers and dimers in the vapour respectively.

In the biological area much of the SMC work is concerned with biological effects of microwaves—a field in which the SMC is now an important dosimetric tool.[165,166,189] But Kremer and Genzel[190] report briefly on absorption measurements on a concentrated yeast paste for a temperature range −100 C to 0 C and a frequency range 40–90 GHz. At −10 C the absorption was found to be about two order of magnitude higher than that of ice. Such measurements promise to provide useful information on the nature of the binding processes of water in biological cells. Further work is briefly reported in a second paper.[180]

7 Concluding Remarks

We have attempted to provide a broad survey of state-of-the art techniques which are used at millimetre and near-millimetre wavelengths for accurate dielectric metrology and, by the inclusion of a selection of experimental results, to describe the present capabilities of the metrological systems and their significance for industrial developments and scientific research. Our survey cannot pretend to be comprehensive but it would be wrong to conclude without mentioning that there are a wide variety of important and commonly used techniques which are used to provide geometry-dependent sample properties. We have only briefly touched on these here. They are economical to implement and indeed are of great value in their own right but, in general, minimum uncertainty in measuring intrinsic (geometry-independent) properties is achieved by utilizing purpose-built instrumentation which is both characterizable in the absence of the sample and calculable in its presence. It is with the description of such systems that our review has been chiefly concerned. Full appreciation of the

physics or chemistry of a material must ultimately be based upon evaluation of such intrinsic properties, as must any impartial assessment of its value for potential applications.

8 Acknowledgments

The authors are indebted to Dr T. G. Blaney and Mr C. B. Rosenberg, both of NPL, for reading and commenting upon the manuscript.

9 References

1 Report of the Electronic Research Council Solid State Physics and Devices Committee on 'Millimetre Wave Devices and Components'. ERC Report 2661B, June 1979.
2 Kulpa, S. M. and Brown, E. A. 'Near millimeter wave technology base study, Vol. 1', US Army Material Development and Readiness Command, Harry Diamond Laboratories, Report HOL-SR-7a-8, November 1979.
3 Button, K. J. and Wittman, H. R., 'Proceedings and recommendations of the ARO workshop on short millimetre wave nonreciprocal materials and devices', *Internat. J. Infrared and Millimetre Waves*, **3**, pp. 1–10, 1982.
4 Kruse, P. W., 'Why the military interest in near-millimeter wave imaging?', *Proc. Soc. Photo-Opt. Instrum. Eng. USA*, **259**, pp. 94–9, 1980.
5 Crone, G. A. E., Rudge, A. W. and Taylor, G. N., 'Design and performance of airborne radomes: a review', *IEE Proc.*, **128**, Pt. F, pp. 451–64, 1981.
6 Plourde, J. K. and Ren, C. L., 'Application of dielectric resonators in microwave components', *IEEE Trans.* **MTT-29**, pp. 754–70, 1981.
7 Costley, A. E., 'Cyclotron radiation from magnetically confined plasmas', Trends in Physics 1978, Proc. 4th General Conference of the European Physical Society, York, 1978, (Adam Hilger, Bristol, 1978).
8 Luhmann, Jr., N. C., 'Instrumentation and techniques for plasma diagnostics: an overview' in 'Infrared and Millimetre Waves, Vol. 2', K. J. Button (ed.) (Academic Press, New York 1979).
9 Pethig, R., 'Dielectric and Electronic Properties of Biological Materials' (Wiley, New York, 1979).
10 Romero-Sierra, C. *et al.*, 'Bioeffects of electromagnetic waves', 'Review of Radio Science, 1978–1980', chap. 2, S. A. Bowhill (Ed.), (URSI, Brussels, 1981).
11 Afsar, M. N. *et al.*, 'A comparison of dielectric measurement methods for liquids in the frequency range 1 GHz to 4 THz', *IEEE Trans.*, **IM-29**, pp. 283–8, 1980.
12 Birch, J. R., *et al.*, 'The far-infrared dispersion of acetonitrile in dilute solution in carbon tetrachloride', *Infrared Phys.*, **21**, pp. 9–15, 1981.
13 Chamberlain, J. and Chantry, G. W., (Eds.), 'High Frequency Dielectric Measurement', Conf. Proc., Teddington, UK, 1972, (IPC Science and Technology Press, Guildford, 1973).
14 Bangham, M. J. *et al.*, 'Physical measurement in the 100–1000 GHz frequency range', *The Radio and Electronic Engineer*, **49**, pp. 403–17, 1979.
15 Cook, R. J. and Jones, R. G., 'Measurement of electrical properties: Relative permittivity and loss angle.' *Plastics and Rubber Materials and Applications*, **1**, pp. 216–24, Sept. 1976.
16 Kaatze, U. and Giese, K., 'Dielectric relaxation spectroscopy of liquids: frequency domain and time domain experimental methods', *J. Phys. E*: **13**, pp. 133–41, 1980.
17 Lynch, A. C. and Ayers, S., 'Measurement of small dielectric loss at microwave frequencies', *Proc. IEE*, **119**, pp. 767–70, 1972.
18 Ayers, S. *et al.*, 'Low-loss dielectrics for 10–3000 GHz', *Proc. IEE*, **121**, pp. 1447–50, 1974.
19 Stumper, U. and Frentrup, K., 'Precise determination of very low dielectric losses at frequencies of 9 and 29 GHz', *Rev. Sci. Instrum.*, **47**, pp. 1196–1200, 1976.
20 Hermiz, N. A., Hasted, J. B. and Rosenberg, C. B., 'Microwave losses of n-alkanes', *J. Chem. Soc. (Faraday Trans.)* **78**, pp. 147–61, 1982.
21 Koppelman, G. and Rudolph, H., 'Quasioptical millimeter-wave measurements: refractive index of thin plates', *Appl. Phys.*, **23**, pp. 403–6, 1980.
22 Jablonski, D., 'Attenuation characteristics of circular dielectric waveguide at millimeter wavelengths', *IEEE Trans.*, **MTT-26**, pp. 667–71, 1978.
23 Pannell, R. M. and Jervis, B. W., 'Two simple methods for the measurement of dielectric permittivity of low-loss microstrip substrates', *IEEE Trans.*, **MTT-29**, pp. 383–6, 1981.
24 Itoh, T. and Fwu-Jih Hsu, 'Application of inverted strip dielectric waveguides for measurements of material properties at millimeter-wave frequencies', Proc. 8th European Microwave Conference, Paris, 1978, pp. 823–7 (Microwave Exhibitions and Publishers, Sevenoaks, England, 1978).
25 Itoh, T. and Fwu-Jih Hsu, 'Application of inverted strip dielectric waveguides for measurements of the dielectric constant of low-loss materials at millimeter-wave frequencies', *IEEE Trans.*, **MTT-27**, pp. 841–4, 1979.
26 Cook, R. J. and Rosenberg, C. B., 'Measurement of the complex refractive index of isotropic and anisotropic materials at 35 GHz using a free-space microwave bridge', *J. Phys. D*: **12**, pp. 1643–52, 1979.
27 Campbell, C. K., 'Free-space permittivity measurements on dielectric materials at millimetre wavelengths', *IEEE Trans.*, **IM-27**, pp. 54–8, 1978.
28 Newton, J. M., Kozakoff, D. J. and Schuchardt, J. M., 'Methods of dielectric material characterization at millimeter wavelengths', Proc. 15th Symposium on Electromagnetic Windows, pp. 142–8, 1980.
29 Kilp, H., 'Precise measurement of the complex permittivity of low-to-medium-loss standard liquids at 285 GHz', *J. Phys. E*: **10**, pp. 985–9, 1977.
30 Chantry, G. W. (Ed.) *et al.*, 'High Frequency Dielectric Reference Materials', EEC Community Reference Bureau (BCR), BCR Project 148, Final Report of Phase 1, (BCR, Brussels, 1980).
31 Chantry, G. W. (Ed.) *et al.*, 'High Frequency Dielectric Reference Materials', EEC Community Reference Bureau (BCR), BCR Project 148, Final Report of Phase 2, (BCR, Brussels, 1980).
32 Van Loon, R. and Finsy, R., 'Measurement of complex permittivity of liquids at frequencies from 5 to 40 GHz', *Rev. Sci. Instrum.*, **44**, pp. 1204–8, 1973.
33 Van Loon, R. and Finsy, R., 'Measurement of complex permittivity of liquids at frequencies from 60 to 150 GHz', *Rev. Sci. Instrum.*, **45**, pp. 523–5, 1974.
34 Finsy, R. and Van Loon, R., 'Dielectric relaxation in 1,1,1-trichloroethane/cyclohexane solutions', *J. Chem. Phys.*, **63**, pp. 4831–5, 1975.
35 Van Loon, R. and Finsy, R., 'The precise microwave permittivity of liquids using a multipoint technique and curve-fitting procedure', *J. Phys. D: Appl. Phys.*, **8**, pp. 1232–42, 1975.
36 Szwarnowski, S. and Sheppard, R. J., 'Precision waveguide cells for the measurement of permittivity of lossy liquids at 70 GHz', *J. Phys. E: Sci. Instrum.*, **10**, pp. 1163–7, 1977.
37 Khanna, R. K. and Sobhanadri, J., 'Simple microwave interferometer for measurement of electric permittivity and losses of liquids at 4·23 mm wavelength', *Ind. J. Pure Appl. Phys.*, **12**, Pt. 4, pp. 268–72, 1974.
38 Jeyaraj, M., Kumaraswamy, A. and Sobhanadri, J., 'Numerical curve fitting technique for evaluating complex permittivity of liquids at millimetre and centimetre wavelengths', *J. Phys. E.*, 12, pp. 1179–82, 1979.
39 Blue, M. D., 'Permittivity of ice and water at millimeter wavelengths', *J. Geophys. Res. (USA)*, **85**, Pt. C2, pp. 1101–6, 1980.
40 Andreyev, G. A. *et al.*, 'Investigation of the dielectric properties of ground covers at millimeter wavelengths', *Telecommun. Radio Eng. (USA)*, **34**, pp. 126–7, 1979.
41 McCrackin, F. L., 'Analysis and corrections of instrumental errors in ellipsometry', *J. Opt. Soc. Am.*, **60**, pp. 57–63, 1970.
42 Thorpe, T. L., Barnes, F. S. and Gage, D. S., 'Millimeter wave ellipsometer', *Proc. Soc. Photo-Opt. Instrum. Eng.*, USA, **248**, pp. 158–65, 1980.
43 Goulon, J., Roussy, G. and Rivail, J. L., 'Réalisation d'un interféromètre de Michelson en guide superdimensionné. Mesure de la permittivité complexe des liquides en ondes millimétrique', *Rev. Phys. Appliquée*, **3**, pp. 231–6, 1968.
44 Goulon, J., Roussy, G. and Rivail, J. L., 'Optimisation de la permittivité complexe d'un liquide a partir de mesures interférométriques en ondes millimétriques', *Rev. Phys. Appliquée*, **4**, 413–9, 1969.
45 Goulon, J., *et al.*, 'Mesures interferometriques précises de la permittivité complexe des liquides dans un large domaine de fréquences', *Rev. Phys. Appliquée*, **8**, pp. 165–74, 1973.
46 Read, L. A. A., Dagg, I. R. and Reesor, G. E., 'Improved microwave Michelson interferometer operating at 140 GHz', *Rev. Sci. Instrum.*, **50**, pp. 1553–60, 1979.
47 Engen, G. F., 'Advances in microwave measurement science', *Proc. IEEE*, **66**, pp. 374–84, 1978.
48 Yell, R. W., *et al.* 'Electromagnetic metrology', 'Review of Radio Science, 1978–1980', chap. 1, Ed. S. A. Bowhill, (URSI, Brussels, 1981).
49 Stumper, U., 'Prospects for a six-port reflectometer working at submillimetre wavelengths', Proc. IEE Colloquium on Measurements at millimetre and near millimetre wavelengths, Digest No. 1981/44, Section 9, (IEE, London, 1981).
50 Rossenbluh, M., Temkin, R. J. and Button, K. J., 'Submillimetre laser wavelength tables', *Applied Optics*, **15**, pp. 2635–44, 1976.
51 Knight, D. J. E., 'Ordered List of Far Infra-red Laser Lines. Continuous $\lambda > 12\,\mu m$', NPL Report Qu 45, (1st revision), 1981.
52 Chamberlain, J. F. and Gebbie, H. A., 'Determination of the refractive index of a solid using a far-infrared maser', *Nature*, **206**, pp. 602–3, 1965.
53 Chamberlain, J., Haigh, J. and Hine, M. J., 'Phase modulation in far infrared (submillimetre-wave) interferometers. III—Laser refractometry', *Infrared Phys.*, **11**, pp. 75–84, 1971.
54 Chantry, G. W. and Chamberlain, J. in 'Materials Science of Polymers', A. D. Jenkins (Ed.) (North-Holland, Amsterdam, 1971).
55 Chamberlain, J. (Ed.) *et al.* 'Complex permittivity at 29·7 cm^{-1} of some organic liquids and solutions', *Trans. Faraday Soc.*, **63**, pp. 2605–9, 1967.
56 Fellgett, P., Thesis, University of Cambridge, 1951.
57 Fellgett, P., 'A propos de la théorie du spectrometre interferential multiplex', *J. Phys. Radium*, **1a**, pp. 187–91, 1978.
58 Jacquinot, P. and Dufor, C., 'Condition optiques d'emploi des cellules photo-electrique dans les spectrographes et les interferometres', *J. Rech CNRS*, **6**, pp. 91–103, 1948.
59 Jacquinot, P., 'The luminosity of spectrometers with prisms, gratings or Fabry-Perot etalons', *J. Opt. Soc. Am.*, **44**, pp. 761–5, 1954.
60 Chantry, G. W., 'Submillimetre Spectroscopy' (Academic Press, New York, 1971).
61 Bell, R. J., 'Introducing Fourier Transform Spectroscopy' (Academic Press, New York, 1972).
62 Chamberlain, J., 'The Principles of Interferometric Spectroscopy' (Wiley, Chichester, 1979).
63 Bell, F. E., 'Optical constants and their measurement', *Handbuch der Physik*, **25**, pp. 1–58, 1967.
64 Chamberlain, J., 'Interface effects in Fourier transform spectroscopy', *Infrared Phys.*, **12**, pp. 145–64, 1972.
65 Birch, J. R. and Parker, T. J., 'Dispersive Fourier transform spectrometry', in 'Infrared and Millimetre Waves, 2, pp. 137–271, K. J. Button, (Ed) (Academic Press, New York, 1979).
66 Birch, J. R. 'Recent progress in dispersive Fourier transform spectroscopy', Proc. Conf. on Fourier Transform Infrared Spectroscopy, Columbia, South Carolina, 1981, Soc. Photo-Optical Instrum. Engrs., **289**, pp. 362–84, 1981.
67 Birch, J. R., 'A far infrared reflection interferometer', *Infrared Phys.*, **12**, pp. 29–34, 1972.
68 Birch, J. R., Dromey, J. D. and Nicol, E. A., 'The effect of detector port radiation on the determination of insertion loss by Fourier transform spectroscopy', *Infrared Phys.*, **21**, pp. 17–24, 1981.
69 Kinch, M. A. and Rollin, B. V., 'Detection of millimetre and submillimetre wave radiation by free carrier absorption in a semiconductor', *Brit. J. Appl. Phys.*, **14**, pp. 672–6, 1963.
70 QMC Instruments Ltd, 229 Mile End Road, London.
71 Chamberlain, J. and Gebbie, M. A., 'Phase modulation in far infrared interferometers, Part 1' *Infrared Phys.*, **11**, pp. 25–55, 1971.
72 Chamberlain, J. and Gebbie, M. A., 'Phase modulation in far infrared interferometers Part 2', *Infrared Phys.* **11**, pp. 57–73, 1971.
73 Chamberlain, J. and Gebbie, M. A., 'Use of phase modulation in submillimetre-wave interferometers', *Appl. Opt.*, **10**, pp. 1184–5, 1971.
74 Martin, D. H. and Puplett, E., 'Polarised interferometric spectroscopy for the millimetre and submillimetre spectrum.' *Infrared Phys.*, **10**, pp. 105–9, 1970.
75 Parker, T. J., Ledsham, D. A. and Chambers, W. G., 'Analysis of the mode of operation of a polarizing interferometer in dispersive Fourier transform spectroscopy', *Infrared Phys.*, 18, pp. 179–83, 1978.
76 Afsar, M. W., Hasted, J. B. and Chamberlain, J., 'New techniques for dispersive Fourier transform spectroscopy of liquids', *Infrared Phys.*, 16, pp. 301–10, 1976.
77 Birch, J. R., *et al.*, 'A variable-thickness variable-temperature liquid cell for the dispersive Fourier transform spectroscopy of liquids', *J. Phys. E.*, **15**, pp. 684–8, 1982.

78 Mok, C. L., *et al.*, 'The far infrared performance and application of free standing wire grids wound from 5 μm diameter tungsten wire', *Infrared Phys.*, **19**, pp. 437–42, 1979.

79 Beunen, J. A., *et al.*, 'Performance of freestanding wire grids wound from 10 μm diameter tungsten wire at submillimetre wavelengths: computation and measurement', *J. Opt. Soc. Am.*, **71**, pp. 184–8, 1981.

80 Ade, P. A. R., *et al.*, 'Free standing wire grids wound from 5 μm diameter wire for spectroscopy at far infrared wavelengths', *Infrared Phys.*, **19**, pp. 599–601, 1979.

81 Parker, T. J., Ford, J. E. and Chambers, W. G., 'The optical constants of pure fused quartz in the far infrared', *Infrared Phys.*, **18**, pp. 215–9, 1978.

82 Birch, J. R., 'A specimen holder for rapid batch processing by transmission dispersive Fourier transform spectrometry at ambient temperatures', *J. Phys. E.*, **13**, pp. 716–7, 1980.

83 Chamberlain, J. E., Gibbs, J. E. and Gebbie, M. A., 'Refractometry in the far infrared using a two beam interferometer', *Nature*, **198**, pp. 874–5, 1963.

84 Birch, J. R. and Jones, R. G., 'A ferrite modulator for the far infrared', *Infrared Phys.*, **10**, pp. 217–24, 1970.

85 Birch, J. R., 'The absolute determination of complex reflectivity', *Infrared Phys.*, **18**, pp. 613–20, 1978.

86 Birch, J. R., Cook, R. J. and Pardoe, G. W. F., 'A millimetre wavelength absorption in soda-lime-silica glass', *Solid State Commun.*, **30**, pp. 693–5, 1979.

87 Birch, J. R., Dromey, J. D. and Lesurf, J., 'The optical constants of some common low loss polymers between 4 and 40 cm^{-1}', *Infrared Phys.*, **21**, pp. 225–8, 1981.

88 Birch, J. R., Dromey, J. D. and Lesurf, J., 'The optical constants of some common low loss polymers between 4 and 40 cm^{-1}', NPL Report DES 69, February 1981.

89 Afsar, M. N. and Button, K. J., 'Millimeter and submillimeter wave measurements of complex optical and dielectric parameters of materials I. 2·5 mm to 0·66 mm for alumina 995, beryllia, fused silica, titanium silicate and glass ceramic', *Intl. J. Millimeter Infrared Waves*, **2**, pp. 1029–44, 1981.

90 Birch, J. R. and Stone, N. W. B., 'The transmission of some glasses in the millimetre wave region', *J. Phys. E.*, **6**, pp. 1101–4, 1973.

91 Bell, E. E. and Russell, E. E., 'Measurement of the far infrared optical properties of solids with a Michelson interferometer used in the asymmetric mode: Part II. The vacuum interferometer', *Infrared Phys.*, **6**, pp. 75–84, 1966.

92 Parker, T. J., *et al.*, 'A Fourier spectrometer for determining the optical constants of transparent solids in the far infrared from 77 to 300 K', *Infrared Phys.*, **18**, pp. 571–6, 1978.

93 Russell, E. E. and Bell, E. E., 'Measurement of the optical constants of crystal quartz in the far infrared with the asymmetric Fourier-transform method', *J. Opt. Soc. Am.*, **57**, pp. 341–8, 1967.

94 Russell, E. E. and Bell, E. E., 'Optical constants of sapphire in the far infrared', *J. Opt. Soc. Am.*, **57**, pp. 543–4, 1967.

95 Gast, J. and Genzel, L., 'An amplitude Fourier spectrometer for infrared solid state spectroscopy', *Opt. Commun.*, **8**, pp. 26–30, 1973.

96 Gauss, K. F., Happ, H. and Rother, G., 'Millimetre wave and far infrared investigation on KDP with asymmetric interferometers', *Phys. Stat. Sol. B.*, **72**, pp. 623–30, 1975.

97 Birch, J. R. and Murray, D. K., 'A modular interferometer for dispersive reflectivity measurements on highly absorbing solids', *Infrared Phys.*, **18**, pp. 283–91, 1978.

98 Parker, T. J. and Chambers, W. G., 'A new technique for dispersive reflection spectroscopy in the far infrared', *IEEE Trans.*, **MTT-22**, pp. 1032–1036, 1974.

99 Parker, T. J., Chambers, W. G. and Angress, J. F., 'Dispersive reflection spectroscopy in the far infrared by division of the field of view in a Michelson interferometer', *Infrared Phys.*, **14**, pp. 207–15, 1974.

100 Staal, P. R. and Eldridge, J. F., 'Improvements in dispersive reflection spectroscopy using a commercial Michelson interferometer', *Infrared Phys.*, **17**, pp. 299–303, 1977.

101 Birch, J. R., 'The absolute determination of the complex and power reflectivities of solid dielectrics between 100 GHz and 3 THz' Proc. Conf. on Dielectric Materials, Measurements and Applications, IEE Conf. Publication, 177, pp. 220–2, Birmingham, (IEE, London, 1979).

102 Chamberlain, J., Gibbs, J. E. and Gebbie, H. A., 'The determination of refractive index spectra by Fourier spectrometry', *Infrared Phys.*, **9**, pp. 185–209, 1969.

103 Chamberlain, J. E., Costley, A. E. and Gebbie, H. A., 'Submillimetre dispersion of liquid tetrabromethane', *Spectrochimica Acta.*, **23A**, pp. 2255–60, 1967.

104 Davies, M., *et al.*, 'Submillimetre- and millimetre-wave absorptions of some polar and non-polar liquids measured by Fourier transform spectrometry', *Trans Faraday Soc.*, **66**, pp. 273–92, 1970.

105 Chamberlain, J., Afsar, M. N. and Hasted, J. B., 'Direct measurement of the refraction spectrum of ethanol at submillimetre wavelengths', *Nature, Phys. Sci.*, **245**, pp. 28–30, 1973.

106 Afsar, M. N., Chamberlain, J. and Hasted, J. B., 'The measurement of the refraction spectrum of a lossy liquid in the far infrared region', *Infrared Phys.*, **16**, pp. 587–99, 1976.

107 Birch, J. R. and Bulleid, C. E., 'Phase errors in dispersive Fourier transform spectrometry', *Infrared Phys.*, **17**, pp. 279–82, 1977.

108 Birch, J. R. and Parker, T. J., 'The role of the origin of computation in the determination of phase spectra by dispersive Fourier transform spectroscopy', *Infrared Phys.*, **19**, pp. 103–5, 1979.

109 Davies, G. J. and Chamberlain, J., 'High accuracy submillimetre-wave solution measurements', *J. Phys. A*, **5**, pp. 767–72, 1972.

110 Afsar, M. N., *et al.*, 'Assessment of random and systematic error in microwave and submillimetre dielectric measurements', *Proc. IEE*, **124**, pp. 575–7, 1977.

111 Afsar, M. N. and Chantry, G. W., 'Reliable measurement of the optical and dielectric parameters of liquid carbon tetrachloride in the wavelength range 3 mm–50 μm (3 cm^{-1}–200 cm^{-1})', *Intl. J. Infrared Millimetre Waves*, **2**, pp. 107–14, 1981.

112 Honijk, D. D., *et al.*, 'The determination of complex refractive indices with Fourier transform interferometry—V. Methods for the determination of complex refractive index spectra of liquids in the far infrared spectral region (5–500 cm^{-1}) using a variable pathlength, variable temperature liquid cell', *Infrared Phys.*, **17**, pp. 9–24, 1977.

113 Afsar, M. N., *et al.*, 'Dispersive Fourier transform spectrometry with variable-thickness variable-temperature liquids cells', *IEEE Trans.*, **MTT-25**, pp. 505–8, 1977.

114 Honijk, D. D., *et al.*, 'The determination of the complex refractive index spectra of liquids in the far infrared spectral region 5–500 cm^{-1}, with dispersive Fourier transform spectrometry', *Infrared Phys.*, **16**, pp. 257–62, 1976.

115 Birch, J. R., *et al.*, 'The far infrared dispersion of acetonitrile in dilute solution in carbon tetrachloride', *Infrared Phys.*, **21**, pp. 9–15, 1981.

116 Bennouna, M., *et al.*, 'The determination of the complex refractive indices of some concentrated aqueous salt solutions at submillimetre wavelengths', *Chem. Phys.*, **62**, pp. 439–45, 1981.

117 Birch, J. R. and Bennouna, M., 'An improved experimental method for reflection dispersive Fourier transform spectrometry of very heavily absorbing liquids', *Infrared Phys.*, **21**, pp. 229–34, 1981.

118 Cook, R. J., 'Microwave cavity methods', in Ref. 13, pp. 12–27, 1973.

119 Jones, R. G., 'Precise dielectric measurements at 35 GHz using an open microwave resonator', *Proc. IEE*, **123**, pp. 285–90, 1976.

120 Stumper, U., 'The measurement of the complex permittivity of low-loss liquids at millimetre wavelengths'. In 'High Frequency Dielectric Measurement', J. Chamberlain and G. W. Chantry, (Eds.), pp. 51–5, 1973.

121 Stumper, U., 'A TE_{01n} cavity resonator method to determine the complex permittivity of low loss liquids at millimeter wavelengths', *Rev. Sci. Instrum.*, **44**, pp. 165–9, 1973.

122 Stumper, U., 'Automatic measurement of the complex permittivity at millimeter wavelengths', *Intl. J. Infrared and Millimetre Waves*, **2**, pp. 999–1014, 1981.

123 Cullen, A. L. and Davies, J. A., 'The new system for microwave Q-factor measurement', *Proc. IEE, Microwaves, Optics, Acoustics*, **2**, pp. 77–84, 1978.

124 Akyel, C. and Bosisio, R. G., 'A new automated absolute Q-measuring method', Proc. IEEE-EEMTIC 1981 Conference, Ottawa, Canada, Report CH1710-3/81/0000, pp. 103–110.

125 Degenford, J. E. and Coleman, P. D., 'A quasi-optical perturbation technique for measuring dielectric constants' *IEEE Proc.*, **54**, pp. 520–2, 1966.

126 Gage, D. S., Lewin, L. and Barnes, F. S., 'Millimetre wave Fabry-Perot interferometer for the measurement of conductivity of thin films for solar cells' *Proc. Soc. Photo-Opt. Instrum. Engrs., USA*, **248**, pp. 148–57, 1980.

127 Deutsch, J. and Lange, K., 'Bestimmung der dielektrischen Eigenschaften von Substraten fur Mikrowellen-Streifenleitungen mittels zylindrischer Hohlraumresonatoren', *Frequenz*, **35**, pp. 220–3, 1981.

128 Rosenberg, C. B., Hermiz, N. A., Cook, R. J., 'Cavity resonator measurements of the complex permittivity of low loss liquids.', *Proc. IEE*, **129**, Pt. H, pp. 71–5, 1982.

129 von Lorenz-Peter Schmidt and Hofmann, H., 'Ein Verfahren zur Ermittlung der komplexen Dielektrizitatskonstante dunner Folien in Millimeterwellenbereich', *Arch. Elektr. Ubertrag.*, **33**, pp. 185–9, 1979.

130 Bernardi, P., Bertolani, F. and Rizzoli, V., 'Frequency- domain shuttle-pulse measurement of losses and mode conversion', *IEEE Trans.*, **MTT-26**, pp. 203–8, 1978.

131 Bertolani, F., Falciaseeca, G. and Rizzoli, V., 'An improved method for measuring the complex permittivity of lossy dielectrics at millimeter-wave frequencies', Proc. 8th European Microwave Conference, Paris, 1978, pp. 538–542, (Microwave Exhibitions and Publishers, Sevenoaks, England, 1978).

132 Clarke, R. N. and Rosenberg, C. B., 'Fabry-Perot and open resonators at microwave and millimetre wave frequencies, 2–300 GHz', *J. Phys. E.*, **15**, pp. 9–24, 1982.

133 Cullen, A. L. and Yu, P. K., 'The accurate measurement of permittivity by means of an open resonator', *Proc. R. Soc. Lond. A.*, **325**, pp. 493–509, 1971.

134 Lynch, A. C., 'Measurement of dielectric properties in an open resonator', Proc. Conf. on Dielectrics Materials Measurement and Applications 1979, IEE Conf. Publ. 177, pp. 373–376, (IEE, London, 1979).

135 Breeden, K. H. and Langley, J. B., 'Fabry-Perot cavity for dielectric measurements', *Rev. Sci. Instrum.*, **40**, pp. 1162–3, 1969.

136 Kogelnik, H. and Li, T., 'Laser beams and resonators', *IEEE Proc.*, **54**, pp. 1312–29, 1966.

137 Cullen, A. L. and Nagenthiram, P., 'Microwave open resonators', in Ref. 13, Chamberlain, J. and Chantry, G. W. (Eds.), pp. 73–7, 1973.

138 Jones, R. G., 'Millimetre-wave dielectric measurements using open-resonators', in Ref. 13, Chamberlain, J. and Chantry, G. W., (Eds.), pp. 78–83, 1973.

139 Boyd, G. D. and Kogelnik, H., 'Generalized confocal resonator theory', *Bell Syst. Tech. J.*, **41**, pp. 1347–69, 1962.

140 Ramo, S., Whinnery, J. R. and Van Duzer, 1965, 'Fields and Waves in Communications Electronics' (Wiley, New York, 1965).

141 Cullen, A. L., Nagenthiram, P. and Williams, A. D., 'Improvement in open-resonator permittivity measurement', *Electronics Letters*, **8**, pp. 577–9, 1972.

142 Weinstein, L. A., 1969. 'Open Resonators and Open Waveguides' (The Golem Press, Boulder, Col. 1969).

143 Schlegel, D. and Stockhausen, M., 'Measurements of dielectric anisotropy of films in the microwave region by resonator perturbation method' *J. Phy. E.*, **5**, pp. 1045–6, 1972.

144 Jones, R. G., 'The measurement of dielectric anisotropy using a microwave open resonator', *J. Phys. D.*, **9**, pp. 819–827, 1976.

145 Harris, D. J. and Batt, R. J., 'Open resonator methods for the measurement of atmospheric propagation characteristics', Proc. IEE Colloquium on 'Measurements at millimetre and near millimetre wavelengths', Digest No. 1981/44, May 1981, (IEE, London, 1981).

146 Luen, C. H. and Auchterlonie, L. J., 'Fine tuning of millimetre-wave open resonator', *Electronics Letters*, **18**, pp. 358–9, 1982.

147 Jones, R. G., 'Effect of mirror resistivity on loss-angle measurements in open-resonators', *Electronics Letters*, **11**, pp. 545–7, 1975.

148 Cook, R. J. and Jones, R. G., 'Precise dielectric measurement techniques for the frequency range 10 GHz to 150 GHz', Proc. 8th European Microwave Conf., Paris, 1978, pp. 528–32, (Microwave Exhibitions and Publishers, Sevenoaks, 1978).

149 Cook, R. J., Jones, R. G. and Rosenberg, C. B., 'Comparison of cavity and open-resonator measurements of permittivity and loss angle at 35 GHz', *IEEE Trans.*, **IM-23**, pp. 438–42, Dec. 1974.

150 Cullen, A. L., 'Improvements in the beam-wave theory of the open-resonator', *Electronics Letters*, **11**, pp. 344–5, 1975.

151 Cullen, A. L., 'On the accuracy of the beam-wave theory of the open resonator', *IEEE Trans.*, **MTT-24**, pp. 534–5, 1976.

152 Cullen, A. L., Nagenthiram, P. and Williams, A. D., 'A variational approach to the theory of the open resonator', *Proc. R. Soc. Lond. A.*, **329**, pp. 153–69, 1972.

153 Erickson, C. W., 'High order modes in a spherical Fabry-Perot resonator', *IEEE Trans.*, **MTT-23**, pp. 218–23, 1975.

154 Erickson, C. W., 'Perturbation theory generalized to arbitrary (p,1) modes in a Fabry-Perot resonator', *IEEE Trans.*, **MTT-25**, p. 958, 1977.

155 Deschamps, G. A., 'Gaussian beam as a bundle of complex rays', *Electronics Letters*, **7**, pp. 684–5, 1971.

156 Deschamps, G., 'Ray techniques in electromagnetics', *IEEE Proc.*, **60**, pp. 1022–35, 1972.

157 Felsen, L. B., 'Evanscent waves', *J. Opt. Soc. Am.*, **66**, pp. 751–60, 1976.

158 Cullen, A. L. and Yu, P. K., 'Complex source-point theory of the open resonator' *Proc. R. Soc. Lond. A*, **366**, pp. 155–71, 1979.

159 Yu. P. K. and Cullen, A. L., 'Measurement of permittivity by means of an open resonator. I. Theoretical', *Proc. Roy. Soc. Lond.*, A, **380**, pp. 49–71, 1982.
160 Lynch, A. C., 'Measurement of permittivity by means of an open resonator II. Experimental', *Proc. Roy. Soc. Lond.*, A, **380**, pp. 73–76, 1982.
161 Waterhouse, R. V., 'Statistical Properties of reverberant sound fields', *J. Acoust. Soc. Am.*, **43**, pp. 1436–44, 1968.
162 Morse, P. M. and Bolt, R. H., 'Sound waves in rooms', *Rev. Mod. Phys.*, **16**, pp. 69–145, 1944.
163 Elterman, P., 'Integrating cavity spectroscopy', *Appl. Opt.*, **9**, pp. 2140–2, 1970.
164 Hulls, P. and Shute, R., 'Dielectric heating in industry: application of radio frequency and microwaves', *IEE Proc.*, **128**, Pt.A, pp. 583–8, 1981.
165 Justesen, D. R., *et al.*, 'A microwave oven for behavioural and biological research: electrical and structural modifications, calorimetric, dosimetry, and functional evaluation.' *J. Microwave Power*, **6**, pp. 237–57, 1971.
166 Bernardi, P. and D'Ambrosio, G., 'Bio-electromagnetic research: review of some important aspects', *Alta Freq.*, **49**, pp. 47–54, 1980.
167 D'Ambrosio, G., Di Meglio, F. and Ferrara, G., 'Multimode time-varying enclosures for exposure and dosimetry in bioelectromagnetic experiments', *Alta Freq.*, **49**, pp. 89–94, 1980.
168 Gebbie, H. A. and Llewellyn-Jones, D. T., 'Untuned resonators for near millimeter waves', *Intl. J. Infrared Millimeter Waves*, **2**, pp. 197–206, 1981.
169 Corona, P., Latmiral, G., Paolini, F. and Piccioli, L., 'Use of a reverberating enclosure for measurements of radiated power in the microwave range', *IEEE Trans.*, EMC-18, pp. 54–59, 1976.
170 Corona, P., 'Comments and corrections to "Use of a reverberating enclosure for measurements of radiated power in the microwave range"', *IEEE Trans.*, EMC-18, p. 205, 1976.
171 Corona, P., 'Electromagnetic reverberating enclosures: behaviour and applications', *Alta Freq.*, **49**, pp. 154–8, 1980.
172 Lentz, R. R., 'Use of a reverberating chamber in microwave oven choke design', *J. Microwave Power*, **14**, pp. 29–33, 1979.
173 Lentz, R. R. and Anderson, H. C., 1979, 'Reverberating Chambers for EMC Measurement', IEEE Electromagnetic Compatibility Symposium Record, pp. 446–51, 1979.
174 Llewellyn-Jones, D. T., Knight, R. J. and Gebbie, H. A., 'Use of an untuned cavity for absolute power measurements of the harmonics above 100 GHz from an IMPATT oscillator', *J. Phys. D*, **13**, pp. L111–3, 1980.
175 Lamb, W. E., 1946, 'Theory of a microwave spectroscope', *Phys. Rev.*, **70**, pp. 308–17, 1946.
176 Corona, P., Latmiral, G. and Paolini, E., 'Performance and analysis of a reverberating enclosure with variable geometry', *IEEE Trans.*, EMC-22, pp. 2–5, 1980.
177 Llewellyn-Jones, D. T., *et al.*, 'New method of measuring low values of loss in the near millimetre wavelength region using untuned cavities', *IEE Proc.*, **127**, Pt. A, pp. 535–40, 1980.
178 Kremer, F. and Izatt, J. R., 'Millimetre-wave absorption measurements in low-loss dielectrics using an untuned cavity resonator', *Intl. J. Infrared Millimeter Waves*, **2**, pp. 675–94, 1981.
179 Izatt, J. R. and Kremer, F., 'Millimeter wave measurement of both parts of the complex index of refraction using an untuned cavity resonator', *Appl. Opt.*, **20**, pp. 2555–9, 1981.
180 Kremer, F. and Genzel, L., 'Temperature dependent mm-wave absorption of biological cells and biomolecules', Proc. 5th International Conference on Infrared and Millimeter Waves, Wurzburg, 1980, pp. 219–20.
181 Corona, P., *et al.*, 'The limits for anisotropy of the mixture of field-modes to be satisfied in the reverberating chambers with variable geometry used for power measurements', Proc. 5th International Wroclaw Symp. on EMC, pp. 829–37, 1980.
182 Becker, G. E. and Autler, S. H., 'Water vapour absorption of electromagnetic radiation in the centimeter wave-length range', *Phys. Rev.*, 70, pp. 300–7, 1946.
183 Llewellyn-Jones, D. T., Knight, R. J. and Gebbie, H. A., 'Use of the untuned cavity for millimetre and submillimetre wave measurements of loss in gaseous solid and liquid samples', Proc. European Conference on Precision Electrical Measurement, EUROMEAS '77, IEE Conference Publication 152, p. 70, 1977.
184 Llewellyn-Jones, D. T., Knight, R. J. and Gebbie, H. A., 'Absorption by water vapour at 7·1 cm^{-1} and its temperature dependence', *Nature*, **274**, pp. 876–8, 1978.
185 Hadley, L. N. and Dennison, D. M., 'Reflection and transmission interference filters', *J. Opt. Soc. Am.*, **37**, pp. 451–65, 1947.
186 Willis, H. A., *et al.*, 'Measurement of the absorption spectrum of polytetrafluoroethylene in the near millimetre region by an untuned cavity', *Polymer*, **22**, pp. 20–2, 1981.
187 Fleming, J. W. and Chantry, G. W., 'Accurate radiometric measurements on low-loss polymers at submillimetre wavelengths', *IEEE Trans.*, IM-23, pp. 473–8, 1974.
188 Gebbie, H. A. and Bohlander, R. A., 'Nonresonant cavity as a long path absorption cell', *Appl. Opt.*, **11**, pp. 723–8, 1972.
189 D'Ambrosio, G., *et al.*, 'Entomological experiments on the teratogenic effects of electromagnetic fields', *Alta Freq.*, **49**, pp. 115–9, 1980.
190 Kremer, F. and Genzel, L., 'Application of untuned cavities for millimeter wave spectroscopy', Proc. 6th International Conference on Infrared and Millimeter Waves, Miami, 1981, paper T-1-4.
191 Josyulu, O. S., Gowri Krishna, J. and Sobhanadri, J., 'A method for the evaluation of dielectric parameters of solids at microwave frequencies', *J. Phys.*, 15, pp. 318–21, 1982.
192 Ermert, H., 'Uber die Anwendung quasioptischer Resonatoren zur Messung der Materialparameter von Mikrowellenferriten in Millimeterwellenbereich', *Arch. Elekt. Ubertrag.*, 23, pp. 631–2, 1969.
193 Ermert, H., 'Messungen an Ferriten im Millimeterwellenbereich mit quasioptischen Messverfahren', *Frequenz*, **25**, pp. 171–7, 1971.
194 Chan Song Lint, B. and Priou, A., 'Characterization of magnetic materials in the millimeter-wave range (60–90 GHz)', *IEEE Trans.*, MTT-24, pp. 883–6, 1976.

Manuscript first received by the the Institution on 26th July 1982 and in final form on 10th September 1982.
(Paper No. 2062/MI 31)

Standard Frequency and Time Service

Communication from the National Physical Laboratory

Relative Phase Readings in Microseconds NPL—Station

(Readings at 1500 UTC)

AUGUST 1982	MSF 60 kHz	GBR 16 kHz	Droitwich 200 kHz	SEPTEMBER 1982	MSF 60 kHz	GBR 16 kHz	Droitwich 200 kHz
1	−12·7	32·2	24·8	1	−14·0	31·9	18·4
2	−13·0	32·6	24·6	2	−14·1	32·1	18·3
3	−13·3	32·4	24·3	3	−14·1	32·0	18·1
4	−13·6	32·0	24·1	4	−14·1	31·9	17·9
5	−13·4	32·0	23·9	5	−14·1	31·6	17·7
6	−13·3	32·2	23·7	6	−14·1	32·9	17·4
7	−13·3	32·4	23·6	7	−14·1	—	17·3
8	−13·5	32·1	23·4	8	−14·2	31·4	17·1
9	−13·6	32·0	23·2	9	−14·3	32·0	16·9
10	−13·7	32·0	22·9	10	−14·5	31·6	16·6
11	−13·6	32·2	22·6	11	−14·3	33·2	16·3
12	−13·7	32·3	22·4	12	−14·3	31·4	16·0
13	−13·5	32·4	22·0	13	−14·3	31·6	15·7
14	−13·5	32·2	21·7	14	−14·4	31·9	15·5
15	−13·5	32·2	21·5	15	−14·6	31·4	15·3
16	−13·5	32·5	21·1	16	−14·6	31·6	14·2
17	−13·5	32·4	20·8	17	−14·5	31·6	13·7
18	−13·6	32·5	20·6	18	−14·6	32·7	13·6
19	−13·5	32·1	20·4	19	−14·4	32·4	13·8
20	−13·7	32·3	20·3	20	−14·4	32·3	—
21	−13·7	32·2	20·2	21	−14·3	31·2	15·3
22	−13·7	32·3	20·0	22	−14·4	31·8	16·3
23	−13·7	32·6	19·8	23	−14·4	31·9	17·0
24	−13·7	32·2	19·6	24	−14·3	31·7	17·7
25	−13·7	—	19·5	25	−14·2	32·1	19·1
26	−13·9	—	19·4	26	−14·2	—	21·5
27	−13·9	—	19·3	27	−14·4	32·7	23·5
28	−13·9	—	19·2	28	−14·4	32·5	25·8
29	−13·9	—	19·1	29	−14·4	32·2	27·4
30	−14·0	31·6	18·7	30	−14·4	32·1	27·7
31	−14·0	32·0	18·5				

Notes: (a) Relative to UTC scale (UTC_{NPL}–Station) = +10 at 1500 UT, 1st January 1977.
(b) The convention followed is that a decrease in phase reading represents an increase in frequency.
(c) 1 μs represents a frequency change of 1 part in 10^{11} per day.
(d) It may be assumed that the satellite stations on 200 kHz at Westerglen and Burghead will follow the day to day changes in these phase values.

UDC 621.317.341 : 621.391.812.029.65
Indexing Terms: Radio transmission, propagation effects, Measurements, field strength, attenuation

Sub-millimetre-wave propagation measurement techniques

STEPHEN L. JOHNSTON, B.E.E., M.S.E.E., SMIEEE*

SUMMARY

A number of propagation measurements have been made in the sub-millimetre (s-mm) wave region (about 1 mm to 10 μm wavelengths or frequencies of 300 GHz to 3 THz) using four basic techniques. While those measurements have been reported in the literature, s-mm propagation measurement survey papers to date have concentrated on the reported propagation data. This paper describes measurement techniques used in 33 s-mm propagation measurement papers and discusses various aspects of their techniques including characteristics of the apparatus employed. Factors to be considered in using those techniques are discussed. Certain propagation measurements which are needed for the s-mm region are cited.

* *Editor-in-Chief, International Radar Directory, 4015 Devon Street, Huntsville, Alabama 35802, USA.*

1 Introduction

During the performance of a sub-millimetre (s-mm) wave radar preliminary design study, propagation data from experimental measurements of others were needed for use in the radar performance analysis and in the selection of the radar frequency. A literature search yielded about one hundred s-mm propagation references, of which about half pertained to actual measurements. Review of this group resulted in attracting the author's attention to thirty-three[1-33] for consideration of the measurement techniques reported. An IEEE EASCON-79 paper[34] treated propagation data needs for millimetre/sub-millimetre wave radar systems design and reviewed available data but did not consider measurement techniques.

Exploration and utilization of a new part of the electromagnetic spectrum require a knowledge of the propagation characteristics of that region. Theoretical studies are necessary to predict what is to be expected; however, experimental propagation measurements are needed to verify the validity of the theoretical studies. Experimental measurements require that adequate apparatus for the region under study be available. While fully adequate apparatus is desirable, frequently valuable (although limited) data can be obtained from very rudimentary apparatus. Many years before adequate apparatus for the microwave region was developed, Hertz through his classical experiments in 1889 generated 60 cm waves using a spark gap transmitter.

The s-mm region (variously defined as wavelengths of about 1 mm to 10 μm or frequencies of 300 GHz to 3 THz, i.e. 3000 GHz) is the last electromagnetic frontier. Several theoretical studies have been conducted on propagation characteristics of this region. Experimental measurements have been beset by two problems: apparatus availability/adequacy and the nature of this region itself. Both detector (receiver) and radio frequency signal sources have been a problem. While considerable progress has been made in each of these areas, currently available apparatus still does not permit making all the propagation measurements that are needed for this region. This region is characterized by much higher atmospheric attenuation than the centimetre ('microwave') region, thus greater receiver sensitivity and/or power output of r.f. sources are needed. Present apparatus characteristics have permitted a number of propagation measurements to be made however. While several papers have addressed comparison of theoretical and experimental s-mm propagation data[35-41], usually the various measurement techniques have been described only briefly in individual papers on measurement results. However, measurement techniques are important both as a guide in the assessment of resulting data and in the planning of additional measurements to be made. Measurement conditions, e.g. path description, and technical characteristics of the measurement apparatus are of further interest. This paper will survey s-mm propagation measurement techniques used by various workers and will discuss various aspects of their techniques.

0033-7722/82/110585+15 $1.50/0

2 Data Base and Frequency Region

The previously mentioned literature search identified nearly 100 papers on s-mm wave propagation. This included both theoretical computations and experimental measurements from 1·4 mm to 100 μm wavelengths. From this collection, only those papers containing experimental measurements in the frequency region that are anticipated for the experimental radar were selected. Operating frequency of the radar was to be as high as permissible to achieve the smallest antenna possible beamwidth for a given antenna diameter yet commensurate with availability of adequate r.f. source power output.

Three types of r.f. sources were considered for the s-mm radar: solid-state, thermionic and laser. Amboss[42] has presented an excellent review of various types of r.f. sources with emphasis on the 100–300 GHz region. Solid-state devices are very attractive due to their small size and simple power supply requirements. Purcell[43] has described British and Japanese experimental solid-state devices operating up to 400 GHz. At present, their low power output and unavailability for general use made them unsuitable for the contemplated experimental s-mm radar.

Optically-pumped lasers have been operated at many discrete lines in the s-mm region with average powers of a few milliwatts at some lines in the lower frequencies.[44] While that power is adequate for some purposes, higher power and tunability are desirable. About 20 dB greater power output has been achieved from r.f. tubes in the vicinity of 1 mm.

The only thermionic r.f. source currently available for operation in the s-mm region is the backward-wave oscillator. Golant[45, 46] described a series of b.w.o.s covering the frequency range of 37–612 GHz. In the West, the Thomson-CSF carcinotrons† (b.w.o.s) operate at various frequencies up to 1000 GHz.[47–49] Power outputs vary from 1 W at 300 GHz to about 1 mW at 1000 GHz. These tubes are usually operated c.w. although a previous paper[50] discussed pulsed operation.

The extended interaction oscillator (e.i.o.)[51–53] has been developed in c.w. and pulsed versions currently operating at several frequencies up to 280 GHz. Power output at 280 GHz of 1 W c.w. or 10 W peak for pulsed operation at duty cycles of 0·1 were reported. An amplifier version, the extended interaction amplifier (e.i.a.), has also been developed at 95 GHz.[54]

Availability of the e.i.o. and the carcinotron caused interest in the radar operating frequency to be centred in the 200–300 GHz region.

For convenience, the octave 180–360 GHz was chosen for this paper. This octave also includes two absorption lines: 183 and 325 GHz as well as the atmospheric window near 220 GHz. Techniques have been used in this region which have not been used yet in the shorter wavelength portions of the s-mm band. Some of the references used in this paper included measurements made at shorter wavelengths. Concentration on the 180–360 GHz region excluded few s-mm propagation measurements papers from this paper even though this octave is only a small portion of the s-mm band. Measurement techniques to be described in this paper are representative of the entire s-mm band.

Thirty-three references[1–33] pertaining to propagation measurements/apparatus in this octave were selected to illustrate s-mm propagation measurements techniques. A review of these papers indicated that they could be classified either by measurement purpose or by measurement technique. The former include atmospheric attenuation, rain attenuation, snow attenuation, fog attenuation, solar spectrum, H_2O absorption, rain backscatter, etc.

These papers cover the years 1953–1982. Interestingly, the five year period of 1965–1969 reported the most measurements with the largest single year being 1966. The paucity of current s-mm propagation papers may be in part due to the high interest now in millimetre wave systems, especially radar.[55] Countries of the authors include Venezuela, UK, USA, and USSR. Measurement purposes were 16 atmospheric attenuation, 13 H_2O absorption, 3 rain attenuation, 2 snow attenuation, 2 fog attenuation and 1 rain backscatter (some reported multipurposes).

The four basic measurement techniques used include those employing a radiometer, those made in a chamber, measurements made on an outdoor direct path and outdoor reflectivity. For brevity these will be referred to in this paper as 'radiometer', 'chamber', 'outdoor direct' and 'outdoor reflectivity'.

All measurements include an r.f. source, a propagation medium, and an appropriate receiver. Radiation from the Sun is usually used as the r.f. source in radiometers. Measurements may be made either by assuming a constant propagation medium and changing path length, by observing effects of variation of the propagation medium with time as in outdoor measurements in a rain storm, or by varying the propagation medium as in chamber measurements. Figure 1 shows the measurement frequencies and techniques used for the 33 measurement papers. Frequencies which have been allocated in this octave by the World Administrative Radio Conference on Space Telecommunications (WARC/ST)[56] are also shown, along with the WARC-79 allocations for radiolocation.[57]

3 Sub-millimetre-Wave Propagation

Sub-millimetre waves are propagated in a vacuum with the well-known spreading loss or free space loss of $20 \log (4\pi D/\lambda)$, i.e. 20 dB/decade. S-mm waves suffer attenuation, refraction and scattering in addition when propagated through the atmosphere. Absorption by water vapour and its mixtures with other gases causes severe attenuation at the several absorption lines, e.g. 183 and 325 GHz. Thus it is of extreme importance to determine the nature of these lines, both their frequency and width. These lines were the subject of theoretical treatment by Van Vleck and Weisskopf,[58] Van Vleck[59] and others later. Extensive experimental investigation has also been devoted to the characteristics of these lines. The extremely large values of attenuation even in some of the shorter wavelength 'windows', e.g., greater than

†Trade mark registered.

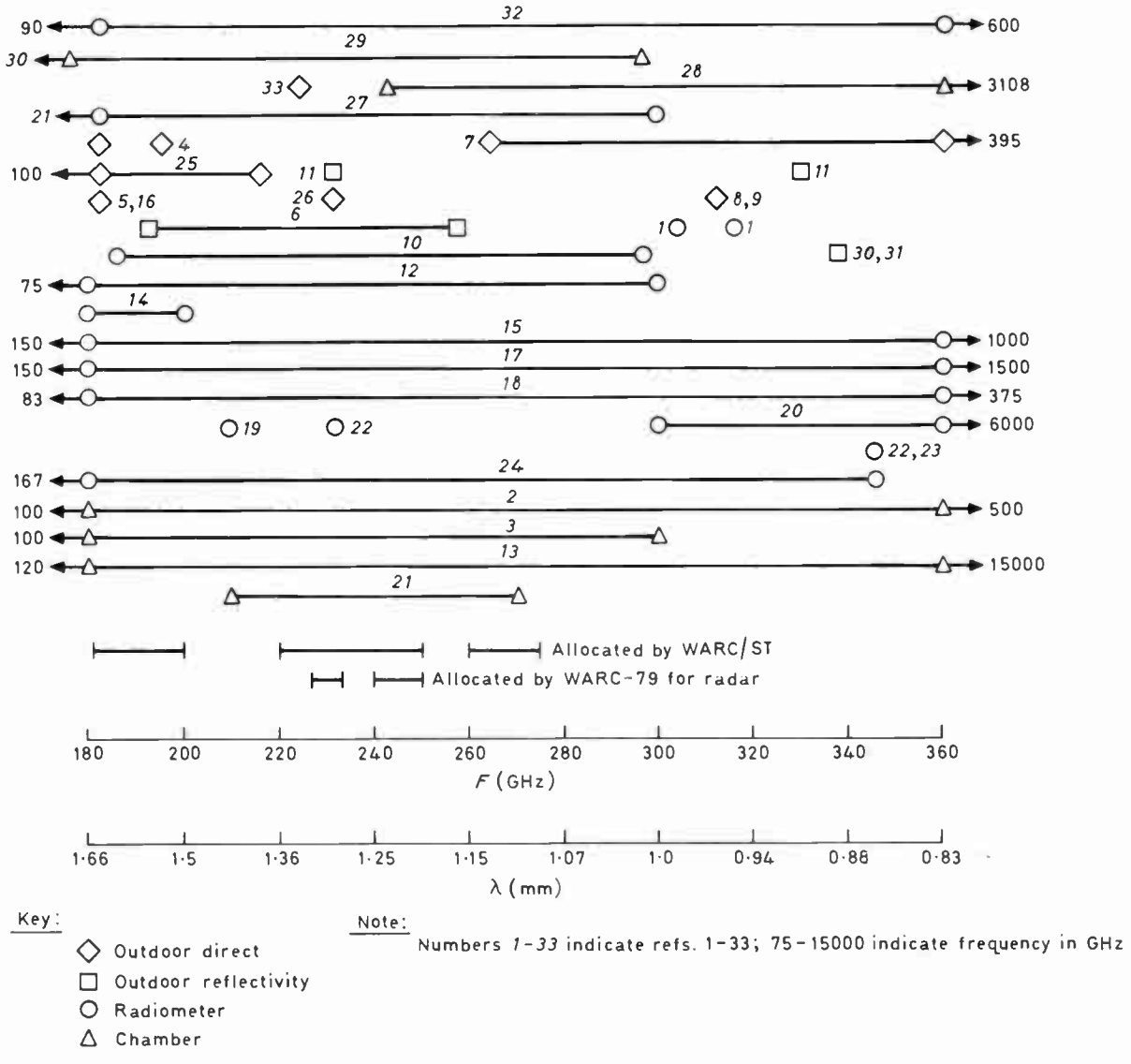

Fig. 1. Frequencies and techniques used in sub-millimetre atmospheric attenuation measurements.

500 dB/km, together with problems of suitable r.f. sources and detectors make s-mm propagation measurements at the shorter wavelength very difficult.

4 Sub-millimetre-Wave Propagation Measurement Techniques

It is only natural that s-mm propagation measurement techniques are extensions of millimetre and microwave propagation measurement techniques. Since the s-mm region lies between the millimetre and infrared (i.r.) regions, s-mm propagation measurement techniques are a mixture of millimetre and i.r. propagation measurement techniques. R.f. sources and detectors from these two adjoining regions have been extended into the s-mm region.

The four basic s-mm propagation measurement techniques (radiometer, chamber, outdoor direct, and outdoor reflectivity) will now be described and illustrative s-mm employments will be presented.

4.1 Radiometer S-mm Propagation Measurements

The radiometer has been widely used in both millimetre and i.r. regions. A radiometer uses the Sun (or the Moon) or the radiation of the atmosphere as the r.f. source which is detected by an appropriate detector using a directional antenna. Various techniques are used to filter the incoming energy to select the desired frequency region. Long and Rivers[60] proposed the use of a direct detection radiometer in the s-mm region since suitable superheterodyne receivers were unavailable for this region at that time. Altshuler[61] treated two different methods for extracting atmospheric attenuation from radiometer data. Kislyakov[41] also treated this topic. Kislyakov[62] and Dryagin and Fedoseev[63] presented reviews of Soviet millimetre and s-mm radiometer technology. Williams and Chang[64] described an s-mm radiometer using the interferometric modulator.

The radiometer is an attractive method for investigating water vapour absorption of s-mm waves

Table 1. Summary of s-mm radiometer measurements

Ref.	Year of measurement	Country	Frequency (GHz)	Wavelength (mm)	Measurement purpose	Altitude (m)	Detector type	Detector sensitivity	Chopping frequency (Hz)	Diameter optics (cm)	Integration time (s)	Experiment variable	Special features
19	1953	US	200±	1·5±	Atmospheric attenuation	≈ s.l.	Golay	10^{-10} W	9	61	5	Sun angle	Black filters
18	1955	US	83, 375	3·6, 0·8		≈ s.l.	Golay	NS	5	152	NS	Sun angle	Wire mesh filters
12	1963	UK	75, 300	4, 1		40 & 2000	Golay	NS	NS	165	1, 180	Sun angle	Differential Golay cells
23	1964	USSR	345	0·87		3860	Optical-acoustic	5×10^{-10} W	10	90	40, 60, 120	Sun angle	OAP-2 receiver
20	1965	US	300, 6000	1–0·05		2134	He-cooled Ge bolometer	NS	NS	30	NS	Sun angle	Michelson-Dicke interferometric radiometer
17	1966	UK	150, 1500	2, 0·2		2880	Golay	NS	NS	160	10	Sun angle	Fabry-Perot interferometer
1	1967	US	304, 316	0·99, 0·95		≈ s.l.	Point contact diode	3·16 K	165	25	10	Sun reflecting plate distance	Dicke superheterodyne
24	1960, 67	USSR	167, 345	1·8, 0·87		s.l. 4 km	NS	NS	NS	NS	NS	NS	NS
15	1957, 67	UK	150, 1000	2, 0·3		3580	NS	NS	NS	76	NS	NS	Michelson interferometer
10	1971	USSR	188, 306	1·6, 0·98		s.l.	He-cooled N-InSb	0·34 K	NS	100	NS	Sun angle	Echellete monochromator
22	1973	US	230, 345	1·3, 0·87		1280	Schottky diode	NS	20	305	NS	Sun angle	Dicke superheterodyne
27	1980	Venezuela	21–300	14·3–1·0		N S	Golay	7×10^{-11} W	NS	10	Few seconds	Sun angle	Rotating mirror
32	1980	UK	90, 600	3·33, 0·5		2400	Liquid He-cooled Ge Bolometer	7×10^{-13} W	100	NS	0·1	Sun angle	Polarizing Martin-Puplett type interferometer
14	1979, 82	US	180, 200	1·67, 1·5		≈ s.l.	Schottky diode	NS	NS	63	NS	Sun angle	Dicke superheterodyne

since it does not require an r.f. source *per se*. Maximum sensitivity and wave selectivity obtain from a superheterodyne radiometer. An r.f. source at the conversion frequency is required as the local oscillator for a superheterodyne receiver. The most severe problem in the use of a radiometer to provide water vapour absorption data is the need of accurate knowledge of the humidity of the atmospheric path to the Sun. Ryadov *et al.*[23] pointed out this limitation. Goldsmith *et al.*[22] stated that ground level atmospheric humidity is a poor indicator of atmospheric attenuation.

Fourteen papers on the use of radiometer for s-mm propagation measurements in the frequency region of 180–360 GHz were used: 19, 18, 12, 23, 20, 17, 1, 24, 15, 10, 22, 27, 32, 14 (listed chronologically). These are represented by a circle in Fig. 1. All were used for atmospheric attenuation measurement. They cover the time period from 1953 to 1982.

Data on these 14 radiometers are contained in Table 1. Radiometer types vary from the simple direct type of Sinton[19] to the elaborate Michelson-Dicke interferometric radiometer of Williams and Chang.[20, 64] Detectors used included the Golay cells,[19, 18, 12, 17, 27] helium-cooled germanium bolometer,[20, 32] helium-cooled n-InSb,[10, 65], and superheterodynes.[1, 22, 14]. The latter two used Schottky barrier diode mixers.[66–68] Williams and Chang[64] also presented an early review of the characteristics of s-mm detectors. Listvin and Potapov[69] described a millimetre and s-mm semiconductor modulator for radiometers. The apparatus used by Ryadov *et al.*[23] was described more fully by Averkov *et al.*[70] The correlation method for determining spectral characteristics[71] referred to by Kukin *et al*[24] involves the inverse Fourier transform of the interferogram function.[64] Apparatus used by Zamit[32] was more fully described by Hills[72] along with earlier measurements made with this equipment.

Zabolotniy[73] reported attenuation measurements made on the Russian RT-22 radiotelescope using receiving equipment similar to that of Vardanyan *et al.*[10] listed in Table 1.

Williams and Chang[20] traced their interference spectrometer radiometer to Gebbie.[15, 74] Gebbie traced it to Strong.[75] All of the radiometers used a low frequency chopper, typically 20 Hz or less. Chang and Lester[1] however used 165 Hz. Dryagin and Fedoseev[63] proposed the use of 825 Hz to remove flicker noise of the amplifier. Such high frequencies are not permissible with the Golay cell, bolometer, or photoconductive detector.[64]

Most of the radiometers used the sun angle as the variable; however, Chang and Lester[1] were a notable exception. They set up a $5 \times 3{\cdot}6$ m metallic flat plate reflector inclined at 45 deg and located at varying distances (a few metres to 300 m) from the radiometer. Atmospheric attenuation was then determined from differences of radiometer readings at two different distances. This presents problems which will be discussed when considering outdoor direct measurements (Sect. 4.3).

The frequency/wavelengths shown in Fig. 1 and listed

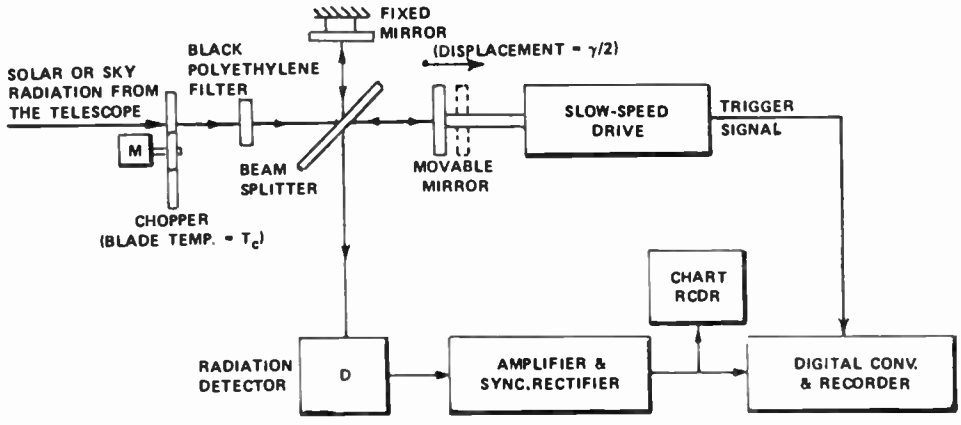

Fig. 2. Block diagram of the Dicke-type sub-millimetre interferometric radiometer receiver (Williams and Chang[20, 64]).

in Table 1 require interpretation. In several cases, e.g. Sinton[19] the radiometer was very broad band. In other cases, e.g. Vardanyan *et al.*[19], an *échellete* monochromator was used to provide a very narrow frequency (wavelength) response. The monochromator was then varied to provide system tuning over a wide s-mm region.

Measurement altitude was generally either near sea level or mountain top. Sensitivity of early s-mm radiometers was inadequate, requiring that s-mm H_2O absorption measurements be made at high altitudes during winter when H_2O content was lowest. Some of the radiometer measurements were made at high altitudes at observatories. Occasionally, the radiometer used a heliostat of the observatory telescope as a collecting system, e.g. Williams and Chang.[20]

Block diagrams of some of these radiometers are shown in Fig. 2 to 5. Figure 2 shows a Dicke-type s-mm interferometric radiometer receiver (Williams and Chang[20, 64]). Figure 3 shows the Dicke superheterodyne receiver of Chang and Lester.[1] It is similar to that in Fig. 4 (Goldsmith *et al.*[22]) and Fig. 5 (Forsythe[14]).

4.2 Chamber S-mm Propagation Measurements

The chamber method is an adaptation of microwave spectroscopy. Here, electromagnetic energy from an appropriate r.f. source is coupled into a chamber (frequently a cylindrical tube) with a detector at the far end of the chamber. Various gases such as H_2O vapour, singly or in combination, are introduced into the chamber. Often a separate empty chamber is used for

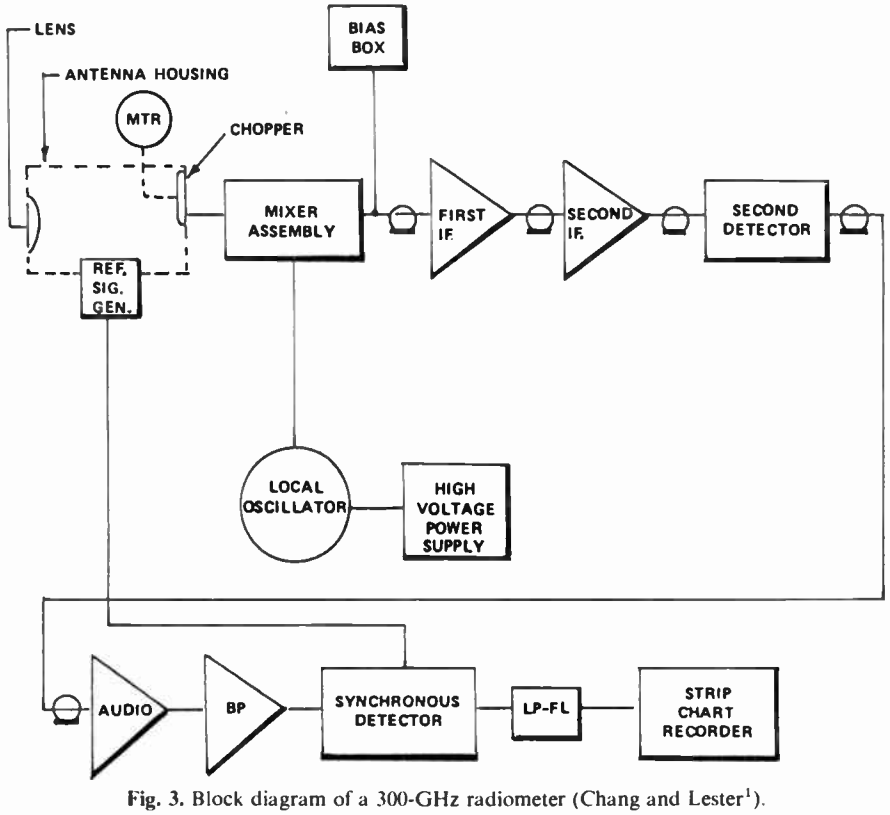

Fig. 3. Block diagram of a 300-GHz radiometer (Chang and Lester[1]).

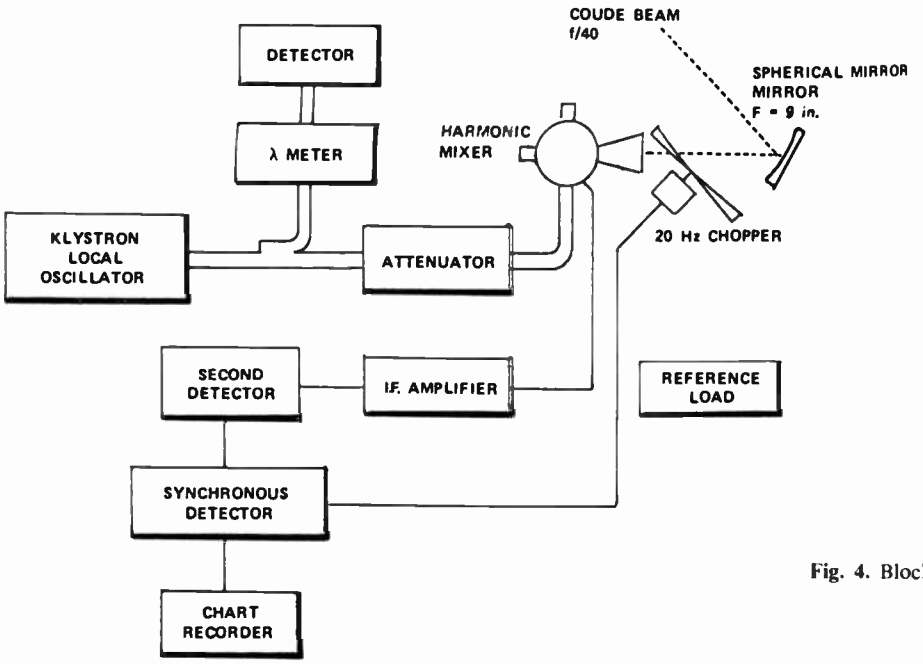

Fig. 4. Block diagram of millimetre wave radiometer (Goldsmith *et al.*[22]).

reference purposes. The chamber technique is attractive in that the atmosphere in the test chamber may be controlled in composition, temperature, and pressure.

Six applications of this technique in this frequency region were noted: Yaroslavsky and Stanevich,[13] Frenkel and Woods,[3] Harries *et al.*,[21] Emery,[2] Simpson *et al.*[28] and Liebe.[29] Characteristics of these six measurements are given in Table 2. The r.f. source was often an Hg lamp; however, Emery[2] was a notable exception: an Elliott 8TK20 klystron with a Froome plasma metal junction harmonic generator with outputs of 10^{-5} to 10^{-9} W served as the r.f. source. Simpson *et al.*[28] used a gas pumped-laser.

Reported effective path lengths were 0·75 to 165 m. Harries *et al.*[21] used White's multipass optical system[76] to provide an increase of effective path-length by multiple passes through the chamber. An optical path of 56 m could be obtained from 90 traverses of the chamber. Valkenburg and Derr[77] showed the equation for effective path-length of a Fabry-Perot resonator of the type used by Frenkel and Woods.[3] A mirror separation of 60 cm and a Q of 10^6 at 300 GHz will give an effective path length of about 162 m. The scheme of Liebe[29] is similar with the addition of a moisture 'lake'.

Figures 6, 7 and 8 from Emery[2] show diagrams of experimental arrangement, optical system, and schematic diagrams of a dual-beam system. The use of two choppers and two phase-sensitive detectors is noteworthy.

Achievable path length is a limitation of the chamber method. This will be discussed below under outdoor direct measurements. Obviously, attenuation of rain or snow cannot be readily measured with a chamber.

4.3 Outdoor Direct S-mm Propagation Measurements

The outdoor direct propagation measurement technique was obtained from both the microwave and optical regions. An r.f. source and appropriate antenna for transmission are required with another antenna and detector for reception. The transmitter and receiver are

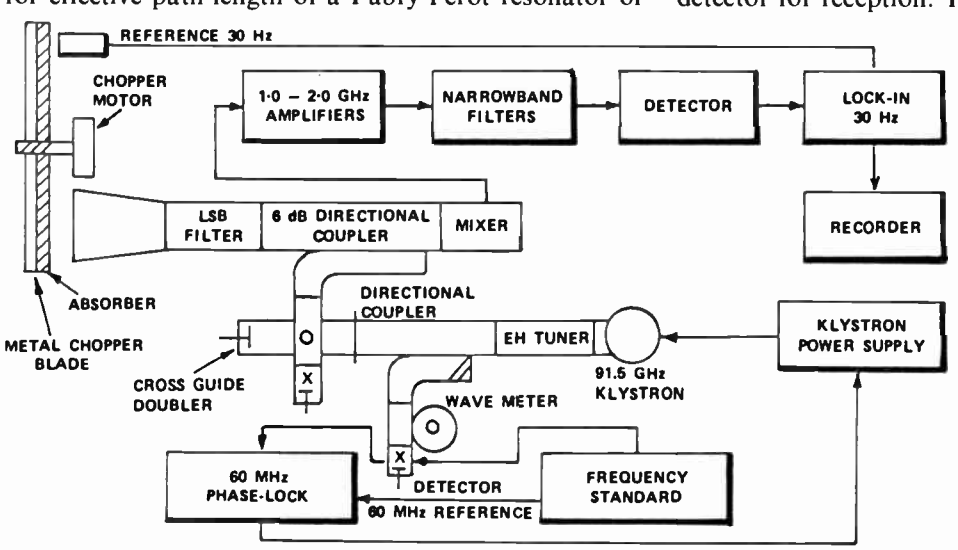

Fig. 5. Millimetre wave radiometer (Forsythe[14]).

Table 2. Summary of the characteristics of s-mm chamber measurements

Ref.	Years of measurement	Country	Frequency (GHz)	Wavelength (mm)	Measurement purpose	Path length (m)	Chamber	Detector	R.F. Source	Special Features
13	1958	USSR	120–15,000	2·5–0·02			Vacuum spectrometer	Optical (acoustic PRK-4Hg	Hg lamp	DIKS-1 spectroscope
3	1965	US	100–300	3·0–1·0		0·75	Fabry–Perot resonant transmission cavity			
21	1969	UK	210–270	1·42–1·11		28	15 cm dia. tube	Photoconductive He-cooled InSb	Hg lamp	Multipass Fourier transform spectroscopy
2	1971	UK	100–500	3·0–0·65	Water vapour absorption	6	5 cm dia. brass tube	Golay cell	Elliott 8TK20 kly	Froome plasma metal junction harmonic generator
28	1980	USA	245–3108	1·22–0·010		3·44	10 cm dia. tube	Golay cell	NS	Digital ratiometer measures ratio of cell input/output
29	1981	USA	30–300	10–1		eff : 165 m at 140 GHz	10 cm dia. tube	NS	NS	Adjustable chamber, temp-ature, pressure, relative humidity

Table 3 Summary of the characteristics of outdoor direct propagation measurements

Ref.	Years of measurements	Country	Frequency (GHz)	Wavelength (mm)	Measurements purpose	Path length (m)	Altitude (m)	R.f. source	Power output (mW)	Antenna diameter (cm)	Antenna type	Antenna polarization	Antenna gain (dB)	Receiver description	Experiment variable	Stated accuracy (dB)
4	1961	USA	172, 183·6, 194	1·55, 1·63, 1·74	H_2O vapour line width	122	NS	3 mm klystron	NS	28	Lens-horn	NS	50	Superhet. 30 MHz i.f.	Halve distance	NS
16	1966	USSR	183·31	1·64		0·5–3000	NS	NS	NS	111, 60, 30	Parabola	NS	55/61	Crystal detector and amplifier	Double distance	NS
7	1966	USSR	261–395	1·15–0·76		1350	12·5	BWO	'a few'	90	Cassegrain	NS	53	10 Hz Mod, OAP-2 pneumatic indicator	Dist, freq, humidity	±1·8
25	1966	USSR	100–221	3·0–1·36	H_2O vapour absorption	1000–6000	7–10	BWO	3–6	Rcvr : 30 Tmtr : 92	Rcvr : Parabola Tmtr : Cassegrain	NS	48/57	Modulation radiometer	Humidity, distance	NS
5	1967	USA	171, 183	1·75, 1·64	do.	122, 183, 244	Rcvr : 6 Tmtr : 2	Klystron	NS	28	Lens-horn	NS	37	Superhet. 30 MHz i.f.	Distance	NS
26	1969	USSR	231	1·3	do.	4000	NS	NS	NS	111, 60, 30	Parabola	NS	50	Crystal detector and amplifier	Distance	±0·1
8	1969	USSR	313	0·96	Rain attenuation	1000	NS	BWO	NS	100	Cassegrain	Vert	68	InSb detector	Rain	NS
9	1969	USSR	313	0·96	Snow attenuation	680	NS	BWO	NS	100	Cassegrain	Vert	68	InSb detector	Snow	NS
33	1981	USA	225	1·33	Atmos. attn, fog and rain attn, rain backscatter target r.c.s.	1000	Various	EIO	70 W peak	61	Cassegrain	Horiz/Vert	NS	Superhet., also crystal detector and amplifier	Various	NS

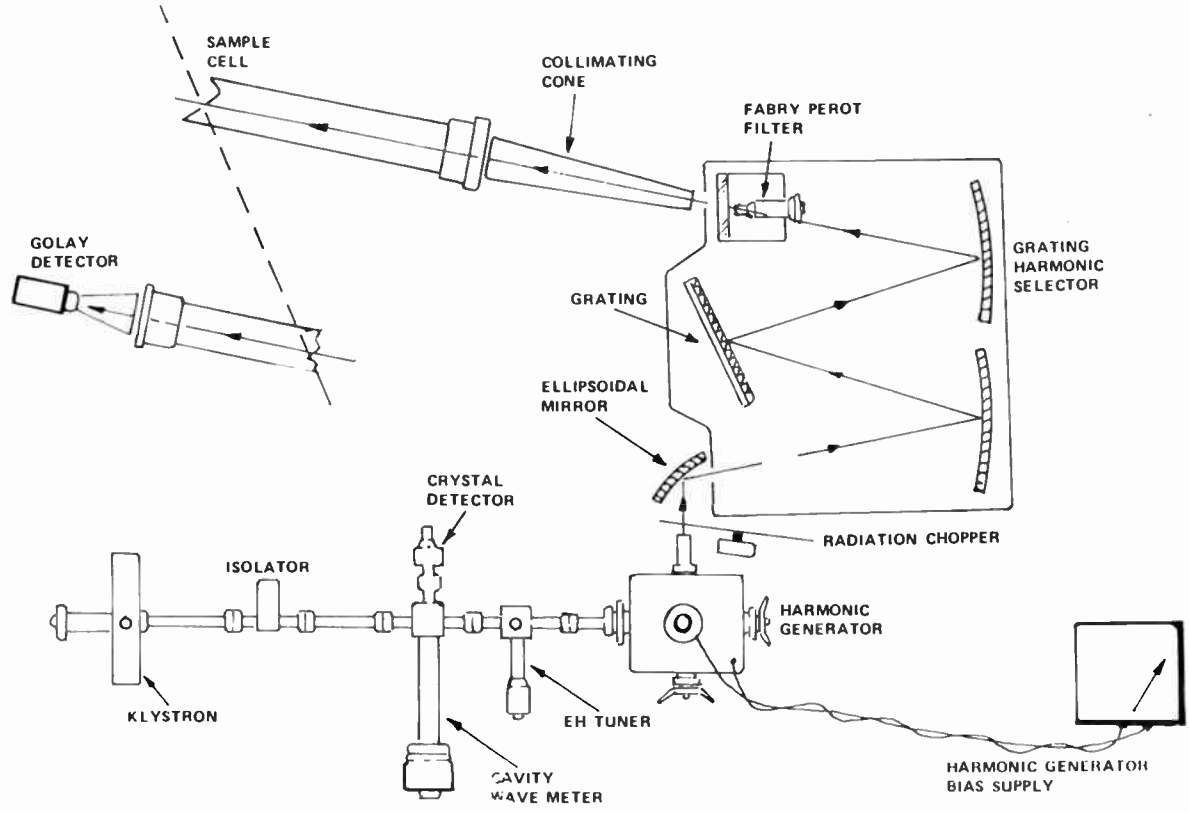

Fig. 6. Diagram showing the experimental arrangement of Emery's[2] generator and optical system for chamber propagation measurements.

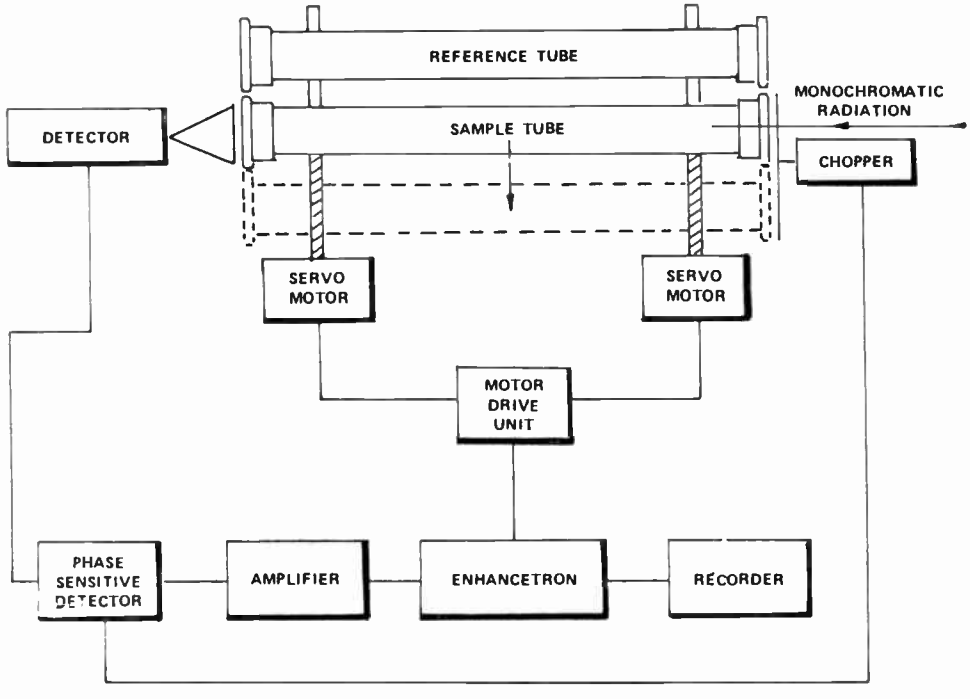

Fig. 7. Schematic diagram showing the system of Fig. 6 with automatic electronic averaging.

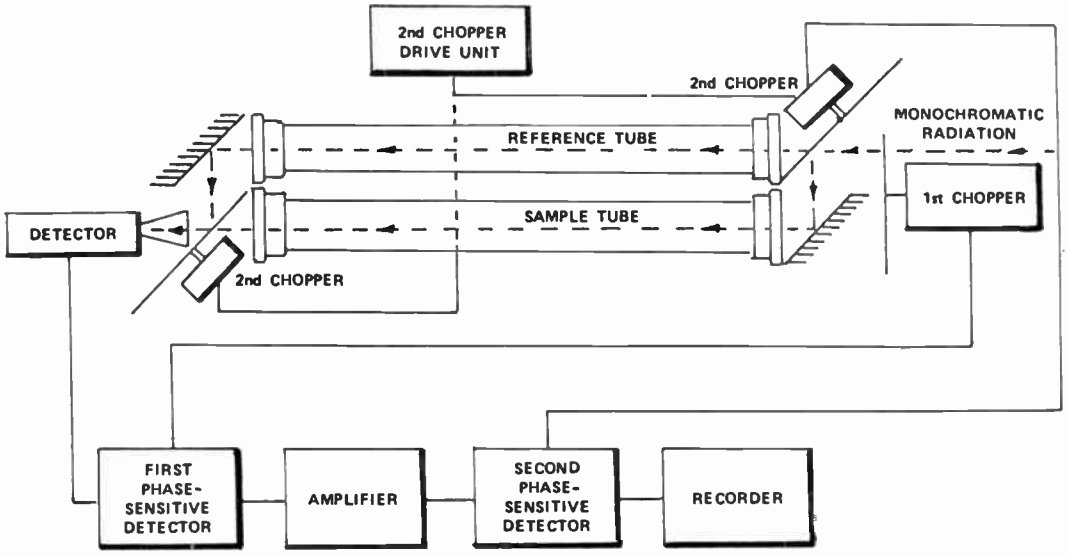

Fig. 8. Schematic diagram of the dual-beam system of Fig. 6.

separated by an appropriate distance, generally less than 10 km at present. In the s-mm region, this must be a line-of-sight path.

Nine of the 33 references[1-33] in the data base for this paper utilized the outdoor direct-propagation measurement technique. These are Coats *et al.*[4] Malyshenko,[16,26] Ryadov and Furashov,[7] Dryagin *et al.*[25] Whaley and Fannin,[5] Babkin *et al.*[8,9] and Nemarich *et al.*[33] Their measurement frequencies are represented by a diamond in Fig. 1, and their characteristics are listed in Table 3.

Date of measurement is interesting; most were made in the 1966–1969 period. All of the measurements except those of Ryadov and Furashov[7], Dryagin *et al.*,[25] and Nemarich *et al.*[33] used single measurement frequencies. The measurement purposes of Babkin *et al.* were rain attenuation[8] and snow attenuation.[9] The purpose of all the others except Nemarich *et al.* was H_2O vapour absorption. Three used path lengths under 700 m, three used about 1000 m, and three used 3000–6000 m. There were no measurements made at high altitudes.

Radio-frequency sources used included klystrons (Coats *et al.*[4]) and Whaley and Fannin[5], the previously cited e.i.o.[51-53] by Nemarish *et al.*,[33] and the b.w.o. of Golant[45,46] in all USSR measurements.[16, 7, 25, 26, 8, 9]

Russian s-mm propagation measurement apparatus was further described by Babkin *et al.*[78] Devyatkov and Golant[79] described electron devices for the millimetre and sub-millimetre wavelengths. Many papers, e.g. Refs. 42, 80–84, have described the gyrotron family. Power levels of 1 kW c.w. at 1 mm wavelength[78] are very impressive. No propagation measurement has been reported using this device family, however.

Variable frequency measurements of Ryadov and Furashov[7] and Dryagin *et al.*[25] are noteworthy. Power outputs of 10 mW or less were generally used except Nemarich *et al.*[33] Path lengths used were such that an adequate signal could be received considering the power output, available antenna gains, receiver sensitivity available, and the expected attenuation.

Apparatus of Nemarich *et al.*[33] further described in Refs. 85–87, is noteworthy. Although not shown in Table 3 it can make simultaneous measurements at 95, 140 and 220 GHz and can measure attenuation on a one-way path or rain backscatter. The associated meteorological characterization system was described elsewhere;[88, 89] this apparatus has many excellent capabilities but does not meet some of the requirements for radar design data.[34] Recent WARC-79 millimetre wave frequency allocations[57] also should be accommodated.

Antenna diameters used varied from 28 to 111 cm and antenna types used included lens-horn, parabola and Cassegrain. Probably the papers which indicated use of a parabola actually meant a Cassegrain[90] since a parabola is not suitable at these frequencies due to feed problems.[91] Antennas for the s-mm and i.r. regions have been described by Rutledge *et al.*[92]

Only three papers,[8, 9, 33] indicated their antenna

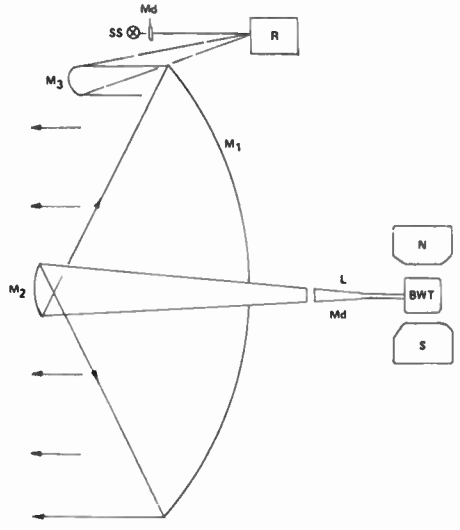

Fig. 9. Optical system of the transmitting equipment for outdoor direct propagation experiment equipment: M_1 transmitting antenna; M_2 antenna radiator; M_3 entrance mirror of the power meter; L waveguide line; Md modulator; SS standard source; R receiver. (Ryadov and Furashov[7]).

polarization. Although connections between the transmitter and antenna or antenna and receiver/mixer are generally short, some form of 'waveguide' is necessary. Harris[93] described waveguides for part of the s-mm frequency region. All USA papers (Coats *et al.*[4] Whaley and Fannin[5] and Nemarich *et al.*[33]) used superheterodyne receivers. All USSR papers used receivers which microwave radar engineers call 'crystal-video'. The superiority of superheterodyne receivers is well-known; however, they require a local oscillator and r.f. mixer. As indicated in the previously discussed radiometers, superheterodyne receivers in the 1 mm region were developed many years ago in the USA. Sub-millimetre detectors in the USSR are described in Refs. 62, 65, 94 and 96.

The PSD-5 and PSD-6 s-mm receivers[94] both employ bulk resistance change of n-InSb cooled to 4·2K. The PSD-5 is suitable for continuous wave signals over 150–2000 GHz (2–0·15 mm) with best sensitivity of $0{\cdot}5 \times 10^{-12}$ W for 1-s time-constant. The PSD-6 used for pulsed signals has a 1-MHz passband and best sensitivity of 5×10^{-9} W. Both receivers are suitable for radiometers, propagation receivers, etc.

Block diagrams of one USSR[7] outdoor direct propagation transmitter and one US transmitter receiver[5] are shown in Figs 9 and 10, respectively. The method of modulation of the r.f. source and the r.f. power monitor of Fig. 9 are noteworthy.

Variables in the measurements of Table 3 include distance, frequency humidity, rain, and snow. Distance and frequency variations can both cause problems. In distance variation, it is assumed that the r.f. source power output, receiver sensitivity, and humidity remain constant during the time the distance is being varied (generally several minutes). Even if they each remain constant within ± 1 dB (very difficult), the total r.m.s. error would be $\pm N$ dB, where there are N error sources each of 1 dB magnitude. This must be further multiplied by $1000/L$, where L is the path length in metres. This multiplication factor arises since attenuation is usually given in decibels/kilometre. A path of 100 m would have a multiplication factor of 10. Battan[97] claims that ± 1 to 5 dB represents typical measurement accuracy in radar meteorology. Bean *et al.*[98] imply a basic radar meteorology accuracy of no better than ± 3 dB. This is in the microwave region where r.f. sources and receivers are much more stable than at s-mm wavelengths. Duffield[99] claims a measurement accuracy at 20 and 30 GHz of 0·5 dB. That system is much more refined than current s-mm systems.

Variation of frequency requires that inherent variation of b.w.o. power output with frequency be included. This also requires that antenna gain (and pattern) and receiver sensitivity be constant over this frequency range. Such may present problems.

4.4 Outdoor Reflectivity S-mm Propagation Measurements

This technique, which is a variant of the outdoor direct propagation measurement technique and could also be called radar, folded path, reflex, etc., was analysed and demonstrated at mm wavelengths by Crawford[100] many years ago. In this method, the transmitter and receiver are co-located and a suitable reflector (often a large flat plate) is located at an appropriate distance. This

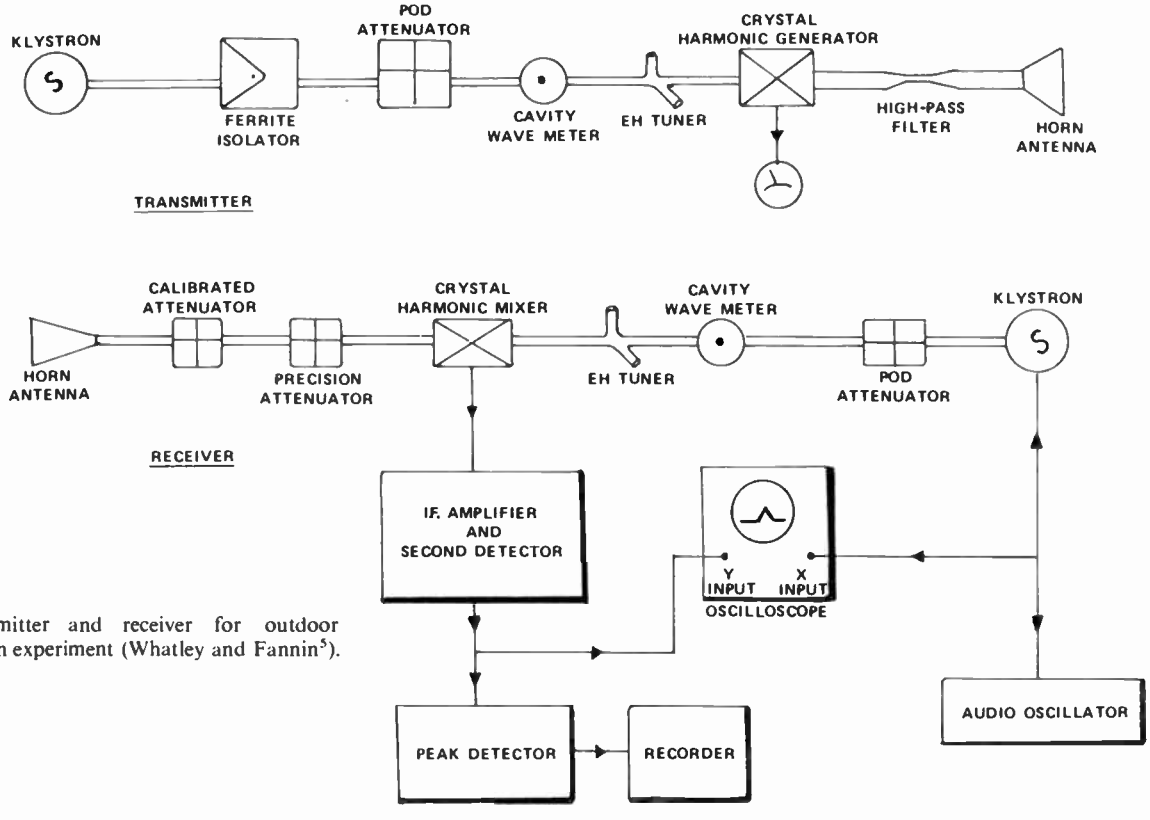

Fig. 10. Transmitter and receiver for outdoor direct-propagation experiment (Whatley and Fannin[5]).

technique has several advantages: (1) only one location with power sources is required; (2) the effective path length is twice the transmitter-reflector distance, since this path is transversed twice; (3) this reduces problems of hydrometeoric inhomogeneity; and (4) co-location makes possible various schemes of compensation of transmitter power variation by incorporating into the receiver correction signals from the transmitter.

Four papers of the data base use this technique: Malyshenko and Vakser,[11] Ryadov and Furashov[6] and Tanton;[30, 31] their measurement frequencies are represented by a square in Fig. 1, and characteristics of these measurements are listed in Table 4. A block diagram of the transmitter portion used by Ryadov and Furashov[6] is shown in Fig. 11.[101] General similarity of Figs. 9 and 11 will be noted. Two of the measurement papers[11, 6] in this group use part of the transmitted signal to compensate the received signal for variation of transmitted power. Both papers provided only brief descriptions of their compensation scheme. Numerous compensation schemes are possible. The optically pumped laser of Tanton[30, 31] is noteworthy. As mentioned previously, Hodges[44] has reviewed optically pumped lasers.

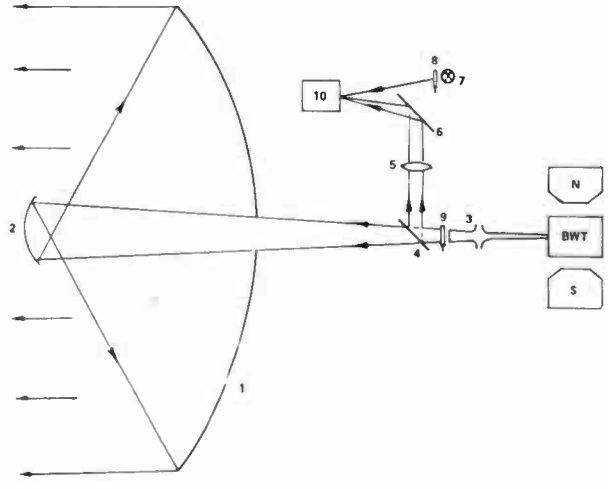

Fig. 11. Diagram of the transmitter used for the outdoor reflectivity method by Ryadov and Furashov[6]: 1 parabolic mirror; 2 elliptical exciter; 3 horn; 4 quartz plate; 5 quartz lens; 6 plane mirror; 7 standard source; 8, 9 modulator; 10 radiation receiver.

Figures 6 and 7, previously discussed under chamber measurements, will be recognized as being adaptable to outdoor reflectivity measurements for this purpose. Figure 12, from the ELTRO Optical Transmissometer[102] could also be used in the s-mm region for this purpose. Usikov *et al.*[103] use a very simple compensation scheme for reflectivity measurements in the millimetre range. In their system, a very sensitive galvanometer is connected to two paralleled diode detectors. These diodes are connected in opposing polarities in such a way that the current from one diode through the galvanometer is opposed by the current from the other diode. One diode is in the directional coupler in the waveguide of the transmitter, the other in the waveguide of the receiver. A variable attenuator in the transmitter is adjusted to give zero

Table 4. Summary of the characteristics of outdoor reflectivity measurements

Ref.	Year of measurement	Country	Frequency (GHz)	Wavelength (mm)	Measurements purpose	Path length (m)	Altitude (m)	R.f. source	Power output (mW)	Antenna diameter (cm)	Antenna type	Antenna polarization	Antenna gain (dB)	Special features	Experiment variable	Stated accuracy (dB)
11	1970	USSR	231, 349	1·3, 0·86	Rain attenuation	2 × 120	NS	NS	NS	Rcvr: 30 Tmtr: 62	Cassegrain	NS	55 61	Tmtr power compensation	Rain	NS
6	1972	USSR	193 261	1·55 1·15	H_2O vapour absorption	2 × 1500	2·6	BWO	100 300	90	Cassegrain	NS	66	10 Hz mod. OAP-4 radiometer (70 cm reflector)	Humidity	±1·5
30 31	1979 1980	USA USA	337 337	0·89 0·89	Atmos. attn. fog attn.	2 × 100	4	Optically pumped laser	0·1	35	Mirror	NS	NS	Golay cell detector corner cube reflector	Humidity fog	NS

galvanometer deflection. Propagation attenuation due to rainfall is measured by determining the change of attenuator setting needed to restore galvanometer null. Unfortunately, system sensitivity at 8 mm wavelength even with a magnetron transmitter only permits use of path lengths of 50–100 m. Use of a superheterodyne receiver and second detector diode current would greatly increase system sensitivity. In this scheme, receiver transfer characteristic is unimportant since this is a null balance system.

Antennas, transmitters, and receivers used in the first two outdoor reflectivity measurements are essentially the same as those used in the outdoor direct propagation measurements. Purposes are also similar. The rain attenuation measurement[11] uses a short path, while the H_2O vapour absorption[6] uses a long path.

Another propagation measurement scheme which has been used at 8·6 mm, but not at s-mm, should be mentioned. Apparatus is shown in Fig. 13.[104] Two antennas (parabola or Cassegrain) are set up about 25 m apart. A pulsed transmitter is connected to one antenna with a receiver to the other. Receiver output feeds two switches, each being connected to an integrator. Ratio of the two integrator outputs is obtained. The two switches are closed at different times, t_1 and t_2. Rain is introduced over about the middle 5 m of the transmitter–receiver path. Each pulse of the transmitter is partially reflected by the receiver antenna back to the transmitter antenna where a portion is reflected back to the receiver antenna, etc., until it is damped out by the attenuation. This technique permits use of only a very short path. Problems of short paths have been cited previously.

5 General Comments on these Sub-millimetre Wave Propagation Measurements

While results are what counts, methodology is also important. Often careful consideration of methodology can indicate limitations of the results obtained. Unfortunately, several papers in this data base gave only a brief description of the experimental apparatus and procedures used. Frequently, some very important information such as antenna polarization was omitted. In several cases, references on the apparatus cited by the main paper were also inadequate.

A very commonly omitted item was the measurement accuracy, e.g., in decibels, and usually the paper did not give sufficient information to permit accuracy estimation. In some papers the stated accuracy appears to be very optimistic. In some papers propagation of measurement errors may not have been considered but has been treated elsewhere.[105]

Measurement/interpretation of rainfall attenuation deserves careful consideration. A radar senses 'integrated path average' values of attenuation. Measurement of rainfall rate requires great care. This is especially true during a thunderstorm. Radar-indicated

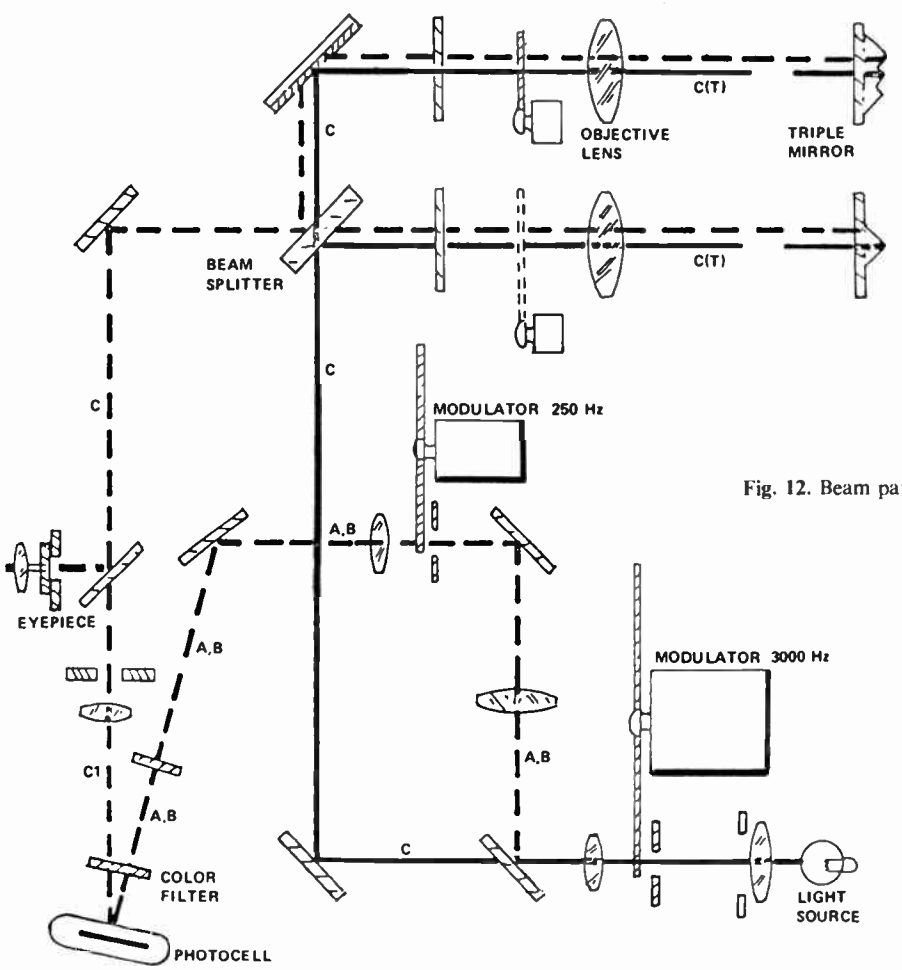

Fig. 12. Beam path within the optics of a transmissometer[102].

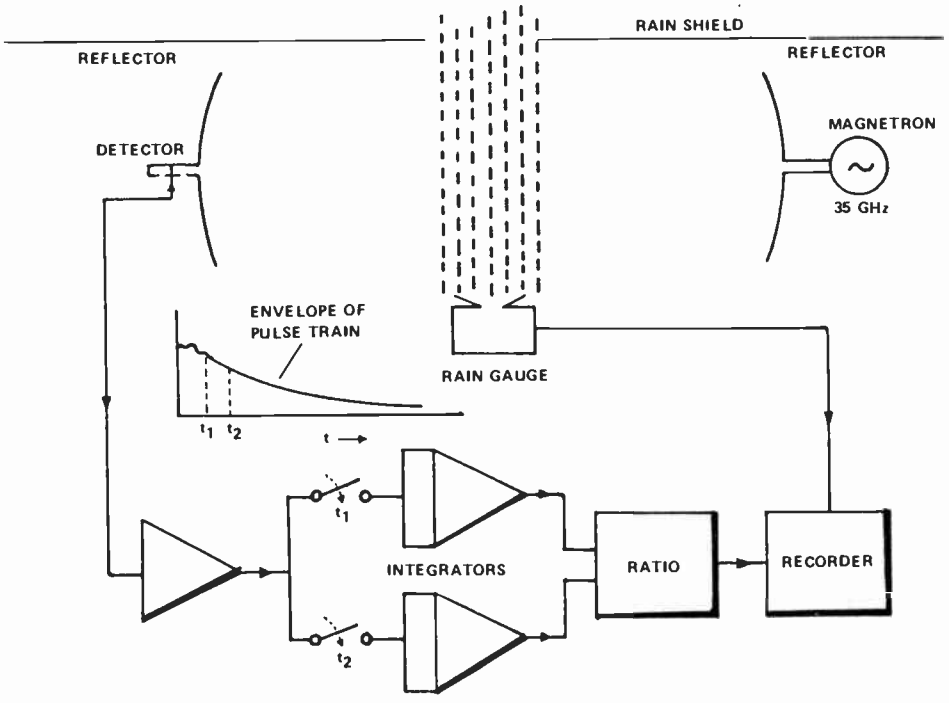

Fig. 13. Rain measurements system (Mink[104]).

attenuation is an indication of instantaneous rainfall rate. Semplak,[106] through use of a capacitor-type rain gauge, showed that instantaneous rainfall rate may reach 280 mm/h, while the rainfall rate averaged over, say, 5 min would be much lower. He also demonstrated severe time lags in rainfall rate derived from tipping bucket rain gauges. Raymond and Wilson[107] developed a water resistance rain gauge and also showed rain rate fluctuation.

Radar meterologists are familiar with the importance of drop size distributions in rain[97, 98, 104, 108–111] in the study of the effects of hydrometeors on radar backscatter/attenuation. Unfortunately, radar meteorologists have only employed one linear radar antenna polarization in this work in the centimetre and millimetre regions so far. Atlas and Ulbrick[112] recently pointed out the fallacy of this. Seliga and Bringi[113] analysed the use of radar differential reflectivity measurements at orthogonal polarizations for measuring precipitation. Unfortunately, Seliga and Bringi did not appear to be aware of the extensive experiments by McCormick, Hendry *et al.*[114–116] of the depolarization effects of rain and snow and their measurements of the canting angle of rain and snow.

Previous comments on large values of peak rainfall rate in thunderstorms and rain depolarization effects indicate that careful interpretation is required for use of published curves on attenuation due to rainfall and fog such as that of Tillotson.[117]

After the completion of the first draft of this paper, the work of Lin and Ishimaru[118] was discovered. It is interesting to note that in 1971 they identified 10 papers on the measurement of attenuation due to rain by millimetre waves covering the time period of 1946–1969. They were designated by the authors as either radio (outdoor direct) or radar (outdoor reflectivity). Parameters summarized were wavelength, method, transmitter and receiver antenna diameters, path length, rain gauge type and how many were used, author, year, and antenna polarization.

Lin and Ishimaru pointed out inadequacies in those papers; many have already been cited in the present paper. They also mentioned the lack of reporting of local climate conditions—ambient temperature, prevailing wind (especially vertical component), and humidity. They concluded: 'Hence it is difficult to compare measurements by different workers'.

6 Additional Sub-millimetre Wave Propagation Measurements Needed

Sub-millimetre propagation measurements needs were very well stated in the summary of millimetre propagation measurements needs which were identified in the ARPA/Tri-Service Millimeter Wave Workshop.[61] The list is legion. Propagation data requirements for mm and s-mm radar design have also been presented along with a review of current mm and s-mm propagation data.[34] Sub-millimetre rain attenuation measurements made so far have used only one linear polarization: simultaneous measurements must be made using orthogonal polarizations in a phase-coherent system. Canting angle effects of rain and snow at s-mm frequencies should be measured and extensive atmospheric fluctuation measurements must be made. Izyumov,[119, 120] Armand *et al.*[121] Sollner,[122] Rainwater,[123] Hill,[124] and Moffat[125] have addressed this problem. Moffat[125] made simultaneous fluctuation measurements at 110 GHz over a 250-m path using two frequencies separated by 0·1 Hz to 10 GHz. Attenuation due to fog should be measured. Richer[126] presented

limited fog attenuation measurements at 140 GHz in the 1970 s-mm symposium, his data indicating that severe fluctuation is to be expected. The apparatus of Nemarich *et al.*[33] and Tanton[31, 32] have been used for limited fog attenuation. Spectral characteristics of fog attenuation are required.

Backscattering from fog, clouds, and rain should be measured at s-mm regions, using simultaneous orthogonal polarizations. Currie *et al.*[108] reported on rain backscatter at 9, 30, 70 and 95 GHz using circular polarization but not simultaneous orthogonal polarization. Backscatter from fog and clouds was measured over 20 years ago at 1·25 cm wavelength[109, 110] but only with one linear polarization. The apparatus of Nemarich *et al.*[33] has been used for limited rain and snow backscatter.

Detection of backscatter from fog, clouds, and rain requires much more performance than is presently available at the shorter s-mm wavelengths. Development of the gyrotron[80–84] and the improved receivers using the Schottky barrier diode[66–68] are very encouraging events. They will permit further s-mm propagation measurements.

Angle of arrival has not been measured at s-mm frequencies. This is extremely important for radar design. Limited angle-of-arrival measurements made at mm wavelengths in Russia and theoretical mm angle-of-arrival analyses have been reported.[34]

It is essential that these various propagation measurements be made at several wavelengths simultaneously. It should be noted that most of the measurements reported to date were made at separate time and places. Accordingly, it is meaningless to try to compare such measurements.

7 Acknowledgments

The assistance of Dr. Dorathy Stewart, Research Directorate, US Army Missile Command, in locating the initial references and for discussions with her on various aspects of meteorology is gratefully acknowledged. Dr. J. C. Wiltse, Engineering Experiment Station, Georgia Institute of Technology, reviewed this paper and made suggestions on some references.

8 References

1 Chang, S. Y. and Lester, J. D., 'Performance characteristics of a 300-GHz radiometer and some atmospheric attenuation measurement,' *IEEE Trans.*, AP 16, no. 5, pp. 588 91, Sept. 1968.
2 Emery, R., 'Atmospheric absorption measurements in the region of 1-mm wavelength,' *Infrared Phys.*, 12, pp. 65 79, 1972.
3 Frenkel, L., and Woods, D., 'The microwave absorption by H_2O vapor and its mixtures with other gases between 100 and 300 Gc/s,' *Proc. IEEE*, 54, pp. 498 505, 1966.
4 Coats, G. T., Bond, R. A. and Tolbert, C. W., 'Propagation measurements in the vicinity of the 183-Gc/s water vapor line', Electr. Eng. Res. Lab. U. of Texas, Rpt. 7 20, 1962.
5 Whaley, T. W., Jr. and Fannin, B. M., 'Characteristics of free space propagation near the 183-GHz H_2O line,' *IEEE Trans.*, AP 17, pp. 682 4, Sept. 1969.
6 Ryadov, V. Ya. and Furashov, N. I., 'Investigation of the spectrum or radiowave absorption by atmospheric water vapor in the 1·15- to 1·5-mm range,' *Radiophys. Quant. Electron.*, 15, no. 10, pp. 1124 8, Oct. 1, 1974.
7 Ryadov, V. Ya. and Furashov, N. I., 'Measurement of the atmospheric absorption of radio waves in the range 0·76 1·15 mm,' *Radiophys. Quant. Electron.*, 9, no. 5, pp. 504 7, 1966.
8 Babkin, Yu. S. *et al.*, 'Measurement of attenuation in rain over 1-km path at a wavelength of 0·96 mm,' *Radio Engng Electron. Phys.*, 15, no. 12, pp. 2164 6, 1970.
9 Babkin, Yu. S. *et al.*, 'Attenuation of radiation at a wavelength of 0·96 mm in snow,' *Radio Engng Electron. Phys.*, 15, no. 2, pp. 2171 4, 1970.
10 Vardanyan, A. S. *et al.*, 'Measurement of the 980- to 1600-μm atmospheric absorption by radioastronomical means,' *Radio Engng Electron. Phys.*, 18, no. 12, pp. 163 5, 1973.
11 Malyshenko, Yu. I and Vakser, Il. Kh., 'Measurement of the attenuation coefficient of 1·3- and 0·86-mm radio waves in rain,' *Radiophys. Quant. ElEctronics*, 14, no. 6, pp. 755 7, June 1971.
12 Bastin, J. A. *et al.*, 'Spectroscopy at extreme infrared wavelengths: III. Astrophysics and atmospheric measurements,' *Proc. R. Soc.*, A, 278, pp. 543 73, 1964.
13 Yaroslavsky, N. G. and Stanevich, A. E., 'The long wavelength infrared spectrum of H_2O vapor and the absorption spectrum of atmospheric air in the region 20 2500 μm (500 4 cm^{-1}),' *Opt. Spectrosc.*, 7, pp. 380 2, 1958.
14 Forsythe, R. E., 'Research in millimeter wave techniques,' Semi-Annual Reports NASA GSFC, NASA Grant NSG-5012, Jan. 1979 to Jan. 1982.
15 Gebbie, H. A. and Burroughs, W. J., 'Observations of atmospheric absorption in the wavelength range 2 mm to 300 μm,' *Nature*, 217, pp. 1241 2, 1968.
16 Malyshenko, Yu. I., 'Measuring the parameters of the 183·31-GHz water-vapor absorption line in the surface atmosphere,' *Ukr. J. Phys.*, 12, no. 8, pp. 1317 22, 1967.
17 Gaitskell, J. N. and Gear, A. E., 'Solar and lunar observations at submillimetre wavelengths,' *Icarus*, 5, pp. 237 44, 1966.
18 Thiessing, H. M. and Caplan, P. J., 'Measurement of the solar spectrum,' *J. Opt. Soc. Am.*, 46, pp. 971 8, 1956.
19 Sinton, W. M., 'Observations of solar and lunar radiation at 1·5 mm,' *J. Opt. Soc. Am.*, 45, pp. 975 9, 1955.
20 Williams, R. A. and Chang, W. S. C., 'Observations of solar radiation from 50 μm to 1 mm,' *Proc. IEEE*, 54, no. 4, pp. 462 70, April 1966.
21 Harries, J. E., Burroughs, W. J., and Gebbie, H. A., 'Millimeter wavelength spectroscopic observations of the water dimer in the vapor phase,' *J. Quant. Spectrosc. Radiat. Trans.*, 9, pp. 799–807, 1969.
22 Goldsmith, P. F. *et al.*, 'Measurement of atmospheric attenuation at 1·3 and 0·87 mm with an harmonic mixing radiometer,' *IEEE Trans.*, MTT-22, no. 12, pp. 1115 6, December 1974.
23 Ryadov, V. Ya., Furashov, N. I. and Sharonov, G. A., 'Measurement of the atmospheric transparency to 0·87-mm waves,' *Radio Engng Electron Phys.*, 9, pp. 733 78, 1964.
24 Kukin, L. M., Lubyako, L. V. and Fedoseev, L. I., 'The measurement of atmospheric absorption in the wavelength range 1·8 0·87 mm,' *Radiophys. Quant. Electron.*, 10, no. 6, pp. 407 12, 1967.
25 Dyragin, Yu. A. *et al.*, 'Measurement of the atmospheric absorption of radio waves in the range 1·36 3·0 mm,' *Radiophys. Quant. Electronics*, 9, no. 6, pp. 624–7, 1966.
26 Malyshenko, Yu. I., 'Measurement of absorption coefficient of water vapor in the transparency window at 1·3 mm,' *Radio Engng Electron. Phys.*, 14, no. 3, pp. 447 8, 1969.
27 de Cosmo, V., 'Automatic radiometer for continual monitoring of atmospheric transmittance at mm and submm frequencies,' Fifth Int. Conf. on Infrared and Millimetre Waves, Conf. Digest, Physics Dept. of the University Würzburg, Federal Republic of Germany, pp. 191 2, 1980.
28 Simpson, G. A. *et al.*, 'Measurements of far infrared water vapor absorption between lines with an optically pumped laser,' *ibid.*, pp. 304 5, Oct. 1980.
29 Liebe, H. J., 'Laboratory studies of water vapor absorption in atmospheric EHF windows,' Sixth Int. Conf. on Infrared and Millimeter Waves, Conf. Digest, IEEE MTT, paper T4 7, 1981.
30 Tanton, G. A., *et al.*, 'Near-ground atmospheric attenuation of 0·89 mm radiation,' Fourth Int. Conf. on Infrared and Millimeter Waves, IEEE MTT, p. 27, Post Deadline Digest, 1979.
31 Tanton, G. A., *et al.*, 'Atmospheric propagation of submillimeter waves: observed correlations with fog conditions at 0·890 mm wavelengths,' Proc. Workshop on Millimeter and Submillimeter Atmospheric Propagation Applicable to Radar and Missile Systems, US Army Missile Command Tech Rpt RR-80 3, pp. 90 4, 1980.
32 Zamit, C. C., 'Absolute atmospheric transparency in the range 90 600 GHz measured from a mountain site,' Fifth Int. Conf. on Infrared and Millimeter Waves, Conf. Digest, Physics Dept. of the University Wurzburg, Federal Republic of Germany, p. 111, 1980.
33 Nemarich, J., *et al.*, 'A near-millimeter wave mobile measurement facility,' *ibid.*, pp. 248 9, 1980.
34 Johnston, S. L., 'A radar system engineer looks at current millimeter-submillimeter atmospheric propagation data,' IEEE EASCON-79 Conf. Record, 1, pp. 27 35; reprinted in Ref. 55.
35 Zhevakin, S. A. and Naumov, A. P., 'The propagation of centimeter millimeter and submillimeter radio waves in the earth's atmosphere,' *Radiophys. Quant. Electronics*, 10, no. 9 10, pp. 1213 43, 1967.
36 Kislyakov, A. G. and Stenkevich, K. S., 'Investigation of the absorption of radio waves in the troposphere using radioastronomical methods,' *Radiophys. Quant. Electronics*, 10, no. 9–10, pp. 1244–65, 1967.
37 Vvedenshiz, B. A., Kolosov, M. A. and Sokolov, A. V., 'Investigations of the propagation of meter, decimeter, centimeter, and submillimeter radio waves,' *Radio Engng Electron. Phys.*, 12, pp. 1752 771, Nov. 1967.
38 Ulaby, F. T. and Straiton, A. W., 'Atmospheric absorption of radio waves between 150 and 350 GHz,' *IEEE Trans.*, AP 18, no. 4, pp. 479 85, July 1970.
39 Bastin, J. A., 'Extreme infrared atmospheric absorption,' *Infrared Phys.*, 6, p. 209, 1966.
40 Guenther, B. D., *et al.*, 'Submillimeter research: A propagation bibliography, US Army Missile Command, Tech. Rpt. RR 77 3, 1976.
41 Kislyakov, A. G., 'Determination of radiowave absorption in atmosphere from the data on radiation,' *Radio Engng Electron. Phys.*, 13, no. 7, pp. 1013 1019, 1968.
42 Amboss, K., 'The current art of millimeter wave solid state and tube type power sources,' Proc. Military Microwaves Conf. MM 80, pp. 520 45, 1980.
43 Purcell, J. J., 'Millimetre wavelength impatt sources,' *The Radio and Electronic Engineer*, 49, no. 7/8, pp. 347 50, July/Aug. 1979; reprinted in Ref. 55.
44 Hodges, D. T., 'A review of advances in optically pumped far-infrared lasers,' *Infrared Phys.*, 18, 375 84, 1978.
45 Golant, M. B., *et al.*, 'A series of wide-band low-power millimeter and sub-millimeter oscillators,' *Instrum. Exp. Tec.*, 8, no. 4, pp. 877 89, July Aug. 1965.
46 Golant, M. B., 'Wide-range oscillators for the sub-millimeter wavelengths,' *Instrum. Exp. Tec.*, 12, no. 3, p. 801, May June 1969.
47 Boissière, J., *et al.*, 'Advances in sub-millimeter-wave carcinotrons,' Sixth Int. Conf. on Infrared and Millimeter Waves, IEEE Conf. Digest, Paper M 5 6, Dec. 1981.
48 Kantrowitz, G., *et al.*, 'New developments in sub-millimeter-wave BWOs,' *Microwave J.*, 22, no. 2, pp. 57 9, Feb. 1979.
49 Epzstein, B., 'Recent progress and future performance of millimeter wave BWOs,' AGARD Conf. Proc CP 245, pp. 36 1 thru 36 11, 1978, reprinted in Ref. 55.
50 Johnston, S. L., 'Radar systems for operation at short millimetric wavelengths,' *The Radio and Electronic Engineer*, 49, no. 7/8, pp. 361 9, July/August 1979.

51 Fujisawa, K., 'The laddertron—a new millimeter wave power oscillator,' *IEEE Trans.* ED-11, no. 8, pp. 381–91, Aug. 1964; reprinted in Ref. 55.
52 Day, W. R. and Noland, J. A., 'The millimeter-wave extended interaction oscillator,' *Proc. IEEE*, **54**, no. 4, pp. 539–43, April 1966.
53 Ewell, G. W., *et al.*, 'High power millimeter wave radar transmitters,' *Microwave J.*, **23**, no. 8, pp. 57ff, Aug 1980; reprinted in Ref. 55.
54 Currie, N. C., *et al.*, 'EIA technology comes of age,' *Military Electronics/Countermeasures*, pp. 34ff, May 1981.
55 Johnston, S. L., 'Millimeter Wave Radar,' (Artech House, Dedham, Mass, 1980).
56 Ward, W. W. and Zolnay, S. L., 'Topics in millimeter wave and optical space communication,' Lincoln Laboratory Technical Note, 1971 43/ESD TR-71-269, AD 731535, 1971.
57 Johnston, S. L., 'New millimeter wave radar operating frequencies,' (In preparation, 1982).
58 Van Vleck, J. H. and Weisskopf, V. E., 'On the shape of collision-broadened lines,' *Rev. Mod. Phys.*, **17**, pp. 227–236, Apr–Jul 1945.
59 Van Vleck, J. H., 'The absorption of microwaves by uncondensed water vapor,' *Phys. Rev.*, **71**, pp. 425–33, Apr. 1947.
60 Long, M. W. and Rivers, W. K., Jr., 'Submillimeter wave radiometry,' *Proc. IRE*, **49**, pp. 1024–7, June 1961.
61 Altshuler, E. E., 'Overt communication review,' Report of the ARPA/Tri-Service Millimeter Wave Workshop, Johns Hopkins University, Applied Physics Lab., JHU QM-75-009, ARPA T I O-75-3, Jan. 1975.
62 Kislyakov, A. G., 'Radioastronomical investigations in the millimeter and submillimeter bands,' *Soviet Phys. Uspekhi*, **13**, no. 4, pp. 495–518, Jan–Feb. 1971.
63 Dryagin, Yu. A. and Fedoseev, L. I., 'Millimeter and submillimeter detector radiometers,' *Radiophys. Quant. Electronics*, **12**, no. 6, pp. 647–51, June 1969.
64 Williams, R. A. and Chang, W. S. C., 'Radiometry in the submillimeter region using the interferometric modulator,' *IEEE Trans.*, **MTT-11**, pp. 513–22, Nov. 1963.
65 Vardanyan, A. S. *et al.*, 'Submillimeter radio telescope with an n-In-Sb detector,' *Soviet Astronomy-AJ*, **16**, no. 5, pp. 806–8, Mar–Apr 1972.
66 Wrixon, G. T., 'Low noise diodes and mixers for the 1- to 2-mm wavelength region,' *IEEE Trans.*, **MTT-22**, no. 12, pp. 1159–65, Dec. 1974.
67 Fetterman, H. R. *et al.*, 'Sub-millimeter heterodyne detection and harmonic mixing using Schottky diodes,' *IEEE Trans.*, **MTT-22**, no. 12, pp. 1013–5, Dec. 1974.
68 McColl, M. and Hodges, D. T., 'Review of mixers for millimeter wavelengths,' Sixth DARPA-Tri-Service Millimeter Wave Conf.; reprinted in Ref. 55.
69 Listvin, V. N. and Potapov, V. T., 'A semiconductor modulator for the millimeter and submillimeter wave bands,' *Radio Engng Electron. Phys.*, **16**, no. 7, pp. 1168–70, July 1971.
70 Averkov, S. E. *et al.*, 'Astronomical station for far-infrared observation,' *Soviet Astronomy-AJ*, **8**, no. 3, pp. 432–4, Nov.–Dec. 1964.
71 Fedoseev, L. I. and Kozitsyn, D. M., 'Correlation method of determining spectral characteristics in the millimeter and submillimeter wave bands,' *Instrum. Exp. Tec.*, **10**, pp. 129–33, Jan.–Feb. 1967.
72 Hills, R. E. *et al.*, 'Absolute measurements of atmospheric emission and absorption in the range 100–1000 GHz,' *Infrared Phys.* **18**, pp. 819–25, 1978.
73 Zabolotniy, V. F., 'Attenuation of radiation at wavelengths of 1·25 and 2·0 mm,' *Infrared Phys.* **18**, pp. 815–7, 1978.
74 Gebbie, H. A., 'Detection of submillimeter solar radiation,' *Phys. Rev.*, **107**, pp. 1194–5, 1957.
75 Strong, J. 'Interferometry for the far infrared,' *J. Opt. Soc. Am.*, **47**, no. 5, pp. 354–7, May 1957.
76 White, J. U., 'Long optical paths of large aperture,' *J. Opt. Soc. Am.*, **32**, pp. 285–8, May 1942.
77 Valkenburg, E. P. and Derr, V. E., 'A high-Q Fabry-Perot interferometer for water vapor absorption measurements in the 100- to 300-Gc/s frequency range,' *Proc. IEEE*, **54**, no. 4, pp. 493–8, April 1966.
78 Babkin, Yu. S. *et al.*, 'Apparatus for investigating the propagation of submillimeter radio waves,' *Instrum. Exp. Tec.*, **11**, no. 1, pp. 243–4, Jan–Feb. 1968.
79 Devyatkov, N. D. and Golant, M. B., 'Development of electron devices for the millimeter and submillimeter wavelength ranges,' *Radio Engng Electron. Phys.*, **12**, no. 11, pp. 1835–46, Nov. 1967.
80 Zaytsev, N. I. *et al.*, 'Millimeter and submillimeter wave gyrotrons,' *Radio Engng Electron. Phys.*, **19**, no. 5, pp. 103–7, May 1974.
81 Kurayev, A. A. *et al.*, 'Efficiency-optimized output cavity profiles that provide a higher margin of gyroklystron stability,' *Radio Engng Electron Phys.*, **19**, no. 5, 96–104, May 1974.
82 Andronov, A. A. *et al.*, 'The gyrotron: high-power source of millimetre and sub-millimetre waves,' *Infrared Phys.*, **18**, pp. 385–93, 1978.
83 Godlove, T. F. *et al.*, 'Prospects for high power millimeter radar sources and components,' IEEE EASCON-77 Conf. Rec., pp. 16-2A thru F; reprinted in Ref. 55.
84 Jory, H. R. *et al.*, 'Gyrotrons for high power millimeter wave generation,' IEEE ED meeting digest, pp. 234–7, Dec. 1977; reprinted in Ref. 55.
85 Dudley, E., 'A mobile facility for target/background characterization at near-millimeter wavelengths,' US Army Missile Command Technical Report, RR 80-3, pp. 151–2, Feb. 1980.
86 Gallagher, J. J. *et al.*, 'Near millimeter wave mobile measurement facility (NMMW/MMF),' US Army Missile Command Technical Report RR-80-3, pp. 153–60, 1980.
87 Nemarich, J. *et al.*, 'A system for measuring near-millimeter-wave target signature and propagation characteristics,' IEEE EASCON-81 Proc., pp. 226–9, 1981.
88 Brown, D. R. *et al.*, 'The US Army atmospheric sciences laboratory transportable atmospheric characterization station (TACS),' Fifth Int. Conf. on Infrared and Millimeter Waves, Conf. Digest, Physics Dept. of the University Wurzburg, Federal Republic of Germany, pp. 250–1, 1980.
89 Snider, D. E. and Brown, D. R., 'The transportable atmospheric characterization system,' US Army Missile Command Technical Rpt. RR-80-3, pp. 161–3, 1980.
90 Hannan, P. W., 'Microwave antennas derived from the Cassegrain telescope,' *IRE Trans.*, **AP-9**, pp. 140–53, March 1961.
91 Kay, F., 'Millimeter wave antennas,' *Proc IEEE*, **54**, no. 4, pp. 641–7, April 1966; reprinted in Ref. 55.
92 Rutledge, D. B. *et al.*, 'Infrared and submillimetre antennas,' *Infrared Phys.*, **18**, pp. 713–30, 1978.
93 Harris, D. J., 'Waveguides for the 100–1000 GHz frequency range,' *The Radio and Electronic Engineer*, **49**, no. 7/8, pp. 389–94, July/Aug. 1979.
94 'The PSD-5 and PSD-6 receivers for the submillimeter range,' *Instrum. Exp. Tec.*, **9**, part 2, no. 4, pp. 1019–20, July/Aug. 1966.
95 Vystavkin, A. N. and Migulin, V. V., 'Receiver for millimeter and submillimeter waves,' *Radio Engng Electron. Phys.*, **12**, no. 11, pp. 1847–1860, Nov. 1967.
96 Afinogenov, V. M., 'A high-sensitivity receiver of submillimeter radiation based on n-GaAs,' *Radiophys. Quant. Electronics*, **15**, no. 10, pp. 1207–12, Oct. 1972.
97 Battan, J. J., 'Radar Observation of the Atmosphere,' (University of Chicago Press, 1973.)
98 Bean, B. R., Dutton, E. J. and Warner, B. D., 'Weather effects on radar,' '*Radar Handbook*', Chapter 24, Section 24·17, M. I. Skolnik, (ed.) (McGraw-Hill, New York 1970.)
99 Duffield, T. L., 'Ground station hardware for the ATS-F millimeter wave experiment,' Final Report, Martin Marietta Corp. Rpt. DR 12,395 (NASA(CR-132802, N73-31409), Feb. 1973.
100 Crawford, A. B. and Hogg, D. C., 'Measurement of atmospheric attenuation at millimeter wavelengths,' *Bell Syst. Tech. J.*, **35**, no. 4, pp. 907–16, July 1956.
101 Ryadov, V. Ya. and Furashov, N. I., 'Investigation of the absorption of radiowaves in the atmospheric transparency window 0·73 mm,' *Radiophys. Quant. Electronics*, **15**, no. 10, pp. 1129–37, Oct. 1972.
102 ELTRO Transmissometer, ELTRO GmbH, Heidelberg, Germany.
103 Usikov, A. Ya., German, V. L. and Vakser, I. Kh., 'Investigation of the absorption and scattering of millimeter waves in precipitation,' *Ukr. J. Phys.*, **6**, no. 5, pp. 618–40, 1961.'
104 Mink, J. W., 'Rain-attenuation measurements of millimetre waves over short paths,' *Electronics Letters*, **9**, no. 10, pp. 198–9, 17 May 1973.
105 Worthing, A. G. and Geffner, J., 'Treatment of Experimental Data,' 9th Printing, (Wiley, New York, 1943).
106 Semplak, R. A., 'Gauge for continuously measuring rate of rainfall,' *Rev. Sci. Instrum.*, **37**, no. 11, pp. 1554–8, Nov. 1966.
107 Raymond, D. J. and Wilson, K., 'Development of a new rainfall intensity gauge,' *J. Appl. Meteorol.*, **13**, pp. 180–2, Feb. 1974.
108 Currie, N. C., Dyer, F. B. and Hayes, R. D., 'Analysis of radar return at frequencies of 9·375, 35, 70 and 95 GHz,' Georgia Inst. of Technology, Engr. Exp. Station Technical Rpt. No. 2, Proj. A-1485, Cont. DAAA 25 73-C-0256, 1975.
109 Donaldson, R. J. *et al.*, 'Quantitative 1·25-cm observations of rain and fog,' Proc. Conf. on Radio Meteorol., Austin, Texas, 1953.
110 Donaldson, R. J., Jr., 'The measurement of cloud liquid-water content by radar,' *J. Appl. Meteorol.*, **12**, pp. 238–44, June 1955.
111 Plank, V. G. *et al.*, 'The nature and detectability of clouds and precipitation as determined by 1·25-cm radar,' *J. Appl. Meteorol.*, **12**, pp. 358–78, Aug. 1955.
112 Atlas, D. and Ulbrick, C. W., 'Path-and-area integrated rainfall measurements by microwave attenuation in the 1-cm region,' Proc. Seventeenth Radar Meteorol. Conf., pp. 406–413, American Meteorological Society, Boston, Mass, 1976.
113 Seliga, T. A. and Bringi, V. N., 'Potential use of radar differential reflectivity measurements on orthogonal polarizations for measuring precipitation,' *J. Appl. Meteorol.*, **15**, pp. 69–76, Jan. 1976.
114 Hendry, A. G., McCormick, C. G. and Barge, B. L., 'Ku-band and S-band observations of the differential propagation constants in snow,' *IEEE Trans.*, AP-24, pp. 521–5, July 1976.
115 McCormick, C. G. and Hendry, A., 'Polarization related parameters for rain: measurements obtained by radar,' *Radio Sci.*, **11**, no. 8, 9, pp. 731–40, 1976.
116 McCormick, C. G., Hendry, A. and Allen, L. E., 'Depolarizations over a link due to rain: measurements of the parameters,' *Radio Sci.*, **11**, no. 8–9, pp. 741–9, 1976.
117 Tillotson, L. C., 'Millimeter-wavelength radio systems,' *Science*, **70**, pp. 31–6, 2 Oct. 1970.
118 Lin, J. C. and Ishimaru, A., 'Propagation of millimeter waves in rain,' U. of Washington Tech Rpt. 144, AFCRL 71-0310, AD735291, May 1971.
119 Izyumov, A. O., 'Amplitude and phase fluctuations of a plane monochromatic wave in a near-ground layer of moisture-containing turbulent air,' *Radio Engng Electron. Phys.*, **13**, no. 7, pp. 1009–13, 1968.
120 Izyumov, A. O., 'Frequency spectrum of amplitude fluctuations of a plane electromagnetic wave in submillimeter range propagating in a surface layer of turbulent atmosphere,' *Radio Engng Electron. Phys.*, **14**, no. 10, pp. 1609–12, 1969.
121 Armand, N. A. *et al.*, 'Fluctuations of submillimeter radio waves in a turbulent atmosphere,' *Radio Engng Electron. Phys.*, **16**, no. 8, pp. 1259–66, 1971.
122 Sollner, G., 'Frequency spectrum of fluctuations in submillimetre sky emission and absorption,' *Astronomy Astrophys.* **55**, pp. 361–8, 1977.
123 Rainwater, J. H. *et al.*, 'Spectral and temporal characteristics of atmospheric emissions at 94 GHz,' Fifth Int. Conf. on Infrared and Millimeter Waves, Conf. Digest, Physics Dept. of the University Wurzburg, Federal Republic of Germany, pp. 109–10, 1980.
124 Hill, R. J. *et al.*, 'Refractive-index and absorption fluctuations in the infrared caused by temperature, humidity and pressure fluctuations,' *J. Opt. Soc. Am.*, **70**, no. 10, pp. 1192–1205, Oct. 1980.
125 Moffat, P., 'Fluctuations in atmospheric transmission at about 3-mm wavelength,' Inter-Union Commission on Radio Meteorology (IUCRM) Colloquism on Probing of Atmospheric Constitutents, Bournemouth, England, 1975.
126 Richer, K. A., 'Environmental effects on radar and radiometric systems at millimeter wavelengths,' Proc. Symp. on Millimeter Waves, Poly Inst. of Brooklyn, 1970.

Manuscript received by the Institution on 23rd June 1982
(Paper No. 2062/MI 31)

Contributors to this issue

Fritz Arndt received the Dipl.-Ing., the Dr.-Ing. and the Habilitation degrees from the Technical University of Darmstadt in 1963, 1968, 1972 respectively. From 1963 to 1972 he worked on directional couplers and microstrip techniques at the Technical University of Darmstadt. Since 1972 he has been a Professor and Head of the Microwave Department at the University of Bremen. His research activities are at present in the area of the solution of field problems of waveguide and fin-line structures and of antenna design.

Philip Ballard received a B.Sc. honours degree in electrical and electronic engineering from the University of Leeds in 1980, and in September of the same year joined MEL in Crawley, Sussex to work on development of optoelectronic systems. In March 1981 he began a six-month secondment to the Microwave Techniques Group of Philips Research Laboratories, Redhill, Surrey doing research into E-plane techniques for millimetre-wave component and subsystems, becoming a permanent employee there in September 1981.

Robert Bates received the B.Sc. degree in electronics from Chelsea College, London University in 1974. In 1974 he joined Philips Research Laboratories where he has worked on microwave components including mixers, amplifiers, filters and oscillators. In 1980 he received the Ph.D. degree in Electronics from Chelsea College, London University for research work performed at PRL. His current research interests are millimetre wave components and subassemblies.

James Birch joined the National Physical Laboratory on graduation from Brunel University in 1968. His research interests have been in the general area of millimetre and submillimetre wavelength electromagnetic metrology. In particular he has been concerned with the application of the techniques of Dispersive Fourier Transform Spectroscopy to the determination of the complex permittivity of materials. He was awarded a Ph.D. degree by London University in 1979.

Martin Booton received a B.Sc. degree in physics from the University of London in 1970. He was subsequently awarded the Ph.D. degree from the same University for work on submillimetre wavelength gas lasers and on magneto-optical effects in magnetic materials in the same frequency band. He later worked on microwave integrated circuit devices at the GEC Central Research Laboratories at Wembley in Middlesex. Dr. Booton is currently involved with microwave systems and the development of planar integrated circuitry at the Communications Division of EMI Electronics at Wells.

Jens Bornemann received the Dipl.-Ing. degree in electrical engineering from the University of Bremen, West Germany, in 1980. Since 1980 he has been with the Microwave Department of the University of Bremen, where his research interests include discontinuities in waveguide structures, microwave integrated circuits and numerical solutions of electromagnetic field problems.

Matthew Carter became a graduate member of the Institute of Physics in 1970 and a full member in 1977. Since then he has worked at EMI Electronics, Wells, Somerset, first as a materials physicist and then as a microwave engineer. For the past six years, he has been a senior engineer in charge of a section which deals with the microwave hardware of the radio modelling equipment.

Paul Clancy was educated at University College, Dublin, where he received the B.Sc. degree in physics, mathematics and chemistry in 1969. Subsequently at Newcastle upon Tyne Polytechnic he received the M.Sc. degree in semiconductor physics in 1970 and the Ph.D. degree in 1974 for a thesis entitled 'Gaseous impurity effects in high frequency discharge plasma'.

In 1973 Dr Clancy joined Marconi Space and Defence Systems in Stanmore, England, where he worked on the elimination of multipactor and other discharge problems in space communications hardware. Since 1975 he has been employed by ESA at the European Space Research and Technology Centre, Noordwijk, working on research and development activities in the fields of microwave technology and microwave amplifier and filter development. In particular he has co-ordinated and managed development contracts for material science instrumentation and for submillimetre and far infra-red spacecraft payload hardware.

Robert Clarke joined NPL on graduation from the University of Bristol in 1969. As a member of the Radio-frequency and Microwave Measurements Group of the Division of Electrical Science at NPL he has been concerned with the measurement of impedance and attenuation and the determination of the dielectric properties of low loss materials.

Nigel Davey graduated from the University of Hull in 1970 with a degree in chemistry, following which he undertook post graduate research and lecturing duties at Newcastle-upon-Tyne Polytechnic. He subsequently joined the staff of Welwyn Electric, Northumberland, to carry out research into new materials and processes for use in the manufacture of discrete passive components and hybrids. Currently he is Principal Chemist in the Electronics Technology Department, ERA Technology, where his major research interests cover new thick-film deposition techniques and dielectric materials for use at millimetre wavelengths.

F. ARNDT

P. M. BALLARD

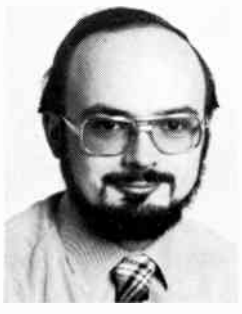

R. N. BATES

J. R. BIRCH

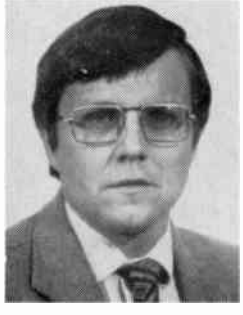

M. W. BOOTON

J. BORNEMANN

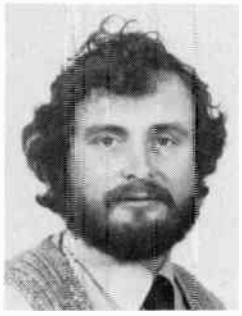

M. C. CARTER

P. F. CLANCY

R. W. CLARKE

N. M. DAVEY

Ian Davies received his B.Sc. degree in chemistry from the University of Aston during 1974 and continued at the same University to carry out research on the chemistry of Group VI compounds for which he was awarded a Ph.D. in 1977. Dr. Davies then joined Plessey Research (Caswell) to work in the two-terminal device fabrication group. His current responsibilities are for the fabrication technologies for mm-wave indium phosphide TEOs and silicon avalanche devices.

Richard Dewey received the B.Sc.(Eng.) degree in electrical engineering from the University of London, King's College in 1968 and Ph.D. from Southampton University in 1978. From 1968 to 1976 he worked as a development engineer with Plessey Radar at Cowes, IOW, initially designing antennas and microwave receiver front-ends and finally working on radar systems design.

Following an 18-month period with ERA-RF Technology Centre, Leatherhead, working on low cross-polar feed systems for satellite antennas, he joined Philips Research Laboratories, Systems Division in 1978. His present research interests include wideband ESM receiver techniques and millimetre wave systems.

Ian Eddison studied electrical and electronic engineering at the University of Leeds from 1970 to 1976, obtaining a B.Sc. in 1973 and a Ph.D. for work on microwave TEOs in 1978. During 1976 he joined Plessey Research (Caswell) to undertake the development of mm-wave gallium arsenide TEOs. In 1979 his interests turned towards research on the possibilities of indium phosphide as the basis of improved mm-wave oscillator devices. Dr. Eddison was made a project leader in 1980 with special responsibility for transferred electron device research at Caswell.

Robert Gelsthorpe graduated from the University of Salford in 1971 and in 1975 received the degree of Ph.D. from the same University for a thesis on precision microwave loss measurements on low loss liquids. He was then appointed Research Fellow at Chelsea College where he worked on broadbanding the electronic tuning range of microwave oscillators. In 1977 he was appointed to the staff of Jundi Shapur University in Iran and on his return to England early in 1979 he worked as Research Fellow in satellite communications at the University of Birmingham. He joined ERA at the end of 1979 and his principal current research interests are high performance millimetric antennas and low cost dielectric waveguide circuits.

Dietrich Grauerholz received the Dipl.-Ing. in 1971 and for the next two years worked in the High-Frequency Laboratory of Elektro-Spezial (Philips). In 1973 he joined the Microwave Department of the University of Bremen, where he has been engaged in the research and development of microstrip circuits, fin-line structures, and microwave measurements.

Ann Henderson received the B.Sc. degree in applied science and the Ph.D. degree at the Royal Military College of Science. She has since carried out research work on a wide variety of mathematical problems in electromagnetic engineering. She has contributed to several publications on antennas and is currently a member of the Institution of Electrical Engineers Professional Group on electromagnetic theory.

Stephen Johnston gained the B.E.E. degree with Honours in 1948 and the M.S.E.E. degree in 1949 from the Georgia Institute of Technology. He continued at Georgia Tech. until 1950 as a research assistant in the Engineering Experiment Station, and then entered the Federal Civil Service in 1950 at the Joint Long Range Proving Ground, Patrick AFB, Florida. He was employed by the US Army Missile Command at Redstone Arsenal, Alabama from 1951 until his retirement in 1980.

Mr Johnston has published and presented over fifty papers at numerous international technical symposia, both professional and government, including the Tri-Service Radar Symposia, Joint EW Conferences and AOC EW Symposium and he holds several patents. His areas of interest include electronic warfare, weapon system simulation, penetration aids

I. DAVIES

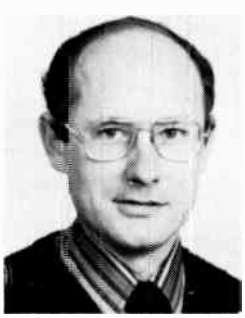

R. J. DEWEY

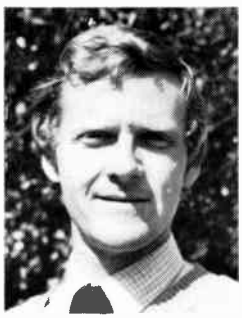

I. G. EDDISON

R. V. GELSTHORPE

D. GRAUERHOLZ

A. HENDERSON

S. L. JOHNSTON

S. J. NIGHTINGALE

M. J. SISSON

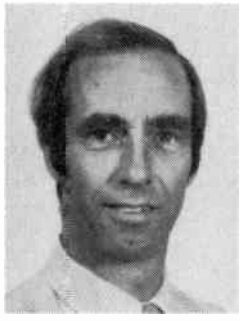

E. G. STEVENS

for ballistic missiles, radar analysis, target signature characteristics, ballistic missile trajectory and guidance analysis, counter-mortar radars, magnetic bubbles, and millimetre/submillimetre wave radar.

A member of the Radar Systems Panel of the IEEE Aerospace and Electronic Systems Society and Chairman of the Radar ECCM Committee of that panel, Mr Johnston created the term 'ECCM Improvement Factor' which was recently incorporated into the IEEE Standard Radar Definitions. He is Editor in Chief of the International Radar Directory and author of 'Radar Electronic Counter-Countermeasures' and 'Millimeter Wave Radar'.

Stephen Nightingale joined Philips Research Laboratories in September 1967 and received his first degree from South Bank Polytechnic, London, in 1974 under the joint sponsorship of Philips and the IEE. He was awarded his Ph.D. from the University of Kent at Canterbury in 1980 for his work on loss and noise characteristics of microwave mixers. His work in recent years has been concerned with the design and construction of microwave/millimetre-wave components for frequencies up to 100 GHz. This work included the design and development of millimetre-wave radiometer systems for target tracking and imaging applications in the 27–40 and 75–110 GHz frequency bands.

In 1977/78 he was seconded to Philips Forschungs-laboratorium, Hamburg, W. Germany, where he worked on the noise characteristics of Schottky barrier diodes and radiometric measurement techniques. In September 1982 Dr Nightingale joined the Electronics Laboratory of General Electric Company, Syracuse, New York, USA, where he is currently engaged in developing a 30 GHz monolithic receive module for phased-array applications.

Michael Sisson read physics at Liverpool University obtaining the B.Sc. degree in 1966. From 1966–1969 he worked on infrared sensing devices at the EMI Research Laboratories and during this period studied at Chelsea College for the MSc. degree of the University of London on Physics of Solid State Devices which he was awarded in 1968. He received his Doctorate in 1976 for a thesis on the Development of Microwave Receiving Diodes. From 1969 to the present Dr. Sisson has been employed by GEC Hirst Research Centre working on various microwave devices including mixers, detectors, p-i-n and Gunn diodes. He was responsible for the development of the GaAs beam lead diodes marketed by Marconi Electronic Devices and currently is Leader of the Microwave Diodes Project within the Microwave Division.

Edward Stevens (Member 1968, Graduate 1964) is leader of the Advanced Technology Group of the Communications Division, EMI Electronics, Wells. He began his career in 1954 at the Central Research Laboratories of EMI as a student apprentice studying physics at Acton Technical College/Brunel College of Technology. He was involved in the development of low-power reflex klystrons until 1959. After working on radar in the RAF from 1959 to 1961, he joined G.V. Planer Ltd. and was engaged in research into thin films, both superconducting and magnetic, for high-speed computer memories. This work was extended to include thin-film circuit elements and circuitry. In 1964 Mr. Stevens rejoined EMI as Leader of the Thin-Film Circuits Section at EMI Electronics; his current interests include microwave integrated circuits, active microwave devices, and passive waveguide components.

Neil Williams graduated at Sheffield University in 1970 and later obtained a Ph.D. degree at Imperial College of Science and Technology, University of London. Since 1975 he has worked at ERA Technology in the R.F. Technology Centre. His current research interests include reflector and array antenna design and radar system analysis.

Rüdiger Vahldieck received his Dipl.-Ing. degree in electrical engineering from the University of Bremen in 1980. Since that time he has been working with the Microwave Department of the University of Bremen, where his research activities have been in the area of field problems of waveguide discontinuities and currently in the design and development of fin-line structures.

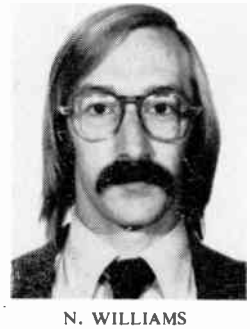

N. WILLIAMS

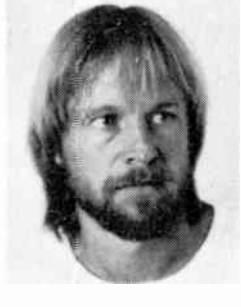

R. VAHLDIECK

Conferences, Courses and Exhibitions, 1982-83

The date and page references in italics at the end of an item are to issues of *The Radio and Electronic Engineer (REE)* or *The Electronics Engineer (EE)* in which fuller notices have been published.
The symbol ★ indicates that the IERE has organized the event.
The symbol ● indicates that the IERE is a participating body.
An asterisk * indicates a new item or information which has been amended since the previous issue.

Further information should be obtained from the addresses given.

1982

DECEMBER

TENCON '82 *6th to 8th December HONG KONG*
International Conference on the development and application of integrated circuits, organized by the Hong Kong Section of the IEEE, will be held in Hong Kong. Information: Hong Kong Trade Development Council, 14–16 Cockspur Street, London SW1Y 5DP. (Tel. 01-930 7955)

INDEX-EL '82 *10th to 15th December ATHENS*
Second International Electrical & Electronics Engineering Exhibition, will be held at The Zappio Palace, Athens. British exhibits sponsored by EEA. Information: EEA, 8 Leicester Street, London WC2H 7BN. Tel. 01-437 0678.

Computers *14th December BIRMINGHAM*
A one-day Seminar on Using Personal Computers in Industry, organized by Sira Institute, will be held at the University of Aston in Birmingham. Information: Conference Unit, Sira Institute, South Hill, Chislehurst, Kent.

Remote Sensing *15th to 17th December LIVERPOOL*
Annual Conference on Remote Sensing and the Atmosphere to be held in Liverpool. Information: Dr A. Henderson-Sellers, Geography Department, University of Liverpool, P.O. Box 147, Liverpool L69 3BX

1983

JANUARY

Visodata *17th to 21st January MUNICH*
Fifth Visodata display and exhibition will be held at the Munich Trade Fair Grounds. Information: Visodata '83, Messegelande, Postfach 12 10 09, D-8000 Munchen 12. (Tel. (089) 51 07-1)

Computer Simulation *27th to 29th January SAN DIEGO*
Multiconference on Modelling and Simulation on Microcomputers organized by The Society for Computer Simulation, will be held at the Holiday Inn, Embarcadero, San Diego. Information: SCS, P.O. Box 2228, La Jolla, California 92038, U.S.A.

FEBRUARY

MECOM *'83 7th to 10th February BAHRAIN*
Third Middle East Electronic Communications Show and Conference, organized by Arabian Exhibition Management, to be held at the Bahrain Exhibition Centre. Information: Dennis Casson, MECOM '83, 49/50 Calthorpe Road, Edgbaston, Birmingham B15 1TH. (Tel. (021) 454 4416).

MARCH

Component Assembly *March BRIGHTON*
Brighton Electronics Exhibition on matching components with insertion, connection and assembly aids and techniques, to be held in Brighton. Information: The Press Officer, Trident International Exhibitions Ltd, 21 Plymouth Road, Tavistock, Devon PL19 8AU. (Tel. (0822) 4671).

Audio-Video *6th to 10th March ABU DHABI*
First comprehensive international exhibition for consumer electronics in the Gulf Area organized by AMK Berlin in association with the Gulf Arab Marketing and Exhibition Company, will be held in Abu Dhabi. Information: AMK Berlin, Postfach 191740, Messedamm 22, D-1000 Berlin 19. (Tel. (030) 30 38-1)

● Telecommunications Networks *21st to 25th March BRIGHTON*
Second International Network Planning Symposium (Networks '83), organized by the Institution of Electrical Engineers with the association of the IERE, to be held at the University of Sussex, Brighton. Information: IEE Conference Department, Savoy Place, London WC2R 0BL. (Tel. 01-240 1871).

Inspex *'83 21st to 25th March BIRMINGHAM*
Tenth International Measurement and Inspection Technology Exhibition, sponsored by *Measurement and Inspection Technology* in association with IQA and Gauge and Tool Makers' Association, to be held at the National Exhibition Centre, Birmingham. Information: Exhibition Manager, Inspex '83, IPC Exhibitions Ltd, Surrey House, 1 Throwley Way, Sutton, Surrey SM1 4QQ. (Tel. 01-643 8040).

APRIL

Engineering Education *6th to 8th April PARIS*
Second World Conference on Continuing Engineering Education, organized by the European Society for Engineering Education, to be held at UNESCO Headquarters in Paris. Information: Mr N. Krebs Ovesen, Danish Engineering Academy, Building 373, DK 2800, Lyngby, Denmark.

● ICAP *'83 12th to 15th April NORWICH*
Third International Conference on Antennas and Propagation organized by the IEE in association with the URSI, IEEE, IMA, IoP and the IERE, will be held at the University of East Anglia, Norwich. Information: IEE Conference Department, Savoy Place, London WC2R 0BL. (Tel. 01-240 1871, ext. 222)

***Engineering Software** *11th to 13th April LONDON*
Third International Conference and Exhibition on the Use and Applications of Computers in Engineering, will be held at Imperial College. Information: Conference Secretary, 125 High Street, Southampton, SO1 0AA (Tel. (0703) 21397)

Electrostatics *13th to 15th April OXFORD*
Sixth conference on Static Electrification organized by the Institute of Physics in association with the Institution of Electrical Engineers, will be held at St Catherine's College, Oxford. Information: Meetings Officer, Institute of Physics, 47 Belgrave Square, London SW1. (Tel. 01-235 6111)

ICASSP *'83 14th to 16th April BOSTON*
Eighth International Conference on Acoustics, Speech, and Signal Processing organized by the IEEE, will be held at the Sheraton-Boston Hotel, Boston, Massachusetts. Information: Publicity Chairman, Richard Kurth, Sperry Research Center, 100 North Road, Sudbury, MA 01776, USA. (Tel. (617) 369-4000)

***IFSSEC** *'83 18th to 22nd April LONDON*
Fire, Security and Safety Exhibition and Conference, will be held at Olympia, London. Information: Victor Green Publications, 106 Hampstead Road, London NW1 2LS. (Tel. 01-388 7661)

***Computer Aided Engineering** *20th to 21st April LONDON*
Technical Conference on Computer Aided Engineering — Today's Technology and the Second Exhibition of Numerical Engineering Equipment and Services, organized by the Institution of Production Engineers, will be held at the Wembley conference Centre. Information: The Manager, Conferences & Exhibitions, IProdE, Rochester House, 66 Little Ealing Lane, London W5 4XX. (Tel. 01-579 9411)

MAY

Test and Measurement *2nd to 5th May SAN JOSE*
The Second Annual Test and Measurement World Expo will be held at the San Jose Convention Center. Information: Meg Bowen, Test and Measurement World Expo, 215 Brighton Avenue, Boston, MA 02134 U.S.A.

Noise *17th to 20th May MONTPELLIER, FRANCE*
Seventh International Conference on Noise in Physical Systems/Third International Conference on 1/f Noise, will be held in Montpellier, France. Information: Dr B. Jones, Department of Physics, University of Lancaster, (Tel. Lancaster 65201); or Professor H. Sutcliffe, Department of Electronic & Electrical Engineering, University of Salford.

Electron Tubes *18th to 20th May GARMISCH-PARTENKIRCHEN, F.R.G.*
Conference on Electron Tubes organized by VDE (NTG) in association with the German Section of the IEEE, will be held in Garmisch-Partenkirchen, Bavaria. Information: Conference Chairman, Dr H. Heynisch, Siemens AG, Werk fur Rohren und Sondergebiete, St Martinstrasse 76, D-8000 Munchen 80.

***Multiple-valued Logic** *23rd to 25th May KYOTO, JAPAN*
Thirteenth International Symposium on all aspects of multiple valued logic, organized by the IEEE in association with ISMVL, Japan, will be held at the Holiday Inn Kyoto. Information: Dr S. L. Hurst, School of Electrical Engineering, University of Bath, BA2 7AY. (Tel. (0225) 61244)

JUNE

***Eurochem** *'83 6th to 10th June BIRMINGHAM*
International Chemical and Process Engineering Show and Conference, organized by the Institution of Chemical Engineers in association with Clapp and Poliak, will be held at the National Exhibition Centre, Birmingham. Information: Conference: Gillian Nelson or Jane Ellis, IChemE Conference Section, 165–171 Railway Terrace, Rugby, CV21 3HQ. (Tel. (0788) 78214) Exhibition: Andrew Dedman, Clapp & Poliak, 232 Acton Lane, London W4 5DL. (Tel. 01-747 3131)

***Tectronica** *'83 14th to 17th June LONDON*
Exhibition of Laboratory Technology, organized by Industrial and Trade Fairs, will be held at Earls Court. Information: Industrial and Trade Fairs, Radcliffe House, Blenheim Court, Solihull, W. Midlands. (Tel. 021-705 6706)

***Radio Communications** *19th to 22 June BOSTON*
International Conference on Communications, organized by the IEEE, will be held in Boston, Massachusetts. Information: IEEE, Conference Coordination, 345 East 47th Street, New York, NY10017, USA.

***Laser and Opto-Electronics** *27th June to 1st July MUNICH*
Sixth International Congress and Exhibition on Laser Opto-Electronik, organized by MMG, will be held in Munich. Information: MMG, Messegelande, Postfach 121009, D-8000 Munchen 12.

IOOC *'83 27th to 30th June TOKYO*
The Fourth International Conference on Integrated Optics and Optical Fibre Communication, sponsored jointly by the Institute of Electronics and Communication Engineers of Japan and the Institute of Electrical Engineers of Japan, will be held at Keio Plaza Hotel, Tokyo. Information: Y. Suematsu, Department Elec. Phys. Tokyo Institute of Technology, 2-12-1, O-okayama, Meguro-ku, Tokyo, 152 Japan.

***Security Tradex** *'83 28th June to 1st July BIRMINGHAM*
Security Trade Exhibition sponsored by the IPSA, in association with the Institute of Industrial Security, will be held at the National Exhibition Centre, Birmingham. Information: Queensway House, 2 Queensway, Redhill, Surrey. (Tel. (07373) 68611)

JULY

***Software Engineering** *4th to 8th July LUND*
Fifth International Conference on Software Engineering for Telecommunication Switching Systems, organized by the IEE

in association with SER, The British Computer Society, Institute of Mathematics and its Applications and the IERE. Information: Conference Department, IEE, Savoy Place, London WC2 0BL (Tel. 01-240 1871)

Reliability '83 *6th to 8th July BIRMINGHAM*
Fourth National Reliability Conference organized by the National Centre of Systems Reliability in association with the Institute of Quality Assurance, will be held at the National Exhibition Centre, Birmingham. Information: Mr A. Cross, National Centre of Systems Reliability, UKAEA, Wigshaw Lane, Culcheth, Warrington WA3 4NE.

SEPTEMBER

***Microwaves** *5th to 9th September NUREMBERG*
Thirteenth European Microwave Conference, organized by IEEE-URSI-VDE, will be held in Nuremberg. Information: IEEE, Conference Coordination, 345 East 47th Street, New York NY 10017, USA. VDE, Zentralstelle Tagungen, Stresemannalle 21, D-6000, Frankfurt am Main 70.

Weightech '83 *13th to 15th September LONDON*
Third International Industrial and Process Weighing and Force Measurement Exhibition and Conference, organized by Specialist Exhibitions in association with the Institute of Measurement and Control, to be held at the Wembley Conference Centre. Information: Specialist Exhibitions Ltd, Green Dragon House, 64/70 High Street, Croydon, CR9 2UH. (Tel. 01-686 5741) Conference Information: IMC, 20 Peel Street, London W8 7PD. (Tel. 01-727 0083).

***ESSDERC '83** *13th to 16th September CANTERBURY*
Thirteenth European Solid State Device Research Conference and Eighth Symposium on Solid State Device Technology, organized by the Institute of Physics in association with the European Physical Society, the IEE, IERE, IEEE, the Dutch Physical Society and the German Physical Society, will be held at the University of Kent at Canterbury. Information: Meetings Officer, Institute of Physics, 47 Belgrave Square, London SW1X 8QX. (Tel. 01-235 6111)

C.A.S.T. '83 *13th to 15th September BIRMINGHAM*
First International Conference and Exhibition on Cable and Satellite Television organized by Cable and Satellite Television Exhibitions, will be held at the Birmingham Metropole Hotel. Information: Exhibition, Michael Hyams, Managing Director, Cable & Satellite TV Exhibitions Ltd, 5 Barratt Way, Tudor Road, Harrow HA3 5QG. (Tel. 01-863 7726) Conference, The Economist Conference Unit, 25 St James's Street, London SW1 1HG. (Tel. 01-839 7000)

***Pattern Recognition** *19th to 21st September OXFORD*
Second International Conference on Pattern Recognition, organized by BRPA, will be held at the University of Oxford. Information: Dr Frank Harris, Nuclear Physics Laboratory, Keble Road, Oxford OX1 3RH (Tel. (0865) 59911)

Simulators *26th to 30th September BRIGHTON*
International Conference on Simulators, organized by the IEE, will be held at the University of Sussex. Information: IEE Conference Department, Savoy Place, London WC2R 0BL (Tel. 01-240 1871) *(Synopses by 4th October.)*

★NEOS '83 *26th to 30th September READING*
International Conference on Networks and Electronic Office Systems, organized by the IERE, will be held at the University of Reading. Information: Professional Activities Department, IERE, 99 Gower Street, London WC1E 6AZ. (Tel. 01-388 3071) *(Synopses by 1st February 1983, Papers by 1st May 1983).*

OCTOBER

Computer Graphics '83 *4th to 6th October LONDON*
Conference and Exhibition on Computer Graphics organized by Online Conferences. Information: Online Conferences Ltd, Argyle House, Northwood Hills, Middlesex HA6 1TS. (Tel. (09274) 28211)

***Technical Diagnostics** *4th to 6th October SOCHI, USSR*
Third Symposium on Technical Diagnostics organized by the IMEKO Technical Committee TC10 will be held in Sochi, USSR. Information: IMEKO Secretariat, 1371 Budapest, POB457, Hungary. (Tel. 324 116)

Security Technology *4th to 6th October ZURICH*
17th Carnahan Conference on Security Technology, organized by the Institute for Communication Technology at the Eidg. Technische Hochschule Zurich, in association with the College of Engineering, University of Kentucky, will be held in Zurich. Information: P de Bruyne, ETH Zentrum-KT, CH-8092 Zurich, Switzerland. (Tel 411-2562792)

Viewdata '83 *18th to 20th October LONDON*
Conference and Exhibition organized by Online Conferences. Information: Online Conferences Ltd, Argyle House, Northwood Hills, Middlesex HA6 1TS. (Tel. (09274) 28211).

Telecom '83 *26th October to 1st November GENEVA*
Second World Telecommunication Exhibition, organized by the International Telecommunications Union, to be held at the New Exhibition Conference Centre in Geneva. Information: Telecom '83, ITU, Place des Nations, CH-1211 Genève 20, Switzerland. (Tel. (022) 99 51 11).

Organizers of appropriate events are invited to submit details to the Editor for inclusion in this calendar.